Photochemical Control of Covalent Bonds and Noncovalent Interactions in Polymer Materials – Gels, Thin Films and Colloids

A dissertation submitted by

Xiaoran Hu

in partial fulfillment of the requirements for the degree of

Doctor of Philosophy

In

Chemistry

TUFTS UNIVERSITY

August 2017

Advisor: Professor Samuel W. Thomas III

Abstract

Understanding of structure-property relationships and advancements in synthetic strategies of stimuli-responsive polymers allow the development of novel functional materials for a variety of applications. Of particular interest are photoresponsive polymers incorporating photolabile groups, as light can offer real-time spatiotemporal control of material properties. In this thesis, we describe the use of stimuli-responsive groups, especially photocleavable groups, to control covalent bonds and non-covalent intermolecular interactions in polymer materials ranging from soft materials (hydrogels and organogels) to solid-state polymer films (polyelectrolyte multilayers and conjugated polymer thin films) to polyelectrolyte colloids. Incorporation of photoresponsive moieties into polymer structures enables the photomodulation of material properties (e.g., electrostatic properties, mechanical properties, and solubility), and provides new approaches including triggered release and photolithographic patterning.

Chapter 2 describes a series of photodegradable ROMP gels covalently linked by structurally different *o*-nitrobenzyl (ONB) groups of different photosensitivity. Inclusion of photocleavable ONB groups in the crosslinkers enables photochemical control of the covalent crosslinking density in the gels, and therefore over swelling, viscoelastic properties, and solubility of these gels.

Chapter 3 describes multi-responsive polyelectrolyte multilayers (PEMs) prepared via layer-by-layer (LBL) assembly. A series of rationally designed and synthesized stimuli-responsive polycations can "charge-shift" from positively charged polymers to polymers with less positive net charge upon photodegradation or increasing pH. Such charge-shifting can disrupt ion-pairing non-covalent intermolecular interactions in PEMs comprising these

polycations, and therefore render PEMs soluble in buffered solutions. We also developed an approach to bond guest molecules to PEMs covalently via a redox sensitive disulfide bond; cleavage of disulfide bond triggered by chemical reduction leads to the release of guests from the PEMs. These two general approaches to tunable physical or chemical bonds, combined with the capability for spatial segregation of chemical functionality in LBL films, enable a versatile method (Chapter 3.2) to prepare free-standing PEM films that can release covalently bound and physically trapped cargo upon application of different stimuli (light, pH or chemical reduction). This general strategy also allows for light-controlled selective disruption, multilevel patterning, and sequential release with PEMs incorporating four photocleavable chromophores fabricated in this manner (Chapter 3.3).

Photo-disruption and triggered release with polyelectrolyte colloidal nanoparticles is described in Chapter 4. Irradiation of polyelectrolyte complex nanoparticles incorporating a photolabile polycation, which can "charge-shift" into a polyanion upon photolysis, causes disruption of the attractive ion-pairing interactions between the oppositely charged polymers and leads to the dissolution of the polyelectrolyte colloid nanoparticles.

Finally, chapter 5 describes photochemical control of conjugated polymer solubility via a sidechain engineering approach. The use of ONB linkage between solubilizing alkyl sidechains and a polythiophene mainchain enables the photocleavage of the solubilizing alkyl sidechains and, therefore, yields a photolyzed polymer insoluble in nonpolar solvents. Moreover, photolysis of the ONB junctions reveals carboxylic acid pendant groups on the polymer backbone and, therefore, increases the solubility of the photolyzed polymer in aqueous solutions. This conjugated polymer can be used as a positive- negative dual-tone photoresist.

Acknowledgements

Foremost, I would like to express my sincere gratitude to my advisor Prof. Samuel W. Thomas III for all his help, support and encouragement. The door to Sam's office was always open whenever I had a question in chemistry or research, or any questions related to my professional career. From Sam I have learned how to be a better chemist, a patient mentor, and a supportive and thoughtful colleague. I would also like to thank Professor Ayse Asatekin and Professor Krishna Kumar for their support throughout my PhD study at Tufts, and Prof. Katherine Mirica for graciously being my outside committee member. I would also like to thank Dr. Sherry Zhu for being a knowledgeable and helpful mentor during my Schlumberger internship.

I would thank members of Team Thomas: Dr. Patricia Gumbley, Dr. Jingjing Zhang, Dr. Robert Pawle, Dr. Esra Altinok, Dr. Zach Smith, Rom Baral, Fanny Frausto, Brendan Duran, Matt Feeney, Seth Sharber, Will Mullin, Dr. Valentina Brega, and the undergraduates and high school students I got to interact with over the years (John Lawrence, Ethan McIntosh, Zaid Qureishi, James Mullahoo and many others) for helping make an amazing lab atmosphere. I would also like to thank collaborators from different departments and all Chemistry department staff members for providing generous help during my PhD study.

Last, but not least, I would like to thank my family and friends for all their support over the years!

Table of Contents

1. Introduction to Photoresponsive Polymers……2
   1.1. Introduction to Stimuli-Responsive Polymers……3
   1.2. Photochemistry of Organic Compounds……..……...4
   1.3. Photocleavable Groups……...7
      1.3.1 *o*-Nitrobenzyl (ONB) Groups……10
      1.3.2 Coumarin Groups……..13
      1.3.3 Phenacyl Groups……...15
   1.4 Selective Photocleavage……..16
      1.4.1 Wavelength Selectivity of Photocleavable Groups.. ……...17
      1.4.2 Quantum Efficiency Selectivity of Photocleavable Groups…..……...18
   1.5 Conclusions…..……18
   1.6 References ……...…20

2. Photochemical Control of Covalent Bonds in Polymer Gels……..24
   2.1. Introduction…….……..25
      2.1.1 Photodegradable Polymer Gels……25
      2.1.2 Ring Opening Metathesis Polymerization (ROMP) ……26
   2.2. Experimental Design and Synthesis of ONB Functionalized Crosslinkers……..29
   2.3. Preparation of ONB Functionalized ROMP Gels……36
   2.4. Photodegradation of ONB Functionalized ROMP Organogels……37
      2.4.1 Visual Observation of Gel Dissolution……38
      2.4.2 Monitoring Dissolution of Fluorescent Polymer Chains……..39
      2.4.3 The Effect of Crosslink Density on Gel Photoreactivity……..42
   2.5. Photocontrolled Release from ONB Functionalized Hydrogels……..43
   2.6. Conclusions……..45
   2.7. Attempts to Develop Anthracene Functionalized Photolabile Hydrogels……46
   2.8. Experimental Section……48
   2.9. References……59

3. Controlling Covalent Bonds and Non-Covalent Intermolecular Forces in Solid-State Polyelectrolyte Multilayers……..74
   3.1. Introduction……...75
      3.1.1 Ion-Pairing Driven Polyelectrolyte Self-Assembly……..75
      3.1.2 Stimuli-Responsive Layer-by-Layer (LBL) Films……76
   3.2. Multi-Responsive Free-Standing LBL PEMs……77
      3.2.1 Experimental Design and Synthesis of Light-, Chemical Reduction-, and pH-Responsive PEMs……..……78
      3.2.2 Response of LBL PEMs to Different Stimuli……..82
      3.2.3 General Approach to Stimuli-Responsive Free-Standing PEMs—Another Example: Photodisruptable Freestanding PEMs……87

3.2.4 Conclusions……91
3.2.5 Experimental Section……92
3.3. Multi-Level Photopatterning and Programmable, Light-Controlled Release from Photoresponsive PEMs Incorporating Four Photocleavable Groups……98
3.3.1 Design and Synthesis of a Series of Photolabile PEMs……99
3.3.2 PEM Deposition via LBL Self-Assembly……103
3.3.3 Photodisruption of PEMs Deposited on Quartz Slides……106
3.3.4 Photocontrolled Orthogonal Release from PEM-Coated Microspheres……116
3.3.5 Conclusions……122
3.3.6 Experimental Section……123
3.4. Conclusions……127
3.5. References……129

4. Photochemical Control of Noncovalent Interactions in Polyelectrolyte Colloids……136
4.1. Introduction……137
4.2. Experimental Design and Synthesis of Charge-Shifting Polycation……138
4.3. Preparation of Polyelectrolyte Colloidal Nanoparticles……140
4.4. Photochemical Disruption of Polyelectrolyte Complexes……143
4.5. Light Triggered Release of Encapsulated Cargo from PEC Colloid Nanoparticles……149
4.6. Conclusions……150
4.7. Experimental Section……150
4.8. References……155

5. Photochemical Control of Non-Covalent Intermolecular Forces Governed by Hydrophobicity……162
5.1. Introduction to Patternable Organic Electronic Materials……163
5.2. Design and Synthesis of Dual-Tone Photoresist **PT$_{o\mathbf{NB}}$** ……166
5.3. Photochemistry……168
5.3.1 Photolysis of Monomer **T1**……168
5.3.2 Photolysis of Thin Films……171
5.4. Photopatterning of **PT$_{o\mathbf{NB}}$** Films……178
5.4.1 Dual-Tone Photopatterning with **PT$_{o\mathbf{NB}}$**……178
5.4.2 Multi-Level CP Micropatterning……179
5.5. Conclusions……182
5.6. Experimental Section……183
5.7. References……189

List of Tables

Table 3.1……102
Table 3.2……106
Table 4.1……140
Table 4.2……141
Table 4.3……148

List of Figures

Figure 1.1……6
Figure 1.2……7
Figure 1.3……8
Figure 1.4……9
Figure 2.1……27
Figure 2.2……28
Figure 2.3……29
Figure 2.4……30
Figure 2.5……31
Figure 2.6……35
Figure 2.7……38
Figure 2.8……39
Figure 2.9……41
Figure 2.10……43
Figure 2.11……45
Figure 2.12……48
Figure 3.1……76
Figure 3.2……77
Figure 3.3……77
Figure 3.4……79
Figure 3.5……80
Figure 3.6……82
Figure 3.7……83
Figure 3.8……84
Figure 3.9……85
Figure 3.10……85
Figure 3.11……87
Figure 3.12……88
Figure 3.13……89
Figure 3.14……90
Figure 3.15……91
Figure 3.16……99
Figure 3.17……100
Figure 3.18……101
Figure 3.19……103
Figure 3.20……104
Figure 3.21……105
Figure 3.22……108
Figure 3.23……110
Figure 3.24……112

Figure 3.25……...114
Figure 3.26……...115
Figure 3.27……...118
Figure 3.28……...120
Figure 3.29……...122
Figure 4.1……...138
Figure 4.2……...139
Figure 4.3……...142
Figure 4.4……...143
Figure 4.5……...143
Figure 4.6……...144
Figure 4.7……...146
Figure 4.8……...147
Figure 4.9……...148
Figure 4.10……149
Figure 5.1……...166
Figure 5.2a……...169
Figure 5.2b……...170
Figure 5.3……...171
Figure 5.4……...172
Figure 5.5a……174
Figure 5.5b……...175
Figure 5.6……...176
Figure 5.7……...177
Figure 5.8……...179
Figure 5.9……...180
Figure 5.10……...182

List of Schemes

Scheme 1.1……...9
Scheme 1.2……...9
Scheme 1.3……....13
Scheme 1.4……....14
Scheme 1.5……....15
Scheme 2.1……....32
Scheme 2.2……....35
Scheme 2.3……....36
Scheme 2.4……....43
Scheme 2.5……....45
Scheme 2.6……....46
Scheme 3.1……....79
Scheme 4.1……...139
Scheme 5.1……...166

Photochemical Control of Covalent Bonds and Noncovalent Interactions in Polymer Materials – Gels, Thin Films and Colloids

Chapter 1:

Introduction to Photoresponsive Polymers

1.1 Introduction to Stimuli-Responsive Polymers

Responsive polymers are macromolecules capable of altering their chemical and/or physical properties upon exposure to external stimuli. Advanced stimuli-responsive systems have been widely used in a diverse range of applications including chemical or biochemical sensors, drug delivery systems, tissue engineering, and actuators.[1, 2] Both physical stimuli (e.g., changes in temperature,[3, 4] light,[5] mechanical stress,[6] and magnetic field[7]), and chemical stimuli (e.g., redox,[8] pH,[9] and enzyme[10]) are useful for triggering changes such as phase transition, small molecule retention and release, changes in ionic mobility, and changes in wettability.

Among the various stimuli used to control properties, light uniquely offers real-time remote control over spatiotemporal distribution, energy and stoichiometry. Rational design of polymers incorporating photolabile groups allows new approaches to photo-modulate material properties. Photoresponsive polymer structures, in general, can be classified into two categories: photoresponsive groups are either (1) positioned in the side chains, or (2) onto the polymer backbones. Commonly used photoresponsive groups include photocleavable groups (e.g., o-nitrobenzyl groups, p-methoxyphenacyl groups, dialkylaminocoumarin groups and others),[5, 11-15] photochromic groups (e.g., spiropyran groups),[16-18] photo-crosslinkable groups,[19-23] and photoisomerizable groups (e.g., azobenene groups).[24, 25] Functional polymers incorporating such photoresponsive groups have enabled photochemical control over the assembly or disassembly of polymer nanocarriers such as micelles,[26] photomodulation of the physical and chemical properties of polymer gels,[27, 28] photolithographic patterning of polymers,[16, 29-31] and others.

1.2 Photochemistry of Organic Compounds

Photochemical reactions are chemical reactions induced by interaction of light with matter. Light is one of the reactants in a photochemical system. A simplified description of molecular organic photochemistry is: R + hν → *R → P, where an organic molecule (R) absorbs a photon (hν) to produce the excited state (*R). This excited state can exhibit chemical properties that are largely different from the ground-state (R). *R can react to produce the photochemical product(s) (P). Light with wavelengths ranging from ~800 nm (near-IR) to ~150 nm (far UV) is of primary importance for photochemistry. The wavelength range of 150-800 nm (~ 8.3 eV - 1.5 eV) corresponds to energies comparable to energies of chemical bonds. Recent advancements in multiphoton photochemistry made IR radiation of particular interest for biological applications.[32, 33]

The first law of photochemistry states that only light absorbed by a molecule can induce photochemical modifications in the matter. The second law of photochemistry states that one molecule is excited for each quantum of light absorbed, and less than one photochemical product molecule is produced for each excited molecule. Under given irradiation condition, the photoreaction rate of a chromophore molecule is dictated by the multiplication of the molecule's molar extinction coefficient (defined as the absorbance for a molar concentration of a substance with a path of 1 cm determined at a specific wavelength) with its photochemical quantum yield (defined as the number of times a chemical reaction occurs per photon absorbed).

According to quantum mechanics, a photochemical reaction can be described by a wavefunction, a function that is provided upon solving the Schrodinger equation. Generally, there is an infinite number of wavefunctions with the corresponding values of the system energy. The energy of molecular system is quantized because only some wavefunctions with

characteristic values of the energy are physically acceptable. In photochemistry, therefore, only photons with a definite quantity of energy corresponding to a difference between two allowed energy values can be absorbed. Because the Schrodinger equation cannot be solved exactly for many body systems, determination of the energy of molecular systems requires approximate methods: in Born-Oppenheimer approximation, electronic and nuclear motions are separated – nuclei can be considered as fixed centers because they are much heavier than the electrons and their motion is much slower than that of electrons. A first approximation separates different types of nuclear motion: translation, rotation and vibration. Translational motion can be well described with classical mechanics, while rotational and vibrational motion require quantum mechanical treatment, leading to discrete energy levels as shown in **Figure 1.1**. The energy corresponding to the difference between two allowed rotation states is much smaller than that for vibrational states, and the latter is much smaller than the energy corresponding to electronic motion. Population of molecular energy states can be described by Boltzmann distribution. At room temperature, the vast majority of molecular systems is populated in the ground electronic and vibrational state. In a typical photochemical process, excited electronic states are populated by light absorption. Understanding of the transition between ground state (S_0) and first excited state (S_1) is of primary importance in understanding photochemical reactions with organic molecules.

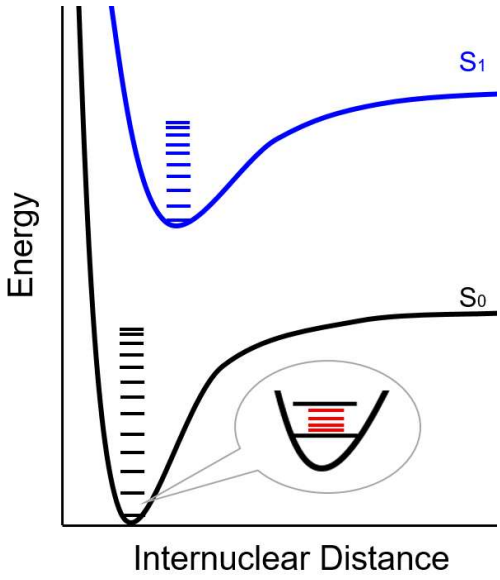

Figure 1.1: Potential energy curves corresponding to the singlet ground state (black, S_0) and singlet first excited state (blue, S_1) of a diatomic molecule. The energy levels for the vibrational motion are shown as black and blue lines inside the curves; the rotational levels for the zero-vibrational level of S_0 are shown as redlines in the insert.

A schematic representation of various pathways between two hypothetical potential energy surfaces (the ground state and the excited state) can be seen in **Figure 1.2**. The Franck Condon principle suggests that vertical excitation typically leads to vibrationally excited species ("hot" molecules). Hot molecules may first relax to an excited state intermediate with a minimum on the excited-state energy surface (path a). Return from the minimum may produce new photochemical product(s) (path c *left*) via a non-radiative transition, or may proceed through a photophysical process without producing a new species (path c *right*). The excited intermediate may also be modified further (path b) in the excited state and then return to the ground state surface to produce photochemical product(s) via a radiative path (path d). Moreover, the reaction

may proceed through a funnel and then the vibrational relaxation occurs in the ground state (path e and f).

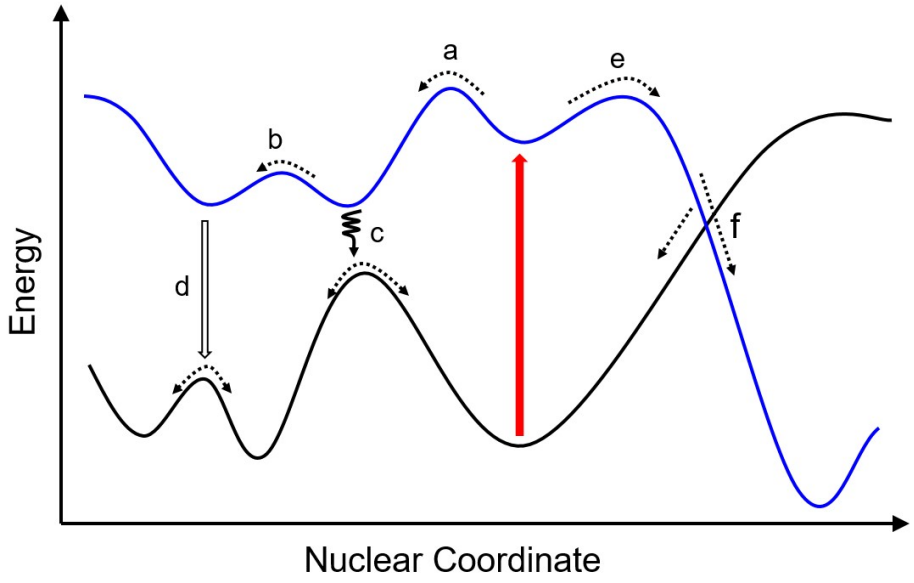

Figure 1.2: Potential energy surfaces of the ground and an excited state with various deactivation pathways (dashed lines) following the light absorption (red arrow).

1.3 Photocleavable Groups

Photolabile protecting groups is a unique class of protecting groups because they can be selectively photolyzed without added chemical reagent. Photocleavable groups have been widely used as protecting groups in organic synthesis and chemical biology for a variety of applications.[34-39] This general class of photoresponsive moieties has also found important application in functional polymer materials.[5, 40] Photocleavable groups can be incorporated into the polymer main chains and behave as linkers between segments (**Figure 1.3**, *top*); cleavage of such linker groups can change the molecular weight, shape or architecture of polymers, and can be used to change the solubility of the materials.[11, 41-43] For example

(**Figure 1.4a**), photocleavable groups can be used as crosslinkers to covalently link individual polymer chains together into three-dimensionally crosslinked, insoluble polymer networks (i.e., polymer gels). Photolysis of the photocleavable groups can break the covalent interchain linkage and release individual, soluble polymer chains.

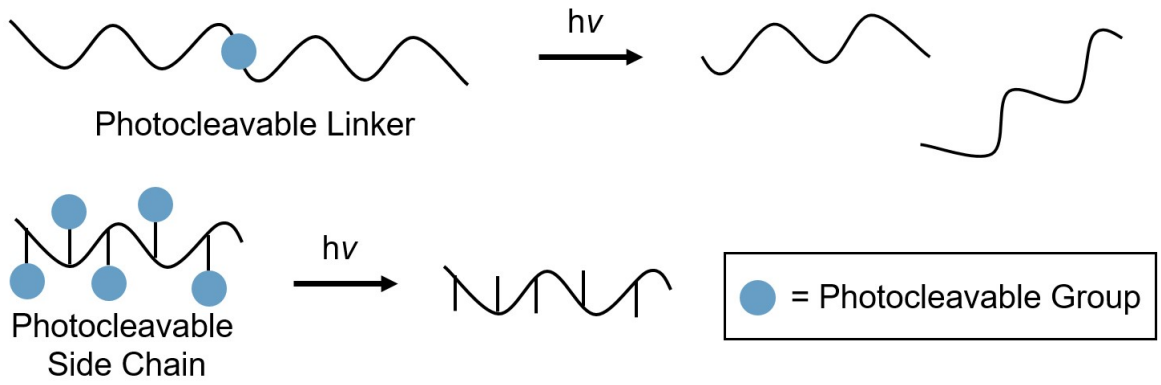

Figure 1.3: *Top*: Incorporation of photocleavable groups in polymer backbones as linkers. *Bottom*: Incorporation of photocleavable groups in polymers as side chains.

Another typical strategy to introduce photocleavable groups into polymers is to position photocleavable groups into polymer side chains (**Figure 1.3**, *bottom*). Most commonly, photolysis of such side chains modifies the hydrophobic-hydrophilic balances, and therefore transforms the structures of the polymer assemblies.[26, 44] **Figure 1.4b** illustrates the formation of polymer micelles from a amphiphilic block copolymer, one block of which bears hydrophobic photocleavable side chains. Photolysis of the photoclevable side chains produces hydrophilic pendant groups, rendering the photoproduct polymer soluble in aqueous solutions. Micelles assembled from such polymers can dissolve upon the photoinduced change in the hydrophobicity-hydrophilicity balances.

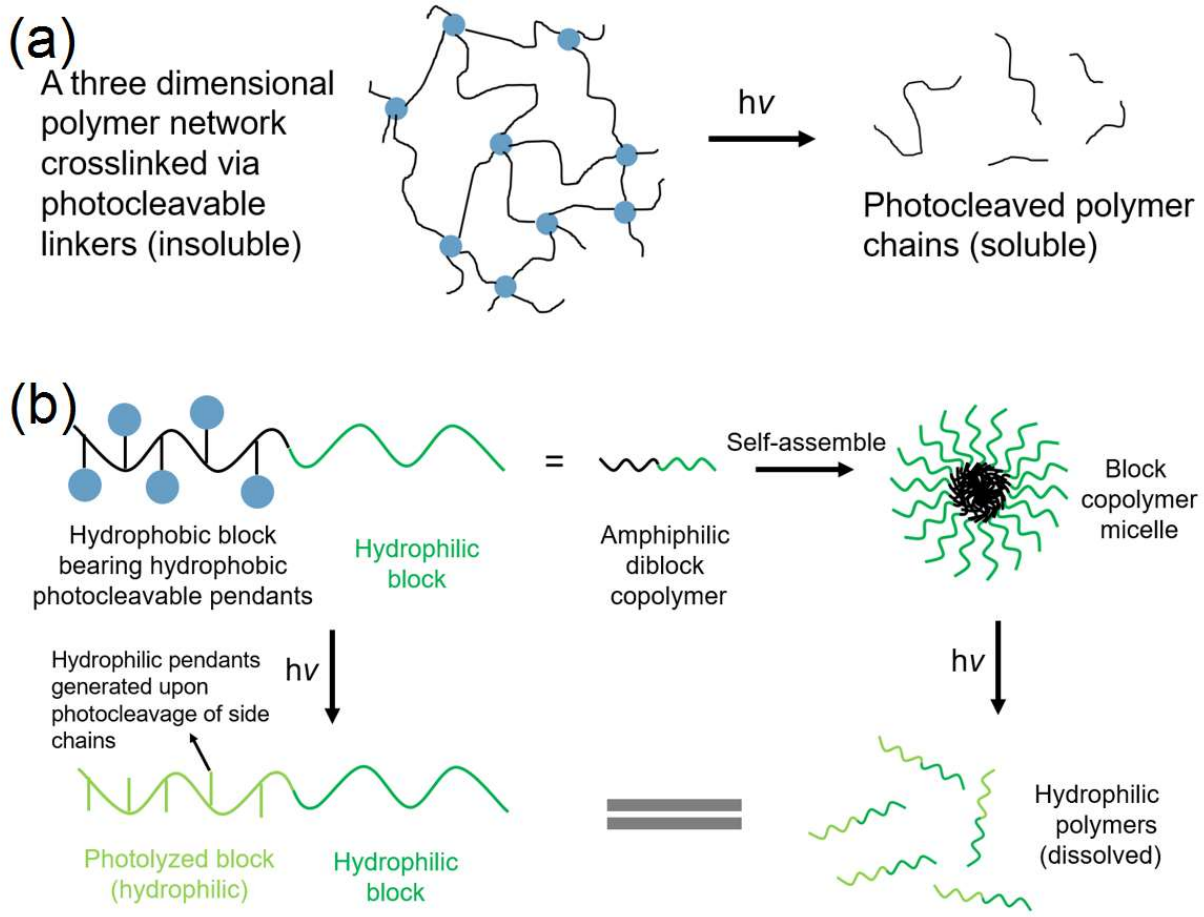

Figure 1.4: (a) Schematic of a polymer network covalently crosslinked via photocleavable groups, and its degradation into solubilizing polymer chains upon photolysis. (b) Illustrative representation of the photolysis of an amphiphilic block copolymer bearing photocleavable pendants; micelles assembled form such photoresponsive block copolymers dissolve upon the photocleavage of side chains.

In the following section, we focus on the photochemistry and applications of three classes of photocleavable groups, that is, the o-nitrobenzyl (ONB) groups, coumarin groups and phenacyl groups.

1.3.1 *o*-Nitrobenzyl (ONB) Groups

1.3.1.a Mechanism of ONB Photolysis

Since first described by Barltrop and coworkers,[45] *o*-nitrobenzyl (ONB) groups have been widely used as protection groups for functional groups including hydroxyl groups, carboxylic acids, and amino groups. ONB groups photolyzes through Norrish type II reaction (**Scheme 1.1**):[12, 38] Absorption of a photon first excites the nitro group; subsequent intramolecular hydrogen abstraction produces the aci-nitro intermediate, followed by rearrangement which produces the nitroso derivative. Photodegradation of an o-nitrobenzyl ester (NBE) group results in a deprotected carboxylic acid and an o-nitrosobenzaldehyde byproduct (**Scheme 1.2**). The photogenerated carboxylic acid is more hydrophilic than the parent NBE moiety, making the NBE group an interesting photocleavable group especially useful to photomodulate hydrophobicity/hydrophilicity of molecules.

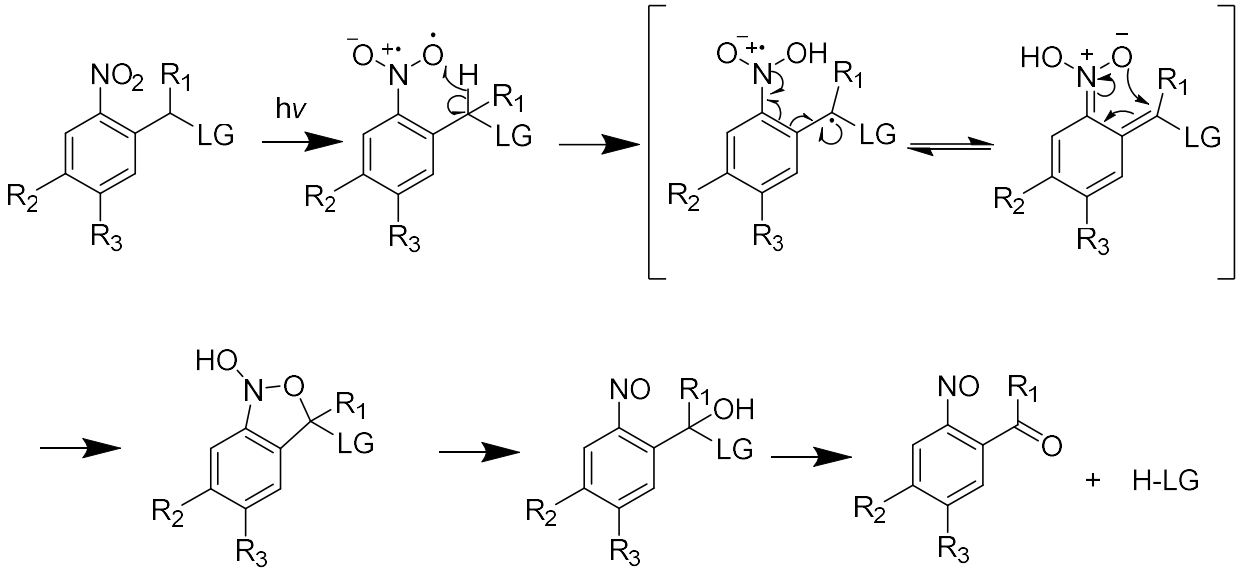

Scheme 1.1: Photocleavage mechanism of ONB groups.

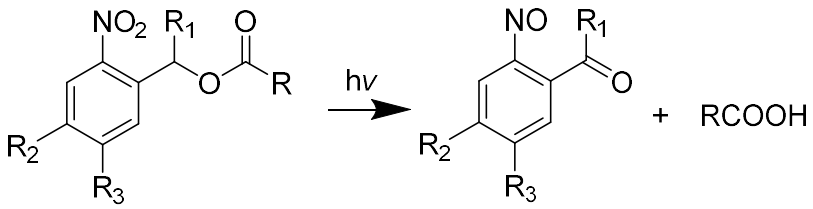

Scheme 1.2: Photolysis of NBE groups.

A variety of ONB derivatives that absorb different wavelengths of light with different quantum yield has been developed.[12, 38] In the following section, we will discuss the structure-property relationships of ONB groups.

1.3.1.b Structure-Property Relationships of ONB Groups

Rational structural design of ONB derivatives allows fine-tuning of their photochemical properties (e.g. quantum efficiency and absorption wavelengths). Generally, substitution of benzylic hydrogen with hydrocarbons can lead to approximately five-fold increase in the relative photolysis rate of ONB groups due to the stabilization of the photoexcited intermediate by the secondary benzylic carbon center.[46-48] Substitution of benzylic hydrogen also lowers the probability of side reactions between the photochemical products because the photoproduct of a substituted ONB group is a ketone, which is usually less prone to side reactions compared with aldehyde photoproduct produced from unsubstituted nitrobenzyl groups. For example, the recovery of protected amine groups is usually significantly lowered by the side reaction between the released amine with the aldehyde photoproduct, which can be suppressed by having the benzylic substitution because the ketone byproduct is less prone to the imine formation.[12]

Moreover, grafting moieties onto the aromatic ring (R2 and R3 in **Scheme 1.1**) shifts the absorption of ONB groups: generally, grafting electron-rich moieties (e.g., alkoxy groups) onto the aromatic ring red-shift the absorption of NB derivatives and reduces the quantum yield of the photocleavage. [39, 47, 49-51]

Leaving groups (LG in **Scheme 1.1**) also influence the quantum efficiency by providing stabilization or destabilization to the ONB type radical intermediates and hence lower or increase the barrier of the photocleavage reaction.[47, 52]

1.3.1.c Applications of ONB Groups

ONB groups have been widely used in the fields of organic synthesis, photolithography, and chemical biology.[12, 13, 53] ONB groups have also found important applications in stimuli-responsive macromolecules.[54] One common approach to photoresponsive polymers is to incorporate NBE groups into the macromolecule side chains; photolysis of the hydrophobic NBE groups generate carboxylic acid groups, and therefore increase the hydrophilicity of the polymer. For example, amphiphilic diblock copolymer with the hydrophobic block bearing NBE pendants can change from amphiphilic to hydrophilic; such block copolymers have been used to construct photoresponsive polymer nanoassemblies, such as photodisruptable micelles, with promise for drug delivery applications.[55] Photolabile polymers with NBE pendant groups also find important applications in photolithography.[56, 57]

Moreover, ONB groups can be incorporated in the polymer backbones: block copolymers with ONB junctions between the hydrophilic and hydrophobic blocks have been used in self-assembled photoresponsive nanocarriers;[11, 58, 59] ONB linkers bridging polymer and glass

surface allows detaching of polymer brush from the substrates;[60] ONB based cross-linkers also enable to photomodulate crosslinking density and, therefore, physical properties of polymer networks.[41]

1.3.2 Coumarin Groups

Coumarin groups are another class of extensively studied photocleavable groups useful in protecting various functional groups including carboxylic acids, phosphates, amino and hydroxyl group.[12, 15, 38] Modifications of the coumarin type moieties by substitution changes the light absorption wavelength, quantum efficiency, and other properties (such as hydrophilicity) of these molecules.[13]

Coumarin groups photolyze through a C-O bond heterolysis mechanism (see **Scheme 1.3** for the photolysis mechanism of diethylaminocoumarin).[13, 61] Upon absorption of a photon, the excited molecule first relaxes to the lowest excited state S_1. The excited intermediate turns to ground-state starting molecule via fluorescence emission or nonradiative deactivation paths, or proceed via heterolytic bond cleavage to produce a tight ion pair as an intermediate. The tight ion pair either (1) reacts with nucleophiles to form a new stable coumarinylmethyl product, or (2) escapes the solvent cage and becomes solvent separated ion pair that can react with available nucleophiles, or (3) recombines and regenerates the ground-state starting molecule without producing a new species.

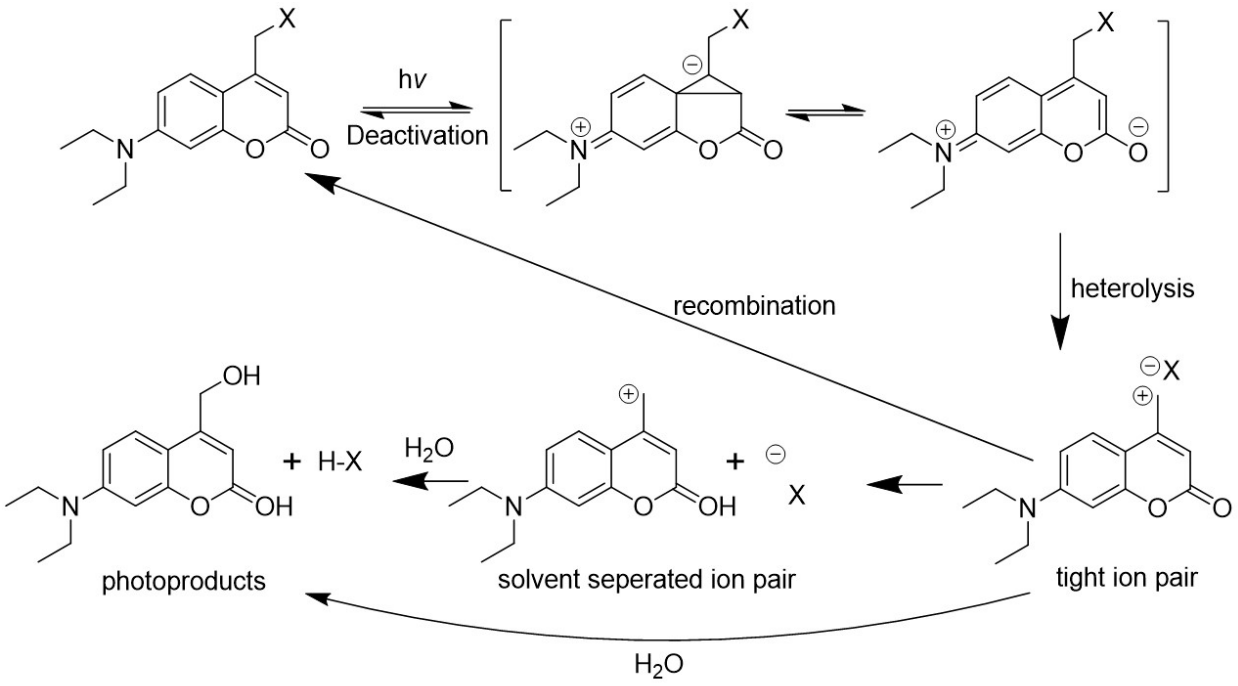

Scheme 1.3: Photocleavage mechanism of diethylaminocoumarin groups.

Compared with nitrobenzyl groups, coumarin derivatives can have red shifted absorbance. Coumarins that photolyze effectively under visible light have drawn significant attention for biological applications. Examples of photolabile polymers incorporating photocleavable coumarin groups include photolabile hydrogels based on coumarin-containing cross-linkers, photodisruptable nanoparticles of polymers that incorporate coumarin groups along the backbones, photodisruptable micelles based on block copolymers containing coumarin pendant groups, and photosensitive polyelectrolyte multilayers [26, 42, 62-64]

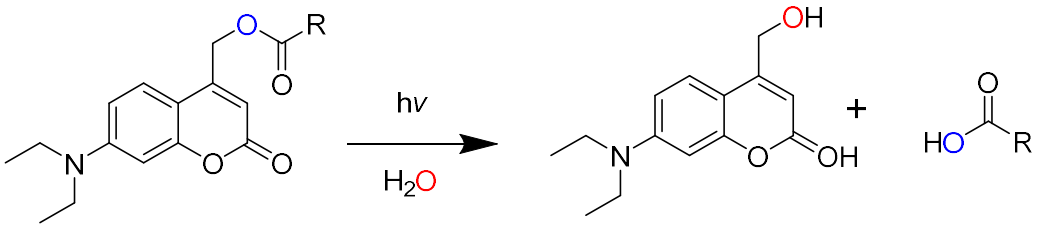

Scheme 1.4: Photocleavage of a coumarinyl ester.

1.3.3 Phenacyl groups

For the phenacyl class of photoprotecting groups, the leaving group is attached to the C_α position of the carbonyl group. Photolysis of α-substituted esters of phenacyl chromophore can liberate carboxylic acid groups. The deprotection mechanism of phenacyl moieties significantly depends on the modification on the phenacyl skeleton, the leaving group, and the reaction conditions (e.g., solvent).[13, 38]

Generally, phenacyl groups with no substitution on the phenacyl skeleton photolyze via a photoreduction mechanism that involves either (1) hydrogen abstraction from hydrogen atom donors by the excited phenacyl groups (**Scheme 1.5**, entry 1), or (2) reduction of the excited phenacyl groups via electron transfer in presence of good electron donors (**Scheme 1.5**, entry 2), followed by the liberation of the leaving group from the α-position.[13, 65] One the other hand, skeleton-substituted phenacyl protection groups, such as *p*-hydroxyphenacyl groups (pHP) and *p*-methoxyphenacyl groups (pMP), typically react through different mechanisms. The pHP groups were reported to undergo a skeletal rearrangement (a photo-Favorskii rearrangement) to release the leaving group (**Scheme 1.5**, entry 3).[13, 66] For the photoreaction of pMP

compounds, the photo-Favorskii rearrangement mechanism (**Scheme 1.5**, entry 4) competes with photoreduction pathways.[13, 67, 68]

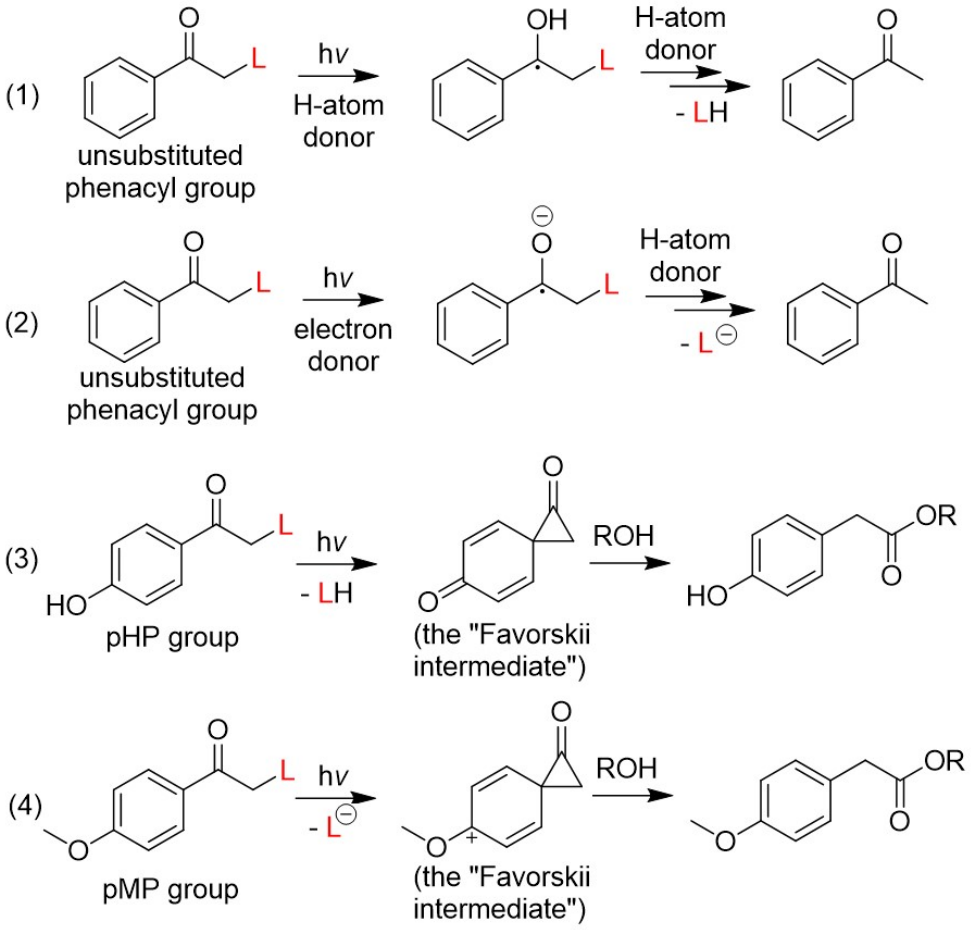

Scheme 1.5: Photochemistry of phenacyl groups that release a leaving group (L). (1) and (2): photolysis of unsubstituted phenacyl groups via photoreduction mechanisms; (3): photolysis of *p*-hydroxyphenacyl (pHP) groups via a photo-Favorskii rearrangement mechanism; (4) a photo-Favorskii rearrangement path of the photolysis of *p*-methoxyphenacyl (pMP) groups.

1.4 Selective Photocleavage

A variety of photocleavable groups, including the above mentioned ONB groups, coumarin groups and phenacyl groups, have been developed to enable efficient and predictable photochemical reactions useful in organic synthesis and chemical biology.[13-15] An interesting feature of photocleavable groups is that they can be selectively excited: one photocleavable group may be cleaved in presence of other photoreactive groups that do not react under the same condition. Such feature makes photocleavable groups promising for applications including sequential delivery of therapeutics[50, 69, 70] and functional surface patterning. [71, 72] To develop photoresponsive groups that can be selectively photocleaved, it is important to control the photochemical reaction rates of these groups. This rate can be controlled via two conceptually different approaches: i) controlling the chromophore absorbance, and ii) controlling the photolysis quantum efficiency.

1.4.1 Wavelength Selectivity of Photocleavable Groups

Photocleavable groups that absorb different wavelengths of light allow wavelength-selective photocleavage for various applications. For example, Conway and coworkers [70] described wavelength-orthogonal photolysis of neurotransimitters in vitro using a combination of 4-methoxyphenacyl caging group and 4,5-dimethoxy-2-nitrobenzyl caging group; del Campo *et al* and other groups [71, 72] studied wavelength selective cleavage of surface immobilized photoclevable groups; Thomas and coworkers [62] demonstrated wavelength-selective disruption and triggered release with photolabile polyelectrolyte multilayers comprising two compartments that photodegrade sequentially, first using visible light to photolyze diethylaminocoumarin groups, followed by using ultraviolet light to cleave NBE groups.

1.4.2 Quantum Efficiency Selectivity of Photoclevable Groups

Selective photolysis of different photocleavable groups with similar absorbance can be enabled by tuning their quantum yields. Bochet and coworkers [73, 74] reported selective photocleavage of ONB groups using monochromatic light; photosensitivities of these ONB groups were altered by fine-tuning their quantum yields through kinetic isotope effect without altering their absorbance: the deuterated ONB compounds react slower than the nondeuterated. Thomas and coworkers [48] reported a series of conjugated polymers with side chains containing structurally different ONB groups; polymers incorporating different ONB derivatives photodegraded with different rates upon exposure to UV light at 365 nm. Although all ONB groups reported in this work had similar light absorbance at 365 nm (i.e., similar molar extinction coefficient), the different quantum yields of the structurally varied ONB groups result in different rate of photolysis under the same irradiation condition.

1.5 Conclusions

Understanding of structure-property relationships and advancements in synthetic strategies of stimuli-responsive polymers enable development of functional materials for a variety of applications including sensors, drug delivery, surface modification, and others.[1, 2] Of particular interest is photoresponsive polymers incorporating photolabile groups, as light offers real-time spatiotemporal control of the material properties without the need of added reagent. In this thesis, we describe the use of stimuli-responsive groups, especially photocleavable groups, to control covalent bonds and non-covalent intermolecular interactions in polymer materials ranging from soft materials to solid-state polymer films to polyelectrolyte

colloids. These materials provide new approaches to photomodulate material properties including electrostatic properties, mechanical properties, and solubilities, and are promising for applications such as drug delivery and photolithographic pattering.

1.6 References

1. Stuart, M.A.C., et al., *Emerging applications of stimuli-responsive polymer materials.* Nature Materials, 2010. **9**(2): p. 101-113.
2. Theato, P., et al., *Stimuli responsive materials.* Chemical Society Reviews, 2013. **42**(17): p. 7055-7056.
3. Roy, D., W.L.A. Brooks, and B.S. Sumerlin, *New directions in thermoresponsive polymers.* Chemical Society Reviews, 2013. **42**(17): p. 7214-7243.
4. Jochum, F.D. and P. Theato, *Temperature- and light-responsive smart polymer materials.* Chemical Society Reviews, 2013. **42**(17): p. 7468-7483.
5. Thomas, S.W., *New Applications of Photolabile Nitrobenzyl Groups in Polymers.* Macromolecular Chemistry and Physics, 2012. **213**(23): p. 2443-2449.
6. Davis, D.A., et al., *Force-induced activation of covalent bonds in mechanoresponsive polymeric materials.* Nature, 2009. **459**(7243): p. 68-72.
7. Fu, J., Q. Wang, and J.B. Schlenoff, *Extruded Superparamagnetic Saloplastic Polyelectrolyte Nanocomposites.* ACS Applied Materials & Interfaces, 2015. **7**(1): p. 895-901.
8. Huo, M., et al., *Redox-responsive polymers for drug delivery: from molecular design to applications.* Polymer Chemistry, 2014. **5**(5): p. 1519-1528.
9. Kocak, G., C. Tuncer, and V. Butun, *pH-Responsive polymers.* Polymer Chemistry, 2017. **8**(1): p. 144-176.
10. Hu, J., G. Zhang, and S. Liu, *Enzyme-responsive polymeric assemblies, nanoparticles and hydrogels.* Chemical Society Reviews, 2012. **41**(18): p. 5933-5949.
11. Lu, W., et al., *Application of new photolabile protecting groups as photocleavable joints of block copolymers.* Chemical Communications, 2013. **49**(83): p. 9636-9638.
12. Bochet, C.G., *Photolabile protecting groups and linkers.* Journal of the Chemical Society, Perkin Transactions 1, 2002(2): p. 125-142.
13. Klán, P., et al., *Photoremovable Protecting Groups in Chemistry and Biology: Reaction Mechanisms and Efficacy.* Chemical Reviews, 2013. **113**(1): p. 119-191.
14. Hansen, M.J., et al., *Wavelength-selective cleavage of photoprotecting groups: strategies and applications in dynamic systems.* Chemical Society Reviews, 2015. **44**(11): p. 3358-3377.
15. Yu, H., et al., *Chemistry and biological applications of photo-labile organic molecules.* Chemical Society Reviews, 2010. **39**(2): p. 464-473.
16. Friedle, S. and S.W. Thomas, *Controlling Contact Electrification with Photochromic Polymers.* Angewandte Chemie International Edition, 2010. **49**(43): p. 7968-7971.
17. Fumio, T., et al., *Photochromic Rewritable Memory Media: A New Nondestructive Readout Method.* Japanese Journal of Applied Physics, 1993. **32**(9R): p. 3987.
18. Ercole, F., T.P. Davis, and R.A. Evans, *Photo-responsive systems and biomaterials: photochromic polymers, light-triggered self-assembly, surface modification, fluorescence modulation and beyond.* Polymer Chemistry, 2010. **1**(1): p. 37-54.
19. Jensen, J., et al., *Direct Photopatterning of Electrochromic Polymers.* Advanced Functional Materials, 2013. **23**(30): p. 3728-3737.
20. Tucker-Schwartz, A.K., R.A. Farrell, and R.L. Garrell, *Thiol–ene Click Reaction as a General Route to Functional Trialkoxysilanes for Surface Coating Applications.* Journal of the American Chemical Society, 2011. **133**(29): p. 11026-11029.
21. Lowe, A.B., et al., *Combining Ring-Opening Metathesis Polymerization and Thiol-Ene Coupling Chemistries: Facile Access to Novel Functional Linear and Nonlinear Macromolecules.* Macromolecular Rapid Communications, 2014. **35**(4): p. 391-404.

22. Davis, A.R. and K.R. Carter, *Controlling Optoelectronic Behavior in Poly(fluorene) Networks Using Thiol–Ene Photo-Click Chemistry.* Macromolecules, 2015. **48**(6): p. 1711-1722.
23. Manhart, J., et al., *Design and application of photo-reversible elastomer networks by using the [4πs+4πs] cycloaddition reaction of pendant anthracene groups.* Polymer, 2016. **102**: p. 10-20.
24. Katayama, H., et al., *Stereocontrolled Synthesis and Optical Properties of All-cis Poly(phenylene vinylenes) (PPVs): A Method for Direct Patterning of PPVs.* Journal of the American Chemical Society, 2005. **127**(12): p. 4350-4353.
25. Li, L., *A Review of: "Smart Light-Responsive Materials—Azobenzene-Containing Polymers and Liquid Crystals, edited by Yue Zhao and Tomiki Ikeda".* Molecular Crystals and Liquid Crystals, 2010. **518**(1): p. 172-172.
26. Zhao, Y., *Light-Responsive Block Copolymer Micelles.* Macromolecules, 2012. **45**(9): p. 3647-3657.
27. Kloxin, A.M., M.W. Tibbitt, and K.S. Anseth, *Synthesis of Photodegradable Hydrogels as Dynamically Tunable Cell Culture Platforms.* Nature Protocols, 2010. **5**: p. 1867-1887.
28. Kloxin, A.M., et al., *Photodegradable Hydrogels for Dynamic Tuning of Physical and Chemical Properties.* Science, 2009. **324**: p. 59.
29. Thomas, S.W., et al., *Patterns of electrostatic charge and discharge in contact electrification.* Angewandte Chemie-International Edition, 2008. **47**(35): p. 6654-6656.
30. Nie, Z.H. and E. Kumacheva, *Patterning surfaces with functional polymers.* Nature Materials, 2008. **7**(4): p. 277-290.
31. DeFranco, J., et al., *Photolithographic Patterning of Organic Electronic Materials*, in *Functional Supramolecular Architectures*. 2011, WILEY-VCH Verlag & Co. KGaA. p. 399-420.
32. Olejniczak, J., et al., *Highest Efficiency Two-Photon Degradable Copolymer for Remote Controlled Release.* ACS Macro Letters, 2013. **2**(8): p. 683-687.
33. Yoshii, T., M. Ikeda, and I. Hamachi, *Two-Photon-Responsive Supramolecular Hydrogel for Controlling Materials Motion in Micrometer Space.* Angewandte Chemie, 2014. **126**(28): p. 7392-7395.
34. Rodrigues-Correia, A., et al., *Selective Uncaging of DNA through Reaction Rate Selectivity.* Organic Letters, 2014. **16**: p. 5128--5131.
35. Rodrigues-Correia, A., X.M.M. Weyel, and A. Heckel, *Four Levels of Wavelength-Selective Uncaging for Oligonucleotides.* Orgainc Letters, 2013. **15**: p. 5500-5503.
36. Klán, P., et al., *Photoremovable Protecting Groups in Chemistry and Biology: Reaction Mechanisms and Efficacy.* Chemical Reviews, 2013. **113**: p. 119-191.
37. Yu, H., et al., *Chemistry and Biological Applications of Photo-Labile Organic Molecules.* Chemical Society Reviews, 2010. **39**: p. 464-473.
38. Wang, P., *Photolabile Protecting Groups: Structure and Reactivity.* Asian Journal of Organic Chemistry, 2013. **2**(6): p. 452-464.
39. Bochet, C.G., *Photolabile Protecting Groups and Linkers.* Journal of the Chemical Society, Perkin Transactions. 1, 2002: p. 125.
40. Bertrand, O. and J.-F. Gohy, *Photo-responsive polymers: synthesis and applications.* Polymer Chemistry, 2017. **8**(1): p. 52-73.
41. Kloxin, A.M., et al., *Photodegradable Hydrogels for Dynamic Tuning of Physical and Chemical Properties.* Science, 2009. **324**(5923): p. 59-63.
42. Chamsaz, E.A., et al., *Photoresponsive polyesters by incorporation of alkoxyphenacyl or coumarin chromophores along the backbone.* Photochemical & Photobiological Sciences, 2014. **13**(2): p. 412-421.

43. Mo, B., et al., *Facile synthesis of photolabile dendritic-unit-bridged hyperbranched graft copolymers for stimuli-triggered topological transition and controlled release of Nile red.* Polymer Chemistry, 2015. **6**(18): p. 3489-3501.
44. Gohy, J.-F. and Y. Zhao, *Photo-responsive block copolymer micelles: design and behavior.* Chemical Society Reviews, 2013. **42**(17): p. 7117-7129.
45. Barltrop, J.A., P.J. Plant, and P. Schofield, *Photosensitive protective groups.* Chemical Communications (London), 1966(22): p. 822-823.
46. Wieboldt, R., et al., *Photolabile precursors of glutamate: synthesis, photochemical properties, and activation of glutamate receptors on a microsecond time scale.* Proceedings of the National Academy of Sciences, 1994. **91**(19): p. 8752-8756.
47. Holmes, C.P., *Model Studies for New o-Nitrobenzyl Photolabile Linkers: Substituent Effects on the Rates of Photochemical Cleavage.* The Journal of Organic Chemistry, 1997. **62**(8): p. 2370-2380.
48. Smith, Z.C., et al., *Thiophene-Based Conjugated Polymers with Photolabile Solubilizing Side Chains.* Macromolecules, 2015. **48**(4): p. 959-966.
49. Aujard, I., et al., *o-Nitrobenzyl Photolabile Protecting Groups with Red-Shifted Absorption: Syntheses and Uncaging Cross-Sections for One- and Two-Photon Excitation.* Chemistry – A European Journal, 2006. **12**(26): p. 6865-6879.
50. Griffin, D.R. and A.M. Kasko, *Photodegradable Macromers and Hydrogels for Live Cell Encapsulation and Release.* Journal of the American Chemical Society, 2012. **134**(31): p. 13103-13107.
51. Bochet, C.G., *Wavelength-selective cleavage of photolabile protecting groups.* Tetrahedron Letters, 2000. **41**(33): p. 6341-6346.
52. Solomek, T., et al., *Photolysis of ortho-nitrobenzylic derivatives: the importance of the leaving group.* Photochemical & Photobiological Sciences, 2012. **11**(3): p. 548-555.
53. Wang, P., *Photolabile Protecting Groups: Structure and Reactivity.* Asian Journal of Organic Chemistry, 2013. **2**: p. 452-464.
54. Thomas, S.W., *New Applications of Photolabile Nitrobenzyl Groups in Polymers.* Macromolecular Chemistry and Physics, 2012. **213**: p. 2443-2449.
55. Yang, F., Z. Cao, and G. Wang, *Micellar assembly of a photo- and temperature-responsive amphiphilic block copolymer for controlled release.* Polymer Chemistry, 2015. **6**(46): p. 7995-8002.
56. Guo, L., et al., *Design, synthesis, and photosensitive performance of polymethacrylate-positive photoresist-bearing o-nitrobenzyl group.* Journal of Applied Polymer Science, 2015. **132**(13): p. n/a-n/a.
57. Smith, Z.C., et al., *Thiophene-Based Conjugated Polymers with Photolabile Solubilizing Side Chains.* Macromolecules, 2015. **48**: p. 959.
58. Kalva, N., N. Parekh, and A.V. Ambade, *Controlled micellar disassembly of photo- and pH-cleavable linear-dendritic block copolymers.* Polymer Chemistry, 2015. **6**(38): p. 6826-6835.
59. Zhao, H., et al., *o-Nitrobenzyl Alcohol Derivatives: Opportunities in Polymer and Materials Science.* Macromolecules, 2012. **45**(4): p. 1723-1736.
60. Kang, C., R. Crockett, and N.D. Spencer, *The influence of surface grafting on the growth rate of polymer chains.* Polymer Chemistry, 2016. **7**(2): p. 302-309.
61. Schade, B., et al., *Deactivation Behavior and Excited-State Properties of (Coumarin-4-yl)methyl Derivatives. 1. Photocleavage of (7-Methoxycoumarin-4-yl)methyl-Caged Acids with Fluorescence Enhancement.* The Journal of Organic Chemistry, 1999. **64**(25): p. 9109-9117.
62. Gumbley, P., et al., *Wavelength-Selective Disruption and Triggered Release with Photolabile Polyelectrolyte Multilayers.* Chemistry of Materials, 2014. **26**: p. 1450-1456.

63. Babin, J., et al., *A New Two-Photon-Sensitive Block Copolymer Nanocarrier.* Angewandte Chemie International Edition, 2009. **48**(18): p. 3329-3332.
64. Han, D., X. Tong, and Y. Zhao, *Fast Photodegradable Block Copolymer Micelles for Burst Release.* Macromolecules, 2011. **44**(3): p. 437-439.
65. Literák, J., A. Dostálová, and P. Klán, *Chain Mechanism in the Photocleavage of Phenacyl and Pyridacyl Esters in the Presence of Hydrogen Donors.* The Journal of Organic Chemistry, 2006. **71**(2): p. 713-723.
66. Zhang, K., et al., *Mechanism of Photosolvolytic Rearrangement of p-Hydroxyphenacyl Esters: Evidence for Excited-State Intramolecular Proton Transfer as the Primary Photochemical Step.* Journal of the American Chemical Society, 1999. **121**(24): p. 5625-5632.
67. Givens, R.S., et al., *Photochemistry of phosphate esters: .alpha.-keto phosphates as a photoprotecting group for caged phosphate.* Journal of the American Chemical Society, 1993. **115**(14): p. 6001-6012.
68. Sheehan, J.C. and K. Umezawa, *Phenacyl photosensitive blocking groups.* The Journal of Organic Chemistry, 1973. **38**(21): p. 3771-3774.
69. Griffin, D.R. and A.M. Kasko, *Photoselective Delivery of Model Therapeutics from Hydrogels.* ACS Macro Letters, 2012. **1**(11): p. 1330-1334.
70. Stanton-Humphreys, M.N., et al., *Wavelength-orthogonal photolysis of neurotransmittersin vitro.* Chemical Communications, 2012. **48**(5): p. 657-659.
71. del Campo, A., et al., *Surface Modification with Orthogonal Photosensitive Silanes for Sequential Chemical Lithography and Site-Selective Particle Deposition.* Angewandte Chemie International Edition, 2005. **44**(30): p. 4707-4712.
72. San Miguel, V., C.G. Bochet, and A. del Campo, *Wavelength-Selective Caged Surfaces: How Many Functional Levels Are Possible?* Journal of the American Chemical Society, 2011. **133**(14): p. 5380-5388.
73. Blanc, A. and C.G. Bochet, *Isotope Effects in Photochemistry: Application to Chromatic Orthogonality.* Organic Letters, 2007. **9**(14): p. 2649-2651.
74. Blanc, A. and C.G. Bochet, *Isotope Effects in Photochemistry. 1. o-Nitrobenzyl Alcohol Derivatives.* Journal of the American Chemical Society, 2004. **126**(23): p. 7174-7175.

Chapter 2:

Photochemical Control of Covalent Bonds in Polymer Gels

Reproduced in part with permission from:
Hu, X.; Shi, J.; Thomas, S. W., Photolabile ROMP gels using ortho-nitrobenzyl functionalized crosslinkers. *Polym Chem-Uk* **2015**, *6*, 4966-4971.
Copyright 2015 Royal Society of Chemistry.
Gumbley, P.; Hu, X.; Lawrence, J. A.; Thomas, S. W., Photoresponsive Gels Prepared by Ring-Opening Metathesis Polymerization. *Macromolecular Rapid Communications* **2013**, *34*, 1838-1843.
Copyright 2013 John Wiley and Sons, Inc.

2.1 Introduction

2.1.1 Photodegradable Polymer Gels

Polymer gels are three-dimensionally cross-linked networks of polymers. They are an important class of soft materials which have both solid- and liquid like properties. Physical gels are interconnected via noncovalent linkages, while chemical gels are covalently crosslinked. Gels have been used in numerous applications, including food, cosmetics, medicine, electronics, tissue engineering, and many others.[1-3]

Incorporation of stimuli-responsive groups into the structures of gels can yield materials that change properties upon exposure to a specific stimulus. Such stimuli-responsive gels are a promising material platform for a number of applications.[3] Stimuli-responsive groups, especially stimuli-cleavable groups, can be incorporated in the covalent crosslinkers; polymer networks held by such crosslinkers degrade upon specific stimulus. For example, various acid-sensitive groups (such as acetal groups,[4, 5] imine groups[6] and boronate ester groups[7, 8]) have been incorporated into covalent crosslinkers used to prepare acid-degradable gels; the acidic conditions present in tumor tissues, endosomes or lysosomes can trigger the degradation of these gels, making such gels promising for applications including targeted delivery and tissue engineering.[9, 10] Degradable crosslinkers based on enzyme cleavable groups (e.g., ester groups[10] and phosphate groups[11, 12]), redox cleavable groups (e.g., disulfide groups [13]) and photolyzable groups (such as nitrobenzyl groups[14-17] and coumarin groups[18-20]) have also been developed.

On the other hand, stimuli-responsive groups may also be incorporated into the gel scaffolds. Examples of this class of stimuli-responsive gels include thermal responsive hydrogels

with poly(N-isopropylacryamide) (PNIPAm) scaffolds [21] and pH responsive hydrogels based on amino-functionalized polymers.[22] Recently, stimuli-responsive physical gels crosslinked via supramolecular interactions have also attracted increasing attention.

Using light to control gel degradation has a number of advantages, such as the ability to pattern gels spatiotemporally, the tunable nature of the energy and intensity of light, and the permeability of light through a variety of materials. ONB groups are the most commonly used photolabile moieties in photocleavable crosslinkers.[23, 24] Anseth's group carried out a seminal work exploring photomodulation of the physical and chemical properties of hydrogels:[25] incorporation of photocleavable ONB groups in crosslinker structures allowed to photo-manipulate crosslink densities in hydrogels and therefore to photocontrol the physical properties of hydrogels, while introduction of ONB groups into the pendants enabled to modify the functionalities of hydrogel scaffolds on-demand; such photodegradable gels provide a cell culture platform that allows real-time manipulation of the cell microenvironment, and demonstrates promise as cell culture platforms in which cell-material interactions can be dynamically and remotely controlled.

2.1.2 Ring Opening Metathesis Polymerization (ROMP)

Various polymerization methods have been exploited for the fabrication of polymer gels, including free radical polymerization,[25] atom transfer radical polymerization (ATRP),[26] reversible addition-fragmentation chain-transfer polymerization (RAFT),[27] and step-growth polymerizations.[28] Ring opening metathesis polymerization (ROMP) is a class of controlled chain-growth living polymerization that, depending on the monomer and initiator used, can result

in the favorable polymerization kinetics. Other advantages ROMP can have include high functional group tolerance and mild polymerization conditions.

ROMPs proceed via an olefin metathesis mechanism (**Figure 2.1**); the driving force for ROMP is the relief of ring strain: first, the monomer double bond complexes with the metal catalyst center and forms a four-membered ring; cycloreversion then results in the catalyst being transferred to the "opened" chain; repeated addition of monomer units results in the propagation of the polymer chain. Termination occurs upon chain transfer between the propagating chain end and an added olefin (e.g., ethyl vinyl ether, a traditional terminating agent).[29]

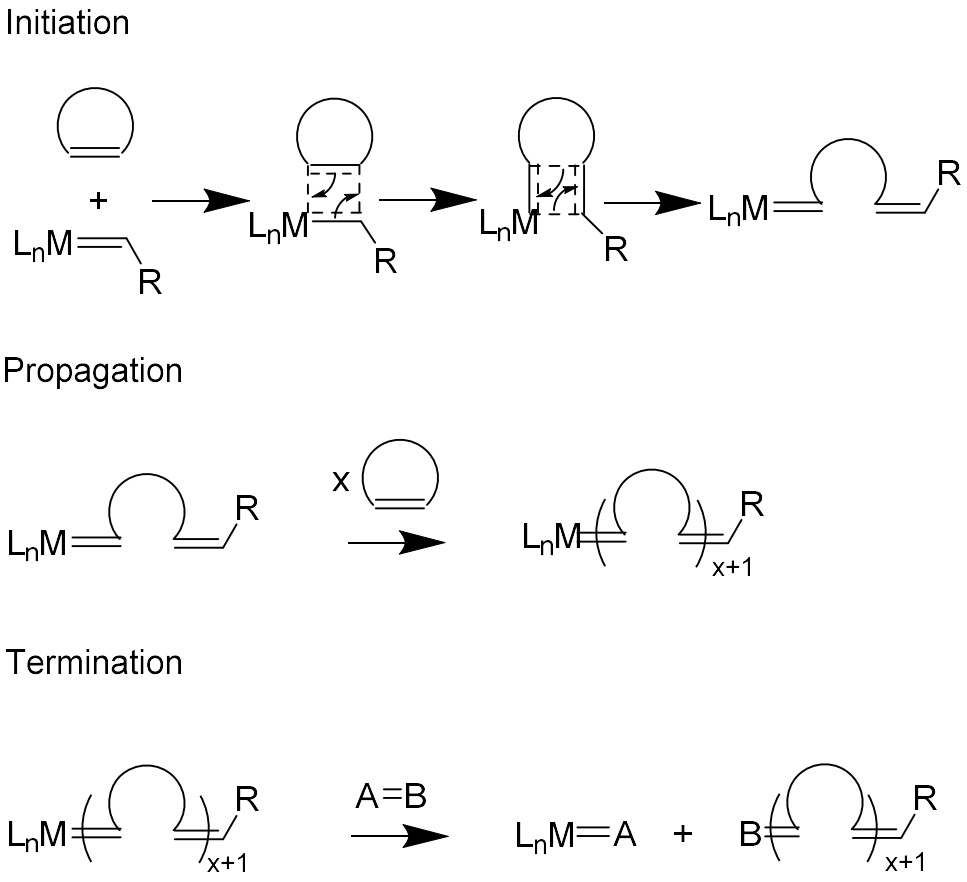

Figure 2.1: General Mechanism of ROMP.

Transition metals useful for ROMP catalysis include tungsten, molybdenum, tantalum, and ruthenium. Commercially available Grubbs ruthenium catalysts (**Figure 2.2**) are among the most well studied metal carbene catalysts for ROMP.[30-34] The Grubbs catalysts have high tolerance to a variety of functional groups such as amide, ester, hydroxyl and nitro groups.[34-36] Incompatibility of ROMP with nitriles, amines and carboxyl groups has been reported, as these groups can coordinate to the ruthenium centers.[37-40] However, with sophisticated molecular design, researchers have successfully polymerized norbornene derivatives containing these functional groups. For example, Sutthasupa *et al* [37, 38] polymerized carboxyl and amine containing monomer via ROMP by introducing a proper spacer to prevent the amines or carboxyl groups from interacting with the metal centers coordinated at the double bond in the metathesis intermediates.

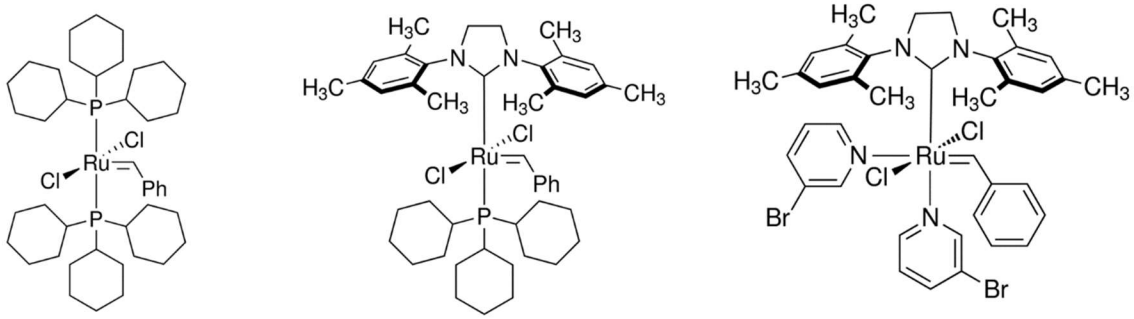

Figure 2.2: Structures of Grubbs Catalysts. *Left*: Grubbs Catalyst 1st Generation; *middle*: Grubbs Catalyst 2nd Generation; *right*: Grubbs Catalyst 3rd Generation.

Despite the advantages of ROMP as a powerful and feasible tool of living polymerization, there are limited amount of studies exploring application of ROMP in the preparation of polymer gels. This chapter describes the use of ROMP for the construction of photoreactive gels

incorporating structurally different ONB groups, each of which has distinct photosensitivity. Inclusion of photocleavable groups in the bis(norbornene) crosslinkers enables photochemical control of the covalent crosslinking density in, and therefore of swelling, viscoelastic properties, solubility of the gels, and allows to photo-control the release of trapped cargo from these gels.

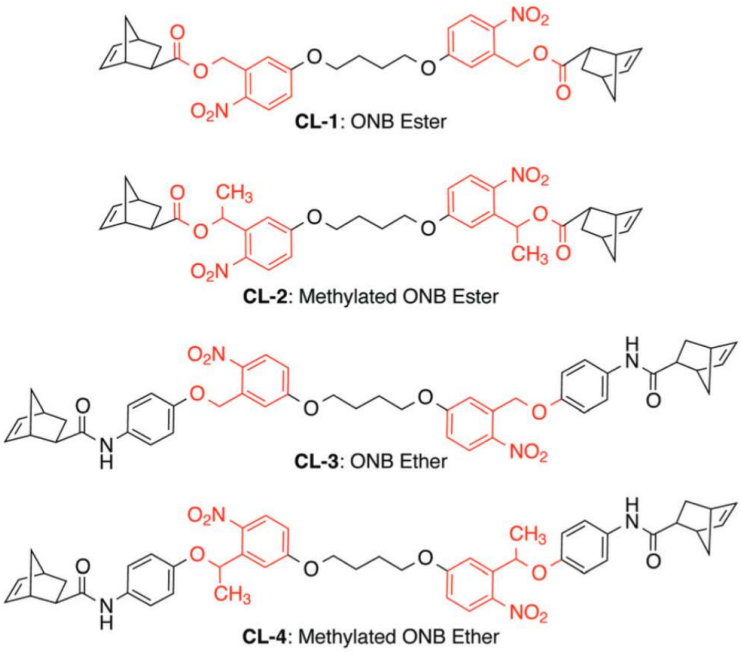

Figure 2.3: Structures of photolabile ROMP crosslinkers with different photosensitivities. The different photosensitive ONB moieties are highlighted in red.

2.2 Experimental Design and Synthesis of ONB functionalized Crosslinkers

Covalent polymer networks generally require a cross-linking molecule that contains two or more monomer moieties for holding individual polymer chains together. We designed and synthesized four ONB-containing bis(norbornene) crosslinkers in this study (**Figure 2.3**), each of which has different photosensitivity because of the structural variations highlighted in red color.

Upon copolymerization of a hydrophilic or hydrophobic monomer with such cross-linkers, an insoluble network of crosslinked polymer chains (i.e., a hydrogel or an organogel, respectively) can be generated (**Figure 2.4**). These gels can photodegrade and become soluble upon the photolysis of ONB containing crosslinkers.

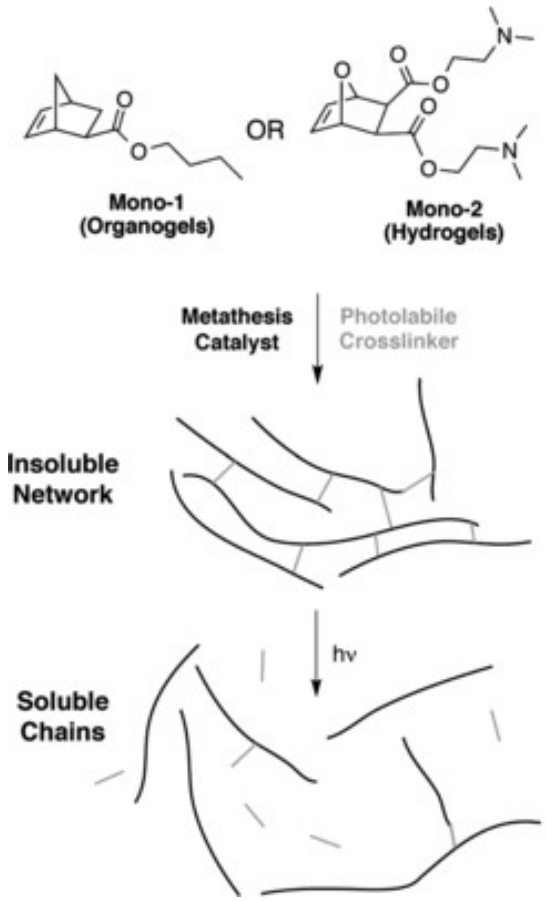

Figure 2.4: Structures of **Mono-1** and **Mono-2**, and the general design for ROMP gels that dissolve upon photocleavage of crosslinkers.

The key differences between these crosslinker molecules are the structures of the ONB units, which are either: ONB esters (**CL-1**), ONB esters methylated in the benzylic positions (**CL-2**), ONB ethers (**CL-3**), or ONB ethers methylated in the benzylic positions (**CL-4**). Both

methylation and substitution of electron donating ethers on the benzylic positions are designed to stabilize the benzylic radical intermediate of the first step of ONB photolysis (**Figure 2.5**). Our expectation in this study was that either of these two modifications would increase the photoinduced sensitivity of the resulting gels, and that combining these modifications (as in **CL-4**) would lead to gels with the fastest response to UV light. Photochemically controlled cleavage of such crosslinkers incorporated in the gels allows for real-time remote control of the crosslinking density in the gels, and therefore of the swelling, modulus, and solubility of these gels. We designed such symmetrical bis(norbornene)-crosslinker structures to ensure equivalent reactivity of the two polymerizable termini of the cross-linkers and increase the number of photolabile groups that could yield photocleavage of the photolabile covalent linkage. **Mono-1** and **Mono-2**, a hydrophobic butyl ester and a hydrophilic amino-functionalized monomer, respectively, were used to prepare organogels and hydrogels.

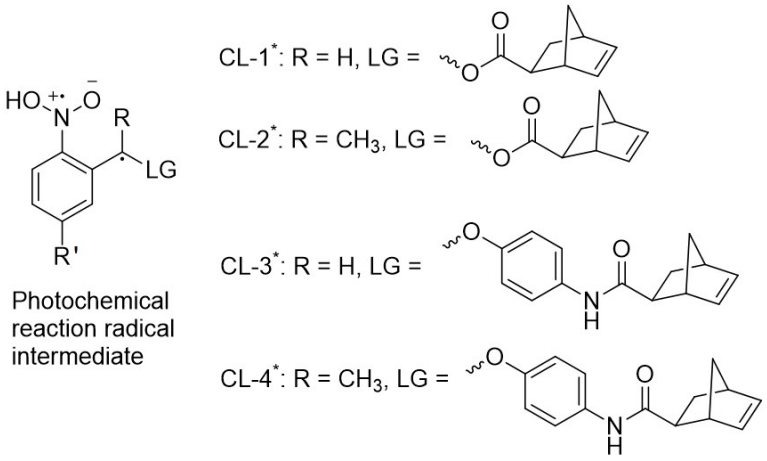

Figure 2.5: Structures of the radical intermediates of the photolysis of photolabile crosslinkers.

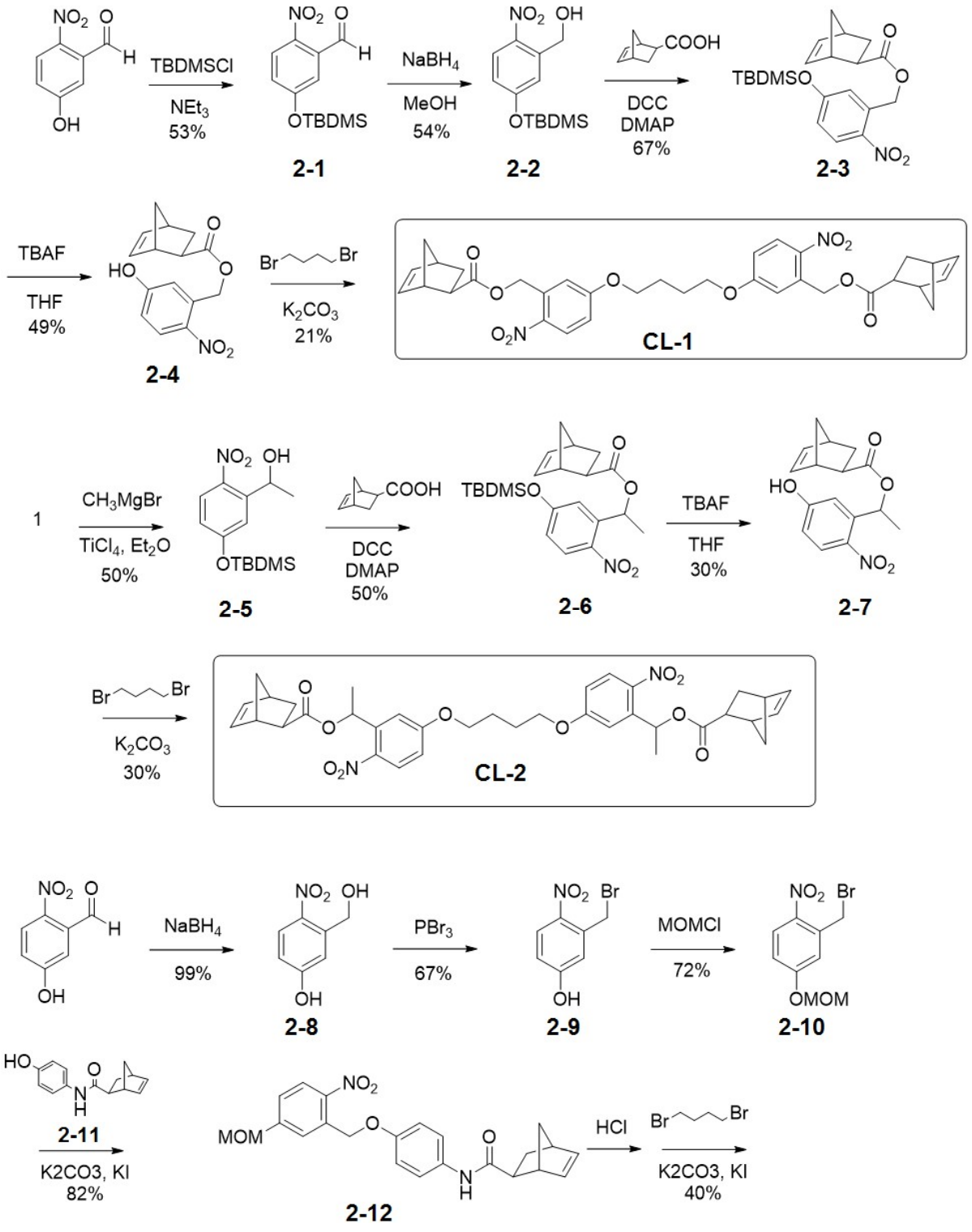
TBDMSCl
NEt3
53%
NaBH4
MeOH
54%
DCC
DMAP
67%
2-1
2-2
2-3
TBAF
THF
49%
2-4
K2CO3
21%
CL-1
1
CH3MgBr
TiCl4, Et2O
50%
2-5
DCC
DMAP
50%
2-6
TBAF
THF
30%
2-7
K2CO3
30%
CL-2
NaBH4
99%
PBr3
67%
MOMCl
72%
2-8
2-9
2-10
2-11
K2CO3, KI
82%
HCl
K2CO3, KI
40%
2-12

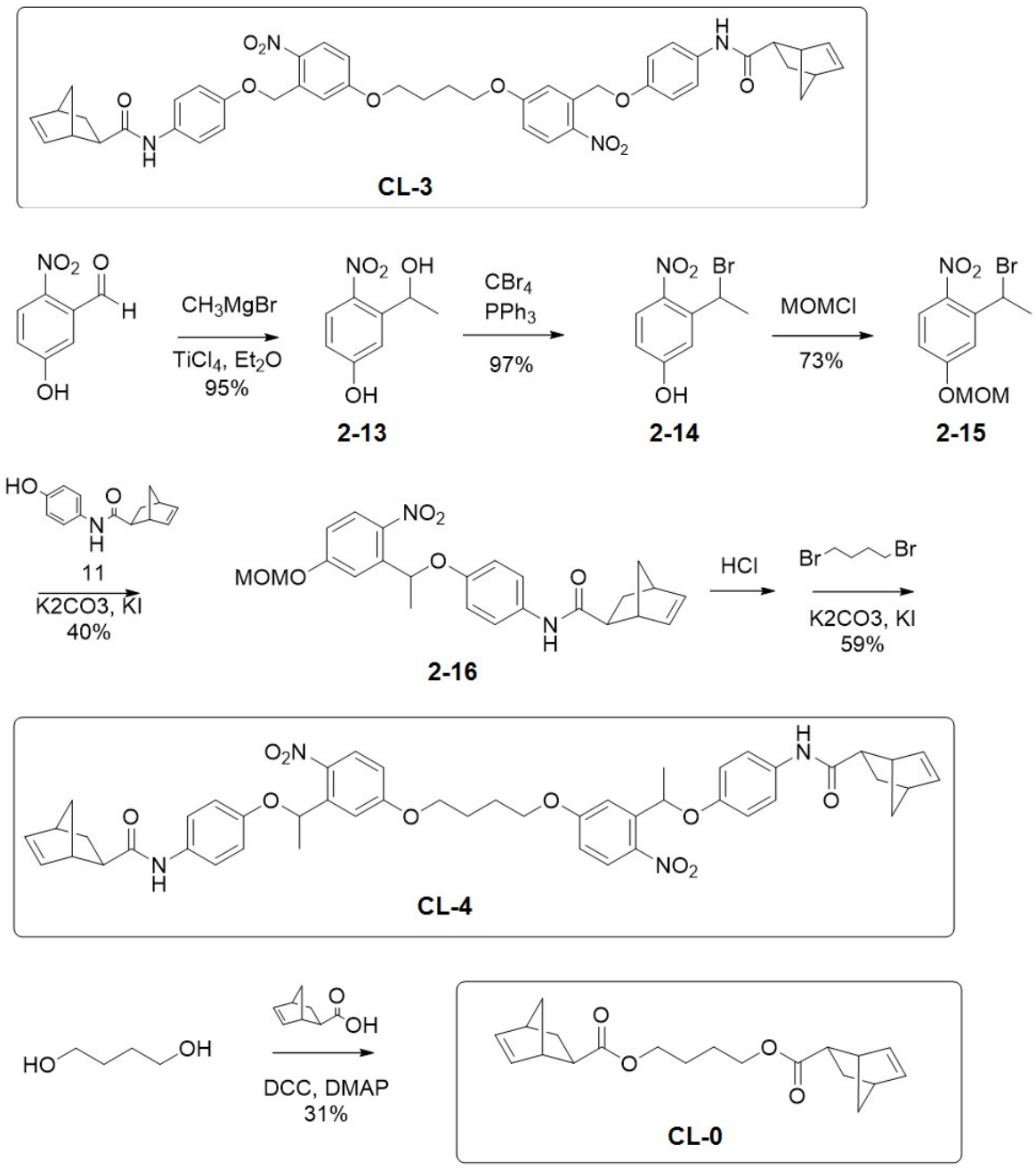

Scheme 2.1: Synthesis of ROMP crosslinkers **CL-0**, **CL-1**, **CL-2**, **CL-3** and **CL-4**.

The synthesis of monomers and crosslinkers is described in detail in our publications on this work. [41, 42] Protection of the phenol of 5-hydroxy-2-nitrobenzaldehyde with tert-

butyldimethylsilyl chloride (TBDMSCl) yielded silyl ether **2-1**, which sodium borohydride reduced to give nitrobenzyl alcohol **2-2**. We then acylated alcohol **2-2**with commercially available exo-5-norbornenecarboxylic acid using dicyclohexylcarbodiimide (DCC) activation to give nitrobenzyl ester **2-3**; esters derived from the *exo* diastereomer present less steric hindrance during ROMP than esters derived from the *endo* isomer. [36, 43] Finally, fluoride-mediated deprotection of the silyl ether and alkylation of the resulting phenol **2-4** with 1,4-dibromobutane in the presence of potassium carbonate gave crosslinker **CL-1**. Synthesis of crosslinker **CL-2** proceeded in an analogous fashion, beginning with the preparation of **2-5** using a methyltitanium nucleophile, followed by esterification of the benzylic alcohol and double alkylation of 1,4-dibromobutane with phenol following deprotection with TBAF.

Preparations of ONB ether crosslinkers **CL-3** and **CL-4** followed similar paths, with reduction of 5-hydroxy-2-nitrobenzaldehyde with either $NaBH_4$ or $CH_3MgBr/TiCl_4$ followed by bromination to yield the corresponding primary or secondary bromides **2-9** and **2-13**. Protection of the phenols with chloromethyl methyl ether (MOMCl) followed by substitution of the bromides with the phenol-functionalized norbornene **2-11** [42] yielded compounds **2-12** and **2-16**. MOM deprotection followed by alkylation with 1,4-dibromobutane yielded the target ONB ether crosslinkers **CL-3** and **CL-4** (**Scheme 2.1**).

Preparation of photoinert cross-linker **CL-0** required only the double acylation of 1,4-butanediol with exo-5-norbornenecarboxylic acid. The UV/vis absorbance spectra of all photolabile crosslinkers in tetrahydrofuran showed absorbance maxima at approximately 300 nm with molar extinction coefficients of $\sim 2\times10^4\ M^{-1}cm^{-1}$, with absorbance confined to the ultraviolet region of the spectrum (**Figure 2.6**).

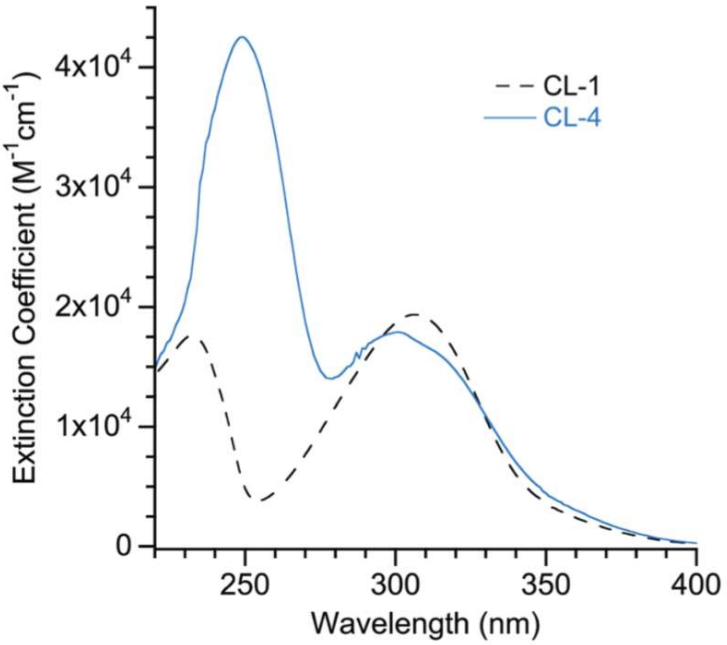

Figure 2.6: UV-vis absorbance spectra of crosslinkers **CL-1** and **CL-4** dissolved in THF.

Hydrophobic monomer **Mono-1** and hydrophilic monomer **Mono-2** were synthesized as reported elsewhere.[40] We also prepared nitrobenzoxadiasole (NBD) labeled fluorescent monomers **Mono-3** and **NBDMA**. Acylation of previously reported[44] nitrobenzoxadiasole alcohol with commercially available exo-5-norbornenecarboxylic acid or methyl methacrylate acid using dicyclohexylcarbodiimide (DCC) activation produced monomer **Mono-3** or **NBDMA**. Copolymerization of **Mono-3** into the gel matrix allowed us to monitor the photo-induced dissolution of the gel scaffolds using fluorescence spectroscopy. **NBDMA** was copolymerized with a hydrophilic monomer poly (ethylene glycol) methyl ether methacrylate via free radical polymerization to yield a water soluble, fluorescently (NBD-) labeled macromolecule **PEGNBD**, which was used as a florescent guest molecule physically trapped in the photolabile gels (see Chapter 2.5).

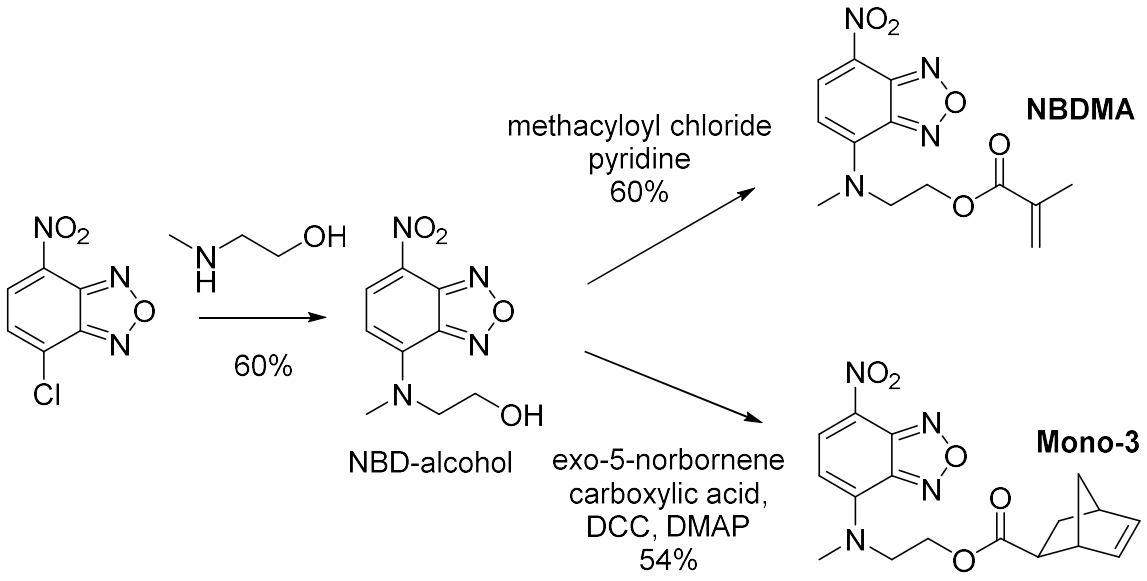

Scheme 2.2: Synthesis of fluorescently labeled monomers **NBDMA** and **Mono-3**.

2.3 Preparation of ONB Functionalized ROMP Gels

All the organogels reported herein, regardless of crosslinker structure, were prepared using the same procedure (**Scheme 2.3**): (1) dissolution of 40 mg of ROMP monomer **Mono-1** and 0.5 mg fluorescent ROMP monomer **Mono-3** containing the nitrobenzofurazan (NBD) dye, together with the crosslinker of interest (**CL1**–**CL4**), into 0.2 mL DMF, (2) dissolution of the Grubbs 2nd generation ruthenium carbene catalyst into 0.2 mL CH_2Cl_2, and (3) mixing the two solutions together. The final concentrations of monomer (0.51 M) and catalyst (0.007 M) in the mixed solutions were the same in all polymerizations. Under these conditions, all four of the crosslinkers yielded gels within 30 s. To study the effect of the gel composition on the properties of the photoresponsive gels (*vide infra*), we prepared gels with molar ratios of crosslinker: catalyst of 1.3 and 1.5. We purified all gels using Soxhlet extraction with dichloromethane for two days to remove soluble polymer chains and monomers. As expected, gels prepared from

crosslinker **CL-4** had a > 50% higher storage modulus (45 Pa) when the ratio of crosslinker : catalyst molar ratio was 1.5 than gels prepared with a ratio of 1.3 (27 Pa). We determined that the somewhat different structures of the ether and ester-based crosslinkers did not affect the ratio of crosslinker to monomer incorporated into the gels: the yield of dry xerogel for organogels prepared with **CL-2** and **CL-4** were the same, within experimental error (89–91%), and ^{1}H NMR analysis of the soluble fractions isolated from Soxhlet extraction showed no evidence of either of the crosslinkers. Further evidence for similar crosslink densities for organogels prepared with either ONB-ether and ONB-ester crosslinkers is that their gravimetric swelling ratios in benzene solutions—22 ± 1 for gel prepared with **CL-2**, 20±2 for gel prepared with **CL-4** at crosslinker : catalyst ratio of 1.3—were not distinguishable within experimental error.

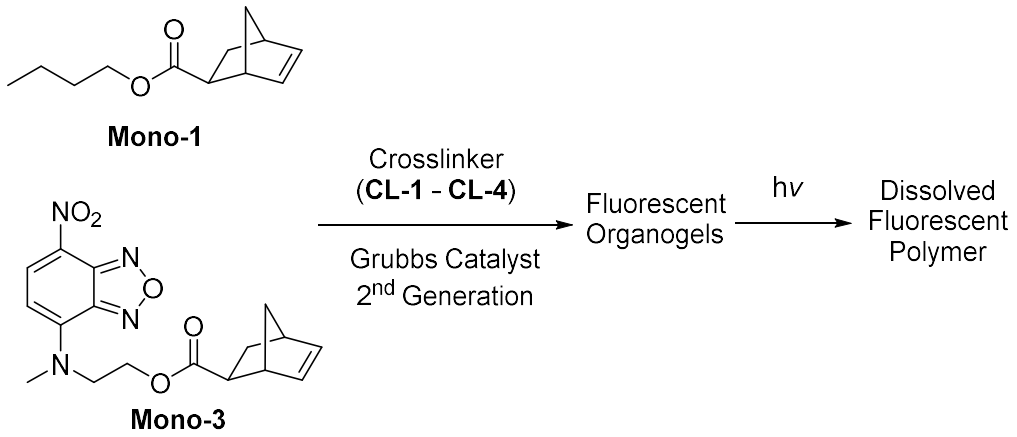

Scheme 2.3: Overall design of photoresponsive gels prepared using **CL-1** – **CL-4**. Fluorescent monomer **Mono-3** was used in the gels at a loading of 1.4 mole percent relative to **Mono-1**.

2.4 Photodegradation of ONB Functionalized ROMP Organogels

We used several approaches to characterize how the structure of the crosslinker and the crosslinker : catalyst ratio affects the sensitivities of gels to UV light; as a function of irradiation

time, we visually monitored of the presence of the organogels in benzene solution and tracked the release of a fluorescent dye covalently attached to a norbornene monomer (**Mono-3**) that was incorporated into the gels. In these experiments, we irradiated gels with a 200 W Hg/Xe lamp equipped with a BG40 bandpass filter to induce the degradation of gels. The power density incident on samples in these experiments was 25 mW cm^{-2}. We also measured the viscoelastic properties of several gels as a function of irradiation time with a portable UV lamp emitting at 365 nm with power density incident on samples of 9 mW cm^{-2}. In all examples, leaving gels in the dark in parallel with our irradiation experiments did not result in any significant degradation as determined by any of our three approaches.

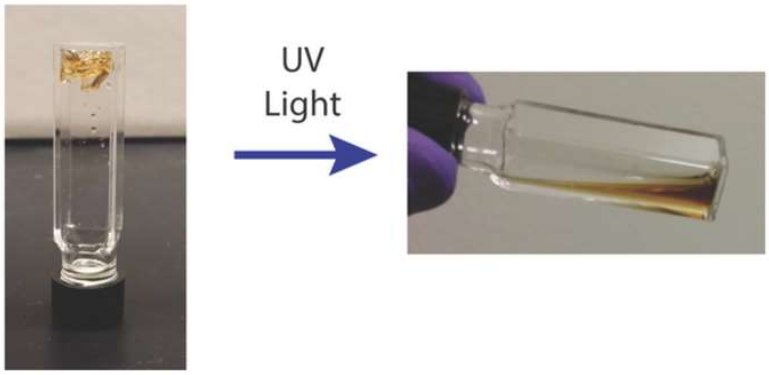

Figure 2.7: Optical photographs of an organogel swollen in benzene (before irradiation, *left*) and of the dissolved product after photodegradation (*right*).

2.4.1 Visual Observation of Gel Dissolution

This approach, in which we note the time of irradiation required for the gel to no longer be visible to the naked eye in benzene, although imprecise, is a quick, low-tech, and direct method for identifying large differences in photosensitivity between gels of different composition. We used this simple method in our initial communication [41] on this subject to

establish that gels prepared with **CL-2** are more reactive than gels prepared with **CL-1**. **Figure 2.8** summarizes the irradiation time required for dissolution of ~2 mg samples of ROMP organogels prepared with a 1.3 crosslinker : catalyst molar ratio with each of the four different ONB crosslinkers. The most reactive gels are those prepared with the methylated ether ONB crosslinker, **CL-4**, which combines the radical stabilizing features of a tertiary benzylic radical with an electron donating ether functional group, and dissolve in about 10 minutes.

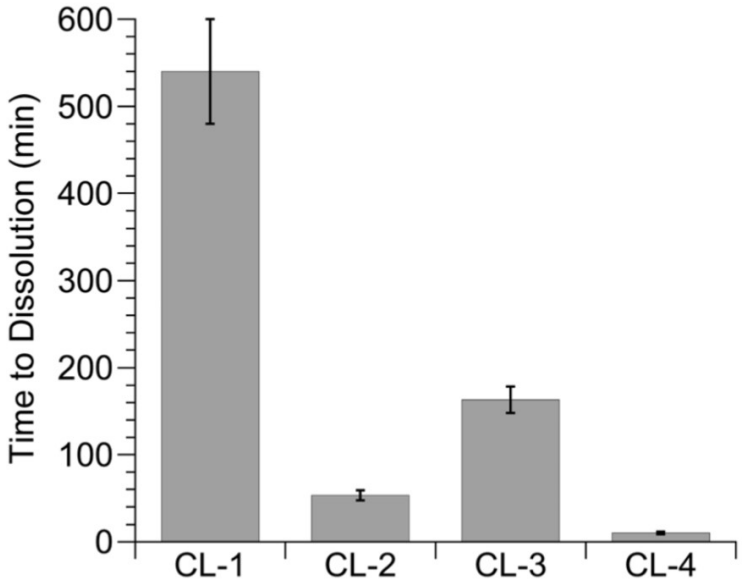

Figure 2.8: UV irradiation time required to dissolve 2 mg of organogels (prepared using a 1.3 molar ratio of crosslinker to catalyst as shown in Scheme **2.3**) in benzene. Error bars are the standard deviations of three measurements for each crosslinker.

2.4.2 Monitoring Dissolution of Fluorescent Polymer Chains

As a number of potential applications of photolabile gels focus on light causing the release of guests, we developed a simple method to follow the release of solubilized polymer chains released from the insoluble polymer network upon UV irradiation. This approach uses a small percentage of norbornene monomer (**Mono-3**) labeled with a fluorophore—NBD in this

case, see **scheme 2.3**—in the synthesis of gels. only upon breaking the ONB crosslinks with UV light can these fluorophores, as part of soluble polymer chain photoproducts, be released into solution. The fluorescence intensity of the NBD dye in the fluid solution as a function of irradiation time reflects the quantity of soluble polymer chains released by photolysis. In these experiments, we used approximately the same mass (2 mg) of dry xerogel swollen in 3 mL of benzene, and irradiated all gels under the conditions described above. The fluorescent side-chains, although they compete for absorbance of UV photons with the photocleavable ONB groups, the molar ratio of monomer **M1** in all polymerizations was the same, such that any differences in competitive absorbance between gels prepared with different crosslinkers are small.

Figure 2.9 summarizes the results of these experiments for gels prepared using a 1.3 crosslinker : catalyst ratio and the four different ONB-containing crosslinkers. In all experiments, the quantity of NBD present in solution before UV irradiation of the gels, as detected by fluorescence, was not distinguishable from background. Fluorescence from the NBD, however, increases with irradiation of the gel suspended in benzene at $\lambda > 320$ nm, consistent with UV-induced dissolution of the gel. In all cases, the intensity of fluorescence from the probe reaches a plateau at durations of irradiation generally consistent with the time required for dissolution of the gel as determined visually; to compare the reactivity of different gels, we set the average integrated fluorescence intensity of the last three data points, corresponding to this plateau in each experiment, to 1.0.

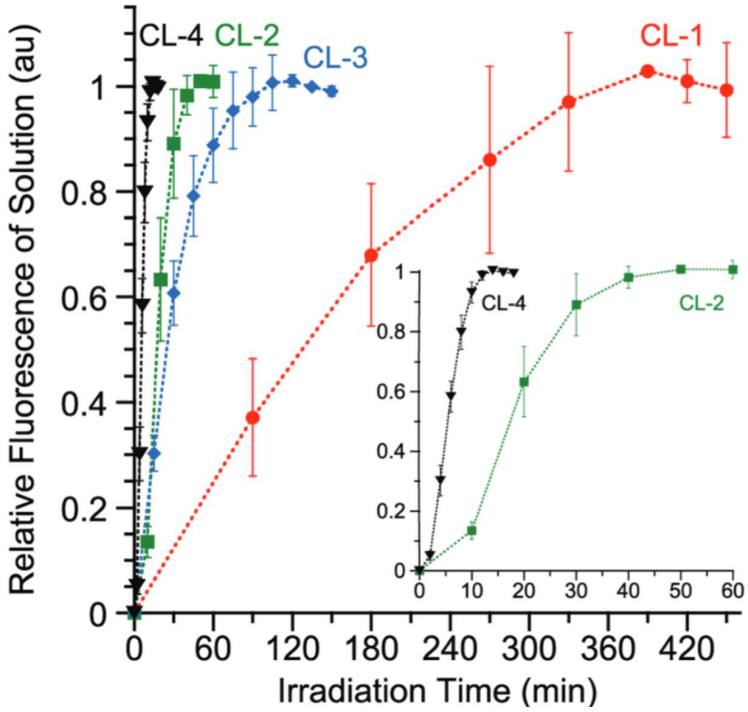

Figure 2.9: The dependence of fluorescence intensity of benzene-soluble portion of NBD-containing ROMP gels crosslinked with each of the ONB crosslinkers on duration of UV irradiation using a BG40 bandpass filter. In each experiment, we used 2 mg of dry xerogel. The wavelength of excitation for fluorescence spectroscopy was 465 nm, while the fluorescence intensities were determined by integrating between λ_{em} = 500 nm and λ_{em} = 550 nm. The data points are the average of three measurements of relative fluorescence intensity in separate irradiation experiments; the error bars represent standard deviations from these measurements.

The order of reactivity of the gels prepared with different crosslinkers, determined using fluorescence spectroscopy, was the same as determined by simple visual inspection: gels prepared with **CL-4**, the methylated ONB ether crosslinker, were most reactive, releasing all fluorophores into solution within 10 minutes, while gels with **CL-1**, the unmethylated ONB ester crosslinker, were the least reactive, taking up to 6 hours to reach a plateau of fluorescence

intensity of soluble fractions; even after this protracted time of irradiation, some quantity of **CL-1** gel still remained insoluble. As negative control experiments, identical samples of gels that were not exposed to UV light showed no fluorescent signal discernible from background. This ordering of reactivity is consistent with our initial hypothesis, as combining both (i) ether-for-ester substitution and (ii) increasing the number of alkyl groups on the benzylic position stabilize the benzylic radical intermediate, increasing the efficiency of photolysis more than either of these two substitutions in isolation.

2.4.3 The Effect of Crosslink Density on Gel Photoreactivity

To characterize the effect of crosslink density on the sensitivity of these gels to UV light, we compared the photoinduced dissolution of gels prepared with the most reactive crosslinker, **CL-4**, with crosslinker : catalyst molar ratios of 1.3 and 1.5. **Figure 2.10** shows the results of two experiments designed for this purpose, which in both cases conformed to our expectations that the gels with larger concentrations of crosslinkers take longer to dissolve than those with smaller concentrations. When we monitored the release of soluble NBD-labelled soluble polymer chains upon ONB photolysis using fluorescence spectroscopy, fluorescence of the solutions containing more highly crosslinked gels took 2–3 times longer to reach a plateau than the solutions containing less highly cross-linked gels (**Figure 2.10** *top*). As a complement to this approach, we also determined the storage moduli of gels with different concentrations of crosslinkers as a function of UV irradiation (**Figure 2.10** *bottom*). As expected, the gels with larger crosslink densities showed larger storage moduli and required more time of UV irradiation to approach storage moduli of zero than gels with smaller crosslink densities.

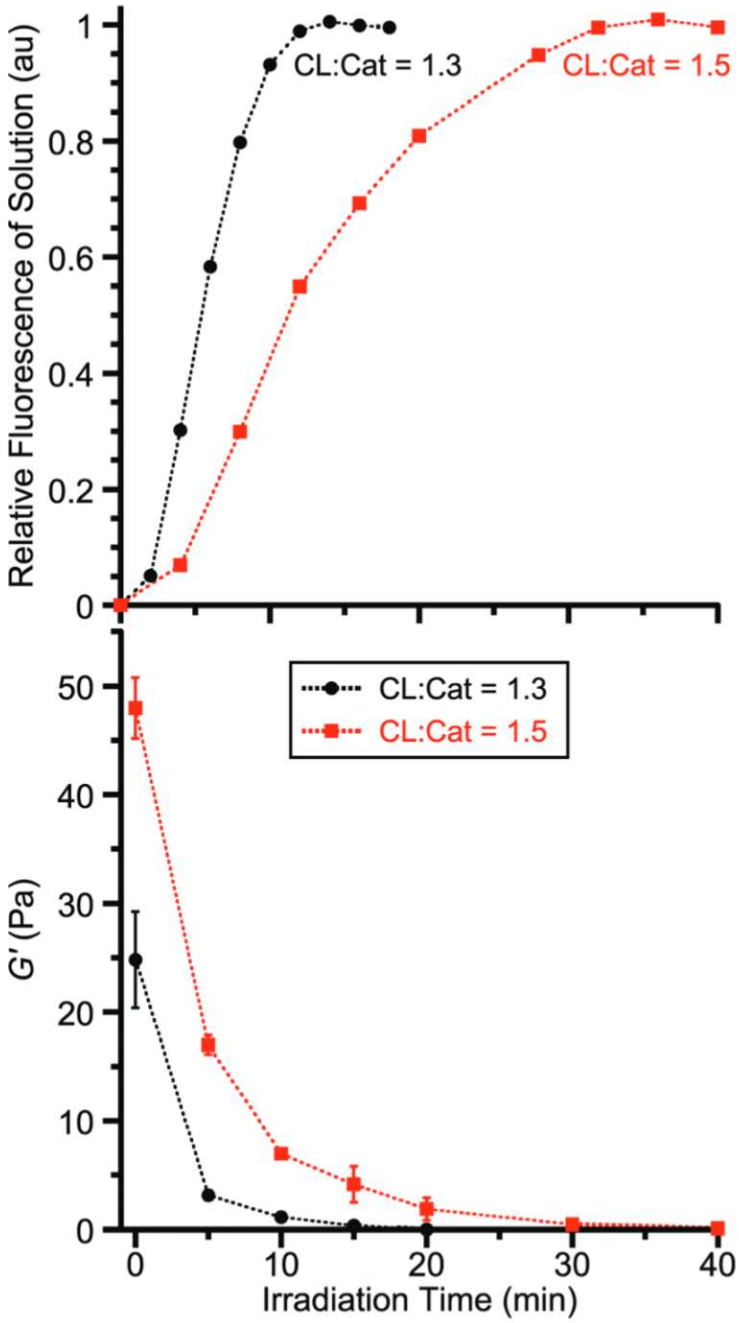

Figure 2.10: Dependence of dissolution of bound fluorescent polymers (*top*) and storage modulus (*bottom*) of gels on ratio of crosslinker (**CL-4**) to catalyst.

2.5 Photocontrolled Release from ONB Functionalized Hydrogels

To demonstrate the potential utility of these materials in aqueous environments, we also prepared photoresponsive ROMP hydrogels using a monomer previously reported by Tew and coworkers (**Mono-2**) (**Scheme 2.4**).[40] To prepare these gels, we used a procedure similar to the procedure for organogel preparation (*vide supra*). We first combined (i) hydrophilic monomer **Mono-2**, (ii) crosslinker **CL-4**, and (iii) a fluorescently-labeled random copolymer **PEGNB** of poly(ethylene glycol)methyl ether methacrylate and 7-nitro-2,1,3-benzoxadia-zole methacrylate (**NBDMA**) in dichloromethane, then to this solution added Grubbs 2nd generation ruthenium carbene catalyst to yield a crosslinker : catalyst molar ratio of 1.5. The gel that resulted after approximately 30 minutes was purified by Soxhlet extraction, resulting in a fluorescent hydrogel due to physically trapped polymer chains bearing NBD fluorophores as pendants. This hydrogel was photolabile, as photolysis with UV light using irradiation conditions identical to those used with the organogels (*vide supra*) in water resulted in the dissolution of the gel and release of the fluorescent polymeric guest (**Figure 2.11**)

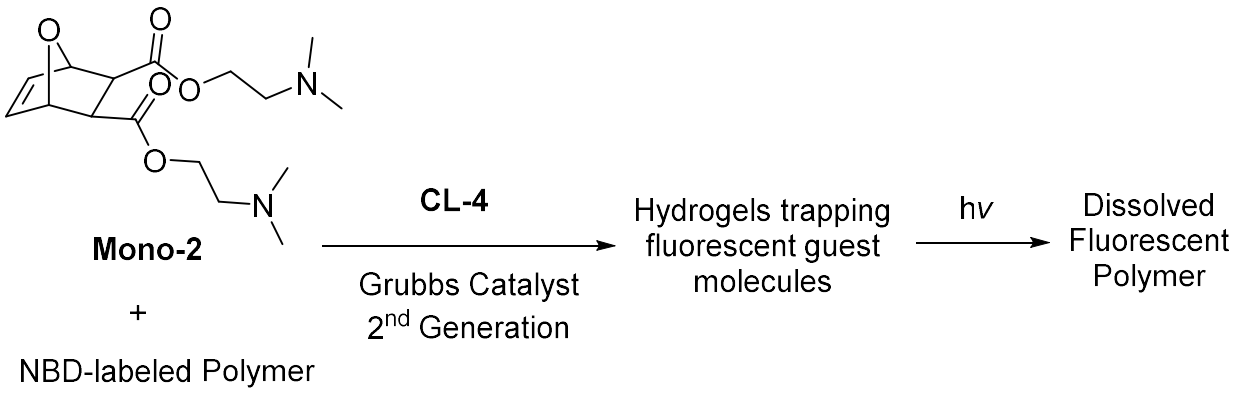

Scheme 2.4: Overall design of photoresponsive hydrogels prepared using hydrophilic monomer **Mono-2** and photolabile crosslinker **CL-4**. Fluorescent polymer **PEGNB** was physically trapped in the gels.

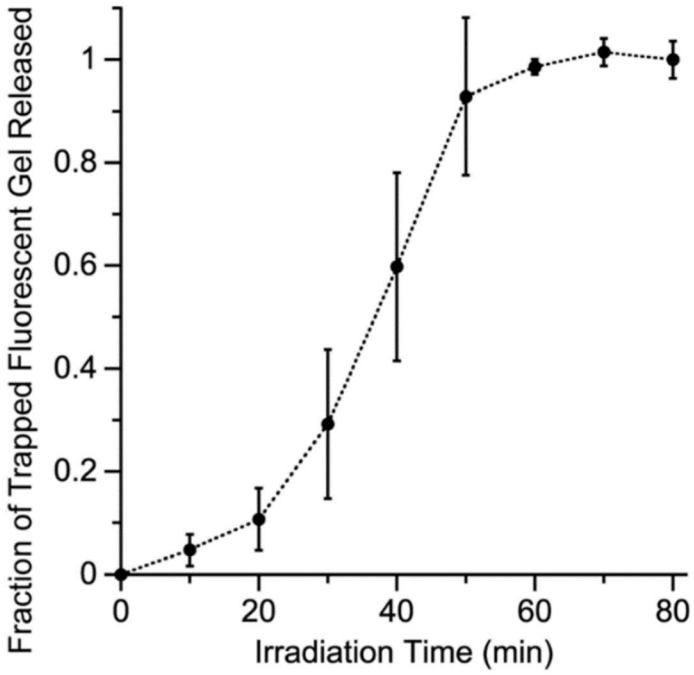

Figure 2.11: UV-induced release of fluorescent NBD-labeled methacrylic polymer **PEGNBD** from hydrogel prepared with hydrophilic monomer **Mono-2** and crosslinker **CL-4**.

2.6 Conclusions

This work combines the structurally tunable nature of the ONB photocleavable groups, the photolysis of which that can occur in many environments, with advantages of ROMP—simple protocols, fast polymerization rates, and high functional group tolerance—for the preparation of organogels and hydrogels that can photodegrade upon photochemical cleavage of covalent crosslinkers. Work described in this chapter also expands the repertoire of photolabile crosslinkers available for photoresponsive gels. The dependence of gel photosensitivity on crosslinker structure is consistent with the previously determined correlation of stability of the intermediate benzylic radical of the mechanism of nitrobenzyl group cleavage on the quantum yield of photolysis.[17, 45] Gels prepared with ONB methyl ether crosslinkers showed the fastest response of all samples investigated, highlighting the potential of this substitution pattern on

photocleavable groups in this and other platforms. Photolabile ROMP hydrogels also allow for light-induced release of physically trapped guests. Finally, our approach opens up the possibility of combining different photocleavable covalent crosslinkers in ROMP gels to achieve wavelength-selective photo-responsive properties.

2.7 Attempts to Develop Anthracene Functionalized Photolabile Hydrogels

One disadvantage of the ONB based photolabile gels is the need for UV light to induce gel decomposition, as opposed to more biologically compatible visible or near-infrared (NIR) light. By incorporating photocleavable moieties sensitive to longer wavelengths of light into crosslinker structure, we hoped to fabricate gels that could photodegrade upon exposure to visible or NIR light.

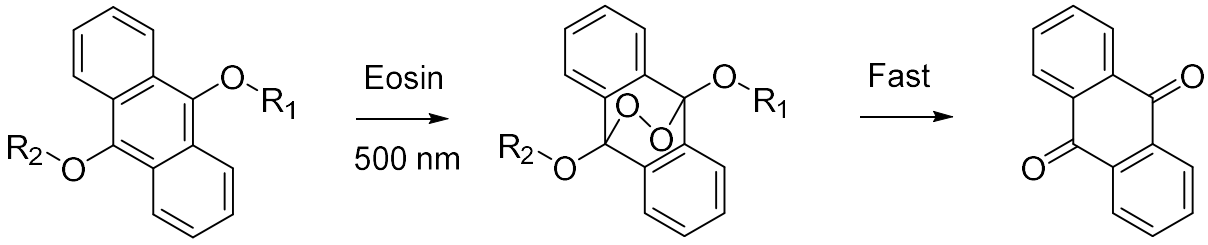

Scheme 2.5: Green light-induced cleavage of anthracene moiety in presence of a singlet oxygen sensitizer Eosin reported by Yuan *et al*.[46]

Yuan *et al* [46] reported the cleavage of anthracene moieties under visible light (540 nm): upon exposure to light, eosin sensitizer can transform triplet oxygen into singlet oxygen in solution, which further scissor two alkoxyl bonds of the dialkoxyanthracene as shown in **Scheme 2.5**. This work inspired us to design an analogous dialkoxyanthracene-containing, bis(methacrylate) crosslinker **CL-AC** as shown in **Scheme 2.6**. We acylated the previously

reported dialcohol compound 17 [46] with methacryloyl chloride using triethylamine (TEA) as the catalyst.

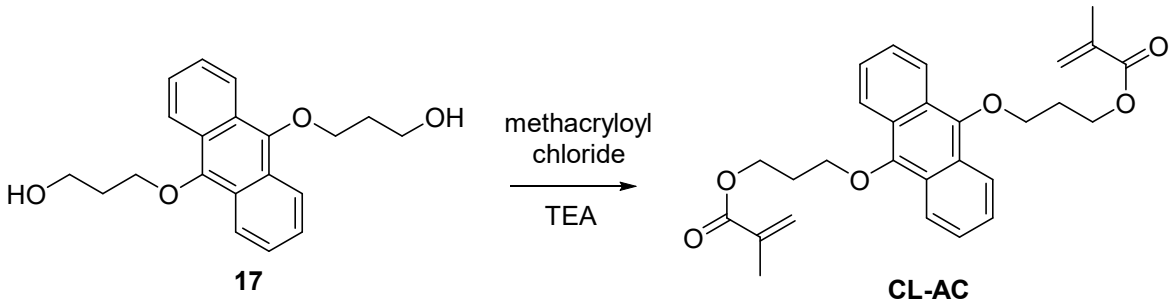

Scheme 2.6: Synthesis of dialkoxyanthracnen-containing crosslinker **CL-AC**.

To prepare **CL-AC** based hydrogel, 0.15 mg poly(ethylene glycol) methyl ether methacrylate (Mn ~ 300 g/mol) (~0.5 mmol), 0.5 mg AIBN (0.003 mmol), 3 mg **CL-AC** (0.0065 mmol) were dissolved in 0.65 mL toluene. After purging the mixture with Argon for 30 min, the reaction mixture was warmed to 65 ^{o}C overnight to yield a fluorescent gel (**Figure 2.12**). The gel obtained was purified using Soxhlet extraction with CH_2Cl_2 over one day and dried in vacuum. This gel can swell both in water and in organic solvents. A control polymerization of poly(ethylene glycol) methyl ether methacrylate performed in an analogous manner without adding the **CL-AC** crosslinker did not produce any insoluble gel, indicating that **CL-AC** crosslinker is necessary to held the gel network.

Figure 2.12: Photo of a fluorescent hydrogel prepared by free radical copolymerization of poly(ethylene glycol) methyl ether methacrylate monomer and **CL-AC** crosslink using AIBN as the initiator.

To test our hypothesis of triggered degradation of the **CL-AC** crosslinked hydrogel (*vide supra*) upon photoinduced generation of singlet oxygen, we irradiated a small piece of such gel (~ 1 mg) swollen in different solutions using red light ($\lambda > 600$ nm): either an aqueous solution of methylene blue (a singlet oxygen sensitizer), or a toluene solution of methylene blue, or a THF solution of methylene blue. In each experiment, the methylene blue concentration was adjusted to result in a sensitizer solution with OD = 0.1~0.2. Upon prolonged irradiation (up to 5 days), however, there was no visible change in the size or the shape of these gels.

2.8 Experimental Section

General Considerations

All synthetic manipulations were performed under standard air-free conditions under an atmosphere of argon gas with magnetic stirring unless otherwise mentioned. Flash chromatography was performed using silica gel (230-400 mesh) as the stationary phase. NMR spectra were acquired on a Bruker Avance III 500 or Bruker DPX-300 spectrometer. Chemical shifts are reported relative to residual protonated solvent (7.26 ppm for $CHCl_3$). All reactants and solvents were purchased from commercial suppliers and used without further purification, unless

otherwise noted. Dry THF, dry CH_2Cl_2, and dry diethyl ether were obtained from an Innovative Technologies PureSolv 400 solvent purifier.

All solution optical spectra were acquired of samples in quartz cuvettes (NSG Precision Cells). Electronic absorbance spectra were acquired with a Varian Cary-100 instrument in double-beam mode using a solvent-containing cuvette for background subtraction spectra. Fluorescence emission spectra were obtained by using either a PTI Quantum Master 4 equipped with a 75 W Xe lamp, or Cary Eclipse Fluorescence Spectrophotometer equipped with a Xe pulse lamp pulsed at 80 Hz, peak power equivalent to 75 kW. Rheological data was obtained on ARES G2 rheometer. Irradiation of gels for storage modulus measurements were performed with a blak-ray B-100A high intensity UV lamp (100 Watt, 365 nm, power density at sample = 9 mW/cm^2) at fixed positions in the light path.

Irradiations of gels in all other experiments were performed with a 200W Hg/Xe lamp (Newport-Oriel) equipped with a condensing lens, recirculating water filter, manual shutter, and FSQ-BG40 blue bandpass filter (Newport Corporation) at fixed positions in the light path. The power density at the sample was 25 mW/cm^2.

Synthetic Procedures

Compound **2-1**—compound **2-7, CL-1, CL-2, Mono-1** and **Mono-2** were synthesized according to our previously published study on photoreactive ROMP gels.[40] Detailed synthesis of these compounds have also been included in Patricia A. Gumbley's doctoral dissertation.

Compound **2-8**: To a 50 mL three neck round bottom flask was added $NaBH_4$ (0.23 g, 6.1 mmol) and methanol, stirred. A methanol solution of 2-nitro-5-hydroxybenzyldehyde (0.50 g, 3.0 mmol) was added dropwise into the flask at 0 °C. The reaction mixture was then allowed to

warm up to ambient temperature and stirred for 2 hours. The reaction was then poured into H_2O. The pH of the solution was adjusted to around 6 by 0.1 M HCl. The solution was then extracted with diethyl ether three times, dried over $MgSO_4$, filtered, and concentrated using a rotary evaporator to yield **2-8** as a light brown solid with no further purification. Yield: 0.50 g (99%). ^{1}H NMR (500 MHz, CD_3OD): 8.09 (d, J=9 Hz, 1 H), 7.26 (dd, J=1, 1.5 Hz, 1 H), 6.78 (dd, J=9, 3Hz, 1 H), 4.94 (s, 2 H).

Compound **2-13**: Dry diethyl ether (100 mL) was cooled to -78 °C in a 250 mL three neck flask. $TiCl_4$ (4.7 g, 0.025 mol) was added into the flask dropwise. The mixture was stirred at -78°C and yielded yellow precipitation. 3 M solution of MeMgBr in ether (8.3 mL, 0.025 mol) was added dropwise into the flask and the mixture turned to an orange color. The reaction was stirred for 30 minutes and the temperature of the mixture was allowed to slowly increase to around -30 °C. Then, 2-nitro-5-hydroxybenzyldehyde (1.7 g, 0.010 mol) was added into the flask very slowly. The reaction was stirred at around -30 ºC for 3 hours, and then poured into water, extracted with ethyl acetate three times, dried over $MgSO_4$, and concentrated using a rotary evaporator to yield **2-13** as a yellow solid with no further purification. Yield: 1.7 g (95%). ^{1}H NMR (500 MHz, CD_3OD): 7.95 (d, J=9 Hz, 1 H), 7.25 (d, J=3 Hz, 1 H), 6.76 (dd, J=2.5, 9 Hz, 1 H), 5.47 (q, J=6 Hz, 1 H), 1.44 (d, J=6 Hz, 3 H).

Compound **2-9**: To a 50 mL three neck round bottom flask was added **2-8** (0.26 g, 0.0015 mol) and 10 mL dry DMF. PBr_3 (1.0 g, 3.7 mmol) was added dropwise into the flask at -78 °C. The reaction was warmed to ambient temperature and stirred overnight. The reaction was poured into water, extracted by ethyl acetate 3 times, dried over Na_2SO_4 and concentrated using a rotary evaporator. The crude product was purified via flash chromatography using hexanes/ethyl acetate (1:1 v:v) as the eluent to yield **2-9** as a yellow solid. Yield: 0.24 g (67%). ^{1}H NMR (500 MHz,

$CDCl_3$): 8.10 (d, 9 Hz, 1 H), 7.00 (d, 2.5 Hz, 1 H), 6.87 (dd, J=2.5, 9 Hz, 1 H), 5.87 (s, 1 H), 4.84 (s, 2 H).

Compound **2-14**: A two neck flask was charged with **2-13** (0.33 g, 1.8 mmol), CBr_4 (1.0 g, 3.0 mol), PPh_3 (0.79 g, 3.0 mmol) and 25 mL dry THF. The reaction mixture was stirred overnight at ambient temperature. The reaction mixture was filtered, concentrated with a rotary evaporator and purified via flash chromatography using hexanes/ethyl acetate (1.5:1 v:v) as the eluent to yield **2-14** as a light brown solid. Yield: 0.43 g (97%). ^{1}H NMR (500 MHz, CD_3OD): 7.94 (d, 9 Hz, 1 H), 7.25 (d, J=3 Hz, 1 H), 6.83 (dd, J=2.5, 9 Hz, 1 H), 5.46 (q, J=6.5 Hz, 1 H), 1.43 (d, 6.5 Hz, 3 H).

Compound **2-10**: To a stirred mixture of **2-9** (1.0 g, 4.3 mmol) in 50 mL CH_2Cl_2 were added MOMCl (5 equiv) at 0 °C, then i-Pr_2NEt (3.0 equiv) was added. The reaction was stirred overnight at ambient temperature. After slow addition of satured NH_4Cl at 0 °C, the mixture was extracted with CH_2Cl_2 3 times. The combined organic layer was washed with brine, dried over Na_2SO_4, filtered, and concentrated in vacuo. The crude product was purified by flash column chromatography using hexanes/ethyl acetate (2.5:1 v:v) to afford **2-10** as a light yellow solid. Yield: 1.0 g (84%). ^{1}H NMR (500 MHz, $CDCl_3$): 8.14 (d, J=9.5 Hz, 1 H), 7.32 (d, J=3 Hz, 1 H), 7.09 (dd, J=2.5, 9 Hz, 1 H), 5.27 (s, 2 H), 5.01 (s, 2 H), 3.48-3.50 (m, 3 H).

Compound **2-15**: To a stirred mixture of **2-14** (0.43 g, 1.8 mmol) in 20 mL CH_2Cl_2 were added MOMCl (5 equiv) at 0 °C, then i-Pr_2NEt (3 equiv) was added. The reaction was stirred overnight at ambient temperature. After slow addition of satured NH_4Cl at 0 °C, the mixture was extracted with CH_2Cl_2 3 times. The combined organic layer was washed with brine, dried over Na_2SO_4, filtered, and concentrated in vacuo. The crude product was purified by flash column chromatography using hexanes/ethyl acetate (5:2 v:v) to afford **2-15** as a light yellow solid.

Yield: 0.37 g (73%). ^{1}H NMR (500 MHz, $CDCl_3$): 7.97 (d, J=9 Hz, 1 H), 7.49 (d, J=2.5 Hz, 1 H), 7.05 (dd, J=2.5, 9 Hz, 1 H), 5.88 (q, J=6.5 Hz, 1 H), 5.24-5.30 (m, 2 H), 3.50 (s, 3 H), 1.88 (d, J=6.5, 3 H).

Compound **2-11**: Exo-5-norbornenecaboxylic (1.4 g, 0.010 mol), 4-aminophenol (1.3 g, 0.012 mol), DMAP (0.20 g, 0.0016 mol) and 100 mL dry THF were added into a 250 mL three neck round bottom flask. DCC (2.5 g, 0.012 mol) in dry THF was added dropwise into the flask at 0 °C. The mixture was stirred overnight at ambient temperature. The reaction mixture was then concentrated *in vacuo* and redissolved in ethyl acetate, washed by HCl solution (pH around 3), brine, and water. The organic phase was dried over Na_2SO_4, filtered, concentrated with a rotary evaporator, and the crude product was further purified via flash chromatography using hexanes/ethyl acetate (2:1) as the eluent. Pink solid obtained was recrystallized from CH_2Cl_2. After filtration **2-11** was obtained as white crystals. Yield: 0.62 g (27%). ^{1}H NMR (500 MHz, CD_3OD): 7.31 (q, J=2.5, 7 Hz, 2 H), 6.72 (q, J=2.5, 7 Hz, 2 H), 6.18-6.19 (m, 2 H), 2.95 (d, J=1.5 Hz, 1 H), 2.92 (s, 1 H), 2.25-2.29 (m, 1 H), 1.93-1.97 (m, 1 H), 1.76 (d, J=8.5 Hz, 1 H), 1.33-1.39 (m, 2 H).

Compound **2-12**: A 25 mL three neck round bottom flask was charged with **2-10** (0.14 g, 0.51 mmol), **2-11** (0.12 g, 0.52 mmol), K_2CO_3 (0.14 g, 1.0 mmol), KI (0.016 g, 0.10 mmol) and 2 mL dry DMF. The reaction was stirred at 40 °C overnight, diluted with brine, and extracted with CH_2Cl_2 3 times. The combined organic phase was washed with water, dried over Na_2SO_4, filtered and concentrated *in vacuo*. The crude product was purified by flash chromatography using hexanes/ethyl acetate (2:1 v:v) as the eluent to yield **2-12** as a yellow solid. Yield: 0.18 g (82%). ^{1}H NMR (500 MHz, $CDCl_3$): 8.23 (d, J=9 Hz, 1 H), 7.51 (d, J= 3 Hz, 1 H), 7.46 (q, J= 2, 7 Hz, 2 H), 7.11 (s, 1 H), 7.07 (q, J= 2.5, 9 Hz, 1 H), 6.97 (q, J=2.5, 7 Hz, 2 H), 6.15-6.19 (m, 2

H), 5.48 (s, 2 H), 5.25 (s, 2 H), 3.48 (s, 3 H), 3.05 (s, 1 H), 2.97 (s, 1 H), 2.11-2.17 (m, 1 H), 2.00-2.06 (m, 1 H), 1.78 (d, J=8.5 Hz, 1 H), 1.38-1.43 (m, 2 H).

Compound **2-16**: A 25 mL three neck round bottom flask was charged with **2-15** (0.11 g, 0.38 mmol), **2-11** (0.070 g, 0.31 mmol), K_2CO_3 (0.083 g, 0.60 mmol), KI (0.010 g, 0.060 mmol) and 2 mL dry DMF. The reaction was stirred at 40 °C overnight, diluted with brine, and extracted with CH_2Cl_2 3 times. The combined organic phase was washed with water, dried over Na_2SO_4, filtered, and concentrated *in vacuo*. The crude product was purified by flash chromatography using hexanes/ethyl acetate (2:1 v:v) as the eluent to yield **2-16** as a yellow solid. Yield: 0.068 g (82%). ^{1}H NMR (300 MHz, $CDCl_3$): 8.08 (d, J=9 Hz, 1 H), 7.33 (d, J=2.7 Hz, 2 H), 7.30 (s, 1 H), 7.20 (s, 1 H), 6.99 (dd, J=2.7, 9 Hz, 1 H), 6.74 (dd, J=2.1, 6.9 Hz, 2 H), 6.12-6.16 (m, 1 H), 6.05-6.12 (m, 2H), 5.16 (s, 2H), 3.43 (s, 3 H), 2.98 (s, 1 H), 2.92 (s, 1 H), 2.06-2.12 (m, 1 H), 1.93-2.03 (m, 1 H), 1.73 (d, J= 8.1 Hz, 1 H), 1.67 (d, J=6.3 Hz, 3 H), 1.30-1.40 (m, 2 H).

CL-3: To a stirred solution of **2-12** (0.77 g, 1.8 mmol) in 12 mL THF was added 2 mL concentrated HCl. The reaction was kept at ambient temperature overnight, diluted with brine, extracted with ethyl acetate 3 times, dried over Na_2SO_4, filtered and concentrated *in vacuo*. The crude product was purified via flash chromatography using hexanes/ethyl acetate (5:2 v:v) to yield **PreCL-3** as a yellow solid. Yield: 0.67 g (97%). ^{1}H NMR (500 MHz, CD_3OD): 8.16 (d, J=18 Hz, 1 H), 7.43-7.48 (m, 2 H), 7.22 (d, J=5, 1 H), 6.93-6.98 (m, 2 H), 6.83 (dd, J=5, 18 Hz, 1 H), 6.18-6.20 (m, 2 H), 5.45 (s, 1 H), 2.90-2.97 (m, 2 H), 2.25-2.31 (m, 1 H), 1.92-1.99 (m, 1 H), 1.76 (d, J=16 Hz, 1 H), 1.31-1.40 (m, 2 H). **PreCL-3** (0.67 g, 1.8 mmol), 1,4-dibromobutane (0.18 g, 0.83 mmol), K_2CO_3 (0.35 g, 2.5 mmol), KI (0.020 g, 0.12 mmol) and 5 mL dry DMF were added into a 25 mL three neck round bottom flask. The reaction was stirred at 50 °C over 3

days, diluted with brine, extracted with CH_2Cl_2 3 times. The combined organic phase was washed with water, dried over Na_2SO_4, filtered, and concentrated *in vacuo*. The crude product was purified via flash chromatography using CH_2Cl_2/ethyl acetate (10:1 v:v) as eluent to yield **CL-3** as a light yellow solid. Yield: 0.27 g (40%). ^{1}H NMR (500 MHz, THF-d_8): 8.90 (s, 1 H), 8.19 (d, J=9 Hz, 1 H), 7.53-7.60 (m, 2 H), 7.37 (d, J=2.5, 1 H), 6.99 (dd, J=2.5, 9 Hz, 2 H), 6.89-6.93 (m, 2 H), 6.10-6.15 (m, 2 H), 5.45 (s, 2 H), 4.16 (s, 2 H), 3.57 (s, 2 H), 2. 92 (s, 1 H), 2.86 (s, 1 H), 2.11-2.17 (m, 1 H), 2.00-2.06 (m, 1 H), 1.97 (s, 2 H), 1.83 (d, J=8 Hz, 1 H), 1.72 (s, 2 H), 1.20-1.30 (m, 2 H). ^{13}C NMR (125 MHz, THF-d_8): 173.7, 164.5, 155.0, 141.0, 139.2, 138.5, 137.0, 135.2, 128.5, 121.4, 115.7, 114.5, 113.9, 69.2, 68.3, 48.7, 46.8, 45.9, 42.7, 31.0, 26.6. HRMS calculated for $C_{46}H_{46}N_4O_{10}$ $(M + Na)^+$: 837.3106; found: 837.3097.

CL-4: To a stirred solution of **2-16** (0.060 g, 0.14 mmol) in 1 mL THF was added 0.17 mL concentrated HCl. The reaction was stirred under ambient temperature overnight, diluted with brine, extracted with ethyl acetate 3 times, dried over Na_2SO_4, filtered and concentrated *in vacuo*. The crude product was purified via flash chromatography using hexanes/ethyl acetate (2:1 v:v) to yield **PreCL-4** as a yellow solid. Yield: 0.056 g (96%). ^{1}H NMR (500 MHz, CD_3OD): 8.06 (d, J=9 Hz, 1 H), 7.32-7.36 (m, 2 H), 7.09 (d, 3 Hz, 1 H), 6.78 (dd, J=3, 9 Hz, 1 H), 6.71-6.76 (m, 2 H), 6.15-6.19 (m, 2 H), 6.05 (q, J=6.5 Hz, 1 H), 2.90-2.94 (m, 2 H), 2.22-2.27 (m, 1 H), 1.89-1.95 (m, 1 H), 1.74 (s, 1 H), 1.72 (s, 1 H), 1.64 (d, J=6.5 Hz, 3 H), 1.28-1.38 (m, 2 H). **PreCL-4** (0.056 g, 0.14 mmol), 1,4-dibromobutane (0.014 g, 0.065 mmol), K_2CO_3 (0.027 g, 0.20 mmol), KI (0.0030 mg, 0.018 mmol) and 0.8 mL dry DMF were added into a 5 mL three neck round bottom flask. The reaction was stirred at 50 °C over 3 days, diluted with brine, and extracted with CH_2Cl_2 3 times. The combined organic phase was washed with water, dried over Na_2SO_4, filtered, and concentrated *in vacuo*. The crude product was purified via flash

chromatography using CH_2Cl_2/hexanes/ethyl acetate (20:2:1 v:v:v) as eluent to yield **CL-4** as a light yellow solid. Yield: 0.036 g (67%).^{1}H NMR (500 MHz, $CDCl_3$): 8.11 (dd, J=2, 9 Hz, 1 H), 7.27-7.33 (m, 2 H), 7.19-7.26 (m, 1 H), 7.15-7.18 (m, 1 H), 6.77-6.82 (m, 1 H), 6.69-6.75 (m, 2 H), 6.14-6.19 (m, 1 H), 6.06-6.13 (m, 2 H), 3.95-4.07 (m, 2 H), 2.98 (s, 1 H), 2.93 (s, 1 H), 2.06-2.13 (m, 1 H), 1.93-2.01 (m, 1 H), 1.92 (s, 2 H), 1.73 (d, J=8 Hz, 1 H), 1.66 (d, J= 6.5 Hz, 3 H), 1.31-1.40 (m, 2 H). ^{13}C NMR (125 MHz, $CDCl_3$): 173.9, 163.6, 153.9, 143.0, 140.2, 138.6, 136.0, 128.0, 121.8, 115.9, 113.6, 112.5, 71.9, 68.1, 47.4, 46.4, 45.7, 41.7, 30.7, 25.6, 23.5. HRMS calculated for $C_{48}H_{51}N_4O_{10}$ $(M+H)^+$: 843.3600; found: 843.3616.

NBD-Norbornene **Mono-3**: **NBD alcohol** (0.16 g, 0.67 mmol), exo-5-norbornene carboxylic acid (0.10 g, 0.72 mmol), DCC (0.17 g, 0.83 mmol), DMAP (0.017 g, 0.14 mmol) were dissolved in 10 mL dry CH_2Cl_2 in a 25 mL three neck round bottom flask. The reaction was stirred at ambient temperature overnight and then diluted with CH_2Cl_2, washed with water 3 times, dried over Na_2SO_4, and concentrated *in vacuo*. The crude product was purified via flash chromatography using hexanes/ethyl acetate (3:1 v:v) as eluent, followed by recrystallization in ethanol to yield **Mono-3** as an orange solid. Yield: 0.13 g (54%). ^{1}H NMR (500 MHz, $CDCl_3$): 8.47 (d, J=9 Hz, 1 H), 6.19 (d, J=9 Hz, 1 H), 6.09-6.12 (m, 1 H), 6.01-6.04 (m, 1 H), 4.42-4.49 (m, 4 H), 3.48 (s, 3 H), 2.87 (d, J=1.5 Hz, 2 H), 2.05-2.09 (m, 1 H), 1.72-1.77 (m, 1 H), 1.34-1.38 (m, 1 H), 1.24-1.32 (m, 2 H). ^{13}C NMR (125 MHz, $CDCl_3$):175.9, 145.3, 144.7, 144.6, 138.2, 135.4, 135.1, 123.5, 101.7, 61.7, 54.2, 46.5, 46.3, 43.0, 41.9, 41.6, 30.3.

NBDMA: **NBD alcohol** (0.29 g, 0.0012 mol), freshly distilled methacryloyl chloride (0.20 g, 0.0019 mol) and dry pyridine (0.15 g, 0.0019 mol) were dissolved in 15 mL dry CH_2Cl_2 in a 50 mL three neck round bottom flask. The reaction was stirred at ambient temperature overnight and then quenched by addition of water. The mixture was washed with CH_2Cl_2 for 3

times, dried over Na_2SO_4, and concentrated *in vacuo*. The crude product was purified via flash chromatography using CH_2Cl_2 as eluent to yield **NBDMA** as an orange solid. Yield: 0.22 g (60%). NMR results are in consistence with previous publications.[47]

Poly (poly(ethylene glycol) methyl ether methacrylate-co-NBDMA) (**PEGNBD**). Poly(ethylene glycol) methyl ether methacrylate (0.50 g), **NBDMA** (0.025 g), AIBN (5.0 mg) and DMF (5 mL) were added into a 25 mL round bottom flask. The mixture was purged with argon for 20 min, and then warmed to 60 °C and stirred overnight. The cooled mixture was precipitated into copious hexane/ether mixture (1:1 v:v), centrifuged, and crude product was collected by decanting. The crude product was redissolved in 10 mL CH_2Cl_2, precipitated into hexane, and centrifuged. After decanting the remaining sticky liquid was dried in vacuum oven for 3 days to yield an orange gum-like liquid. Yield: 0.26 g (50%). ^{1}H NMR (500 MHz, $CDCl_3$): 3.5-4.5 (broad, 18 H, O-CH_2), 3.2-3.5 (broad, 3 H, O-CH_3), 1.6-2.2 (broad, 2 H, CH_2), 0.4-1.3 (broad, 3H, CH_3). Mn=35 kDa, Mw=61 kDa, PDI 1.72.

General conditions for gelation

Organogels: A solution of Grubbs 2nd generation catalyst (2.4 mg) in 0.20 mL CH_2Cl_2 was added into a 20 mL vial charged with 0.20 mL of a DMF solution of monomers (40 mg) and the crosslinker. The vial was swirled and gelation was observed in no more than 30 seconds. All gels were purified using Soxhlet extraction with CH_2Cl_2 over two days and dried in vacuum.

Trapping of water soluble polymer into the hydrogel: Grubbs 2nd generation catalyst (1.8 mg) was added into a 20 mL vial charged with 0.30 mL CH_2Cl_2 solution of **M3** (50 mg), **CL-4** (2.7 mg) and **PEGNBD** (1.0 mg). The vial was swirled and gelation was observed in about 20

minutes. All gels were purified using Soxhlet extraction with CH_2Cl_2 over two days and dried in vacuum.

Rheological measurements

Each set of measurements started with swelling 8.0 mg gel in benzene in a vial for at least 1 hr before measurement. All gel in the vial was transferred onto the rheometer and rheological data was measured. After one data point was obtained, all substance from the sample holder of the rheometer was collected into a quartz cuvette. Gel in the cuvette was either (1) irradiated for a certain amount of time with a blak-ray B-100A high intensity UV lamp, or (2) kept in the dark for certain amount of time in control experiments. Then all the substance in the cuvette was transferred back onto the rheometer to collect another data point. Gel was immersed throughout the experiments and extra benzene was added if there was not enough benzene covering the gel.

Photodegradation experiments monitored by visual inspection or fluorescence spectroscopy

Each set of experiments started with immersing about 2.0 mg of organogel in about 3 mL benzene in a quartz cuvette equipped with a small magnetic stir bar. The gel was swollen for at least 30 minutes, then the sample in the cuvette was irradiated by UV with the micro stir bar stirring at about 100 rpm. After a certain amount of time, the cuvette was left in the dark with no disturbance to allow the gel to settle to the bottom of the cuvette, after which an emission spectrum of the liquid portion of the sample was collected using excitation at 465 nm. If further irradiation was needed, the cuvette containing the sample was irradiated again and another spectrum was obtained following a similar procedure. Cuvettes were always located at the same

position relative to the UV lamp. In control experiments, all conditions were the same other than that the samples were kept in the dark.

Photo-release of guest from the hydrogel

Each set of experiments started with immersing about 1.0 mg of hydrogel that had trapped fluorescent polymer guest in about 3 mL water in a quartz cuvette equipped with a small magnetic stir bar. Other conditions are the same as in photodegradation experiments monitored by visual inspection or fluorescence spectroscopy.

2.8 References

1. Whittell, G.R., et al., *Functional soft materials from metallopolymers and metallosupramolecular polymers.* Nature Materials, 2011. **10**(3): p. 176-188.
2. Ahn, S.-k., et al., *Stimuli-responsive polymer gels.* Soft Matter, 2008. **4**(6): p. 1151-1157.
3. Yoshida, R. and T. Okano, *Stimuli-Responsive Hydrogels and Their Application to Functional Materials*, in *Biomedical Applications of Hydrogels Handbook*, R.M. Ottenbrite, K. Park, and T. Okano, Editors. 2010, Springer New York: New York, NY. p. 19-43.
4. Murthy, N., et al., *A Novel Strategy for Encapsulation and Release of Proteins: Hydrogels and Microgels with Acid-Labile Acetal Cross-Linkers.* Journal of the American Chemical Society, 2002. **124**(42): p. 12398-12399.
5. Richter, M., et al., *Visualization of Real-Time Degradation of pH-Responsive Polyglycerol Nanogels via Atomic Force Microscopy.* Macromolecular Rapid Communications, 2014. **35**(23): p. 2018-2022.
6. Tan, H., et al., *PEG-urokinase nanogels with enhanced stability and controllable bioactivity.* Soft Matter, 2012. **8**(9): p. 2644-2650.
7. Li, Y., et al., *Well-Defined, Reversible Boronate Crosslinked Nanocarriers for Targeted Drug Delivery in Response to Acidic pH Values and cis-Diols.* Angewandte Chemie International Edition, 2012. **51**(12): p. 2864-2869.
8. Chen, W., Y. Cheng, and B. Wang, *Dual-Responsive Boronate Crosslinked Micelles for Targeted Drug Delivery.* Angewandte Chemie International Edition, 2012. **51**(22): p. 5293-5295.
9. Zhang, X., et al., *Micro- and nanogels with labile crosslinks - from synthesis to biomedical applications.* Chemical Society Reviews, 2015. **44**(7): p. 1948-1973.
10. Kharkar, P.M., K.L. Kiick, and A.M. Kloxin, *Designing degradable hydrogels for orthogonal control of cell microenvironments.* Chemical Society Reviews, 2013. **42**(17): p. 7335-7372.
11. Wachiralarpphaithoon, C., Y. Iwasaki, and K. Akiyoshi, *Enzyme-degradable phosphorylcholine porous hydrogels cross-linked with polyphosphoesters for cell matrices.* Biomaterials, 2007. **28**(6): p. 984-993.
12. Xiong, M.-H., et al., *Bacteria-Responsive Multifunctional Nanogel for Targeted Antibiotic Delivery.* Advanced Materials, 2012. **24**(46): p. 6175-6180.
13. Dispinar, T., et al., *Redox-Responsive Degradable PEG Cryogels as Potential Cell Scaffolds in Tissue Engineering.* Macromolecular Bioscience, 2012. **12**(3): p. 383-394.
14. Kloxin, A.M., M.W. Tibbitt, and K.S. Anseth, *Synthesis of photodegradable hydrogels as dynamically tunable cell culture platforms.* Nature Protocols, 2010. **5**(12): p. 1867-1887.
15. Kharkar, P.M., K.L. Kiick, and A.M. Kloxin, *Design of thiol- and light-sensitive degradable hydrogels using Michael-type addition reactions.* Polymer Chemistry, 2015. **6**(31): p. 5565-5574.
16. Griffin, D.R. and A.M. Kasko, *Photoselective Delivery of Model Therapeutics from Hydrogels.* ACS Macro Letters, 2012. **1**(11): p. 1330-1334.
17. Griffin, D.R. and A.M. Kasko, *Photodegradable Macromers and Hydrogels for Live Cell Encapsulation and Release.* Journal of the American Chemical Society, 2012. **134**(31): p. 13103-13107.
18. Azagarsamy, M.A., et al., *Coumarin-Based Photodegradable Hydrogel: Design, Synthesis, Gelation, and Degradation Kinetics.* ACS Macro Letters, 2014. **3**(6): p. 515-519.
19. Huang, Q., et al., *Photocleavable coumarin crosslinkers based polystyrene microgels: phototriggered swelling and release.* Journal of Materials Chemistry, 2012. **22**(35): p. 18275-18282.
20. Griffin, D.R. and A.M. Kasko, *Photodegradable Macromers and Hydrogels for Live Cell Encapsulation and Release.* Journal of the American Chemical Society, 2012. **134**: p. 13103-13107.
21. Lyon, L.A., et al., *Thermoresponsive microgel-based materials.* Chemical Society Reviews, 2009.

38(4): p. 865-874.
22. Li, C., et al., *Temperature-, pH-, and ion-stimulus-responsive swelling behaviors of poly(dimethylaminoethyl methacrylate) gel containing cholic acid.* Journal of Applied Polymer Science, 2014. **131**(6): p. n/a-n/a.
23. Thomas, S.W., *New Applications of Photolabile Nitrobenzyl Groups in Polymers.* Macromolecular Chemistry and Physics, 2012. **213**(23): p. 2443-2449.
24. Lu, W., et al., *Application of new photolabile protecting groups as photocleavable joints of block copolymers.* Chemical Communications, 2013. **49**(83): p. 9636-9638.
25. Kloxin, A.M., et al., *Photodegradable Hydrogels for Dynamic Tuning of Physical and Chemical Properties.* Science, 2009. **324**(5923): p. 59-63.
26. Jiang, C., et al., *Gel formation in atom transfer radical polymerization of 2-(N,N-dimethylamino)ethyl methacrylate and ethylene glycol dimethacrylate.* Journal of Polymer Science Part A: Polymer Chemistry, 2001. **39**(21): p. 3780-3788.
27. Gonçalves, M.A.D., et al., *Stimuli-Responsive Hydrogels Synthesis using Free Radical and RAFT Polymerization.* Macromolecular Symposia, 2013. **333**(1): p. 41-54.
28. Shih, H. and C.-C. Lin, *Cross-Linking and Degradation of Step-Growth Hydrogels Formed by Thiol–Ene Photoclick Chemistry.* Biomacromolecules, 2012. **13**(7): p. 2003-2012.
29. Madkour, A.E., et al., *End-Functionalized ROMP Polymers for Biomedical Applications.* Macromolecules, 2010. **43**(10): p. 4557-4561.
30. Love, J.A., et al., *A Practical and Highly Active Ruthenium-Based Catalyst that Effects the Cross Metathesis of Acrylonitrile.* Angewandte Chemie, 2002. **114**(21): p. 4207-4209.
31. Schwab, P., et al., *A Series of Well-Defined Metathesis Catalysts–Synthesis of [RuCl$_2$(=CHR′)(PR3)2] and Its Reactions.* Angewandte Chemie International Edition in English, 1995. **34**(18): p. 2039-2041.
32. Schwab, P., R.H. Grubbs, and J.W. Ziller, *Synthesis and Applications of RuCl2(CHR')(PR3)2: The Influence of the Alkylidene Moiety on Metathesis Activity.* Journal of the American Chemical Society, 1996. **118**(1): p. 100-110.
33. Scholl, M., et al., *Synthesis and Activity of a New Generation of Ruthenium-Based Olefin Metathesis Catalysts Coordinated with 1,3-Dimesityl-4,5-dihydroimidazol-2-ylidene Ligands.* Organic Letters, 1999. **1**(6): p. 953-956.
34. Leitgeb, A., J. Wappel, and C. Slugovc, *The ROMP toolbox upgraded.* Polymer, 2010. **51**(14): p. 2927-2946.
35. Gumbley, P., D. Koylu, and S.W. Thomas, *Photoresponsive Polymers Containing Nitrobenzyl Esters via Ring-Opening Metathesis Polymerization.* Macromolecules, 2011. **44**(20): p. 7956-7961.
36. Sutthasupa, S., M. Shiotsuki, and F. Sanda, *Recent advances in ring-opening metathesis polymerization, and application to synthesis of functional materials.* Polym J, 2010. **42**(12): p. 905-915.
37. Sutthasupa, S., F. Sanda, and T. Masuda, *Copolymerization of Amino Acid Functionalized Norbornene Monomers. Synthesis of Amphiphilic Block Copolymers Forming Reverse Micelles.* Macromolecules, 2008. **41**(2): p. 305-311.
38. Sutthasupa, S., F. Sanda, and T. Masuda, *ROMP of Norbornene Monomers Carrying Nonprotected Amino Groups with Ruthenium Catalyst.* Macromolecules, 2009. **42**(5): p. 1519-1525.
39. Alfred, S.F., et al., *Water-soluble ROMP polymers from amine-functionalized norbornenes.* Journal of Polymer Science Part A: Polymer Chemistry, 2008. **46**(19): p. 6672-6676.
40. Madkour, A.E., J.M. Grolman, and G.N. Tew, *Synthesis of hydrogels via ring-opening metathesis polymerization: factors affecting gelation.* Polymer Chemistry, 2011. **2**(1): p. 114-119.
41. Gumbley, P., et al., *Photoresponsive Gels Prepared by Ring-Opening Metathesis Polymerization.* Macromolecular Rapid Communications, 2013. **34**(23-24): p. 1838-1843.
42. Hu, X., J. Shi, and S.W. Thomas, *Photolabile ROMP gels using ortho-nitrobenzyl functionalized*

crosslinkers. Polymer Chemistry, 2015. **6**(27): p. 4966-4971.
43. Rule, J.D. and J.S. Moore, *ROMP Reactivity of endo- and exo-Dicyclopentadiene.* Macromolecules, 2002. **35**(21): p. 7878-7882.
44. Chen, B.-Y., et al., *Novel Highly Selective and Reversible Chemosensors Based on Dual-Ratiometric Fluorescent Electrospun Nanofibers with pH- and Fe^{3+}-Modulated Multicolor Fluorescence Emission.* ACS Applied Materials & Interfaces, 2015. **7**(4): p. 2797-2808.
45. Solomek, T., et al., *Photolysis of ortho-nitrobenzylic derivatives: the importance of the leaving group.* Photochemical & Photobiological Sciences, 2012. **11**(3): p. 548-555.
46. Yan, Q., et al., *Visible light-responsive micelles formed from dialkoxyanthracene-containing block copolymers.* Chemical Communications, 2012. **48**(13): p. 1913-1915.
47. Chen, B.Y., et al., *Novel Highly Selective and Reversible Chemosensors Based on Dual-Ratiometric Fluorescent Electrospun Nanofibers with pH- and Fe^{3+}-Modulated Multicolor Fluorescence Emission.* ACS Applied Materials & Interfaces, 2015. **7**(4): p. 2797-2808.

Chapter 2 Appendix

^{1}H and ^{13}C NMR

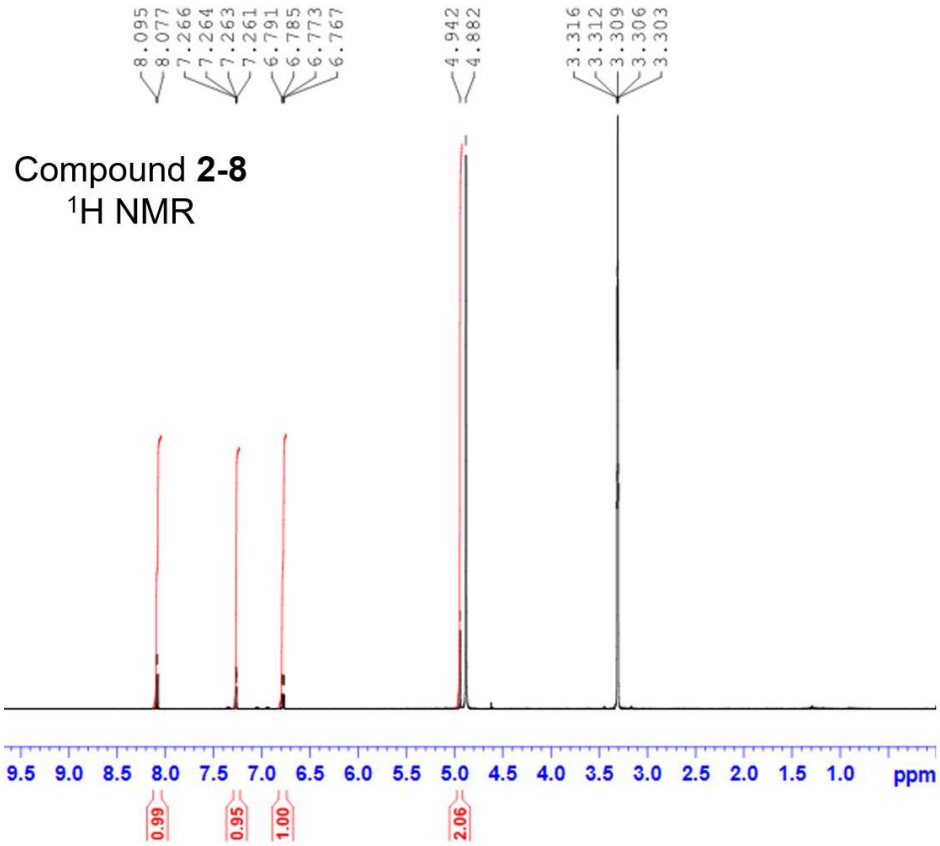
8.095
8.077
7.266
7.264
7.263
7.261
6.791
6.785
6.773
6.767
4.942
4.882
3.316
3.312
3.309
3.306
3.303
Compound 2-8
1H NMR
9.5 9.0 8.5 8.0 7.5 7.0 6.5 6.0 5.5 5.0 4.5 4.0 3.5 3.0 2.5 2.0 1.5 1.0 ppm
0.99
0.95
1.00
2.06

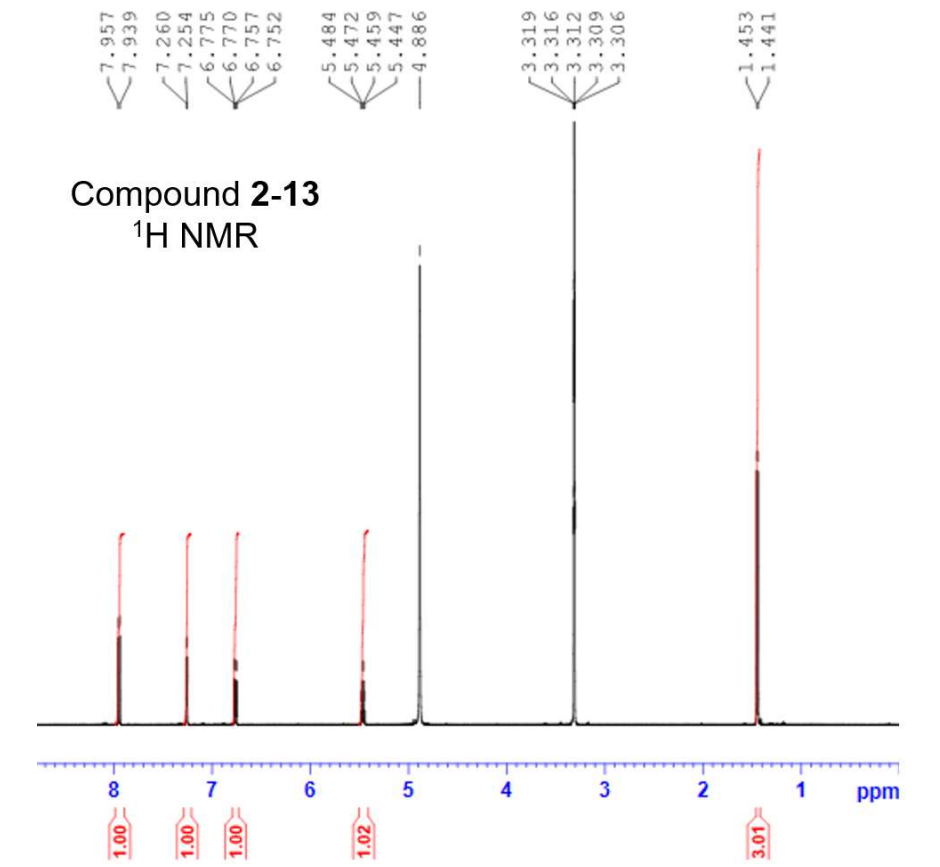
7.957
7.939
7.260
7.254
6.775
6.770
6.757
6.752
5.484
5.472
5.459
5.447
4.886
3.319
3.316
3.312
3.309
3.306
1.453
1.441
Compound 2-13
1H NMR
8 7 6 5 4 3 2 1 ppm
1.00
1.00
1.00
1.02
3.01

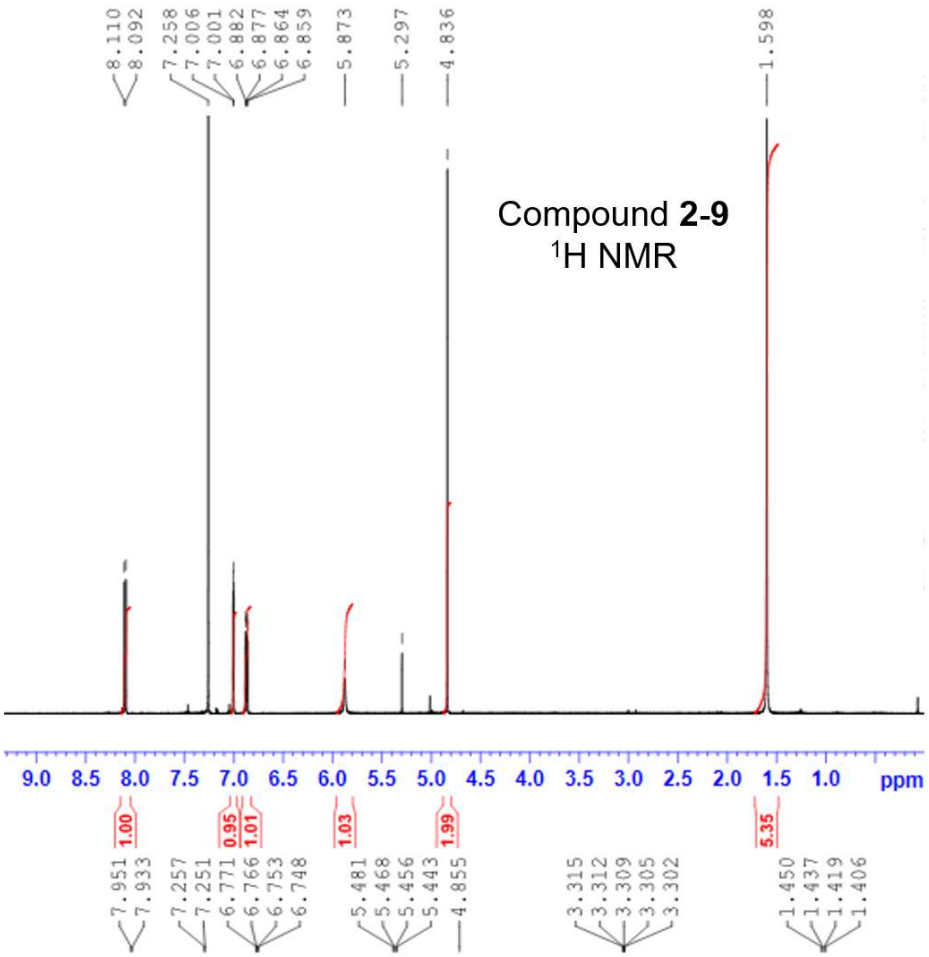
Compound **2-9**
^{1}H NMR
8.110
8.092
7.258
7.006
7.001
6.882
6.877
6.864
6.859
5.873
5.297
4.836
1.598
9.0 8.5 8.0 7.5 7.0 6.5 6.0 5.5 5.0 4.5 4.0 3.5 3.0 2.5 2.0 1.5 1.0 ppm
1.00
0.95
1.01
1.03
1.99
5.35

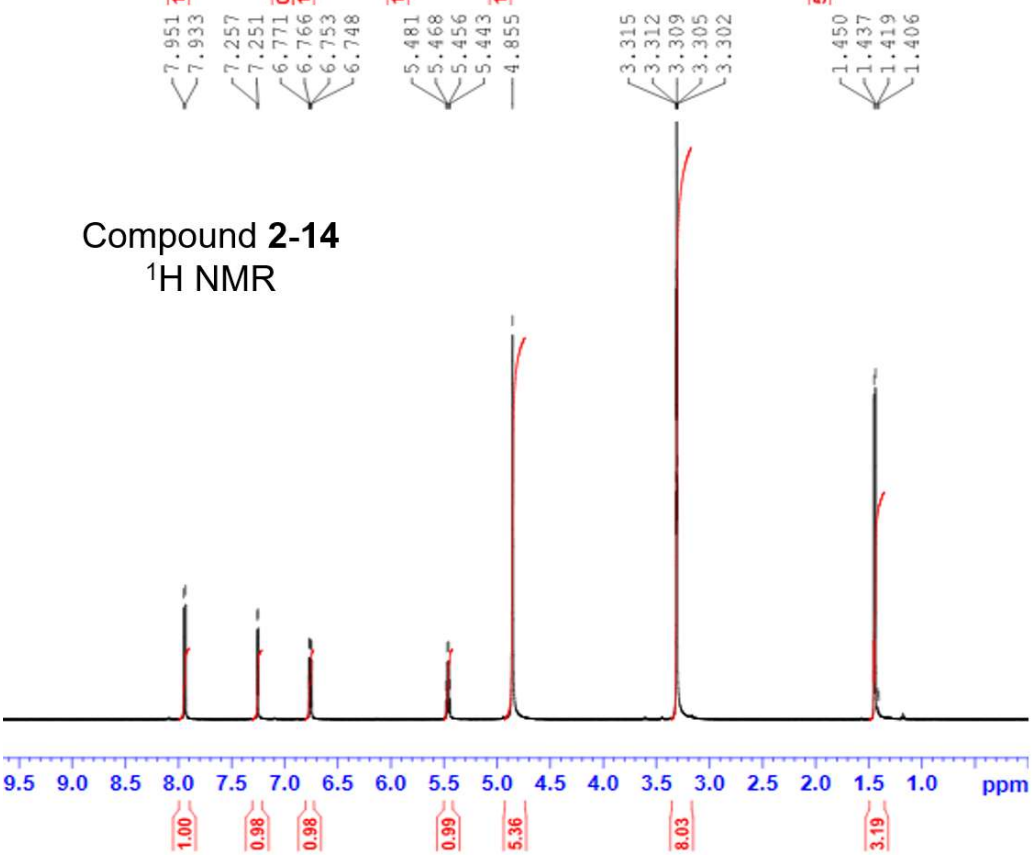
Compound **2-14**
^{1}H NMR
7.951
7.933
7.257
7.251
6.771
6.766
6.753
6.748
5.481
5.468
5.456
5.443
4.855
3.315
3.312
3.309
3.305
3.302
1.450
1.437
1.419
1.406
9.5 9.0 8.5 8.0 7.5 7.0 6.5 6.0 5.5 5.0 4.5 4.0 3.5 3.0 2.5 2.0 1.5 1.0 ppm
1.00
0.98
0.98
0.99
5.36
8.03
3.19

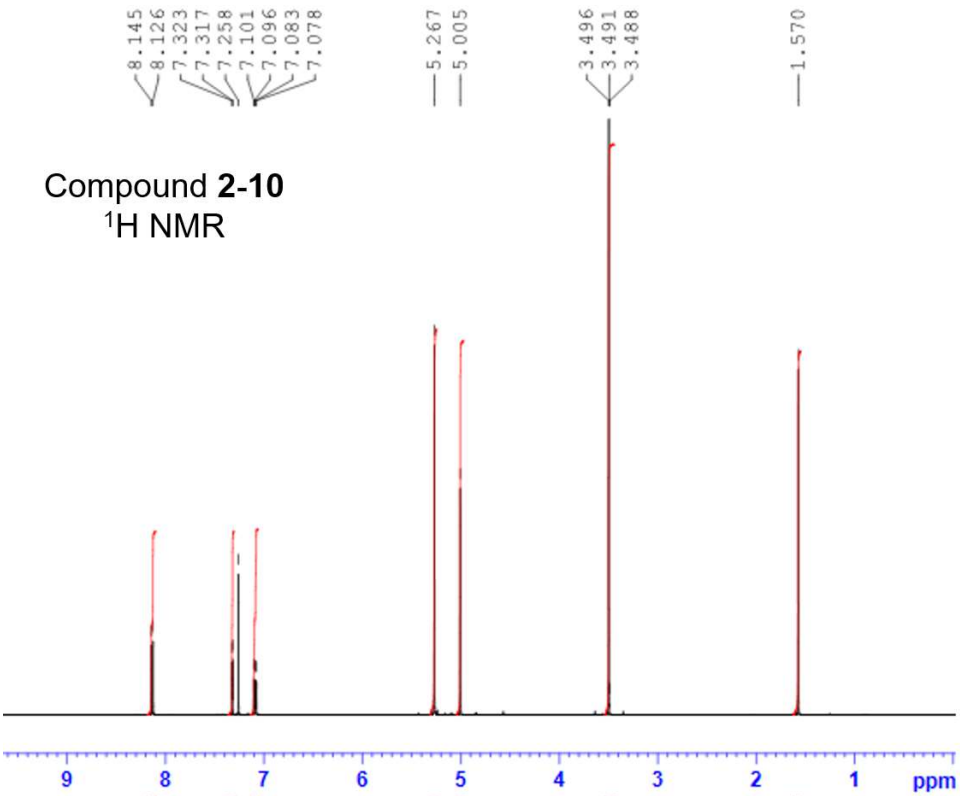
8.145
8.126
7.323
7.317
7.258
7.101
7.096
7.083
7.078
5.267
5.005
3.496
3.491
3.488
1.570
Compound 2-10
1H NMR
9
8
7
6
5
4
3
2
1
ppm
1.00
1.00
1.01
2.11
2.04
3.11
1.98

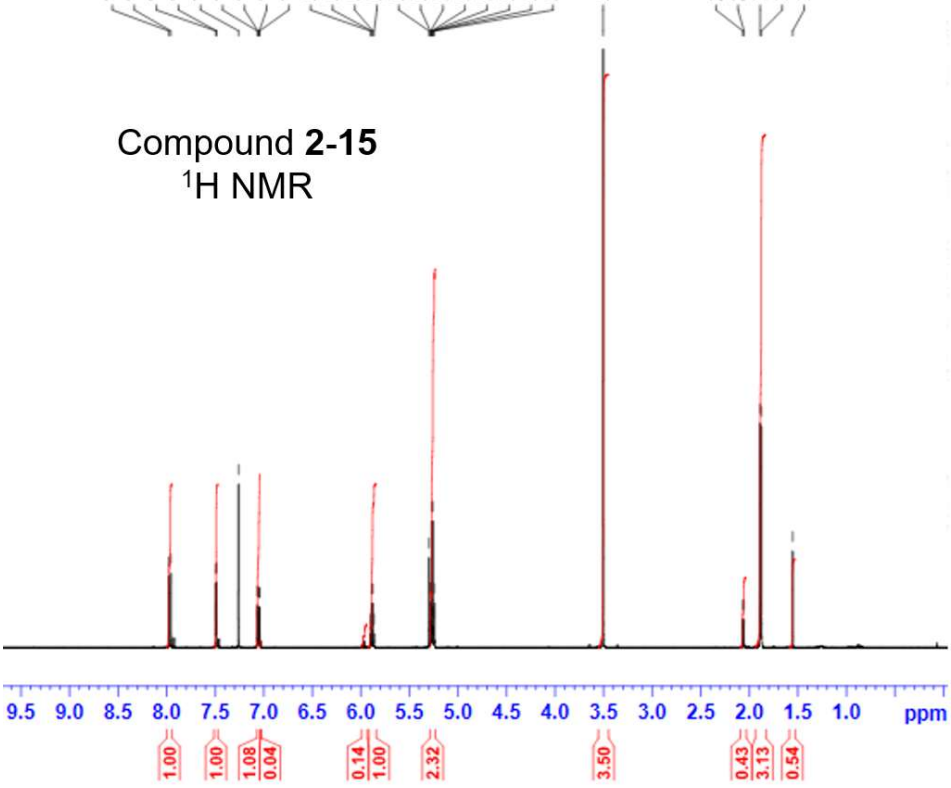
7.978
7.960
7.493
7.488
7.259
7.066
7.061
7.048
7.043
5.904
5.890
5.877
5.864
5.299
5.286
5.282
5.272
5.268
5.258
5.254
5.244
3.504
2.069
2.055
1.888
1.875
1.553
Compound 2-15
1H NMR
9.5
9.0
8.5
8.0
7.5
7.0
6.5
6.0
5.5
5.0
4.5
4.0
3.5
3.0
2.5
2.0
1.5
1.0
ppm
1.00
1.00
1.08
0.04
0.14
1.00
2.32
3.50
0.43
3.13
0.54

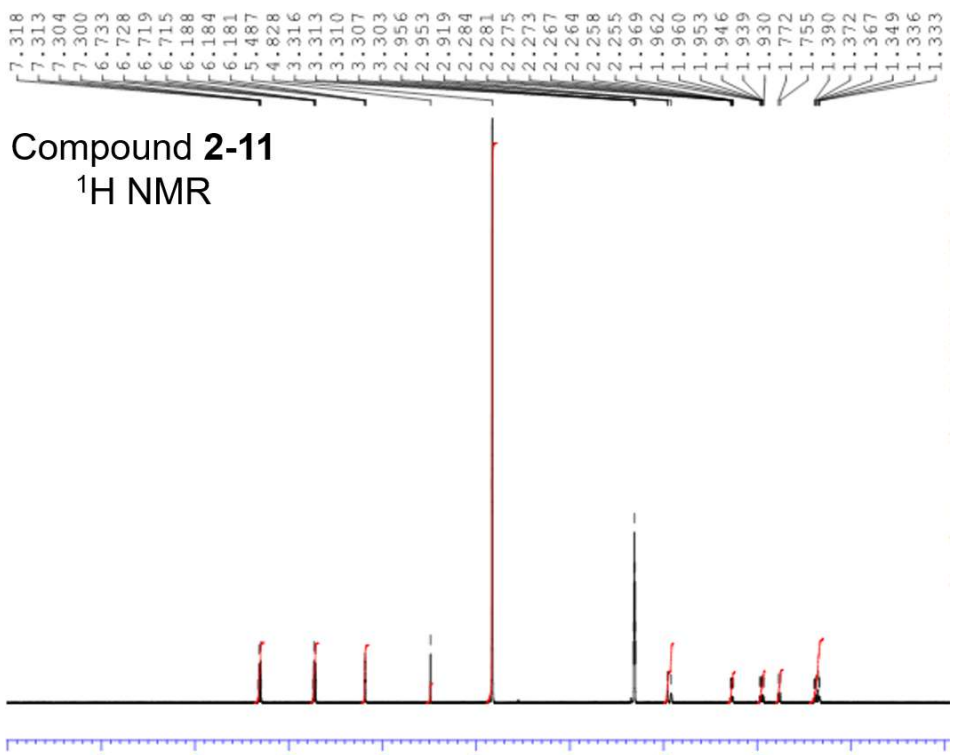

Compound **2-11**
^{1}H NMR

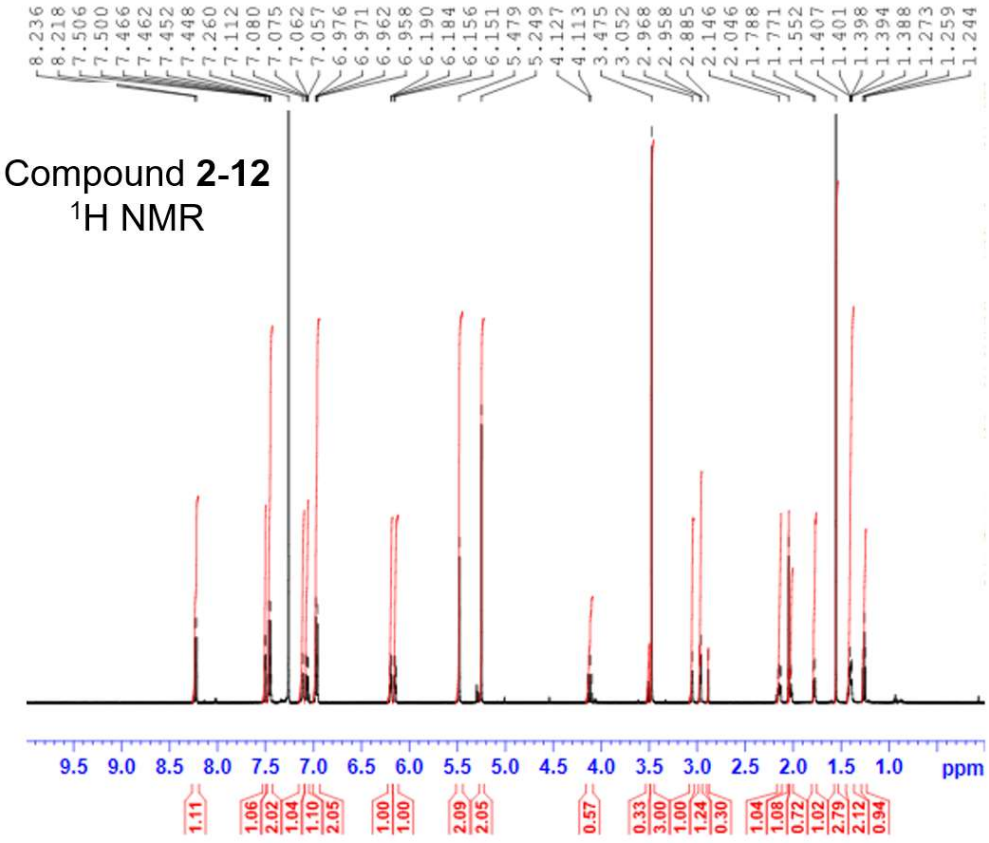

Compound **2-12**
^{1}H NMR

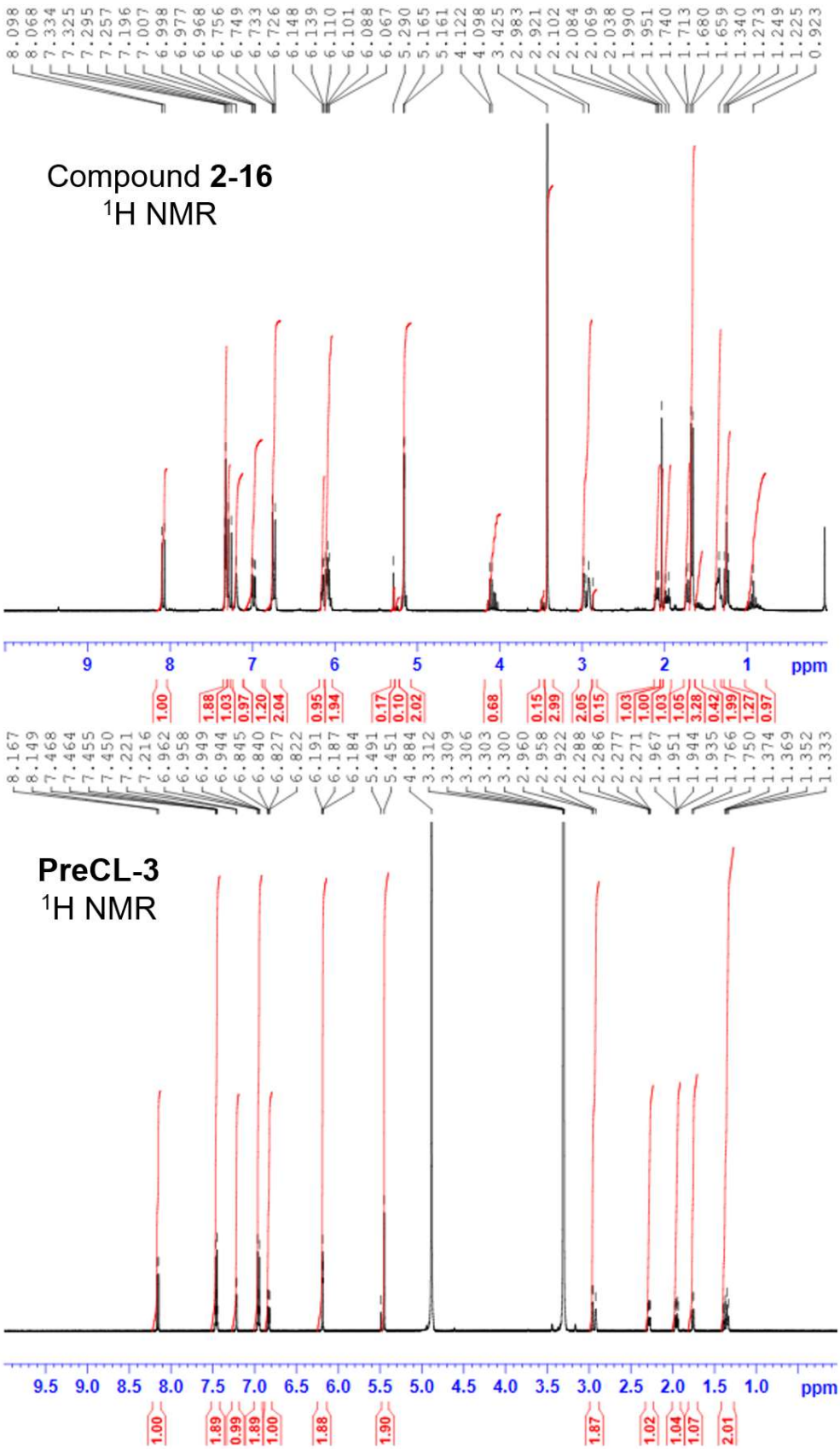
Compound **2-16**
^{1}H NMR
PreCL-3
^{1}H NMR
ppm
ppm

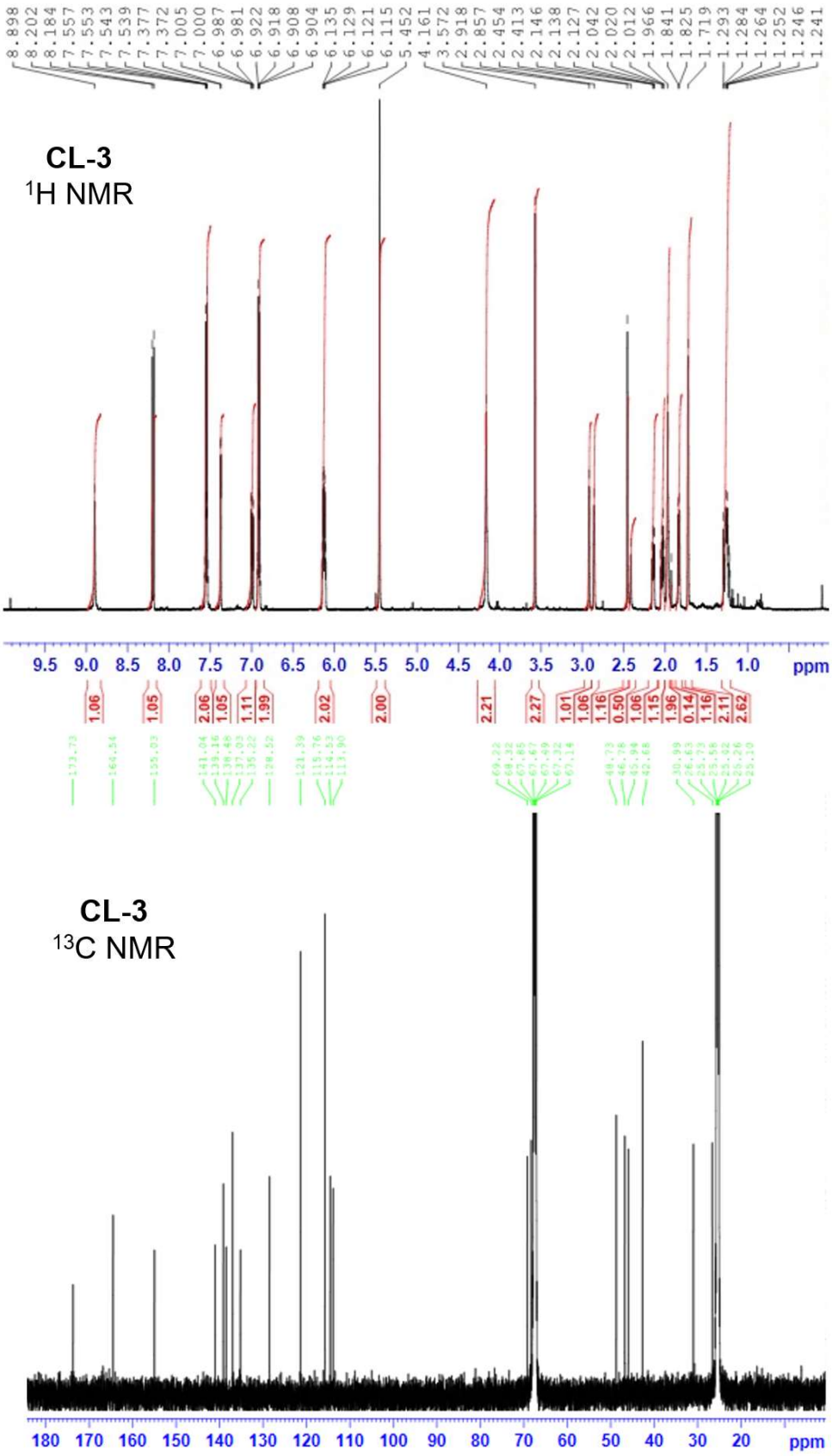
CL-3
1H NMR
CL-3
13C NMR
ppm
ppm

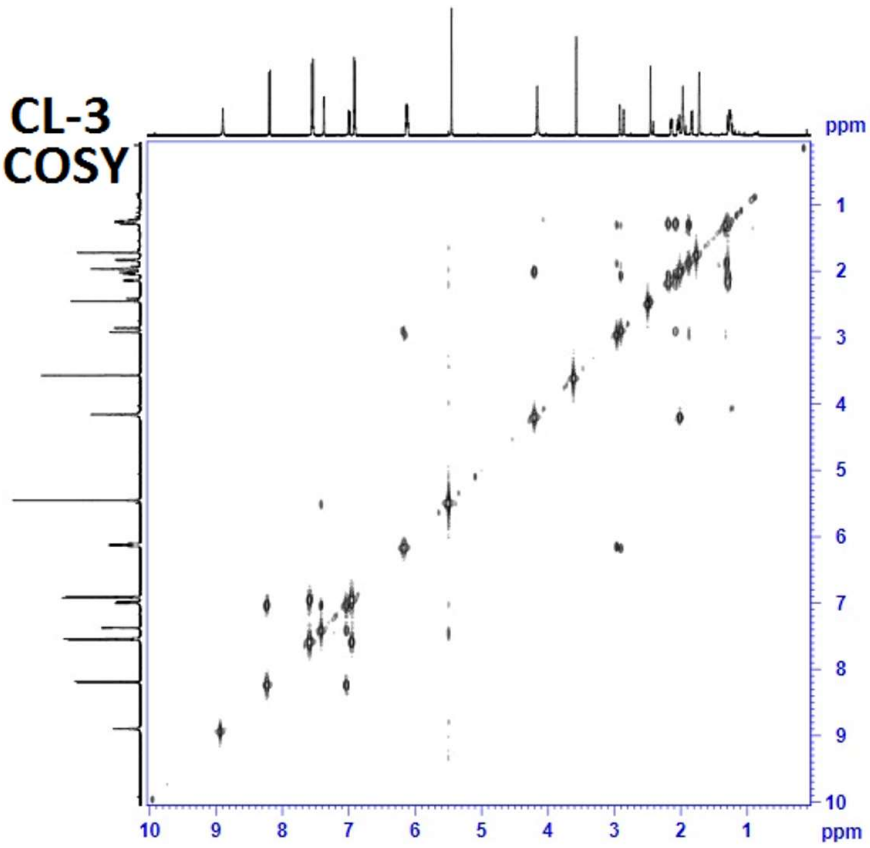
CL-3
COSY
ppm
1
2
3
4
5
6
7
8
9
10
10
9
8
7
6
5
4
3
2
1
ppm

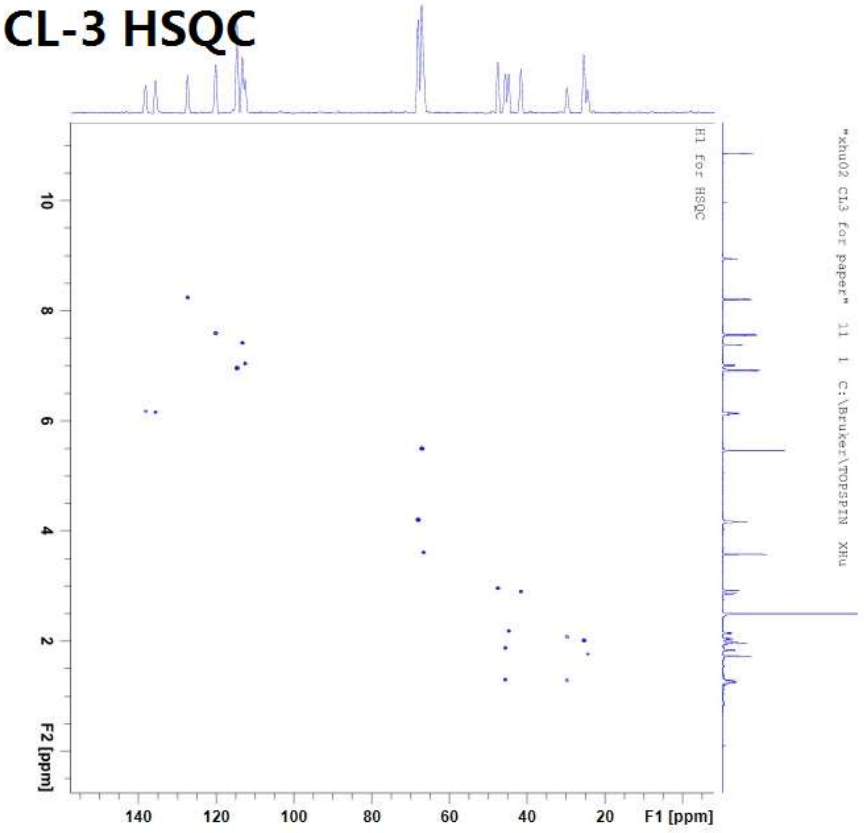
CL-3 HSQC
H1 for HSQC
"xhu02 CL3 for paper" 11 1 C:\Bruker\TOPSPIN XHu
10
8
6
4
2
F2 [ppm]
140
120
100
80
60
40
20
F1 [ppm]

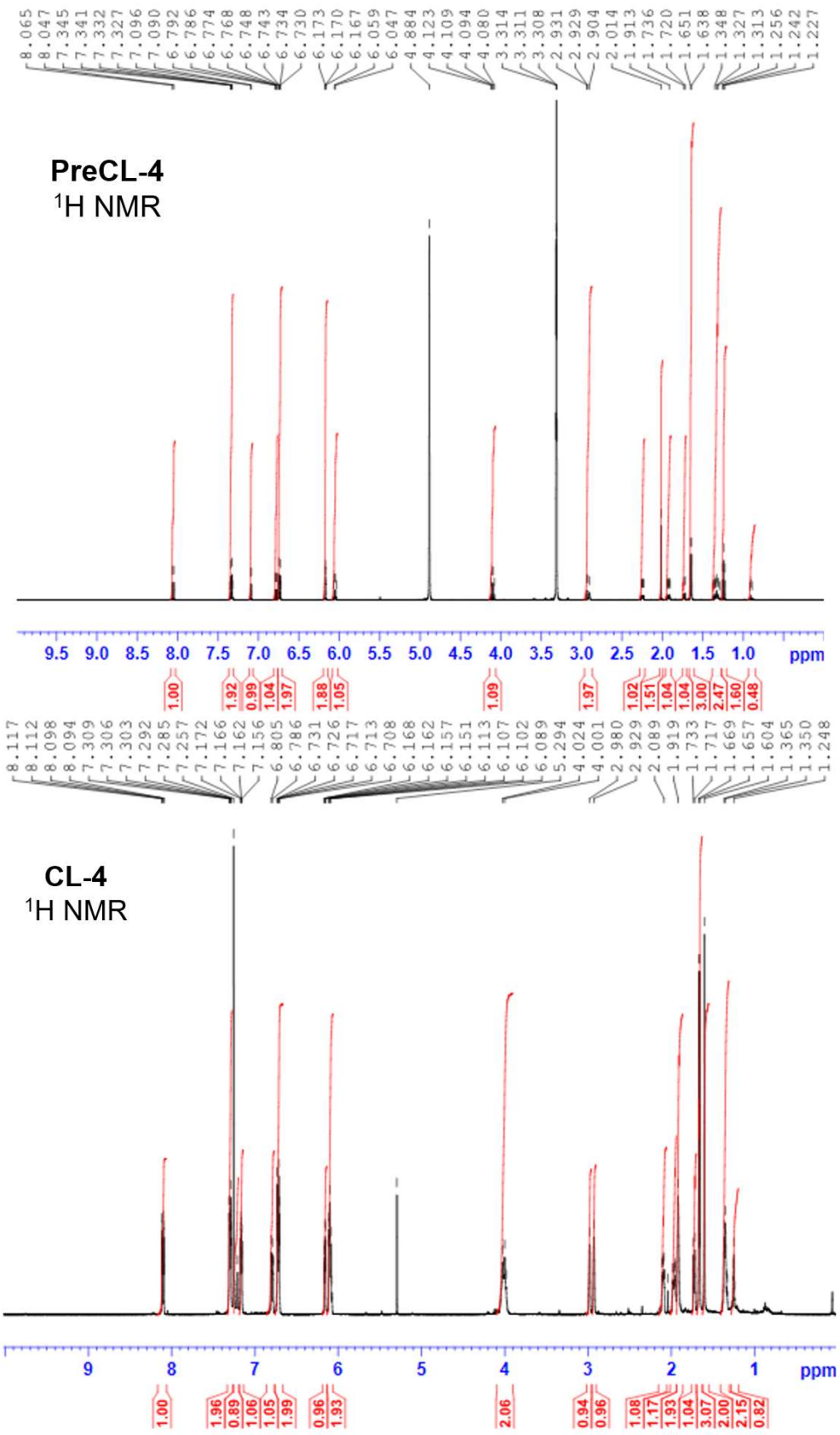
PreCL-4
1H NMR
CL-4
1H NMR
ppm

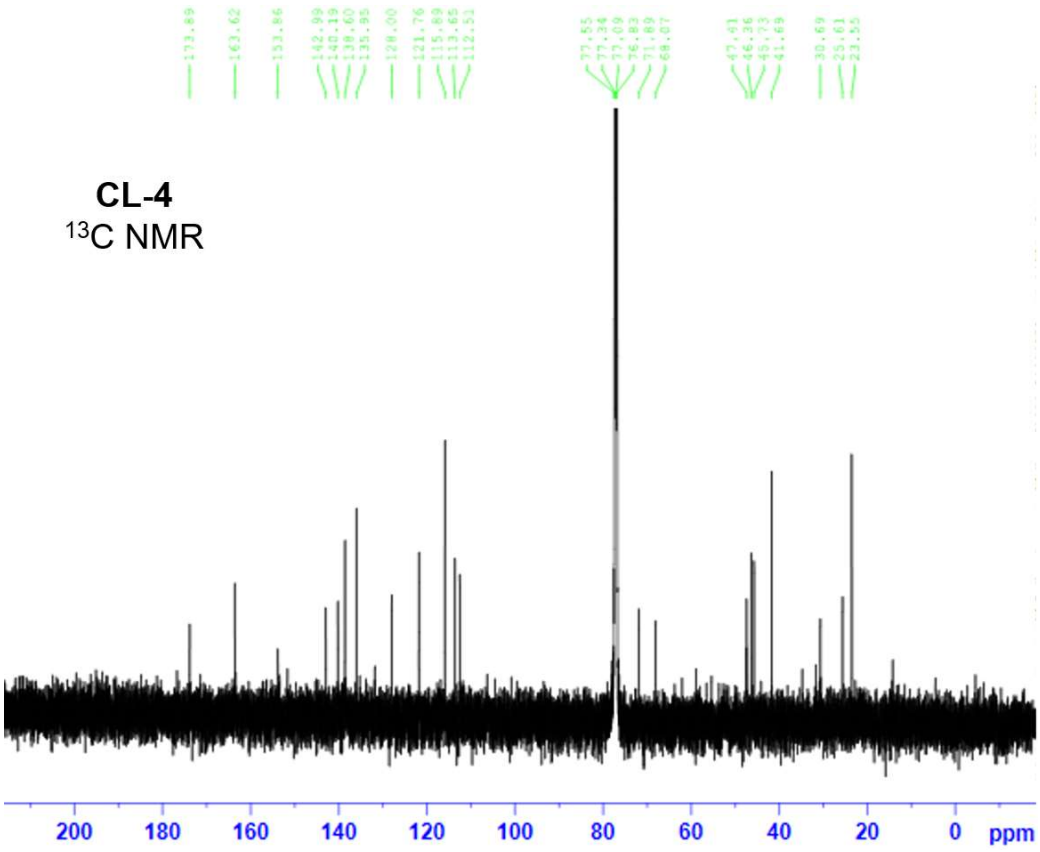
CL-4
13C NMR
200
180
160
140
120
100
80
60
40
20
0
ppm

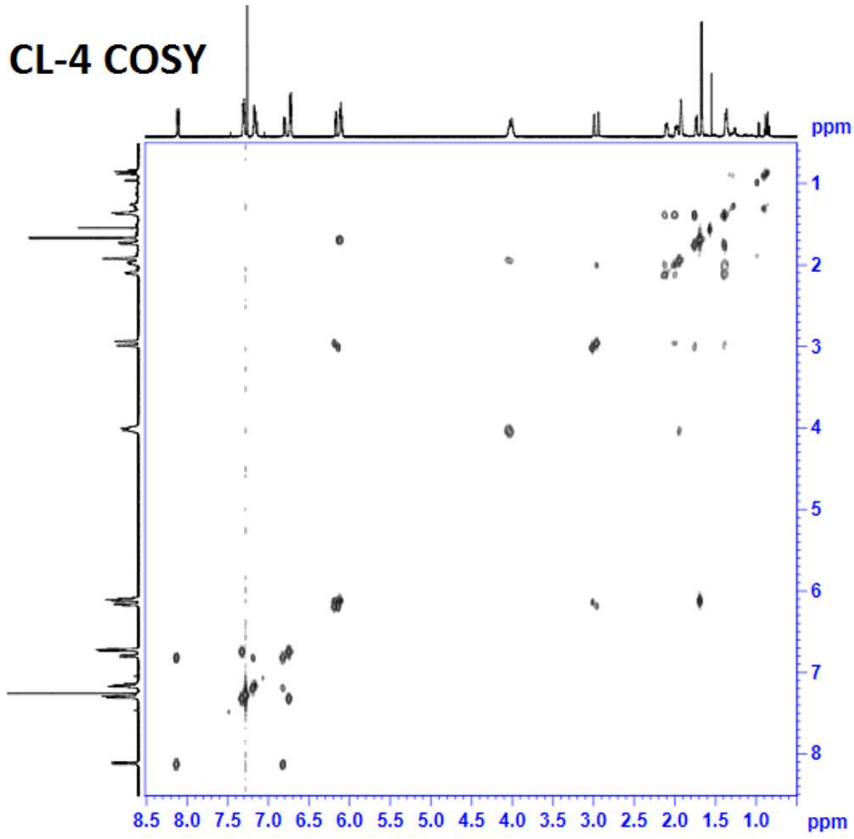
CL-4 COSY
ppm
1
2
3
4
5
6
7
8
8.5 8.0 7.5 7.0 6.5 6.0 5.5 5.0 4.5 4.0 3.5 3.0 2.5 2.0 1.5 1.0
ppm

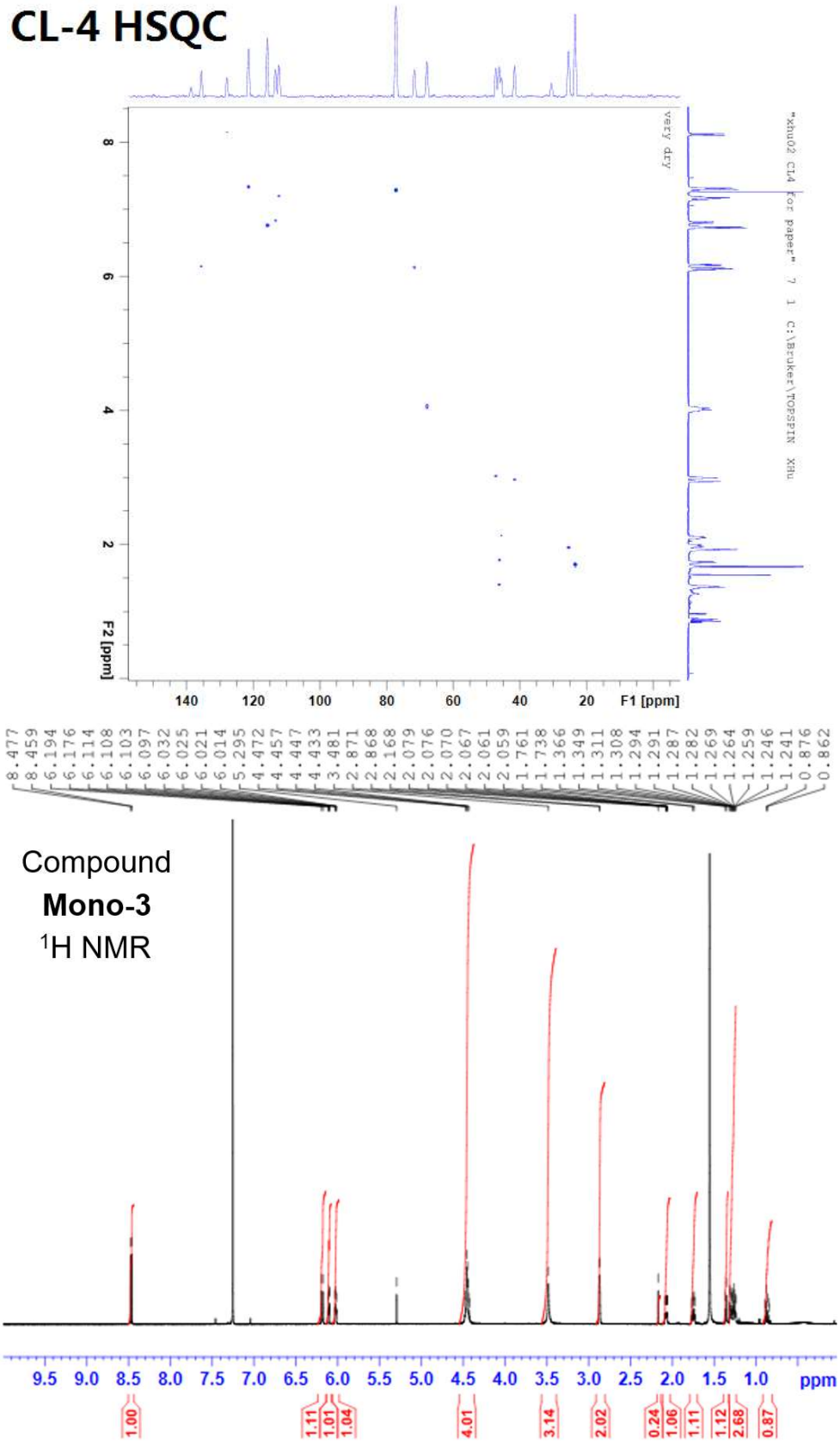
CL-4 HSQC
F2 [ppm]
F1 [ppm]
Compound
Mono-3
1H NMR
ppm

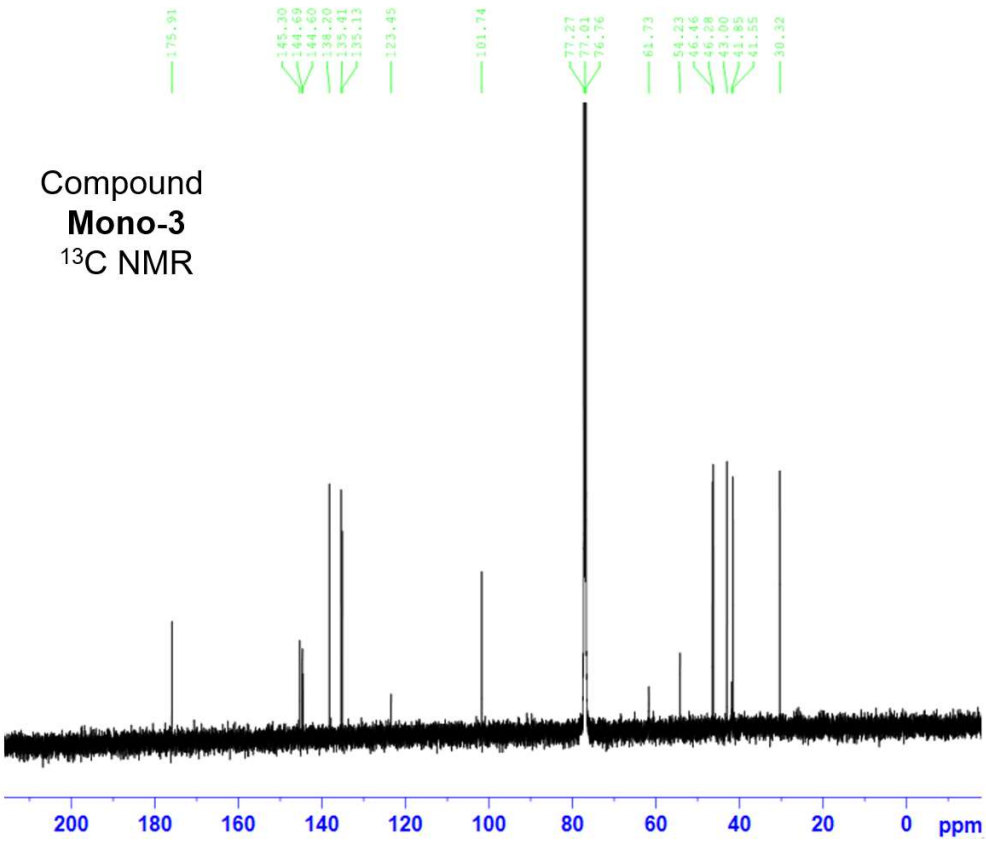
175.91
145.30
144.69
144.60
138.20
135.41
135.13
123.45
101.74
77.27
77.01
76.76
61.73
54.23
46.46
46.28
43.00
41.85
41.55
30.32
Compound
Mono-3
13C NMR
200
180
160
140
120
100
80
60
40
20
0
ppm

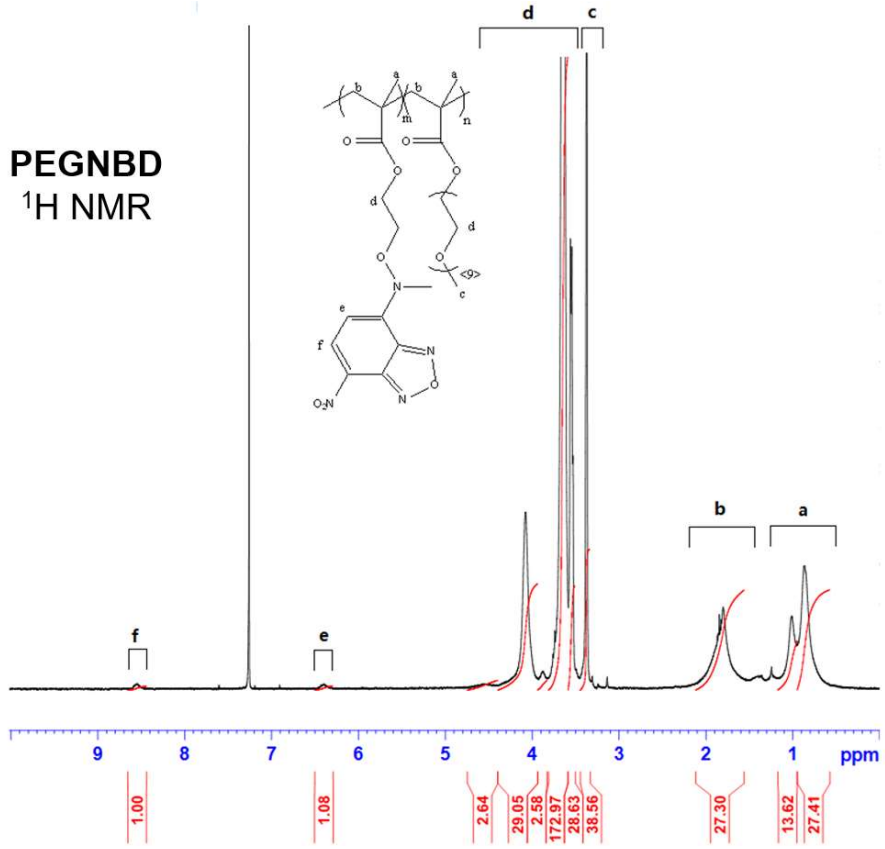
PEGNBD
1H NMR
d
c
b
a
f
e
9
8
7
6
5
4
3
2
1
ppm
1.00
1.08
2.64
29.05
2.58
172.97
28.63
38.56
27.30
13.62
27.41

Chapter 3:

Controlling Covalent Bonds and Non-Covalent Intermolecular Forces in Solid-State Polyelectrolyte Multilayers

Reproduced in part with permission from:
Hu, X.; Qureishi, Z.; Thomas, S. W., Light-Controlled Selective Disruption, Multilevel Patterning, and Sequential Release with Polyelectrolyte Multilayer Films Incorporating Four Photocleavable Chromophores.
Chemistry of Materials **2017**, *29*, 2951-2960.
Copyright 2017 American Chemical Society
Hu, X.; McIntosh, E.; Simon, M. G.; Staii, C.; Thomas, S. W., Stimuli-Responsive Free-Standing Layer-By-Layer Films.
Advanced Materials **2016**, *28*, 715-721
Copyright 2016 Wiley & Sons, Inc.

3.1 Introduction

3.1.1 Ion-Pairing Driven Polyelectrolyte Self-Assembly

Polyelectrolytes are polymers with repeating ionic groups. Polycations are molecules bearing multiple positively charged groups, while polyanions are molecules with negatively charged repeating units. Oppositely charged polyelectrolytes can form associated complexes of different forms upon mixing. The electrostatic attraction between oppositely charged macromolecules, along with van der Waals and hydrophobic interactions, provide the enthalpic driving force for the complexation; the loss of counterions upon association provides the entropic driving force. Morphologies of the associated complexes can range from dense precipitates to coacervates to colloidal nanoparticles, depending on the molecular structure of polymers and the preparation conditions.[1]

The layer-by-layer (LBL) technique is a powerful and flexible approach useful in the design and fabrication of nanoscale composite films. Hierarchically organized LBL composite films can be prepared by simple techniques such as submersion, spin casting, or spray casting. Various materials ranging from inorganic compounds, to macromolecules including inorganic compounds, synthetic polymers and biomacromolecules have been successfully incorporated into LBL films.[2-7] Common interactions used to build LBL films include ion pairing interactions (*vide supra*), hydrogen bonding, and metal coordination. The most common application of LBL technique is construction of polyelectrolyte multilayers (PEMs), multilayer films comprsing alternating layers of polycations and polyanions stabilized by the ion-pairing interactions between oppositely charged polymers (**Figure 3.1**). A unique advantage of the LBL technique, compared with other film deposition methods, is that LBL asssembly can offer feasible, precise control over the nanoscale spatial distribution of chemistry perpendicular to the surface.

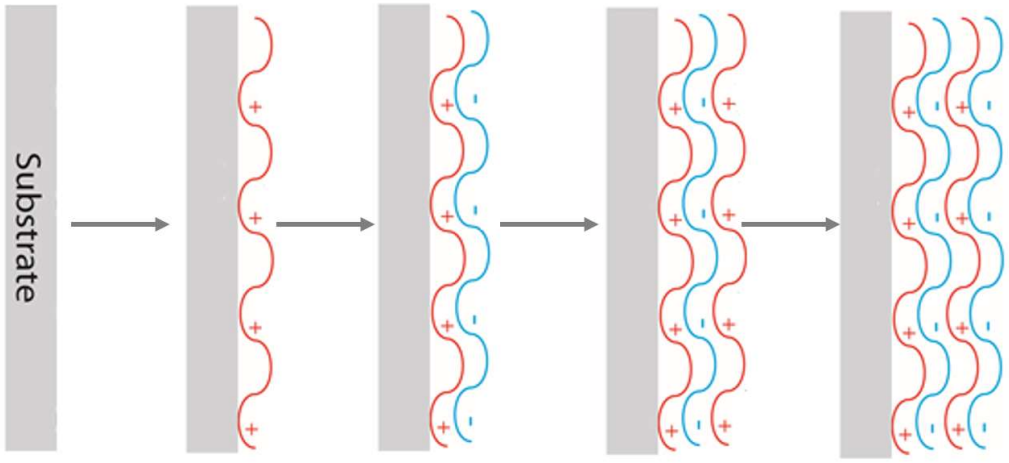

Figure 3.1: Schematic of the LBL deposition of polyelectrolyte multilayers.

3.1.2 Stimuli Responsive LBL films

Of special interest are LBL films incorporating responsive components that undergo changes in structure or properties upon application of external stimuli. Both physical stimuli, (e.g., changes in temperature[8, 9] and light[10, 11]) and chemical stimuli (e.g., changes in pH[12]) are useful for triggering changes including deformation and film dissolution. Such films find applications as biomedical, optical and mechanical materials. Among the various external stimuli used to control the properties of LbL films, light uniquely offers real-time control over spatiotemporal distribution, energy, and stoichiometry. Our group previously reported light-responsive LbL films comprising polycations with photocleavable benzylic esters that yield carboxylic acid groups as polymer side chains upon irradiation with light through mechanisms discussed in Chapter 1.[13, 14] The photo-revealed carboxylic acid groups generate negative charges in aqueous buffer solutions and result in repulsive interlayer electrostatic forces to

disrupt the PEMs (**Figure 3.2**). This "charge shifting" characteristic renders films soluble only in those areas exposed to light of appropriate wavelengths.

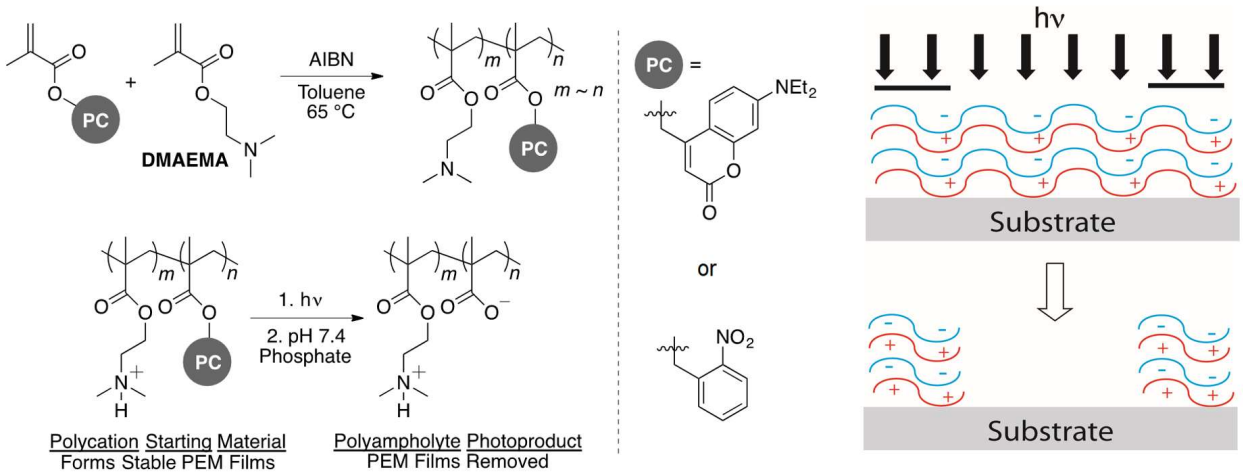

Figure 3.2: Photolysis of polycations generates negatively charged carboxylate groups, disrupting ion-pairing interactions between oppositely charged polyelectrolytes in PEMs and rending the photolyzed PEMs soluble. [13, 14]

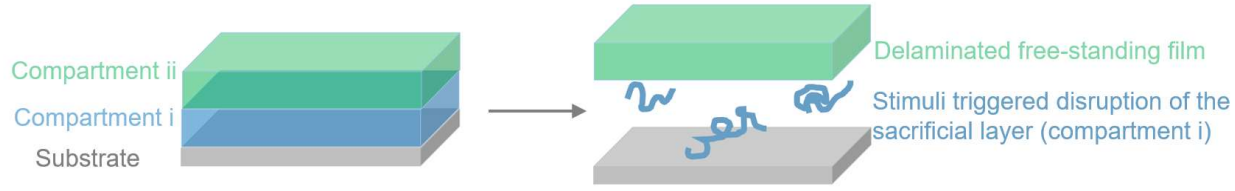

Figure 3.3: Schematic of a stratified film containing two compartments, and the generation of a free-standing film upon stimuli-triggered dissolution of the sacrificial layer.

3.2 Multi-Responsive Free-Standing LBL PEMs

The use of LbL to prepare stratified films, in which groups of bilayers cluster together in compartments at different displacements from the substrate, makes it possible to control the

location of stimuli-responsive moieties within a film. For example, localizing stimulus-responsive moieties in a multilayer film as "sacrificial layers" between a substrate and polymers that do not respond to the stimulus is a route to free-standing thin films (**Figure 3.3**).[12, 15-21] Assemblies of multiple strata, each of which are differentially sensitive to particular stimuli, can yield pre-programmed decomposition of different regions of the film to yield staged decomposition of individual strata, such as the work of Rubner and coworkers with different pH values,[22] and as the group of Sukhishvili demonstrated with layered nanocomposites containing metallic nanoparticles sensitive to different wavelengths of light. [23]

Materials that respond to multiple stimuli can show the same response or different responses upon exposure to different stimuli. A popular and productive approach to multiresponsive materials is to integrate different reactive moieties into individual polymer chains, often taking advantage of controlled and living polymerization techniques.[24, 25] Films prepared by the LbL technique can also respond to multiple stimuli, such polymer/clay LbL films,[26] polymer/gold nanoparticles multilayers,[27] composites of PEGylated nanoparticles and photochromic polymers,[28] and capsules comprising star polyelectrolytes.[29]

Here in Chapter 3.2, we describe two examples of a general approach to designing multiresponsive LBL films that relies on compartmentalizing chemistry in stratified polyelectrolyte multilayer (PEM) films such that different external stimuli perform distinct functions.

3.2.1 Experimental Design and Synthesis of Light-, Chemical Reduction-, and pH- Responsive PEMs

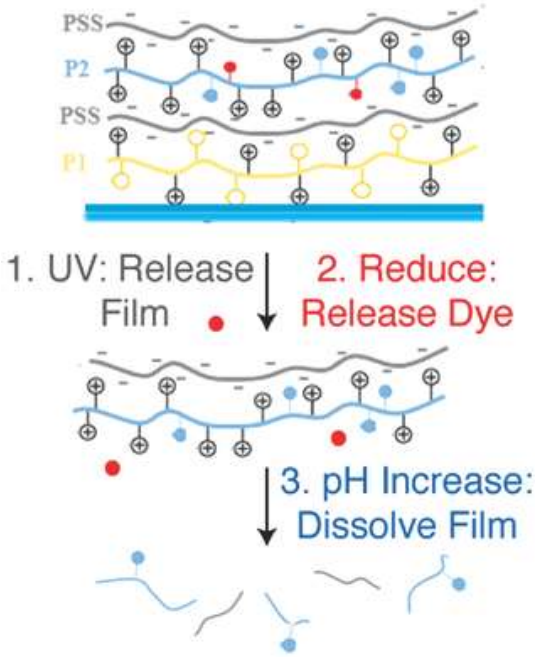

Figure 3.4: Schematic of the multi-responsive PEMs with compartmentalized distribution of chemistry. Each specific external stimulus performs different functions: 1) light enables delamination of a free-standing LBL film, 2) chemical reduction releases a covalently bound dye from the free-standing film, and 3) increase in pH fully dissolves the film.

We focus here on a triple-responsive layer-by-layer film (**Figure 3.4**) in which (i) light enables delamination of a free-standing LBL film, (ii) chemical reduction releases a covalently bound dye from the free-standing film, and (iii) increase in pH fully dissolves the film. We designed a photolabile, charge-shifting polycation **P1** incorporating ONB groups, and a pH/redox dual responsive polycation **P2** bearing rhodamine pendants covalently bond to polymer mainchain through a redox sensitive disulfide bond (**Figure 3.5**). UV exposure can trigger charge-shifting of **P1**, which disrupts ion-pairing interaction in **P1**/poly(styrene sulfonate) (PSS) polyelectrolyte films (*vide supra*). The pH/redox dual responsive **P2** releases the covalently bond rhodamine upon cleavage of disulfide bond triggered by chemical reduction, and gains or losses positive charges upon adjusting pH to lower or higher values because of the protonation or deprotonation of amino groups, respectively. Deprotonation f **P2** under basic conditions (pH > 9.3) can, therefore, disrupt ion-paring interactions between **P2** and PSS, and lead to dissolution of **P2**/PSS PEM films.

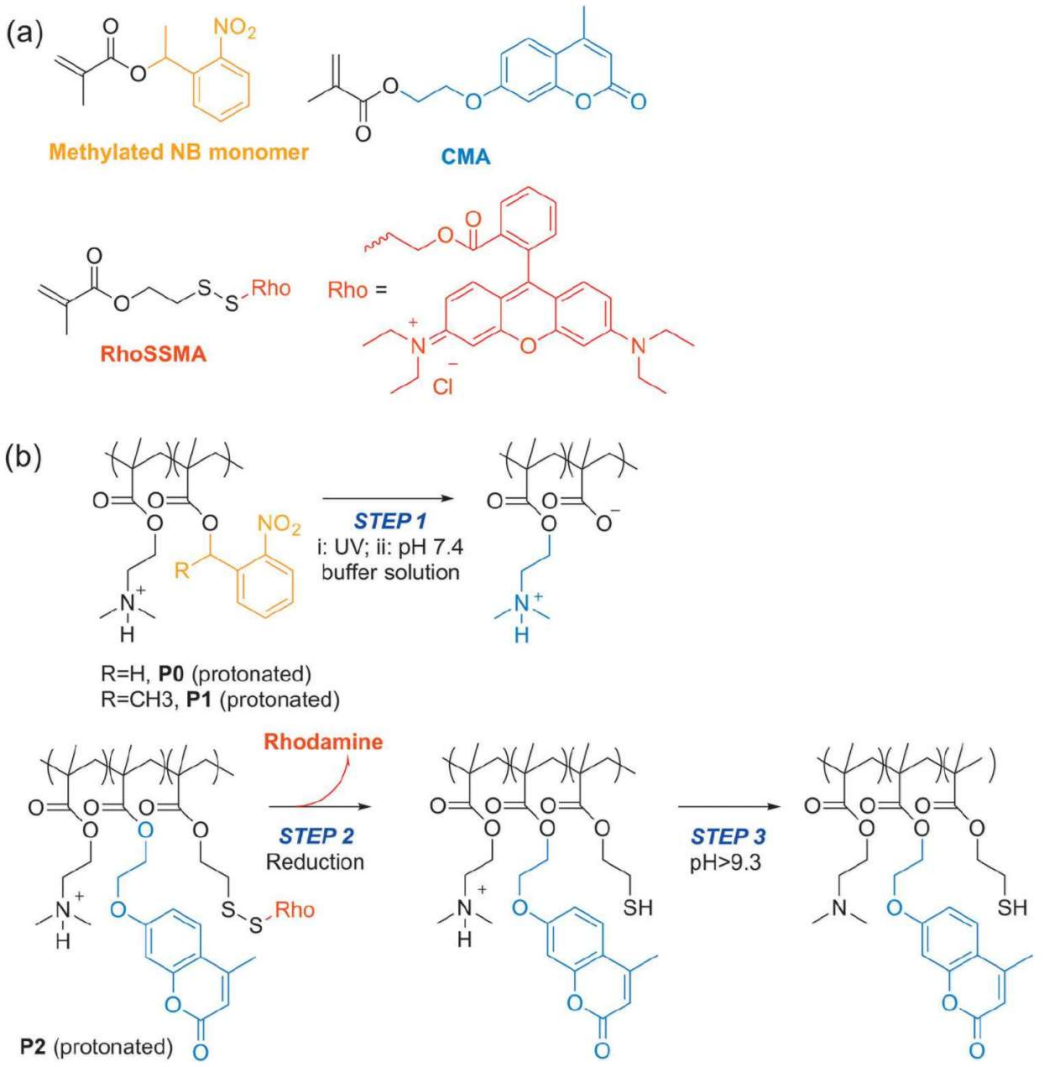

Figure 3.5: (a) Monomers used in this work. (b) Responsive behavior of polycations used in triple-responsive PEM films.

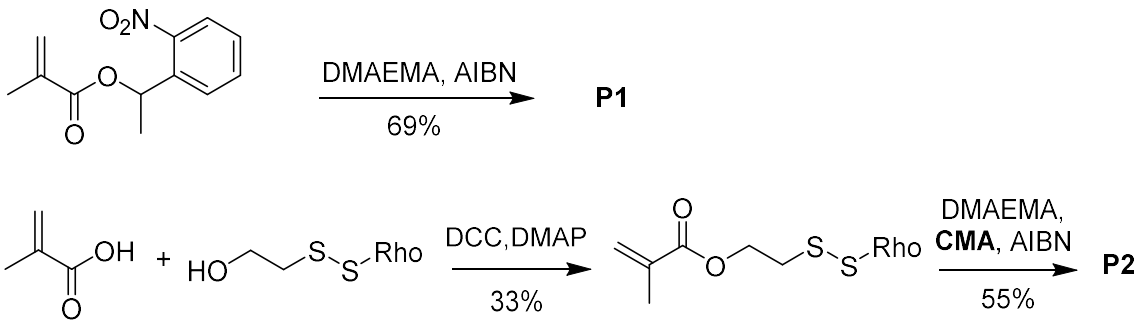

Scheme 3.1: Synthesis of functional polymers **P1** and **P2**.

We synthesized the redox sensitive monomer **RhoSSMA** by reacting a 2-[(2-hydroxylethyl)disulfanyl]ethyl methacrylate with rhodamine B using dicyclohexylcarbodiimide (DCC) and dimethylaminopyridine (DMAP) as the catalyst. **Methylated NB** monomer [30] and the fluorescent monomer **CMA** [31] were synthesized as reported elsewhere. The synthesis of charge-shifting polycation **P1** and dual responsive **P2** were straight forward: free-radical random copolymerization, using AIBN as initiator, of N,N-dimethylaminoethylmethacrylate (DMAEMA) and **Methylated NB** monomer yield the photoresponsive **P1**. Copolymerization of DMAEMA with 0.7% coumarinyl methacrylate (**CMA**), and 0.03% of a **RhoSSMA** yield the redox/pH dual responsive **P2**.

In our design, a stratum of PSS and photodegradable **P1** bilayers is deposited onto a plasma cleaned quartz substrate, onto which an additional stratum of bilayers comprising PSS and the redox/pH dual responsive polycation **P2** is assembled. Alternating immersion of plasma cleaned quartz slides into (1) a 0.2% (w/v) aqueous solution of **P1** or **P2** and (2) a 0.2% (w/v) solution of PSS in 0.1 M NaCl, with intermediate rinsing using deionized water, yielded PEMs that we characterized by UV/vis spectroscopy (**Figure 3.6**). The thicknesses of PEM films reported in this paper increase linearly with average bilayer thicknesses: ~2 nm for **P1**/PSS and about 1.5 nm for **P2**/PSS by AFM. A sacrificial compartment of layers between the rest of the film and the substrate requires suppressed interlayer diffusion of polymer chains during assembly so that individual compartments of the LBL film have independent reactivity and solubility. Here, the linear growth of our PEM films and a bilayer thickness of about 1-2 nm suggest that the degree of layer interpenetration of polymers is limited to 2-3 layers,[14] making it suitable to

produce LBL freestanding films, in which the photolabile **P1**/PSS stratum serves as the sacrificial layer.

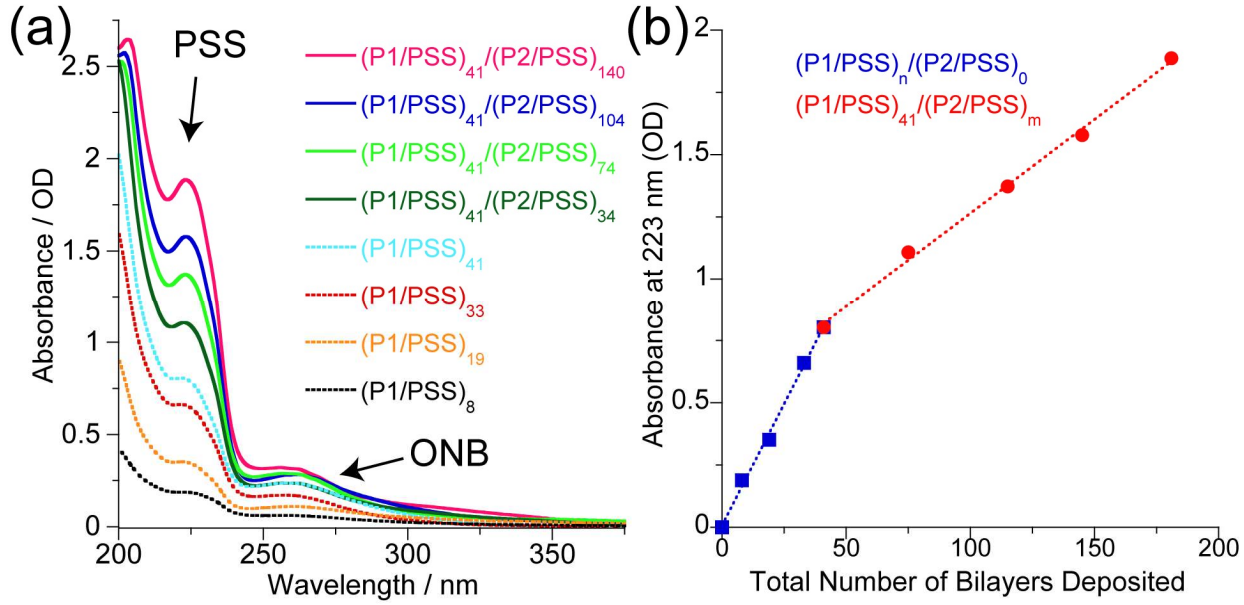

Figure 3.6: (a) UV spectra of PEM films on quartz substrates with varying number of bilayers. (b) Dependence of absorbance at 223 nm on the number of polymer bilayers. The small quantity of coumarin (<1%) precludes its appearance in the UV spectra relative to the larger quantity of the ONB chromophore.

3.2.2 Response of LBL PEMs to Different Stimuli

3.2.2.a Response to Light

Our group previously reported photolabile PEM films based on NB ester groups:[14, 32] photodegradation of ONB groups in **P0** deprotects carboxylate acid groups, generates negative charge in aqueous buffer (**Figure 3.2**), and results in repulsive interlayer electrostatic forces to disrupt the PEM. To enable faster photochemistry, we prepared polycation **P1** that has ONB pendants methylated in the benzylic position, resulting in ONB esters that photochemically

degrade more than five times faster than the unmethylated ONB esters because of increased stability of the key radical intermediate (**Figure 3.7**).

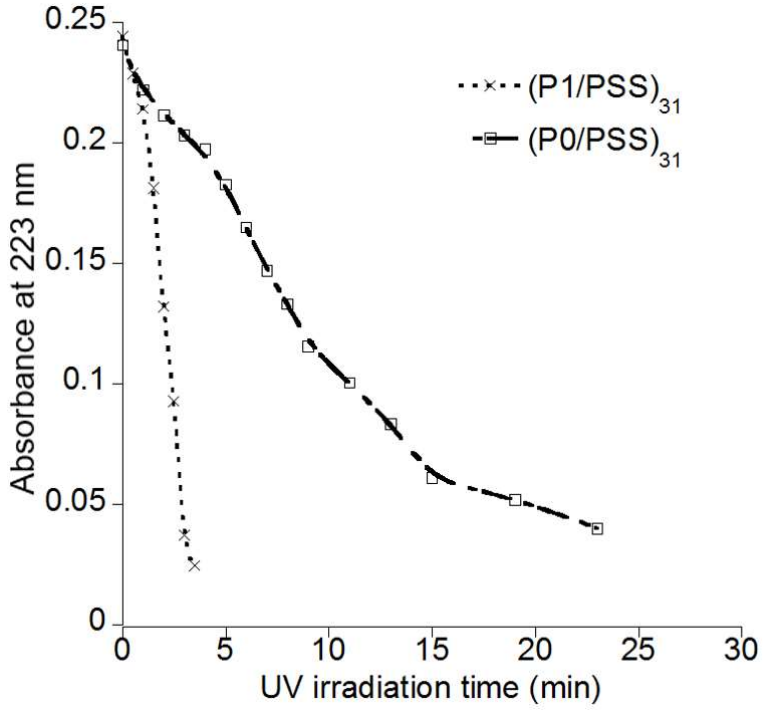

Figure 3.7: Light-induced disruption of photolabile PEMs. Each UV irradiation was followed by 10 min rinsing with pH 7.4 phosphate buffer. PEMs are prepared following the same protocol described in this session, except that DMF solutions of **P1** and **P0** were used in the LBL assembly.

PEM films with a **P1**/PSS stratum adjacent to the quartz substrate and a subsequent **P2**/PSS stratum were irradiated with a 200W Hg/Xe lamp at $\lambda > 295$ nm for 1 hour. Absorption spectra of the double-stratum composite films and of single-stratum photolabile films (**Figure 3.8**), both showed photocleavage of the ONB groups of **P1**. After overnight immersion in pH 7.4 phosphate buffer, the irradiated sacrificial layer dissolved and the remaining **P2**/PSS film could be peeled from the substrate easily as a freestanding PEM film (**Figure 3.9**). A $(\mathbf{P2}/PSS)_{140}$ freestanding film prepared in this manner was ~200 nm thick (**Figure 3.9c**) with a roughness of

~5 nm. Freestanding films obtained in this manner were stored in water, and showed no visible change after two months. Control experiments showed that unirradiated composite films were stable upon immersion (**Figure 3.10**) and did not produce freestanding films. The number of sacrificial bilayers was important in this experiment: 8 sacrificial **P1**/PSS bilayers were not enough to enable delamination of **P2**/PSS PEM after UV irradiation, while 16 **P1**/PSS bilayers were sufficient.

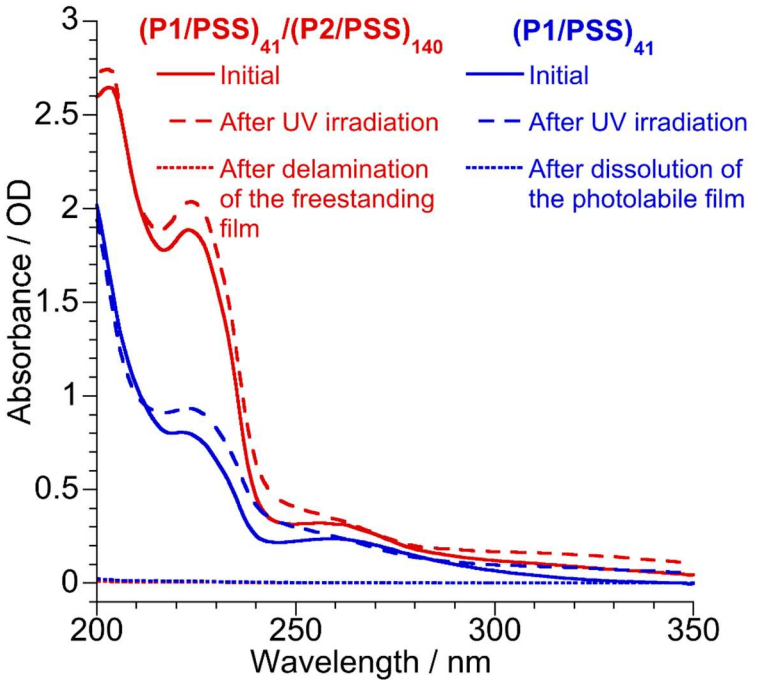

Figure 3.8: UV spectra showing photodegradation of PEMs.

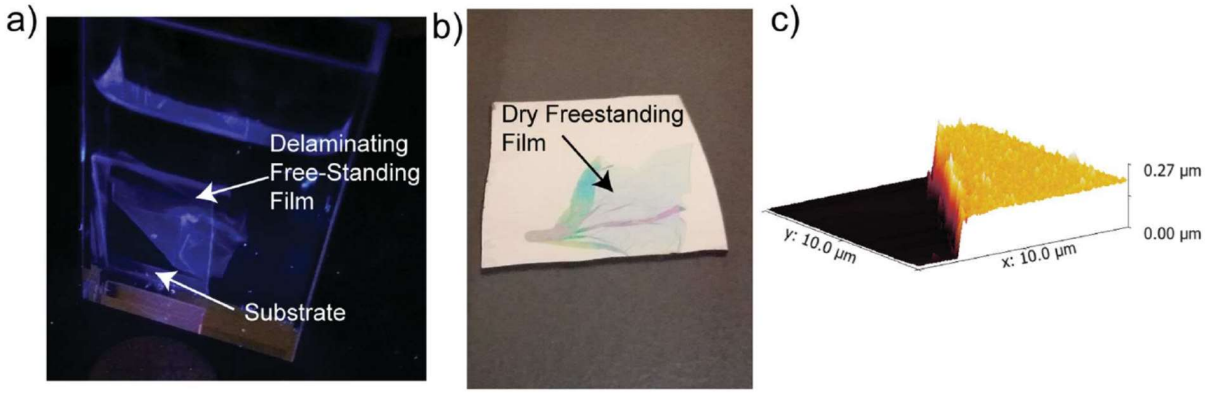

Figure 3.9: Images of free-standing (**P2**/PSS)$_{140}$ films. (a) Optical image of a film delaminating from quartz in buffer solution under UV lamp. (b) Free-standing film on a silica substrate. (c) AFM image.

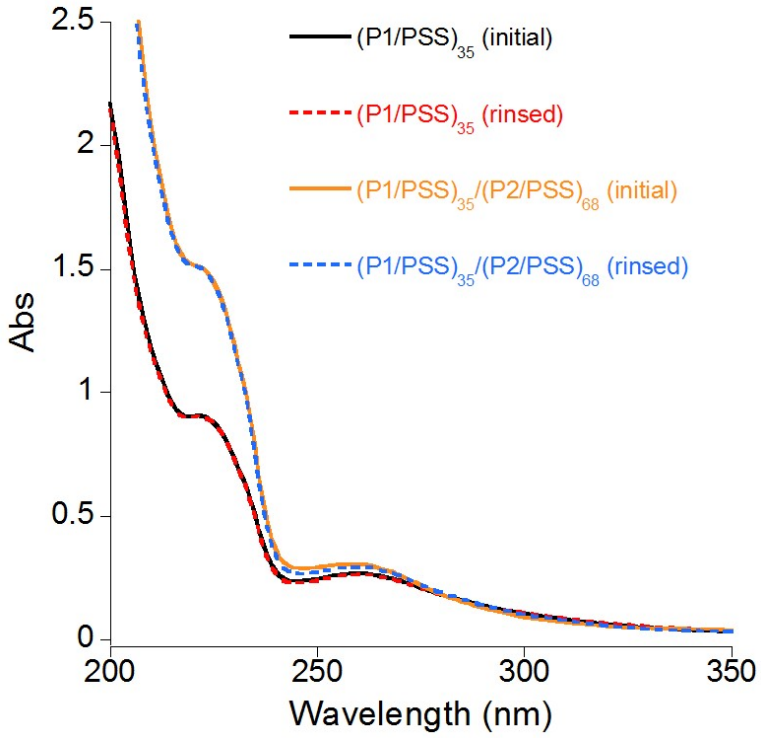

Figure 3.10: UV-vis spectra of unirradiated photolabile **P1**/PSS films and triple responsive (**P1**/PSS)/(**P2**/PSS) composite film before and after being rinsed in 0.1 M pH 7.4 phosphate buffer solution for 10 min.

3.2.2.b Response to Chemical Reduction

As a proof-of-concept demonstration of the triggered release of covalently bound guests from a freestanding film, we used dithiothreitol (DTT) at a concentration of 40 mM to release rhodamine through the well-known nucleophilic attack of DTT thiolate anion on the disulfide bond.[33] This dye had been incorporated into polycation **P2** through covalent disulfide linkages using redox sensitive co-monomer RhoSSMA (Step 2 in **Figure 3.5**). After 7 days of exposure of free standing films as prepared in Step 1, approximately 70% of the rhodamine B bound to the polymer film was released into solution as determined by fluorescence spectroscopy (**Figure 3.11**). Three pieces of evidence confirm that dissolution of polymer chains did not cause this release: i) films treated with DTT show no change visually; ii) almost no fluorescence from coumarin, which was another fluorescent label on **P2** but not bound to the backbone through disulfides, was observed in solution (**Figure 3.11c**); iii) control experiments show that the release of rhodamine is more than a magnitude slower without DTT than with DTT (**Figure 3.11b**). Together, these results support that the cargo covalently bound to freestanding film can be released selectively without further disruption of the film.

3.2.2.c Response to Changes in pH

Under basic conditions, the otherwise protonated ammonium groups of **P2** in the freestanding film deprotonate and convert from positively charged ammonium ions to neutral amines, resulting in negative net charge of the polymer film. The resulting electrostatic repulsion between the polymers in the multilayer film dissolves the freestanding films (Step 3 in **Figure 3.5**). These films were stable over the period of observing time over hours at pH $\leq$ 8.8, but were observed to dissolve in seconds when exposed to solutions with pH $\geq$ 9.3. In addition, the

fluorescence intensities from coumarin in solution increased immediately after adding Na_2CO_3 to a concentration of 0.1 M into the solution containing the freestanding film due to dissolution of the film (**Figure 3.11c**).

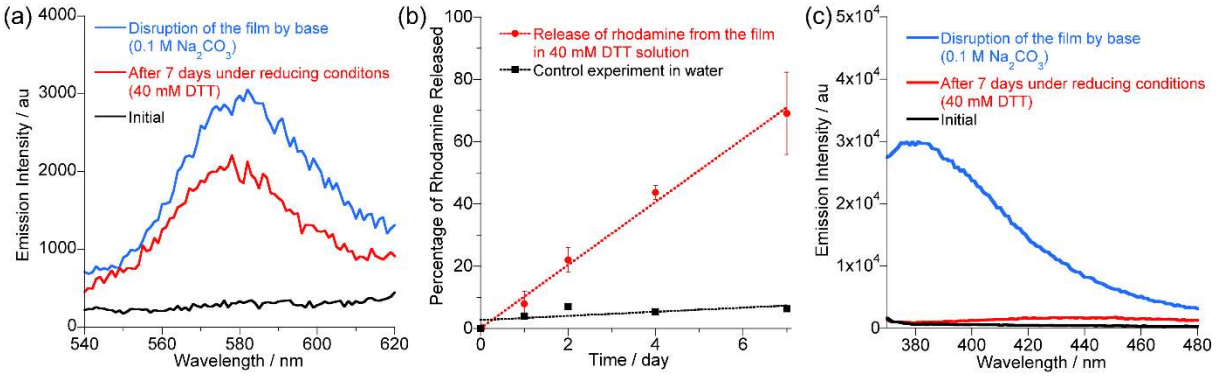

Figure 3.11: (a) Fluorescence spectra (λ_{ex} = 520 nm) showing selective release of rhodamine from free-standing film. (b) Dependence of rhodamine release on time. Error bars show standard deviation of the results from 3 experiments. (c) Fluorescence spectra excited at 320 nm showing coumarin labeled **P2** only dissolved after increasing pH to 9.3

3.2.3 General Approach to Stimuli-Responsive Free-Standing PEMs – Another Example: Photodisruptable Free-Standing PEMs

This general approach for fabricating stimuli-responsive, free-standing films by compartmentalizing different materials in stratified PEM films is more broadly applicable than the above described combination of three stimuli. To demonstrate the potential breadth of this approach, we prepared photodegradable free-standing films by fabricating a dual-compartment film in which both strata respond to light. The sacrificial compartment closest to the substrate comprised **P1** (deposited at pH 6.0) and poly (methacrylic acid) (deposited at pH 5.0), and, therefore, responded to irradiation at 365 nm. A second compartment, only responsive to $\lambda < 350$

nm, comprising bilayers of poly (methacrylic acid) (PMAA) and **P3** (**Figure 3.12**), has photolabile p-methoxyphenacyl esters, derived from the corresponding methacrylate monomer 4-methoxyphenacyl methacrylate (MPMA), which cleaves by a photoreduction mechanism. A combination of nitrobenzyl and phenacyl photocleavable groups has been identified as a pair of wavelength-selective photocleavable groups.[34] Our results with separately prepared, single compartment PEMs incorporating **P1** or **P3** also suggested good photo-selectivity between phenacyl and ONB containing PEMs (**Figure 3.13**): upon exposure to same dose of irradiation at λ = 365 nm, a (**P1**/PMAA) was rendered soluble in rinsing solution, while (**P3**/PSS) or (**P3**/PMAA) films showed negligible spectral change before and after rinsing.

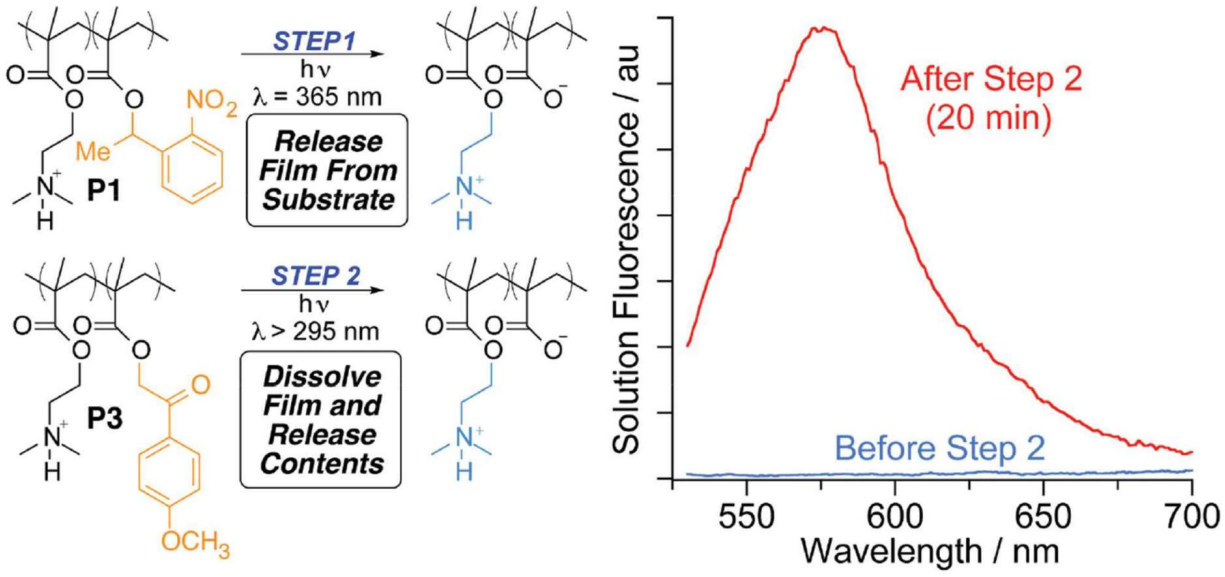

Figure 3.12: *Left*: Steps in using different wavelengths of light to (i) delaminate from a quartz substrate, and (ii) render soluble a free-standing film comprising **P3**/PMAA bilayers. *Right*: Release of rhodamine-functionalized PEI that had been blended in a free-standing film of (**P3**/PMAA) at 2% (w/w) with **P3** in the polycation solution used in film assembly.

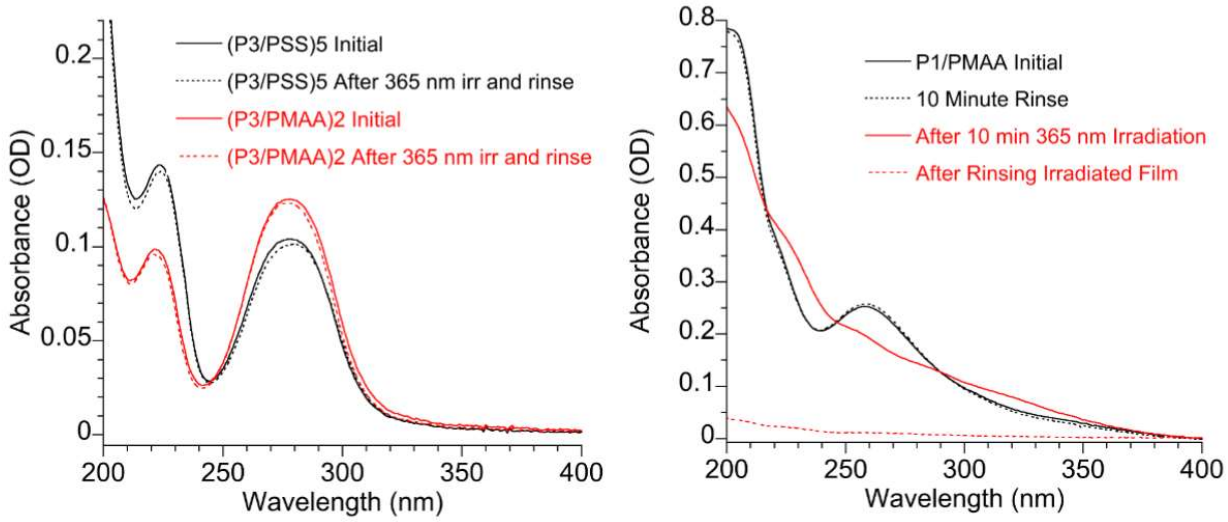

Figure 3.13: Left: Resistance of P3-based PEMs to irradiation at 365 nm. Right: Degradation of **P1**/PMAA PEMs in response to irradiation at 365 nm.

PEM films of **P1** or **P3** with PMAA deposited at pH 5.0 showed a linear response of UV–vis absorbance as a function of number of bilayers deposited (**Figure 3.14**), and resulted in films with a per-bilayer thickness four times greater than those prepared with PSS as determined by AFM (the thicknesses of a (**P3**/PSS)$_9$ film and a (**P3**/PMAA)$_6$ were 27 ± 3 nm and 76 ± 4 nm, respectively), decreasing the number of bilayers that must be deposited for any target film thickness.

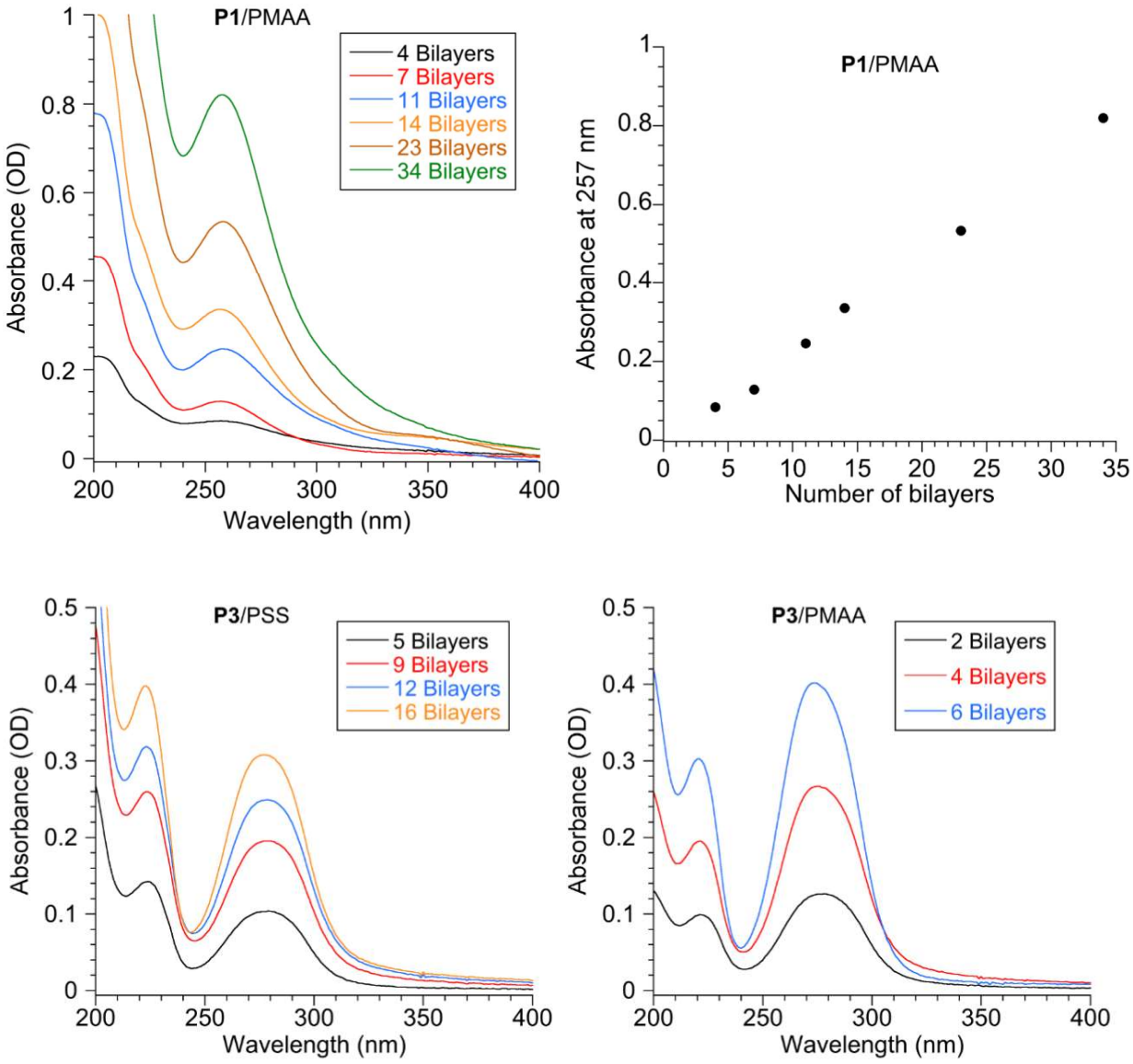

Figure 3.14: Linear dependence of absorbance of **P1**/PMAA or **P3**/PMAA PEM films as a function of number of bilayers.

Irradiation of (**P1**/PMAA) / (**P3**/PMAA) films at 365 nm for 10 min caused **P1**/PMAA layers to dissolve in pH 7.4 phosphate buffer, but left **P3**/PMAA compartments intact as UV-responsive free-standing films. These free-standing films were stable in pH 7.4 phosphate buffer in the dark, but dissolved when irradiated at $\lambda > 295$ nm at 18 mW cm^{-2} for 20 min, which we

confirmed both visually (**Figure 3.15**) and through fluorescence spectroscopy (**Figure 3.12** *right*) of released rhodamine-functionalized poly (ethylene imine) (PEI) that had been included in the polycation deposition solution at a level of 2% (w/w) relative to **P3**.

Figure 3.15: Photographs showing dissolution of pieces of free-standing film of **P3**/PMAA in pH 7.4 phosphate buffer (0.1M) upon irradiation with λ > 295 nm.

3.2.4 Conclusions

Chapter 3.2 demonstrates a versatile method to prepare free-standing PEM films and shows that these films can release covalently bound and physically trapped cargo upon stimuli-induced disruption of covalent bonds or non-covalent ion-pairing interactions. The simple process of layer-by-layer self-assembly enables nanoscale spatial separation of different stimuli-responsive chemistries with polymers prepared by straightforward and scalable techniques. The two examples shown here use stimuli that are all popular for the release of molecular cargo—light, chemical reduction, and pH. We expect that this general approach to multiresponsive materials, in which different stimuli perform discrete operations based on both location of responsive chemistries within a material defined by LbL and chemical structure will be advantageous for the next-generation approaches to applications that multiresponsive materials

have targeted, such as drug delivery and other controlled or triggered release applications, membranes, and logic operations.

3.2.5 Experimental Section

General Considerations

All synthetic manipulations were performed under standard air-free conditions under an atmosphere of argon gas with magnetic stirring unless otherwise mentioned. Flash chromatography was performed using silica gel (230–400 mesh) as the stationary phase. NMR spectra were acquired on a Bruker Avance III 500 or a Bruker DPX-300 spectrometer. Chemical shifts are reported relative to residual protonated solvent (7.26 ppm for $CHCl_3$). All reactants and solvents were purchased from commercial suppliers and used without further purification, unless otherwise noted. Dry tetrahydrofuran (THF) and dry dichloromethane (CH_2Cl_2) were obtained from an Innovative Technologies PureSolv 400 solvent purifier. Molecular weight distributions of polymers were determined using a Shimadzu gel permeation chromatograph with a mobile phase of 2% triethylamine in THF at 0.75 mL min^{-1}. Polystyrene standards (Tosoh) were used for calibration. All solution optical spectra were acquired of samples in quartz cuvettes (NSG Precision Cells). Electronic absorbance spectra were acquired with a Varian Cary-100 instrument in double-beam mode using a solvent-containing cuvette for background subtraction spectra of solution samples. Fluorescence emission spectra were obtained by using either a PTI Quantum Master 4 equipped with a 75 W Xe lamp. Topographical data was acquired using an Asylum Research MFP-3D Atomic Force Microscope (Santa Barbara, CA). Scanning was performed in contact mode with a silicone cantilever, nominal spring constant $k = 2\ N\ m^{-1}$. RMS roughness values were calculated from the AFM scan data using Gwyddion 2.40. Solutions used in the

fabrication, processing and response of films were all aqueous solutions unless otherwise mentioned. All the free-standing films studied in the redox/pH responsive experiments comprise 140 **P2**/PSS bilayers.

LbL Assembly Conditions

Quartz slides (Advalue Technologies) were cleaned with lint-free cloths to remove debris and then plasma cleaned with a Harrick Plasma Cleaner (PDC-32G) for 2 min. LbL assembly was performed with a Midas III Automated Slide Stainer. Slides were first immersed in a positively charged polymer solution (0.30 g polymer in 150 mL of H_2O with 1 equiv. of HCl, unless otherwise mentioned) and then rinsed in deionized (DI) water (500 mL min^{-1}) for 10 min. Next, the slides were immersed in poly(styrene sulfonate) solution (0.30 g polymer in 150 mL 0.1 M NaCl) or poly(methacrylic acid) solution (0.30 g polymer in 150 mL 0.1 M NaCl at pH 5.0) for 10 min and then rinsed in DI water (500 mL min^{-1}) for 10 min. This process was repeated until the desired number of layers was added.

Photogeneration of Free-Standing PEM Films

UV irradiations were performed with a 200W Hg/Xe lamp (Newport-Oriel) equipped with a condensing lens, recirculating water filter, manual shutter, and either (i) a 295 nm longpass (Newport Corporation) or (ii) a 365 nm interference filter (Semrock) at fixed positions in the light path. After irradiation, films with **P1**/PSS or **P1**/PMAA sacrificial compartments were then immersed in 0.1 M pH 7.4 phosphate buffer solution overnight. The edges of the films were scratched with a knife to facilitate the delamination of the film from the substrate. Experiments varying the number of sacrificial bilayers show that after irradiation free-standing

films could be easily removed from the substrate if 16 or more **P1**/PSS bilayers were deposited as sacrificial layers, while **P2**/PSS films deposited over eight **P1**/PSS sacrificial bilayers could not be delaminated after irradiation under the same condition. As few as two **P1**/PMAA bilayers enabled delamination of **P3**/PMAA films. The minimal and maximal numbers of **P2**/PSS bilayers assembled on top of the bottom stack we tried were 70 and 220, and both yielded free-standing films. Free-standing films comprising fewer of bilayers were more fragile than those comprising more bilayers. Irradiating the films at 365 nm (7 mW cm^{-2}) for 20 min followed by immersing the irradiated composite film in pH 7.4 buffer solution for < 10 min is enough to generate free-standing films, although some of the films studied in this article were prepared by irradiating the composite film at $\lambda > 295$ nm (18 mW cm^{-2}) for 1 h and then immersing the film in buffer solution overnight.

Redox Responsive Experiments Monitored by Fluorescence Spectroscopy

Each set of experiments started with transferring about 1 cm^2 of the free-standing film into a quartz cuvette containing about 3 mL DI water. The cuvette was left undisturbed to allow the free-standing film to sink to the bottom of the cuvette before each spectrum acquisition. When adding DTT into a cuvette containing free-standing film in deionized water, the proper amount of DTT solid was measured into a 1 mL vial, into which was added a small amount of water transferred from that cuvette with a pipette. After DTT was fully dissolved, all the DTT solution in the vial was transferred back into that cuvette containing the films, yielding a final concentration of DTT of 40×10^{-3} M. This operation ensured the concentration of substances in that cuvette to be maintained the same before and after adding DTT. The fluorescence emission of the solution in the cuvette was tracked by fluorescence spectroscopy.

pH Responsive Experiments

After each seven-day-long redox responsive experiment, Na_2CO_3 was added to the cuvette in a similar way as adding DTT described above (final concentration of Na_2CO_3: 0.1 M). Visually, the free-standing films immediately disappeared after adding Na_2CO_3. Fluorescence emission spectra were also collected before and after adding Na_2CO_3. pH dependent responsiveness of the free-standing film was also investigated by using 0.1 M buffer solutions of different pH values. The pH responsiveness of free-standing films of **P2**/PSS was studied by exposing free-standing films to pH 7.4 phosphate buffer solution, pH 8.4 tris-HCl buffer solution, pH 8.8 tris-HCl buffer solution, pH 9.3 $NaHCO_3/Na_2CO_3$ buffer solution, 0.1 M $NaHCO_3$ and 0.1 M Na_2CO_3 solution, monitored both by visual inspection of the film as well as through fluorescence spectroscopy measurements. No change was observed for free-standing films exposing to 0.1 M $NaHCO_3$ solution or buffers of pH 7.4, pH 8.4, and pH 8.8. The film dissolved seconds after rinsing in pH 9.3 buffer or 0.1 M Na_2CO_3 solution.

Dual Photochemically Responsive Film

A free-standing film of (**P3**/PMAA)$_{20}$ with 2% rhodamine-PEI was fabricated as described for other free-standing films above using 365 nm irradiation. Approximately 1 cm^2 of this film was immersed in 1.5 mL of 0.1 M phosphate buffer, pH 7.4, in a quartz cuvette. Irradiation was performed using a 295 nm long-pass filter (total incident power density ≈20 mW cm^{-2}). A control experiment in which a free-standing film was kept in the dark showed no observable fluorescence from released rhodamine.

Synthesis

Rhodamine-labeled PEI, **MNBMA**, **CMA**, 2-[(2-hydroxyethyl)disulfanyl]ethyl methacrylate, and **MPMA** were synthesized as reported elsewhere.[30, 31, 35-37]

RhoSSMA: To a 100 mL three neck round bottom flask was added 2-[(2-hydroxyethyl)disulfanyl]ethyl methacrylate (0.40 g, 1.8 mmol), rhodamine B (0.45 g, 0.94 mmol), dimethylaminopyridine (DMAP) (0.050 g, 0.41 mmol), and dry THF (25 mL), stirred. A THF solution of dicyclohexylcarbodiimide (DCC) (0.50 g, 2.4 mmol) was added dropwise into the flask at 0 °C. The reaction mixture was then allowed to warm to ambient temperature and stirred overnight. The reaction was filtered and washed with Na_2CO_3, brine and water, dried over Na_2SO_4, filtered, and concentrated using a rotary evaporator. The crude product was purified via flash chromatography using ethyl acetate: CH_2Cl_2:methanol (3:3:1 v:v:v) as eluent to yield 0.4 g dark purple solid as a crude product ($R_f \approx 0.15$). The crude product was further purified via flash chromatography using CH_2Cl_2:isopropanol:ethyl acetate: TEA in a volumetric ratio of 1:1:1:0.15 as eluent to yield RhoSSMA as a dark purple solid. Fractions eluted from the column were monitored by NMR occasionally to distinguish the desired product from an impurity. Yield: 0.22 g (33%). ^{1}H NMR (500 MHz, $CDCl_3$): δ 8.33–8.30 (m, 1 H), 7.84–7.80 (m, 1 H), 7.76–7.72 (m, 1 H), 7.34–7.30 (m, 1 H), 7.09–7.05 (m, 2 H), 6.93–6.87 (m, 2 H), 6.87–6.84 (m, 2 H), 6.10 (s, 1 H), 5.59–5.57 (m, 1 H), 4.40–4.20 (m, 4 H), 3.50–3.80 (m, 8 H), 2.90–2.80 (m, 2 H), 2.80–2.70 (m, 2 H), 1.92 (s, 3 H), 1.40–1.10 (m, 12 H). ^{13}C NMR (125 MHz, $CDCl_3$): δ 167.1, 164.9, 158.4, 157.8, 155.6, 135.9, 133.6, 133.3, 131.6, 131.5, 131.3, 130.4, 129.7, 126.2, 114.3, 113.6, 96.6, 63.0, 62., 46.2, 37.0, 36.9, 18.3, 12.7.

P1: In a 50 mL round bottom flask, 15 mL toluene solution of DMAEMA (0.50 g, 3.2 mmol), MNBMA (0.69 g, 2.9 mmol) and azobisbutyronitrile (AIBN) (12 mg, 0.073 mmol, 1

wt.%) was purged with argon gas for 20 min. The solution was stirred at 60 °C overnight. The reaction was cooled to room temperature, and precipitated into hexane. The precipitate was collected by filtration. The yellow crude product was dissolved in CH_2Cl_2, and the precipitation was repeated a second time. **P1** was obtained as light yellow solid. Yield: 0.82 g (69%). ^{1}H NMR (500 MHz, $CDCl_3$): δ 8.0–7.8 (broad, 1 H), 7.8–7.3 (broad, 3 H), 6.4–5.8 (broad, 1 H), 4.2–3.7 (broad, 2 H), 2.7–2.3 (broad, 2 H), 2.3–2.1 (broad, 6 H), 2.1–1.4 (broad, 4 H), 1.1–0.3 (broad, 9 H). M_n = 11 kDa, M_w = 20 kDa.

P2: In a 100 mL round bottom flask, DMAEMA (2.0 g, 13 mmol), CMA (25 mg, 0.087 mmol), RhoSSMA (3.0 mg, 0.0044 mmol), and AIBN (20 mg, 0.12 mmol, 1 wt.%) in 25 mL of *N,N*-dimethylformamide (DMF) was sparged with argon gas for 20 min. The solution was stirred at 60 °C overnight. The reaction was then cooled to room temperature and precipitated into hexane. The hexane was decanted and the remaining sticky oil was redispersed in dichloromethane. This precipitation protocol was repeated three additional times to yield a gummy oil. After drying in a vacuum oven overnight, **P2** was obtained as a pink solid. Yield: 1.1 g (55%). ^{1}H NMR (500 MHz, $CDCl_3$): δ 4.2–3.9 (broad, 2 H), 2.7–2.4 (broad, 2 H), 2.3–2.1 (broad, 6 H), 2.1–1.4 (broad, 2 H), 1.1–0.7 (broad, 3 H). M_n = 30 kDa, M_w = 82 kDa.

P3: This polymerization followed a procedure identical to that used for the synthesis of **P1**, except MPMA was used as the monomer instead of MNBMA. ^{1}H NMR (500 MHz, $CDCl_3$) (all resonances broad): δ 7.9–7.7, 7.0–6.7, 5.5–5.1, 4.2–4.0, 3.9–3.8, 2.8–2.5, 2.3, 2.3–1.4, 1.3–0.9. M_n = 25 kDa, M_w = 37 kDa.

3.3 Multi-Level Photopatterning and Programmable, Light-Controlled Release from Photoresponsive PEMs Incorporating Four Photocleavable Groups

The above sub-chapter (Chapter 3.2) describes the application of LBL deposition technique to fabricate multi-responsive stratified films with well-defined, two-compartment architectures, where each of the stimuli performs different functions by disrupting covalent bonds or non-covalent intermolecular forces in the films. This is a general approach to multi-responsive films, in which different stimuli perform discrete operations based on both location of responsive chemistries within a material defined by LbL and chemical structure. Here in Chapter 3.3, we further exploited this approach to develop multi-responsive hybrid PEMs: we describe quadruple-stratified photoresponsive LBL films comprising four spatially confined photodisruptable compartments, each of which responds to different wavelengths of light with different sensitivities. Sequential, photo-controlled disruption of interlayer ion-pairing interactions, and the consequential photo-triggered dissolution of multilayers comprising different materials was performed in a predetermined order under controlled irradiation conditions, yielding wavelength-dependent control over film thicknesses. The spatial arrangement of materials perpendicular to the surface, together with the spatiotemporal distribution of different wavelengths of light on the surface, allows for photo-patterning of films to yield complex micropatterns with multi-level thickness using this approach. We also demonstrate orthogonal release of fluorescent guest molecules from four different samples of photolabile PEM coated microspheres, with each sample of microspheres coated with different photolabile PEM films.

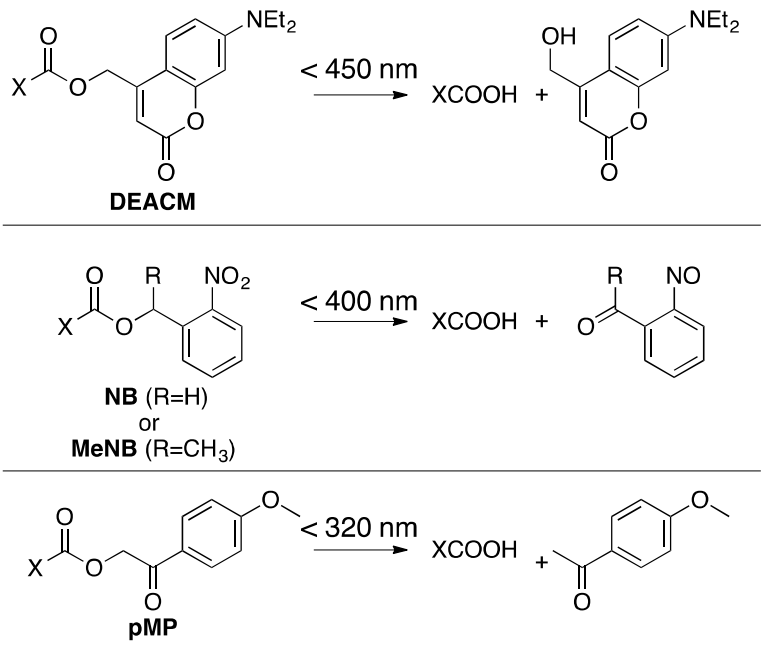

Figure 3.16: Photolysis of the four PPGs used in Chapter 3.3.

3.3.1 Design and Synthesis of a Series of Photolabile PEMs

Inspired in part by the work of del Campo and coworkers, [38] we used a known combination of three families of photocleavable protection groups (PPGs) that absorb light in different wavelength ranges as photolabile methacrylate esters to enable wavelength-selective reactivity as shown in **Figure 3.16**: i) dialkylaminocoumarin (DEACM) groups ($\lambda < 450$ nm), ii) *ortho*-nitrobenzyl (ONB) groups ($\lambda < 400$ nm), and iii) *para*-methoxyphenacyl (PMP) groups ($\lambda < 320$ nm). In a conceptually different approach to enable a fourth level of photolytic selectivity, we used two derivatives of the ONB family that have similar absorbance spectra but different quantum yields of photocleavage: the 2-nitrobenzyl ester (NBE) unsubstituted at the benzylic position, and the α-methyl-2-nitrobenzyl ester (MNBE), which has a methyl group at the benzylic position; the quantum yield of photolysis of the MNBE group is approximately 5 times higher than the quantum yield of photolysis of the unsubstituted NBE group,[39, 40] which we

attribute to increased radical stabilization at the benzylic position from the methyl group of MNBE.

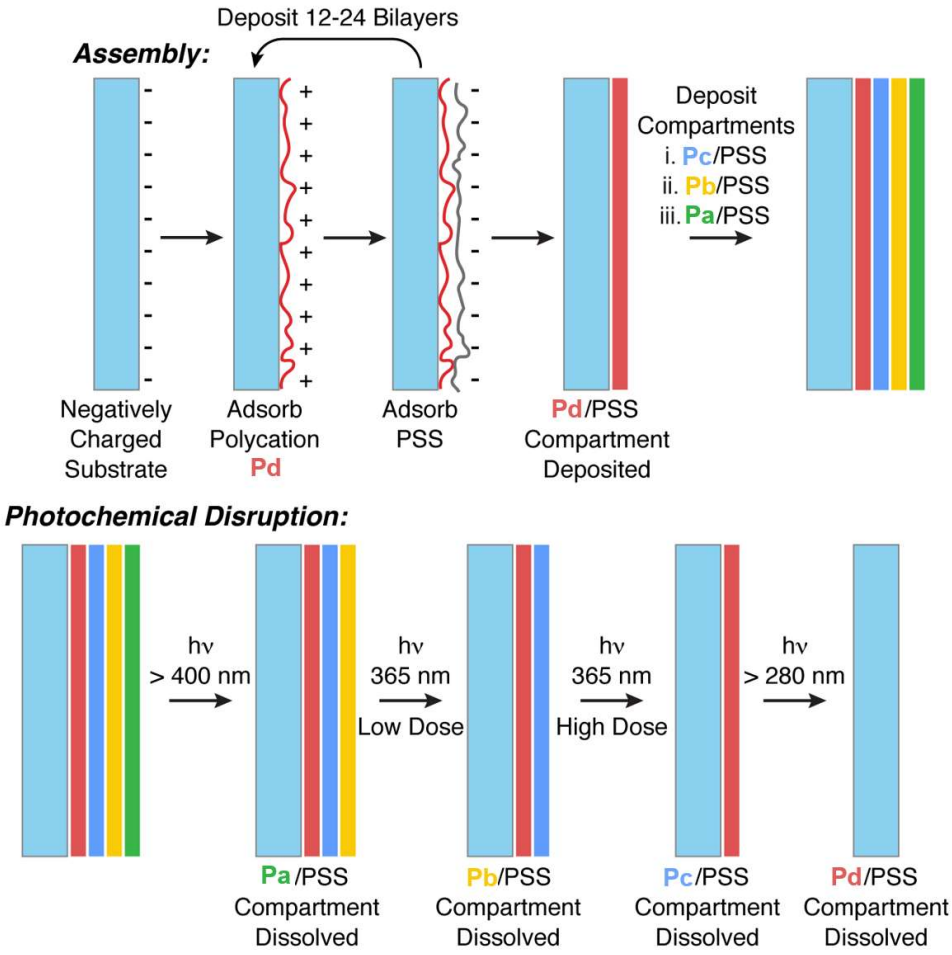

Figure 3.17: *Top*: Bottom-up deposition of hybrid PEMs incorporating four different photocleavable chromophores on a quartz slide substrate through LbL self-assembly. *Bottom:* Top-down light-controlled removal of compartments from the substrate through wavelength-selective photo-triggered disruption of the multilayers. For clarity, the schematic only shows PEMs on one side of the planar quartz substrate, and uses colored blocks to represent compartments each comprising multiple bilayers (Green: **Pa**/PSS; Yellow: **Pb**/PSS; Blue: **Pc**/PSS; Red: **Pd**/PSS).

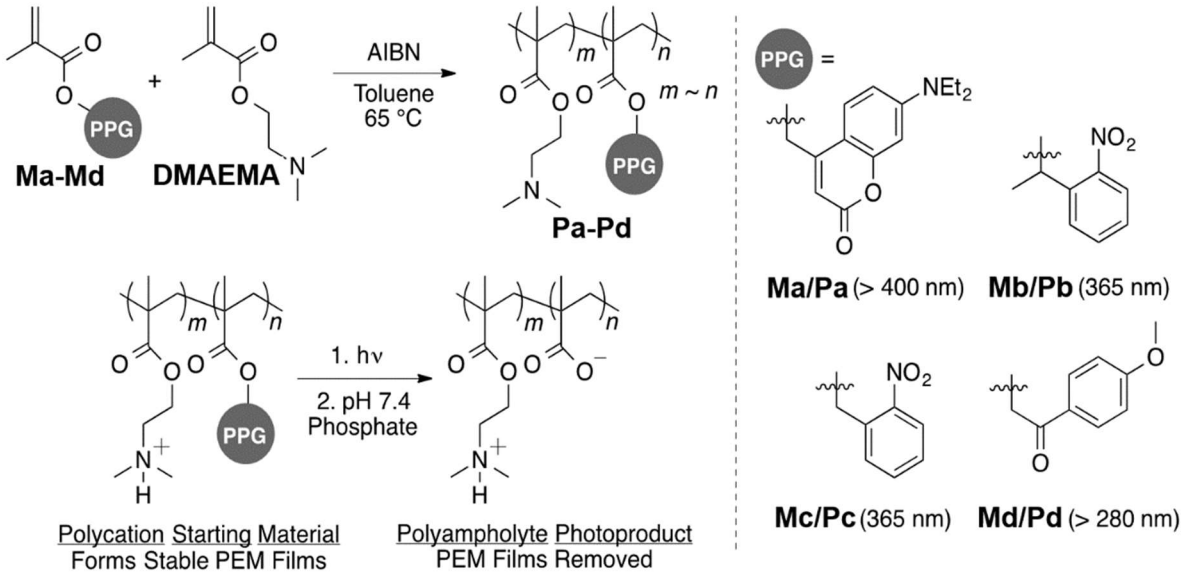

Figure 3.18: Synthesis and photochemical degradation of photolabile polycations in water.

As shown in **Figure 3.17**, our overall design strategy is to integrate each of these polymers into different compartments of LbL films, such that different compartments can be removed from the substrate through selective photodisruption of intermolecular forces under controlled irradiation conditions. We, therefore, designed a series of random copolymers comprising cationic side chains and neutral photocleavable esters that, upon photolysis, yield carboxylic acid groups (**Figure 3.18**). Polycations **Pa**-**Pd** (for clarity, compounds **P3**, **P1**, and **P0** used in Chapter 3.2 are renamed as **Pa**, **Pb**, **Pc** in Chapter 3.3) were prepared via free radical random copolymerization of commercially available monomer *N,N*-dimethylaminoethyl methacrylate (DMAEMA) with 1:1 stoichiometric ratios of photocleavable methacrylate monomers (**Ma**-**Md**) using AIBN as the initiator (**Figure 3.18** and **Table 3.1**). The cationic residues enable ion pairing interactions with negatively charged groups of the polyanion to assist in the formation of PEM films, and render these photoreactive polymers sufficiently soluble in water for all-aqueous processing. The carboxylic acid photoproducts of these polymers become

negatively charged after deprotonation at neutral or basic pH. In these experiments, we used commercially available poly(styrene sulfonate) (PSS) as the polyanion to assemble PEMs with polycations **Pa**-**Pd**. Based on our previous work[14, 35, 41] with this class of polycations incorporated in PEM films, the photoproduct carboxylates disrupt inter-chain interactions sufficiently such that the photolyzed films dissolve in basic or near neutral aqueous solutions.

Table 3.1: Monomer incorporation, based on ^{1}H NMR, and molecular weight distribution statistics (based on GPC in 2% triethylamine in THF) of the photoreactive polymers **Pa**-**Pd**.

Sample	DMAEMA: **Ma-Md**		Mn, kDa	Mw, kDa
	Feed	Incorporation		
Pa	1:1	50% : 50%	11	15
Pb	1:1	50% : 50%	11	20
Pc	1:1	50% : 50%	15	45
Pd	1:1	42% : 58%	25	37

Absorbance spectra of polymers **Pa**-**Pd** (**Figure 3.19**) and previous reports[42-44] reveal that wavelength-selective excitation of DEACM group, ONB groups and pMP group is possible. DEACM has strong absorption over 400 nm ($\varepsilon_{400} \approx 4600$ M^{-1} cm^{-1} [43]). In contrast, ONB groups have local absorbance maxima around 262 nm, molar extinction coefficient values of 100-300 M^{-1} cm^{-1} 365 nm, which approach zero at around 400 nm. pMP groups only absorb deep UV light efficiently (ε_{280nm}=15,000 M^{-1} cm^{-1}) but are essentially transparent at longer wavelengths (λ > 320 nm). In addition to taking advantage of substantially different absorbance spectra of DEACM, ONB, and pMP groups, we introduced a fourth level of selectivity through the higher quantum yields for photolysis of MNBE relative to NBE: this difference in quantum yield has enabled, for example, selective photocleavage of crosslinkers in photolabile hydrogels.[39] Such

different efficiencies of photolysis of these PPGs at different wavelengths suggest the possibility of selective degradation of polycations **Pa**-**Pd**, and therefore, selective disruption of LBL films comprising these photolabile polycations: the DEACM containing polycation **Pa** can be selectively photodegraded under visible light irradiation ($\lambda > 400$ nm) while other polycations will remain essentially unreacted. Similarly, the ONB groups in **Pb** or **Pc** can be photocleaved upon exposure to ~365 nm light with negligible photo-degradation of **Pd** incorporating the deep UV ($\lambda < 320$ nm) sensitive pMP groups. Between the two polycations comprising ONB groups, selective photodegradation of **Pb** or **Pc** can be realized because MNBE has higher photolysis efficiency than NBE. Indeed, selective photo-disruption of these PEMs was successfully performed as discussed in the following sections.

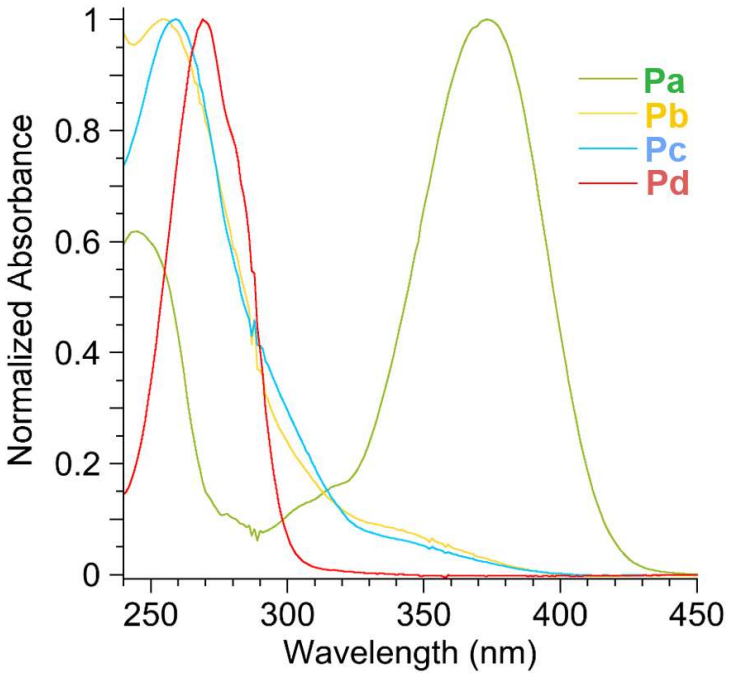

Figure 3.19: Normalized UV/vis spectra of photolabile polycations in water.

3.3.2 PEMs Deposition via LBL Self-Assembly

Photolabile PEMs were successfully deposited on plasma cleaned quartz slides by alternating immersion of the substrate into one of **Pa**-**Pd** at pH 6.0 and a PSS solution, as described in Chapter 3.3.6 (Experimental Section). The ion pairing between the oppositely charged polyelectrolytes, together with van der Waals and hydrophobic interactions, provided the driving force for assembly.[45] The layer-by-layer formation of PEMs can be highly sensitive to parameters such as polymer structure, molecular weight, charge density along polymer chains, polyelectrolyte concentration, and ionic strength.[12, 46-57] It is known that partially charged weak polyelectrolytes favor loopy arrangements of chains, which provides more ion association sites, and thus allows for increased bilayer thickness. [50-54, 58] In order to build thick PEMs, we: (1) used polycation solution of pH 6, as at this pH the partially charged polycations were sufficiently soluble in aqueous solutions, and (2) used NaCl (0.1 M) in polyelectrolyte solutions, as increased ionic strength can also increase average bilayer thicknesses.[52]

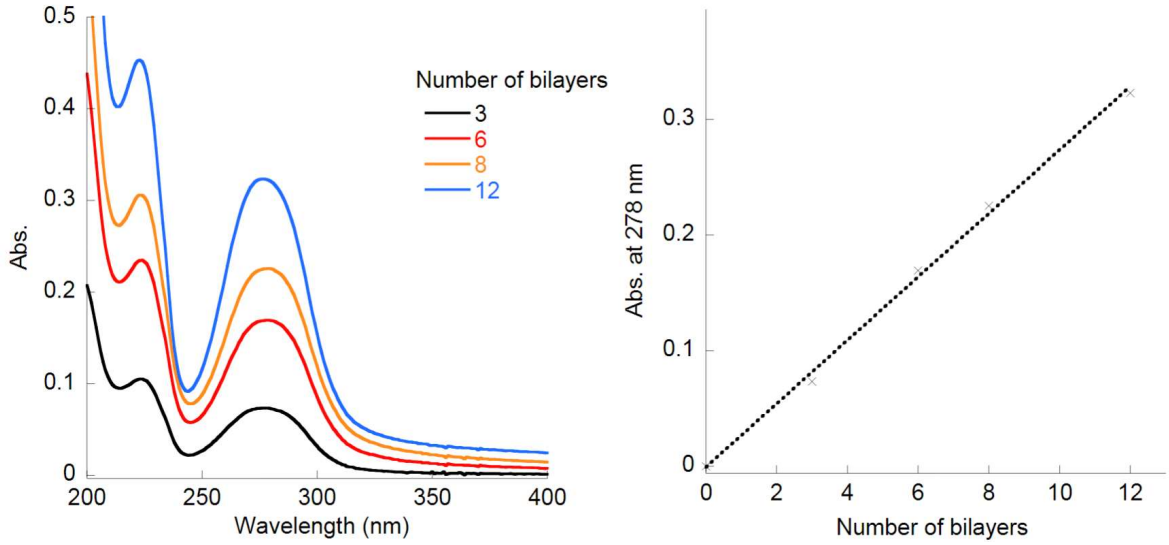

Figure 3.20: Linear relationship between UV absorbance and number of (**Pd**/PSS) bilayers.

UV-vis absorbance spectra of the PEMs showed that photolabile polycations are successfully included in the PEMs prepared via LbL assembly. Consistent with results we reported previously,[35, 41] absorbance of these photolabile PEMs increased linearly with the number of deposited bilayers (see **Figure 3.20** for that of a Pd/PSS film; film growth profilm for Pa/PSS, Pb/PSS and Pc/PSS films can be seen in Chapter 3.2), which suggests limited interlayer diffusion of polymers in these films.[41, 46] Such a characteristic is necessary for the deposition of PEMs comprising multiple compartments stacked in a sequence determined by the LbL process, and the spatial confinement of photochemical functionalities in films designed in this work. The other most common growth profile, superlinear "exponential" growth, is typically ascribed to polymer chain diffusion throughout the entirety of the film, which would preclude the use of this strategy for spatial localization of specific chemistries within films.[12, 46] In addition to characterization by UV/Vis spectrophotometry, the topology of each PEM film deposited on a planar quartz substrate was characterized by atomic force microscopy (AFM, **Figure 3.21**) which allowed for determination of both thicknesses (after scoring) and roughnesses of films (**Table 3.2**).

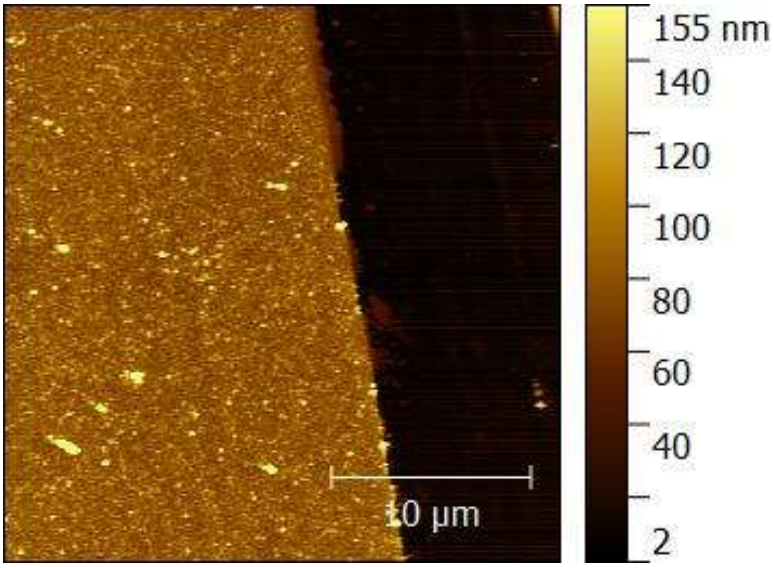

Figure 3.21: A (**Pd**/PSS)$_{12}$ film deposited on planar quartz substrate, scratched with a razor blade to determine thickness.

Table 3.2: Results of AFM characterization of PEMs deposited on quartz slides. Films were scratched with a sharp razor to expose the substrate.

Sample	Average bilayer thickness (nm)	RMS roughness (nm)
(**Pa**/PSS)$_{18}$	5.9	9.3
(**Pb**/PSS)$_{23}$	8.2	10.9
(**Pc**/PSS)$_{24}$	3.5	5.9
(**Pd**/PSS)$_{12}$	6.3	11.6
(PDAC/PSS)$_{35}$	2.6	1.1

3.3.3 Photodisruption of PEMs Deposited on Quartz Slides

3.3.3.a PEMs Comprising One Chromophore

We first prepared single compartment PEMs assembled with polyanion and only one photolabile polycation. All these films prepared are stable to rinsing by 0.1 M pH 7.4 phosphate buffer (UV-vis spectra of the unirradiated films show negligible change after such rinsing), while exposure of these photosensitive PEMs to wavelengths of light discussed above led to degradation of photocleavable groups and resulted in film dissolution in rinsing solutions. Herein we discuss in detail experimental results (**Figure 3.22**) of single compartment PEMs using PSS as polyanion.

Exposure of **Pa**/PSS films to visible light ($\lambda > 400$ nm) resulted in coumarin photolysis, as suggested by irradiation-induced spectral change (**Figure 3.22a**, blue solid curve).[35] Upon rinsing with 0.1 M pH 7.4 phosphate buffer, deprotonation of the resulting carboxylic acid groups in the photoproduct of **Pa** generated negative charge, which resulted in both increased polymer hydrophilicity and disrupted ion pairing interactions between **Pa** and PSS, thus

dissolving the film, as determined by the absorbance decreasing at 380 nm by ~90%. In contrast, **Pb**/PSS and **Pc**/PSS films irradiated at $\lambda > 400$ nm and rinsed in buffer showed less than a 1% change in absorbance after irradiation and rinsing, as expected due to the transparency of the NBE chromophore to visible light.

In contrast, as shown in **Figures 3.22b** and **3.22c**, exposure to 365 nm light degraded ONB groups in **Pb** or **Pc** as indicated by the characteristic absorption peak of the ONB groups in these polymers at 260 nm decreasing, with a new shoulder emerging at ~310 nm. After rinsing the irradiated films incorporating **Pb** or **Pc**, the remaining slides showed little absorption (red solid curves) because the photolyses rendered irradiated **Pb**/PSS and **Pc**/PSS films soluble in rinsing solution. Moreover, although ONB-containing polycations **Pb** and **Pc** have similar absorption spectra and both absorb light at 365 nm, **Pb** photodegrades faster than **Pc**—**Pc**/PSS films require approximately 10 times longer duration of irradiation than **Pb**/PSS films in order to be fully soluble.[41] The dose of light sufficient to render **Pb**/PSS soluble in 0.1 M pH 7.4 phosphate buffer (~ 6 min, 6 mW/cm^2) induced less than 10% decrease in absorbance at $\lambda = 260$ nm of the **Pc**/PSS film after identical irradiation and rinsing steps (**Figure 3.22b**). This difference in photochemical reactivity at $\lambda = 365$ nm enabled selective dissolution of a **Pb**/PSS film using a low dose at 365 nm without significant impact on a similar **Pc**/PSS film. Subsequent irradiation with the same photon flux for longer duration (30 min) rendered **Pc**/PSS films also dissolved (**Figure 3.22c**).

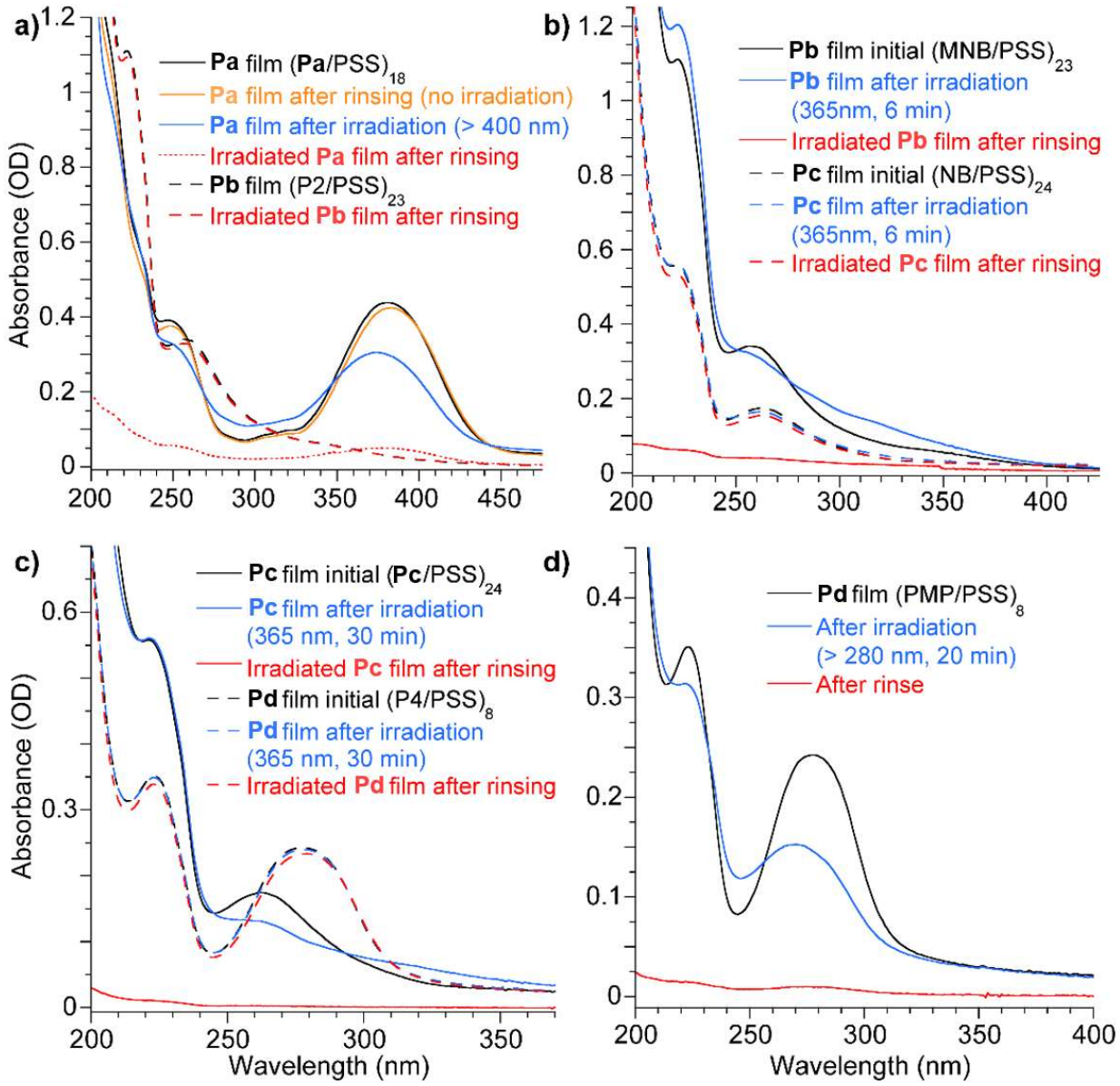

Figure 3.22: Selectivity of film dissolution depending on irradiation conditions. a) Visible light irradiation ($\lambda > 400$ nm) selectively dissolved a (**Pa**/PSS)$_{18}$ film but had little impact on solubility of a (**Pb**/PSS)$_{23}$ film. Irradiation conditions: 30 min duration, 5 mW/cm^2 between 400 nm and 515 nm. b) Irradiation using a Hg/Xe lamp equipped with a 365 nm bandpass filter (6 mW/cm^2) for 6 minutes resulted in dissolution of a (**Pb**/PSS)$_{23}$ film. Identical irradiation and rinsing conditions dissolved <10% of an analogous (**Pc**/PSS)$_{24}$ film. c) 30 min irradiation using a UV lamp equipped

with a 365 nm bandpass filter (6 mW/cm^2) resulted in dissolution of a (**Pc**/PSS)$_{24}$ film with negligible impact on the solubility of a (**Pd**/PSS)$_8$ film. d) Deep UV irradiation (>280 nm, 15 mW/cm^2 between 280 nm and 400 nm) rendered (**Pd**/PSS)$_8$ films soluble. In all cases, the rinsing solutions were 0.1 M pH 7.4 phosphate buffer.

Finally, we demonstrated selective **Pc**/PSS photolysis relative to **Pd**/PSS by exposing the **Pd**/PSS film to identical irradiation conditions to those that result in photo-induced aqueous solubility of **Pc**/PSS (λ = 365 nm, mW/cm^2) for 30 min—the absorbance spectra of **Pd**/PSS films showed no more than a 5% change after exposure to these irradiation and rinsing conditions (**Figure 3.22d**). As discussed in Chapter 3.2,[41] exposure of **Pd**/PSS films to deeper UV light (λ > 280 nm, 14 mW/cm^2 between 280 nm and 400 nm) for 20 min renders them soluble. The photochemical degradation of pMP groups resulted in decrease of the pMP characteristic peak at ~270 nm. The irradiated film (blue curve, **Figure 3.22d**) dissolved almost completely (red curve) in 0.1 M pH 7.4 phosphate buffer.

We also fabricated photolabile PEMs comprising polycations (**Pa**-**Pd**) and PMAA in an analogous fashion, and studied the photo-disruption of these PMAA films (**Figure 3.23**). Such photolabile PMAA films showed similar photoselective disruption as respective photolabile PSS films discussed above, which suggests the versatility of using such photolabile polycations with a variety of polyanions.

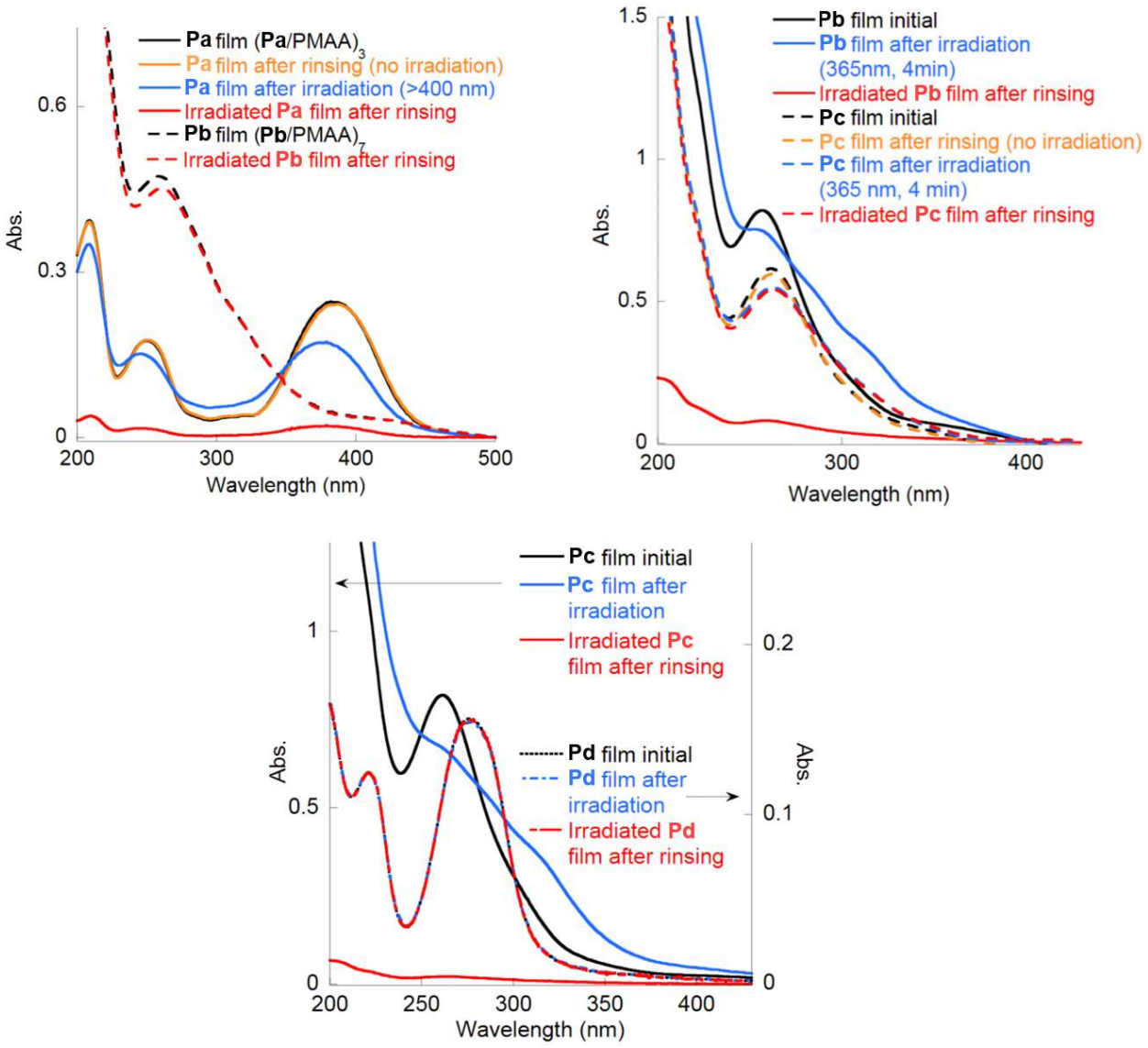

Figure 3.23: *Top left*: Visible light irradiation (λ > 400 nm) selectively dissolved a (**Pa**/PMAA)$_3$ film but had little impact on solubility of a (**Pb**/PMAA)$_7$ film. Irradiation conditions: 30 min duration, 5 mW/cm^2 between 400 nm and 515 nm. *Top right*: Irradiation using a Hg/Xe lamp equipped with a 365 nm bandpass filter (6 mW/cm^2) for 6 minutes resulted in dissolution of a (**Pb**/PMAA)$_{34}$ film. Identical irradiation and rinsing conditions dissolved <10% of an analogous (**Pc**/PMAA)$_{33}$ film. *Bottom*: 30 min irradiation using a UV lamp equipped with a 365 nm bandpass filter (6 mW/cm^2) resulted in dissolution of a (**Pc**/PMAA)$_{33}$ film with negligible impact on the

solubility of a (**Pd**/PMAA)$_3$ film. d) Deep UV irradiation (>280 nm, 15 mW/cm^2 between 280 nm and 400 nm) rendered (**Pd**/PMAA)$_3$ films soluble. In all cases, the rinsing solutions were 0.1 M pH 7.4 phosphate buffer.

3.3.3.b Quadruple PEMs Incorporating Four Chromophores

The LbL technique can enable control over the nanoscale spatial distribution of chemical functionalities within the thickness of deposited films. Rubner, Cohen and coworkers[12] have used this feature of LbL in their reported preparation of hydrogen-bonded films that undergo sequential pH-programmed release of the individual strata of multilayers with different sensitivities to pH. On the other hand, our laboratory has reported wavelength selective sequential release of guest molecules from a two-compartment composite PEM film comprising **Pa**/PSS and **Pc**/PSS.[35] Herein, we prepared quadruple-strata PEM films (substrate)|(**Pd**/PSS)|(**Pc**/PSS)|(**Pb**/PSS)|(**Pa**/PSS) in a manner (**Figure 3.17**) analogous to that we reported previously, and as described in detail in the Experimental Section.[35, 41] In brief, multiple steps of LbL assembly, with each step comprising a number of bilayers of a photoreactive polycation and PSS, were performed sequentially on the same substrate. A photoinert bilayer of PSS/PDAC (represented by "|") was incorporated between each adjacent pair of photolabile compartments—previous studies[35, 46] have shown that similarly thin barrier sections can help to segregate compartments within films prepared by LbL. Increase of UV/Vis absorbance and appearance of characteristic peaks of respective polycations with increasing deposition steps (**Figure 3.24** *right*) demonstrate the successful sequential incorporation of individual compartments comprising respective photoresponsive polymers into composite films. As expected, the film thicknesses as determined by AFM also grew as more

layers were deposited (**Figure 3.24** *left*). Bilayer thickness in each compartment in the composite film (**Pa**/PSS: 5.8 nm, **Pb**/PSS: 9.4 nm, **Pc**/PSS: 3.7 nm, **Pd**/PSS: 7.3 nm) deposited under these conditions were determined by dividing the thickness of each new compartment by the number of bilayers deposited into that compartment, are similar to those determined using the previously discussed single-compartment films (**Table 3.2**).

Upon assembly of the quadruple-compartment composite film, we tested our concept of compartment-selective photochemical disruption under irradiation conditions similar to those established in the single compartment experiments. Altogether, the results described below and in **Figure 3.24** establish that simple approaches to controlling both nanoscale spatial distribution of photoreactive chemistries and irradiation conditions permit integration of photochemically distinct PPGs into multi-compartment PEM films, yielding a quaternary choice for film thickness by controlling irradiation conditions.

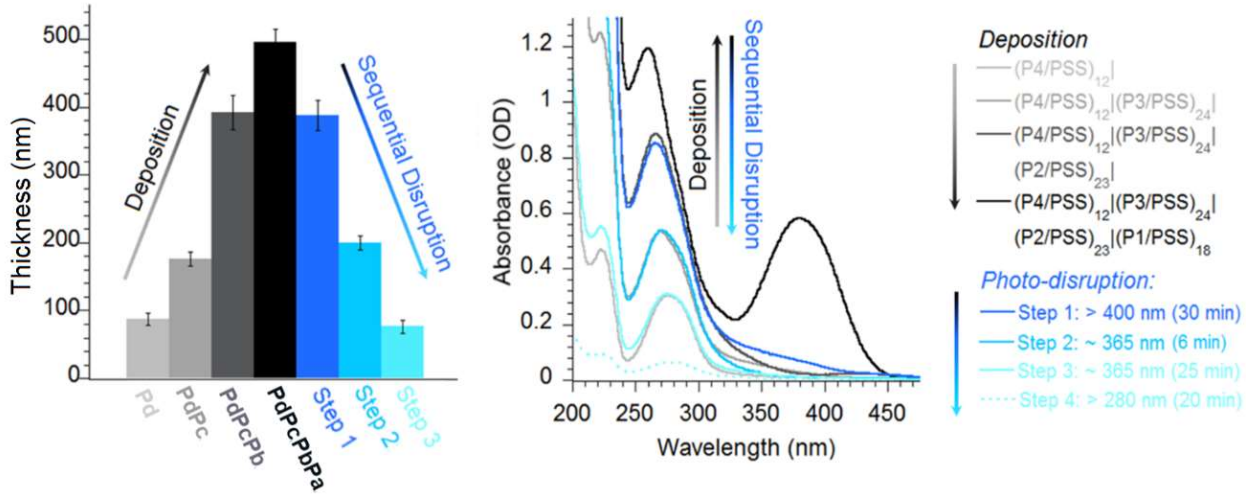

Figure 3.24: Deposition of a (**Pd**/PSS)$_{12}$|(**Pc**/PSS)$_{24}$|(**Pb**/PSS)$_{23}$|(**Pa**/PSS)$_{18}$ film and its photo-triggered sequential dissolution. Error bars represent one standard deviation of thickness in three different areas of a multilayer.

Step 1: Irradiation of the quadruple-compartment film with a 400 nm long pass filter (5 mW/cm^2 between 400 nm and 515 nm) and rinsing with 0.1 M pH 7.4 phosphate buffer solution disrupted **Pa**/PSS, while the rest of the composite film remained on the substrate (**Figure 3.24**). Both the UV/Vis absorbance spectrum of the remaining film and thickness of the remaining film (387 nm) determined using AFM are nearly identical to the those of a (**Pd**/PSS)$_{12}$|(**Pc**/PSS)$_{24}$|(**Pb**/PSS)$_{23}$ film prepared in a control experiment (392 nm).

Step 2: The remaining film was then subjected to UV light (λ = 365 nm, 6 mW/cm^2) for 6 minutes and rinsed with pH 7.4 phosphate buffer. This led to a ~ 190 nm decrease in film thickness, the magnitude of which is indistinguishable from the thickness of a separately prepared single-compartment (**Pb**/PSS)$_{23}$ film. In addition, the leftover film had a UV/Vis spectrum that was nearly identical to that of the separately prepared (**Pd**/PSS)$_{12}$|(**Pc**/PSS)$_{24}$ film. Therefore, both AFM and UV/Vis results indicate that the (**Pb**/PSS)$_{23}$ compartment containing the photolabile MNBE groups was selectively photo-disrupted in this step while preserving the (**Pd**/PSS)$_{12}$|(**Pc**/PSS)$_{24}$| region.

Step 3: Continuing the irradiation at λ = 365 nm for another 25 min yielded dissolution of the (**Pc**/PSS)$_{24}$ compartment into pH 7.4 buffer—the remaining film had similar thickness (77 nm) and UV/Vis spectrum as that of a separately prepared (**Pd**/PSS)$_{12}$| film (87 nm).

Step 4: This remaining film dissolved upon exposure to previous conditions we used to dissolve single-compartment **Pd**/PSS PEMs—20 min irradiation at λ > 280 nm, followed by rinsing in pH 7.4 phosphate buffer.

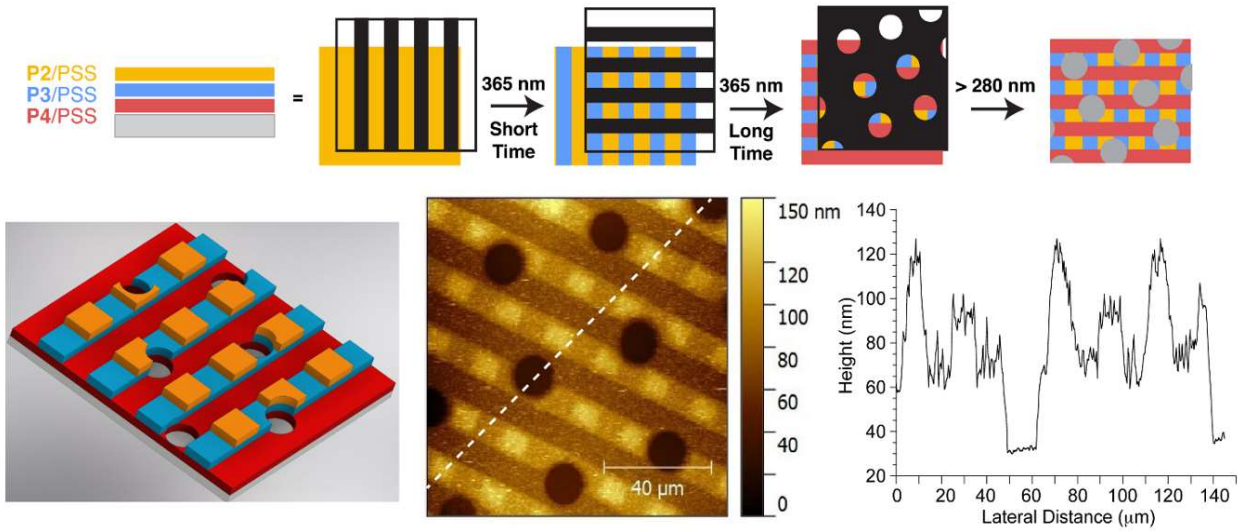

Figure 3.25: *Top:* Scheme for photopatterning using three compartmentalized photolabile polycation/PSS films: (**Pd**/PSS)$_7$|(**Pc**/PSS)$_{11}$|(**Pb**/PSS)$_7$. Four heights are accessible by controlling irradiation conditions in three different masked irradiation steps. Irradiation conditions—**Pb**/PSS photolysis: 365 nm, 6 mW/cm^2, 6 min. duration; **Pc**/PSS photolysis: 365 nm, 6 mW/cm^2, 90 min. duration; **Pd**/PSS photolysis: λ > 280 nm, 15 mW/cm^2 between 280-400 nm, 90 min. duration. *Bottom:* 3-dimensional illustration of patterned surface, and atomic force microscopy image of a film of the triple-patterned film on a quartz substrate; the plot corresponds to the height profile along the white dashed line in the AFM image.

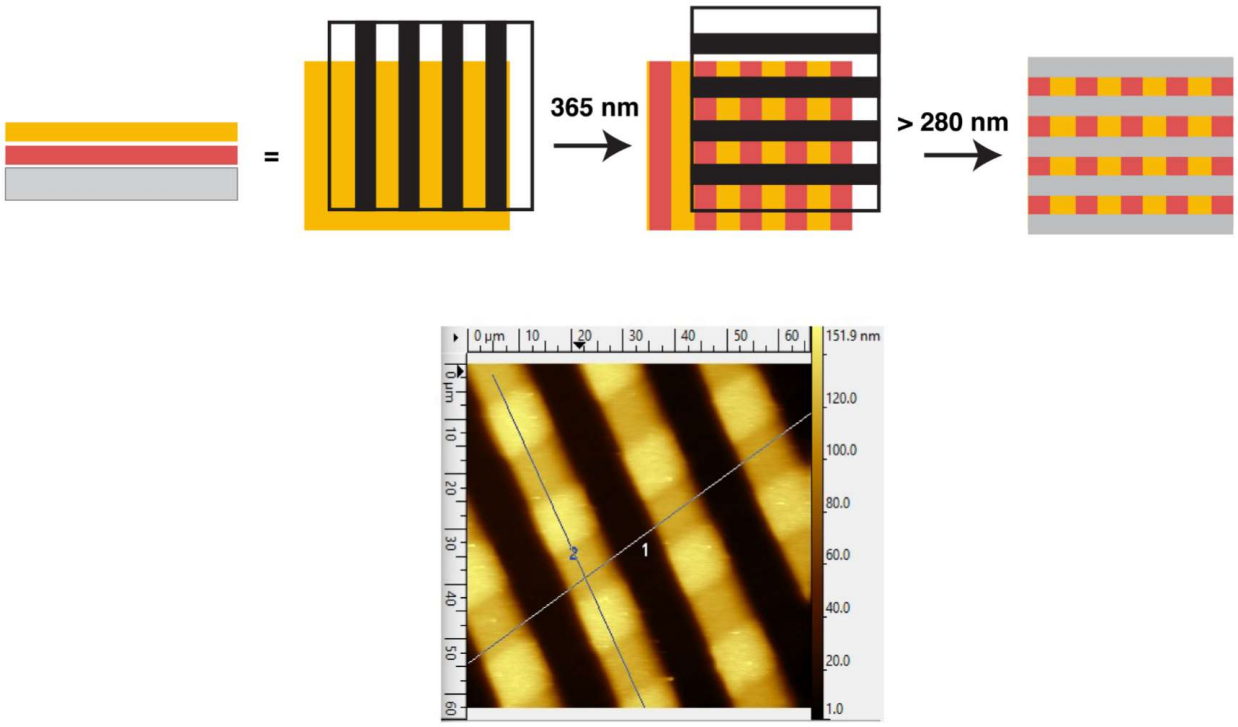

Figure 3.26: *Top*: Scheme for photopatterning using two compartmentalized photolabile polycation/PSS films: (**Pd**/PSS)$_7$|(**Pb**/PSS)$_7$. Three heights are accessible by controlling irradiation conditions in two different masked irradiation steps. Irradiation conditions—Pb/PSS photolysis: 365 nm, 6 mW/cm^2, 6 min. duration; Pd/PSS photolysis: $\lambda > 280$ nm, 15 mW/cm^2 between 280-400 nm, 90 min. duration. *Bottom*: Atomic force microscopy image of a film of the triple-patterned film on a quartz substrate.

3.3.3.d Multilevel Photopatterning with PEMs

Traditional photolithography allows for wide flexibility in patterning in the plane of the substrate, but generally allows for only one film thickness in those locations where the photoresist remains on the substarte. To further demonstrate the unqiue combination of bottom-up and top-down fabrication possible with compartmentalization of photochemically reactive

PEM films, we performed photolithography using 2- and 3-compartment films to yield patterning of resulting film thickness at two or three thickness levels depending on irradiation conditions. **Figure 3.25** shows that using a stratified film containing a combination of **Pb**, **Pc**, and **Pd** allows for patterning at four different heights, as opposed to the two heights available in traditional photolithography. **Figure 3.26** contains a similarly patterned image using **Pd**/PSS and **Pb**/PSS. We are so far unable to achieve similarly resolved patterns using a compartment of **Pa**/PSS as the outermost layer; we preliminarily attribute this difficulty to a combination of the attenuation of UV light caused by the strongly absorbing coumarin moiety, as well as the strong dependence of the efficiency of coumarin photolysis on water content.

3.3.4 Photocontrolled Orthogonal Release from PEM-Coated Microspheres

Beside the capability to construct structurally defined heterogeneous films, another key advantage of LbL is that nano- and macroscale objects can be substrates for assembly of conformal multilayers *via* all aqueous fabrication; such coated objects are promising platforms for biological applications. Combining the advantages of LbL with the photochemical selectivity that light-responsive materials can offer, we prepared PEM-coated silica microspheres and demonstrated quadruple-selective photochemical release of cargo molecules using these microspheres.

As described in the Experimental Section, we prepared PEM coated silica microspheres (diameter: 1 μm) by alternatively dispersing the microspheres in pH 3.5 polycation solutions (0.2% w/w) in 0.1 M NaCl and PSS solutions (0.2% w/w) in 0.1 M NaCl, with centrifugation and rinsing in deionized water between deposition steps. As opposed to using pH 6.0 polycation solutions to deposit thick multilayer films on planar surfaces, we used more acidic polycation

solutions (pH 3.5), because we found that the rate of cargo escaping from unirradiated microspheres prepared using pH 6.0 polycation solutions is about one order of magnitude faster than from those prepared using pH 3.5 polycation solutions. Each coating comprised: i) three sacrificial photolabile bilayers of PSS and the selected photolabile polycation (**Pa**-**Pd**) adjacent to the microspheres to enable the photo-disruption of the coating, ii) one bilayer comprising poly(ethyleneimine) labeled with rhodamine (RhoPEI) and PSS as a fluorescent guest cargo to be released upon photo triggered disruption of sacrificial substrate layers, and iii) one bilayer of PSS and respective photolabile polycation as the outermost bilayer..

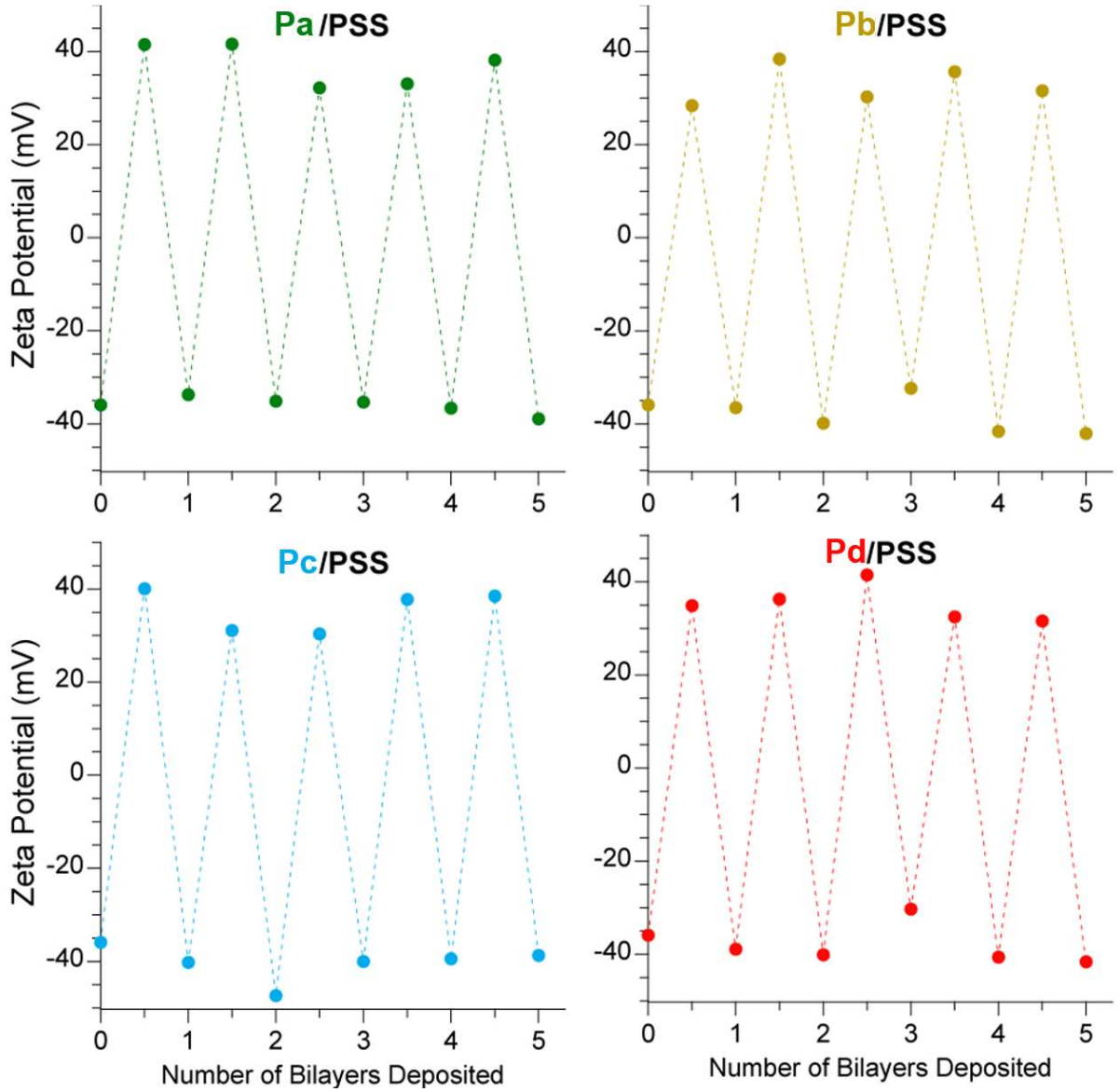

Figure 3.27: Zeta potential of microspheres @a-@d upon deposition of each layer.

We prepared four different samples of fluorescent, PEM-coated microspheres, @a-@d, each of which incorporated one of **Pa**-**Pd** in the photolabile polycations, and monitored the deposition process using the zeta potentials of the microspheres. The bare commercially available microspheres had an initial zeta potential of approximately -35 mV. Generally, the sign

of the zeta potentials of the microsphere suspensions were the same as sign of the polyelectrolyte most recently deposited—the particles had positive zeta potentials after immersion in polycationic solutions, and negative zeta potentials after immersion in polyanionic solutions (**Figure 3.27**).

We studied photo-triggered release of fluorescent cargo from these PEM coated microspheres using fluorescence and UV/Vis spectroscopy. In each experiment, 1.5 mL of colloidal microsphere suspension (concentration: 0.004-0.011% w/w) was irradiated, followed by dispersal of a 0.25 mL aliquot of this suspension into 0.15 mL pH 7.7 Tris-HCl buffer solution. Removal of the microspheres by filtration left only the dissolved polymers and photoproducts that had been released from the beads in fluid solution, including fluorescent polymer. We monitored the fluorescence intensity of each removed aliquot. The average of integrated fluorescence intensities (575–590 nm) of each sample of microspheres, corresponding to the plateau in each experiment, is normalized to 1.0 in each plot in order to quantify the percentage of total release after each irradiation step. We also measured the absorption spectrum of filtered solution before and after each release experiment.

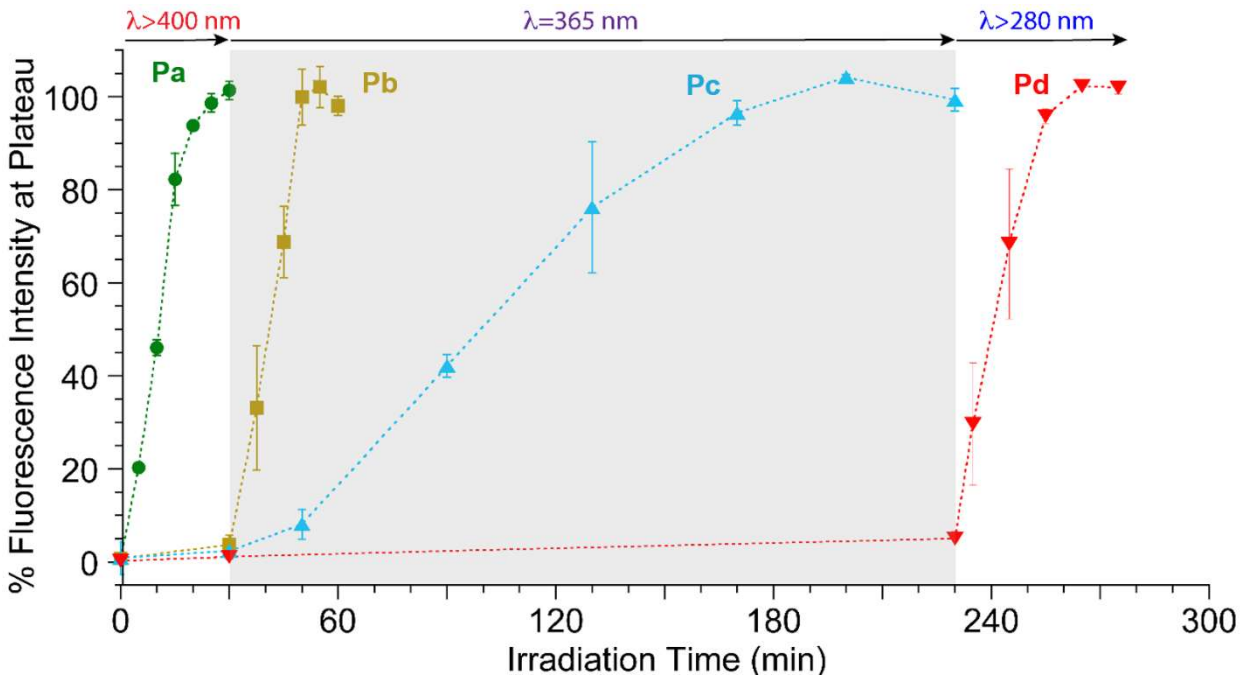

Figure 3.28: Selective release of rhodamine labeled poly(ethyleneimine) from PEM-coated silica microspheres @a-@d under sequentially changing irradiation conditions for each sample. Error bars represent the standard deviations for three trials for each microsphere sample. Fluorescence intensity for each sample of microsphere is normalized (to 100%) to the average of the final three data points, representing the plateau, during each irradiation experiment. The excitation wavelength for all fluorescence spectra was 550 nm.

All four different samples of microspheres (@a-@d) were first subjected to visible light ($\lambda > 400$ nm, 5 mW/cm^2 between 400 nm and 515 nm). Fluorescence intensity of the resulting @a solution increased as irradiation proceeded (**Figure 3.28**, *left*), as the photolabile sacrificial layers disrupted and the cargo layer dissolved. The fluorescence intensity approached to a plateau after ~ 20 min, suggesting the near full release of carried cargo molecules. In addition, the characteristic absorption peaks of **Pa** and the photoproducts emerged around $\lambda = 380$ nm

(consistent with **Figure 3.22**), and the rhodamine peak appears around 560 nm, confirming the dissolution of PEMs on @a (**Figure 3.29**). In contrast, @a solution kept in the dark for a similar duration of time shows < 5% release of fluorophore as monitored by fluorescence spectroscopy, as well as no absorbance bands attributed to either **Pa** or rhodamine via UV/Vis spectrophotometry (**Figure 3.29**). Furthermore, microspheres containing **Pb-Pd** are essentially inert toward visible light irradiation, showing negligible release through either in absorbance and fluorescence.

Further exposure of @b-@d to UV light at λ = 365 nm (6 mW/cm^2) showed release from @b and @c, but not from @d: i) @b reached a plateau of fluorophore release after ~25 min of irradiation, but @c only exhibited ~10% of the maximally released fluorophores during the same photolysis duration (**Figure 3.28**, *middle*). Absorption spectra also show the release of both photodegraded **Pb** (consistent with **Figure 3.22**) and the rhodamine chromophore from @b under these irradiation conditions. Absorption spectra from @c (**Figure 3.29**) only shows the development of photochemical product shoulder around 330 nm (consistent with **Figure 3.22**), but little absorption attributable to any released fluorescent cargo. ii) Prolonged irradiation at λ = 365 nm for another ~2 h resulted in an observed plateau of release of rhodamine fluorescence from @c. Control fluorescence spectroscopy experiments of @b and @c kept in the dark showed <5% rhodamine fluorescence relative to that upon photolysis at 365 nm and also showed negligible rhodamine absorption (**Figure 3.29**).

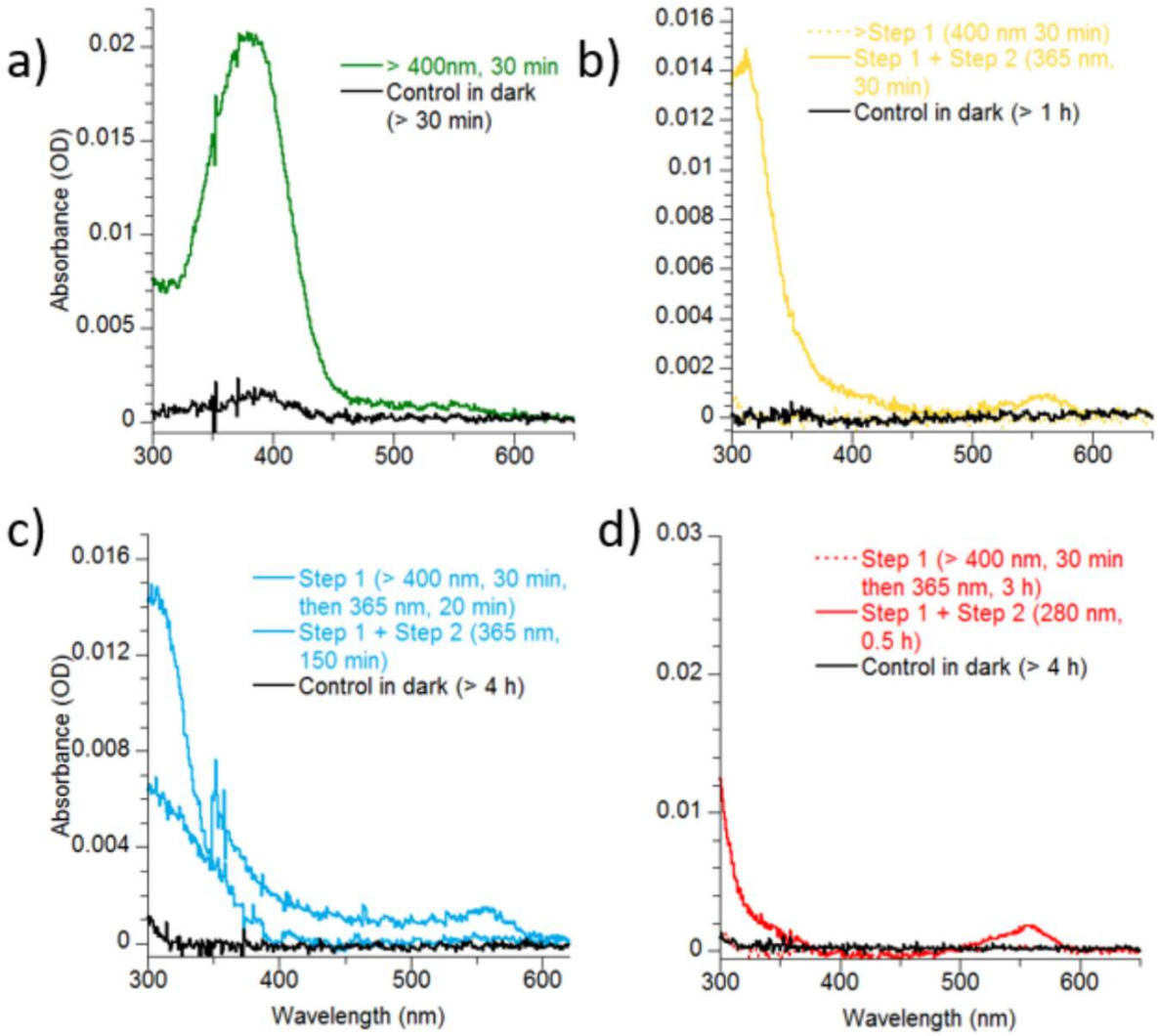

Figure 3.29: UV/vis spectra of @a-@d cargo loaded microspheres solutions subjected to respective irradiation conditions. The absorption peak around 550 nm corresponds to the absorption of rhodamine fluorophore.

3.3.5 Conclusions

Chapter 3.3 demonstrates PEMs that show selective four-stage photo-induced dissolution using two different architectures. By combining the capability for spatial segregation of chemical functionalities in LbL films, the spatiotemporal distribution of light, and the selectivity that

combinations of PPGs can provide, we showed that different strata of an LbL film can be removed selectively through choice of irradiation conditions. This approach represents a merging of different fabrication approaches: bottom-up LbL self assembly dictates the thickness and chemical composition of each stratum in composite films, while top-down photochemical disruption of intermolecular interactions in the films dictates where and which of the LbL-fabricated strata are disrupted. In addition, we utilized the broad applicability of LbL to substrates of different sizes to demonstrate selective four-stage dissolution of and guest release from LbL coatings on silica microspheres. We envision potential applications of this general approach to photoresponsive materials to include all-aqueous photolithographic fabrication in which wavelength of irradiation determines one of several potential film thicknesses, controlling biointerface properties, as well as sequentially controlled triggered release of guest cargo for biological applications. Realization of these applications, however, will require addressing several disadvantages of our approach, such as the potential for limited mechanical strengths of LbL films and the need for tissue-penetrant near infrared light.

3.3.6. EXPERIMENTAL SECTION

General Considerations

NMR spectra were acquired on a Bruker Avance III 500 spectrometer. Chemical shifts are reported relative to residual protonated solvent. Polymer molecular weights were determined using a Shimadzu gel permeation chromatography (GPC) system equipped with a Tosoh TSKgel GMHhr-M mixed-bed column and guard column using a UV detector. The column was calibrated with low polydispersity poly(styrene) standards (Tosoh, PS Quick Kit) with 2% triethylamine in THF as the mobile phase eluting at 0.75 mL/min. All solution optical spectra

were acquired of samples in quartz cuvettes (FireflySci, Inc.). UV/Vis absorbance spectra were acquired with a Varian Cary-100 instrument in double beam mode using a solvent containing cuvette for background subtraction spectra of solution samples, or using a bare quartz slide for background subtraction spectra of solid samples. Fluorescence emission spectra were obtained by using a PTI Quantum Master 4 equipped with a 75 W Xe lamp. Fluorescence spectra were corrected for both the output of the lamp and for the response of the photomultiplier tube detector to different wavelengths. Solutions used in the fabrication and disruption experiments of PEMs were all aqueous solutions unless otherwise mentioned. Zeta potential results were collected using a Malvern Zetasizer Nano-ZS. AFM images were obtained using a Veeco D3100S-1 working in tapping mode. AFM results were processed using software Gwyddion 2.4.

Synthesis

Photoreactive monomers (**Ma**-**Md**), photolabile polymers (**Pa**-**Pd**) and Rhodamine labeled Polyethyleneimine (RhoPEI) were synthesized following methods in literature.[35, 41]

LBL Assembly of the PEMs on Planar Quartz Slides

To protonate the amine groups in the weak polycations (**Pa**-**Pd**) and provide the positive charge for LBL assembly, the pH of **Pa**-**Pd** solutions were adjusted to 6.0 using dilute HCl and NaOH solutions. Photolabile polycation/PSS films were assembled using a Midas III Automated Slide Stainer. Alternating immersion of air-plasma cleaned quartz slides into (1) a 0.2% (w/v) pH 6.0 solution of polycations in 0.1 M NaCl (10 min) and (2) a 0.2% (w/v) solution of PSS in 0.1 M NaCl (10 min), with rinsing using flowing deionized water (10 min, 500 mL/min) between each immersion step, yielded PEMs that we monitored by UV/Vis spectrophotometry.

Poly(diallyldimethylammonium chloride) (PDAC)/PSS layers were deposited in an similar manner, using 0.2% (w/v) solution of PDAC in 0.1 M NaCl and 0.2% (w/v) solution of PSS in 0.1 M NaCl for in the assembly. Polycation/PMAA films were prepared analogously by using a 0.2% (w/v) pH 5.0 solution of PMAA in 0.1 M NaCl as polyanion solution.

Multiple compartments of PEM films, with each compartment comprising a number of bilayers of photoreactive polycations and PSS, were deposited sequentially on the same substrate to construct a quadruple-structured composite film (Figure 2, top). The deep UV responsive, pMP groups containing stack **P4**/PSS was first assembled adjunct to the substrate, followed by a compartment of **P3**/PSS and subsequently a compartment of **P2**/PSS multilayers. **P1**/PSS comprising the visible light sensitive DMAEMA groups was deposited last.

Irradiation Experiments

A 200 W Hg/Xe lamp (Newport-Oriel) with a condensing lens was used in irradiation experiments. The following wavelength filters were used in the photolysis of each polymer: **Pa**, 400 nm long pass filter (FR-GG400, Newport Corp.); **Pb** and **Pc**, 365 nm interference filter (Hg01-365-25, Semrock LLC.); **Pd**, 280 long pass filter (FSQ-WG280, Newport Corp.). Irradiation of PEMs on quartz slides comprising **Pa** was performed inside a closed, visible light transparent chamber with ~100% relative humidity inside at ambient temperature. Irradiation of all other polymers on quartz slides were performed in air at ambient temperature and humidity. After each irradiation step, films were soaked in 0.1 M $NaHCO_3$ (pH 8.2) or 0.1 M phosphate buffer (pH 7.4) for 10 minutes to remove the photocleaved layers, briefly submerged in DI water to remove the remaining rinsing solution, then dried with compressed air. The location of slides remained the same during each irradiation experiment, keeping the photon flux incident on each

film constant. Photomasks comprising chrome patterns on quartz substrates were supplied by Advance Reproductions (North Andover, MA).

LBL Assembly of PEMs on Microspheres

To an aqueous suspension of silica microspheres (0.10 mL, diameter: 1.0 cm, concentration 5.0%, Sigma Aldrich) was first added 1.0 mL of 0.2% (w/v) pH 3.5 polycation solution in 0.1 M NaCl, continuously swirled for 90 min on a VWR digital 3D rotator waver, and collected by centrifugation (2000 g, 1 min). The microspheres were then dispersed in 1.5 mL deionized water, centrifuged and collected by removing the liquid. This rinsing process was repeated three times after each deposition step. Then in an analogous fashion, these microspheres were immersed in 1.0 mL of 0.2% (w/v) PSS solution in 0.1 M NaCl for 60 min with continuous swirling and rinsed, completing the deposition of one bilayer. This process was repeated until the desired number of bilayers were added. To prepare **Pa**/PSS coated and cargo loaded microspheres @a, we first coated the silica microspheres with three **Pa**/PSS bilayers as a photolabile sacrificial layer, followed by assembly of one fluorescently labeled Rhod-PEI/PSS bilayer and subsequent deposition of the outmost **Pa**/PSS bilayer. The other photolabile and cargo loaded microspheres @b-@d were prepared similarly using **Pb**-**Pd** as the photolabile polycation, respectively. Microspheres obtained were dispersed in 1.5 mL of 0.1 M pH 7.7 Tris-HCl buffer solution and stocked in a refrigerator at 4 °C before being used in release experiments.

Release Experiments with Microspheres

A stock suspension of PEM coated microspheres @a-@d (~0.2-0.5 mL) was diluted to 1.5 mL by pH 7.7 Tris-HCl buffer solution (0.1 M) in a quartz cuvette. The suspension in cuvette was mildly stirred with a magnetic stir bar (~60 rpm) and subject to irradiation conditions described in *Irradiation Experiments*. After each duration of irradiation, a 0.25 mL aliquot of the irradiated suspension was removed, and diluted to 0.4 mL by 0.1 M Tris-HCl buffer solution (pH 7.7). The diluted dispersion was then filtered using a syringe filter (Millipore, 0.45 μm), which blocked the microbeads but allowed the dissolved polymers released from the microbeads to pass. The fluorescence intensity of filtered solution was determined using a fluorimeter (PTI Quantum Master 4 equipped with a 75 W Xe lamp), and the absorption spectrum was obtained with UV/Vis spectroscopy (Varian Cary-100, double-beam mode using a solvent-containing cuvette for background subtraction spectra). This process was repeated multiple times during the irradiation until the fluorescence intensity reached a plateau.

3.4 Conclusions

Chapter 3 describes multi-responsive polyelectrolyte multilayers (PEMs) prepared via layer-by-layer (LBL) assembly. This chapter introduces a series of designed and synthesized a series of stimuli-responsive polycations that can “charge-shift” from positively charged polymers to polymers with less positive net charge, upon photodegradation or increasing pH. Such charge-shifting can disrupt ion-pairing non-covalent intermolecular interactions in PEMs comprising these polycations, and therefore render PEMs soluble in buffered solutions. We also describe an approach to bond guest molecules to PEMs covalently via a redox sensitive disulfide bond; cleavage of disulfide bond triggered by chemical reduction leads to the release of guest from the PEM. These two general approaches to tunable physical or chemical bonds, combined with the

capability for spatial segregation of chemical functionality in LBL films, enable a versatile method (Chapter 3.2) to prepare free-standing PEM films that can release covalently bound and physically trapped cargo upon application of different stimuli (light, pH or chemical reduction). This general strategy also allows for light-controlled selective disruption, multilevel patterning, and sequential release with PEMs incorporating four photocleavable chromophores fabricated in this manner (Chapter 3.3).

3.5 References

1. Fu, J., H.M. Fares, and J.B. Schlenoff, *Ion-Pairing Strength in Polyelectrolyte Complexes.* Macromolecules, 2017. **50**(3): p. 1066-1074.
2. Roh, Y.H., et al., *Layer-by-Layer Assembled Antisense DNA Microsponge Particles for Efficient Delivery of Cancer Therapeutics.* ACS Nano, 2014. **8**(10): p. 9767-9780.
3. Richardson, J.J., M. Björnmalm, and F. Caruso, *Technology-Driven Layer-by-Layer Assembly of Nanofilms.* Science, 2015. **348**: p. aaa2491.
4. Yan, Y., M. Björnmalm, and F. Caruso, *Assembly of Layer-by-Layer Particles and Their Interactions with Biological Systems.* Chemistry of Materials, 2014. **26**(1): p. 452-460.
5. Borges, J. and J.F. Mano, *Molecular Interactions Driving the Layer-by-Layer Assembly of Multilayers.* Chemical Reviews, 2014. **114**(18): p. 8883-8942.
6. Tong, W., X. Song, and C. Gao, *Layer-by-layer assembly of microcapsules and their biomedical applications.* Chemical Society Reviews, 2012. **41**(18): p. 6103-6124.
7. Richardson, J.J., et al., *Innovation in Layer-by-Layer Assembly.* Chemical Reviews, 2016. **116**: p. 14828-14867.
8. Zhou, J., M.V. Pishko, and J.L. Lutkenhaus, *Thermoresponsive Layer-by-Layer Assemblies for Nanoparticle-Based Drug Delivery.* Langmuir, 2014. **30**(20): p. 5903-5910.
9. Tan, W.S., et al., *Effect of Block Copolymer Architecture on the Thermally Induced Swelling of Micelle-Containing Multilayer Thin Films.* Macromolecules, 2011. **44**: p. 7767.
10. Gumbley, P., et al., *Wavelength-Selective Disruption and Triggered Release with Photolabile Polyelectrolyte Multilayers.* Chemistry of Materials, 2014. **26**: p. 1450-1456.
11. Bao, C., et al., *Near-Infrared Light-Stimulus-Responsive Film as a Sacrificial Layer for the Preparation of Free-Standing Films.* Langmuir, 2016. **32**(14): p. 3393-3399.
12. Lee, H., et al., *pH-Programmable Sequential Dissolution of Multilayer Stacks of Hydrogen-Bonded Polymers.* ACS Macro Letters, 2013. **2**(10): p. 924-927.
13. Gumbley, P. and S.W. Thomas, *Reversible Photochemical Tuning of Net Charge Separation from Contact Electrification.* ACS Applied Materials & Interfaces, 2014. **6**(11): p. 8754-8761.
14. Koylu, D., et al., *Photochemical Disruption of Polyelectrolyte Multilayers.* Advanced Materials, 2012. **24**(11): p. 1451-1454.
15. Pennakalathil, J. and J.-D. Hong, *Self-Standing Polyelectrolyte Multilayer Films Based on Light-Triggered Disassembly of a Sacrificial Layer.* ACS Nano, 2011. **5**(11): p. 9232-9237.
16. Gui, Z., et al., *Layer-by-layer self-assembly, controllable disintegration of polycarboxybetaine multilayers and preparation of free-standing films at physiological conditions.* Journal of Materials Chemistry, 2010. **20**(8): p. 1467-1474.
17. Gui, Z., et al., *Fabrication of free-standing polyelectrolyte multilayer films: A method using polysulfobetaine-containing films as sacrificial layers.* Journal of Colloid and Interface Science, 2009. **340**(1): p. 35-41.
18. Ma, Y., et al., *Polyelectrolyte Multilayer Films for Building Energetic Walking Devices.* Angewandte Chemie International Edition, 2011. **50**(28): p. 6254-6257.
19. Dubas, S.T., T.R. Farhat, and J.B. Schlenoff, *Multiple Membranes from "True" Polyelectrolyte Multilayers.* Journal of the American Chemical Society, 2001. **123**(22): p. 5368-5369.
20. Ono, S.S. and G. Decher, *Preparation of Ultrathin Self-Standing Polyelectrolyte Multilayer Membranes at Physiological Conditions Using pH-Responsive Film Segments as Sacrificial Layers.* Nano Letters, 2006. **6**(4): p. 592-598.

21. Ma, Y., J. Sun, and J. Shen, *Ion-Triggered Exfoliation of Layer-by-Layer Assembled Poly(acrylic acid)/Poly(allylamine hydrochloride) Films from Substrates: A Facile Way To Prepare Free-Standing Multilayer Films.* Chemistry of Materials, 2007. **19**(21): p. 5058-5062.
22. Lee, H., et al., *pH-Programmable Sequential Dissolution of Multilayer Stacks of Hydrogen-Bonded Polymers.* ACS Macro Lett., 2013. **2**: p. 924.
23. Zhu, Z., et al., *Programmable Light-Controlled Shape Changes in Layered Polymer Nanocomposites.* ACS Nano, 2012. **6**(4): p. 3152-3162.
24. Liao, L., et al., *A Convergent Synthetic Platform for Single-Nanoparticle Combination Cancer Therapy: Ratiometric Loading and Controlled Release of Cisplatin, Doxorubicin, and Camptothecin.* Journal of the American Chemical Society, 2014. **136**(16): p. 5896-5899.
25. Schattling, P., F.D. Jochum, and P. Theato, *Multi-stimuli responsive polymers - the all-in-one talents.* Polymer Chemistry, 2014. **5**(1): p. 25-36.
26. Zhuk, A., R. Mirza, and S. Sukhishvili, *Multiresponsive Clay-Containing Layer-by-Layer Films.* ACS Nano, 2011. **5**(11): p. 8790-8799.
27. Xu, S., et al., *Hollow hierarchical hydroxyapatite/Au/polyelectrolyte hybrid microparticles for multi-responsive drug delivery.* Journal of Materials Chemistry B, 2014. **2**(38): p. 6500-6507.
28. Li, J., et al., *Multi-responsive drug release from hydrogen-bonding multilayers containing PEGylated nanoparticles and azobenzenes.* Journal of Materials Chemistry B, 2014. **2**(28): p. 4422-4425.
29. Xu, W., et al., *Multiresponsive Microcapsules Based on Multilayer Assembly of Star Polyelectrolytes.* Macromolecules, 2014. **47**(22): p. 7858-7868.
30. Wang, Z., et al., *Photoresponsive Cross-linked Polymeric Particles for Phototriggered Burst Release.* Photochemistry and Photobiology, 2013. **89**(3): p. 552-559.
31. He, J., X. Tong, and Y. Zhao, *Photoresponsive Nanogels Based on Photocontrollable Cross-Links.* Macromolecules, 2009. **42**(13): p. 4845-4852.
32. Gumbley, P., et al., *Wavelength-Selective Disruption and Triggered Release with Photo labile Polyelectrolyte Multilayers.* Chemistry of Materials, 2014. **26**(3): p. 1450-1456.
33. Szajewski, R.P. and G.M. Whitesides, *Rate constants and equilibrium constants for thiol-disulfide interchange reactions involving oxidized glutathione.* Journal of the American Chemical Society, 1980. **102**(6): p. 2011-2026.
34. San Miguel, V., C.G. Bochet, and A. del Campo, *Wavelength-selective caged surfaces: how many functional levels are possible?* Journal of the American Chemical Society, 2011. **133**(14): p. 5380-5388.
35. Gumbley, P., et al., *Wavelength-Selective Disruption and Triggered Release with Photolabile Polyelectrolyte Multilayers.* Chemistry of Materials, 2014. **26**(3): p. 1450-1456.
36. Bertrand, O., J.-F. Gohy, and C.-A. Fustin, *Synthesis of diblock copolymers bearing p-methoxyphenacyl side groups.* Polymer Chemistry, 2011. **2**(10): p. 2284-2292.
37. Kock, A., et al., *Disulfide reshuffling triggers the release of a thiol-free anti-HIV agent to make up fast-acting, potent macromolecular prodrugs.* Chemical Communications, 2014. **50**(93): p. 14498-14500.
38. San Miguel, V., C.G. Bochet, and A. del Campo, *Wavelength-Selective Caged Surfaces: How Many Functional Levels Are Possible?* Journal of the American Chemical Society, 2011. **133(14)**: p. 5380-5388.
39. Griffin, D.R. and A.M. Kasko, *Photodegradable Macromers and Hydrogels for Live Cell Encapsulation and Release.* Journal of the American Chemical Society, 2012. **134**(31): p. 13103-13107.
40. Smith, Z.C., et al., *Thiophene-Based Conjugated Polymers with Photolabile Solubilizing Side Chains.* Macromolecules, 2015. **48**(4): p. 959-966.

41. Hu, X., et al., *Stimuli-Responsive Free-Standing Layer-By-Layer Films.* Advanced Materials, 2016. **28**(4): p. 715-721.
42. Rodrigues-Correia, A., X.M.M. Weyel, and A. Heckel, *Four Levels of Wavelength-Selective Uncaging for Oligonucleotides.* Organic Letters, 2013. **15**(21): p. 5500-5503.
43. San Miguel, V., C.G. Bochet, and A. del Campo, *Wavelength-Selective Caged Surfaces: How Many Functional Levels Are Possible?* Journal of the American Chemical Society, 2011. **133**(14): p. 5380-5388.
44. Hansen, M.J., et al., *Wavelength-selective cleavage of photoprotecting groups: strategies and applications in dynamic systems.* Chemical Society Reviews, 2015. **44**(11): p. 3358-3377.
45. Fu, J. and J.B. Schlenoff, *Driving Forces for Oppositely Charged Polyion Association in Aqueous Solutions: Enthalpic, Entropic, but Not Electrostatic.* Journal of the American Chemical Society, 2016. **138**(3): p. 980-990.
46. Gilbert, J.B., M.F. Rubner, and R.E. Cohen, *Depth-profiling X-ray photoelectron spectroscopy (XPS) analysis of interlayer diffusion in polyelectrolyte multilayers.* Proceedings of the National Academy of Sciences, 2013. **110**(17): p. 6651-6656.
47. Ahn, J., et al., *Tuning the Properties of Mucin via Layer-by-Layer Assembly.* Biomacromolecules, 2015. **16**(1): p. 228-235.
48. Tan, W.S., et al., *Effect of Block Copolymer Architecture on the Thermally Induced Swelling of Micelle-Containing Multilayer Thin Films.* Macromolecules, 2011. **44**(19): p. 7767-7774.
49. Itano, K., J. Choi, and M.F. Rubner, *Mechanism of the pH-Induced Discontinuous Swelling/Deswelling Transitions of Poly(allylamine hydrochloride)-Containing Polyelectrolyte Multilayer Films.* Macromolecules, 2005. **38**(8): p. 3450-3460.
50. Choi, J. and M.F. Rubner, *Influence of the Degree of Ionization on Weak Polyelectrolyte Multilayer Assembly.* Macromolecules, 2005. **38**(1): p. 116-124.
51. Mendelsohn, J.D., et al., *Rational Design of Cytophilic and Cytophobic Polyelectrolyte Multilayer Thin Films.* Biomacromolecules, 2003. **4**(1): p. 96-106.
52. Tang, K. and N.A.M. Besseling, *Formation of polyelectrolyte multilayers: ionic strengths and growth regimes.* Soft Matter, 2016. **12**(4): p. 1032-1040.
53. Lundin, M., et al., *Layer-by-Layer Assemblies of Chitosan and Heparin: Effect of Solution Ionic Strength and pH.* Langmuir, 2011. **27**(12): p. 7537-7548.
54. Shiratori, S.S. and M.F. Rubner, *pH-Dependent Thickness Behavior of Sequentially Adsorbed Layers of Weak Polyelectrolytes.* Macromolecules, 2000. **33**(11): p. 4213-4219.
55. Park, S.Y., M.F. Rubner, and A.M. Mayes, *Free Energy Model for Layer-by-Layer Processing of Polyelectrolyte Multilayer Films.* Langmuir, 2002. **18**(24): p. 9600-9604.
56. Vidyasagar, A., et al., *Thermal Transitions in Dry and Hydrated Layer-by-Layer Assemblies Exhibiting Linear and Exponential Growth.* ACS Nano, 2012. **6**(7): p. 6174-6184.
57. Lee, D., et al., *pH-Dependent Structure and Properties of TiO2/SiO2 Nanoparticle Multilayer Thin Films.* Chemistry of Materials, 2007. **19**(6): p. 1427-1433.
58. Vasconcellos, F.C., et al., *Bioactive Polyelectrolyte Multilayers: Hyaluronic Acid Mediated B Lymphocyte Adhesion.* Biomacromolecules, 2010. **11**(9): p. 2407-2414.

Chapter 3 Appendix

^{1}H and ^{13}C NMR

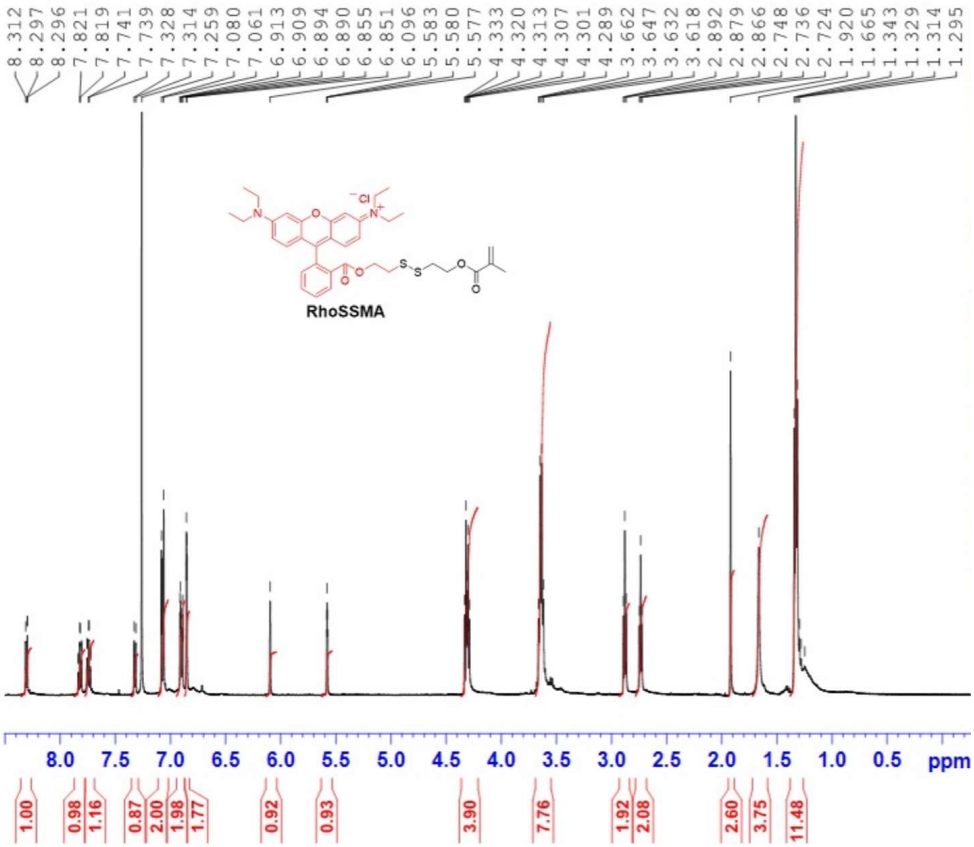
8.312
8.297
8.296
7.821
7.819
7.741
7.739
7.328
7.314
7.259
7.080
7.061
6.913
6.909
6.894
6.890
6.855
6.851
6.096
5.583
5.580
5.577
4.333
4.320
4.313
4.307
4.301
4.289
3.662
3.647
3.632
3.618
2.892
2.879
2.866
2.748
2.736
2.724
1.920
1.665
1.343
1.329
1.314
1.295
RhoSSMA
8.0 7.5 7.0 6.5 6.0 5.5 5.0 4.5 4.0 3.5 3.0 2.5 2.0 1.5 1.0 0.5 ppm
1.00 0.98 1.16 0.87 2.00 1.98 1.77 0.92 0.93 3.90 7.76 1.92 2.08 2.60 3.75 11.48

RhoSSMA

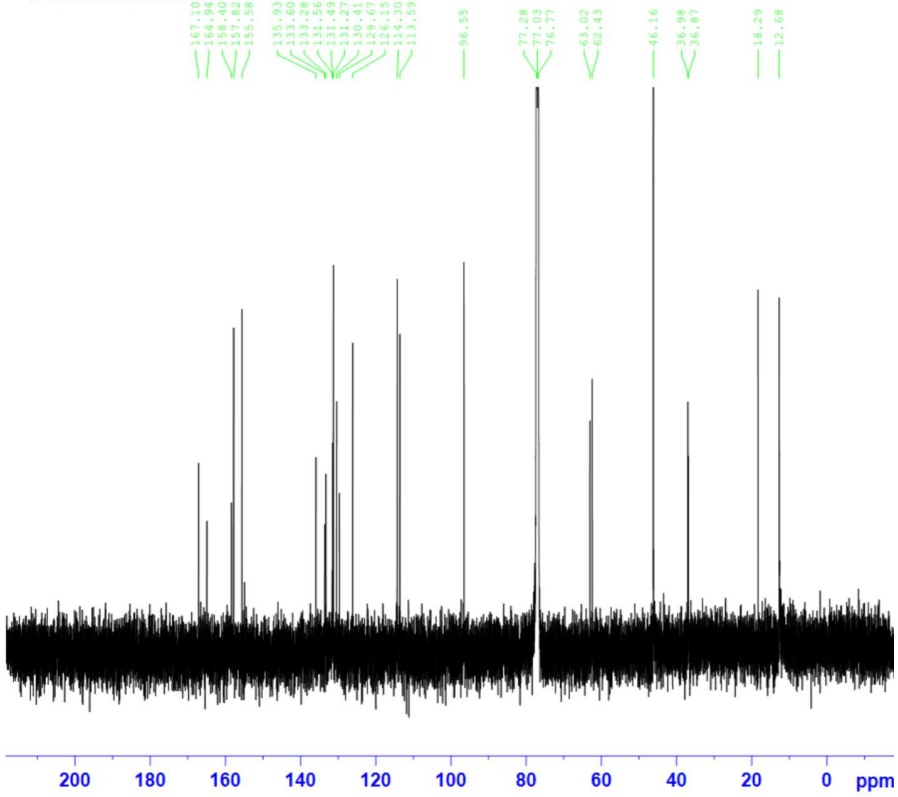
167.10
164.94
158.40
157.82
155.58
135.93
133.60
133.28
131.56
131.49
131.27
130.41
129.67
126.15
114.30
113.59
96.55
77.28
77.03
76.77
63.02
62.43
46.16
36.98
36.87
18.29
12.68
200 180 160 140 120 100 80 60 40 20 0 ppm

P1

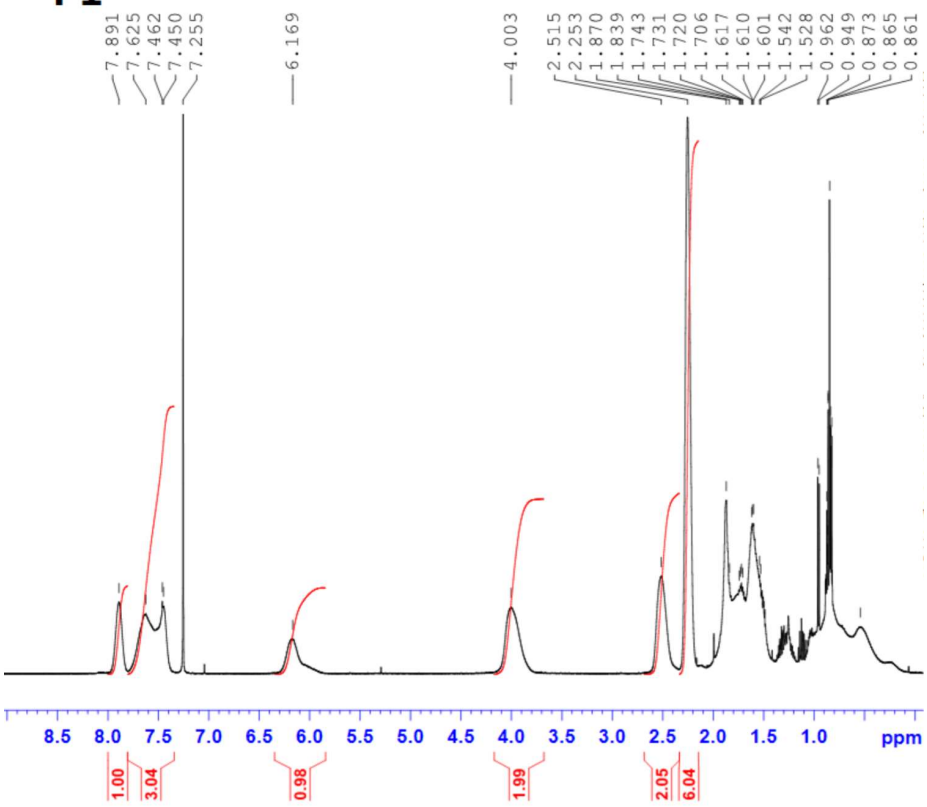
7.891
7.625
7.462
7.450
7.255
6.169
4.003
2.515
2.253
1.870
1.839
1.743
1.731
1.720
1.706
1.617
1.610
1.601
1.542
1.528
0.962
0.949
0.873
0.865
0.861
8.5 8.0 7.5 7.0 6.5 6.0 5.5 5.0 4.5 4.0 3.5 3.0 2.5 2.0 1.5 1.0 ppm
1.00
3.04
0.98
1.99
2.05
6.04

P2

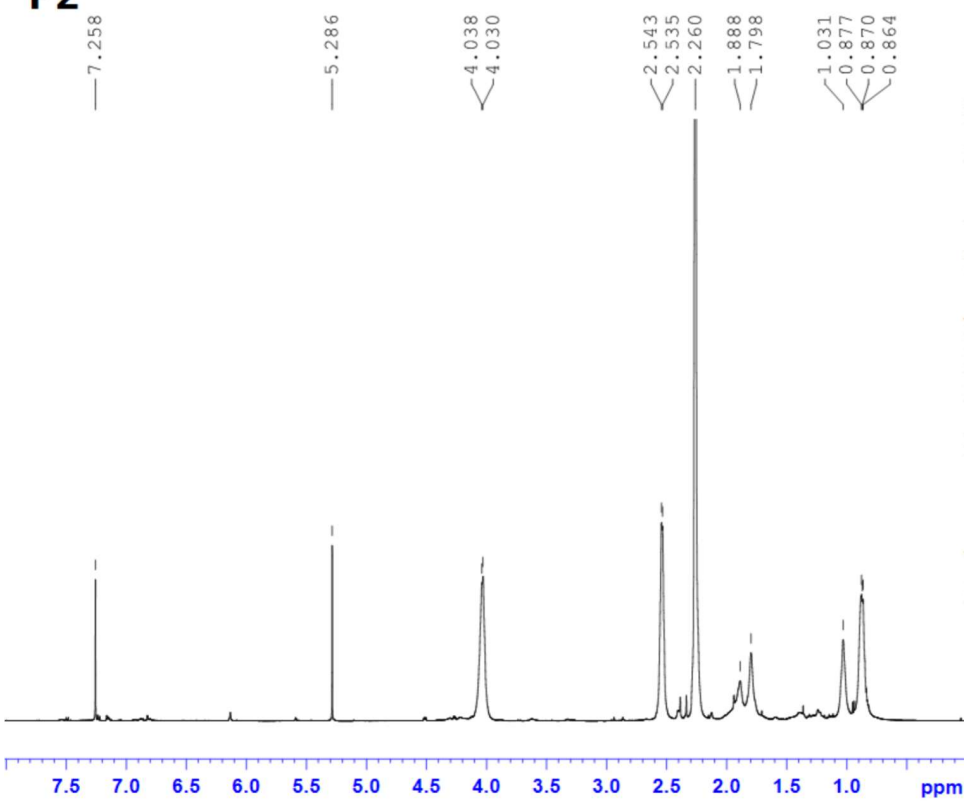
7.258
5.286
4.038
4.030
2.543
2.535
2.260
1.888
1.798
1.031
0.877
0.870
0.864
7.5 7.0 6.5 6.0 5.5 5.0 4.5 4.0 3.5 3.0 2.5 2.0 1.5 1.0 ppm

P3

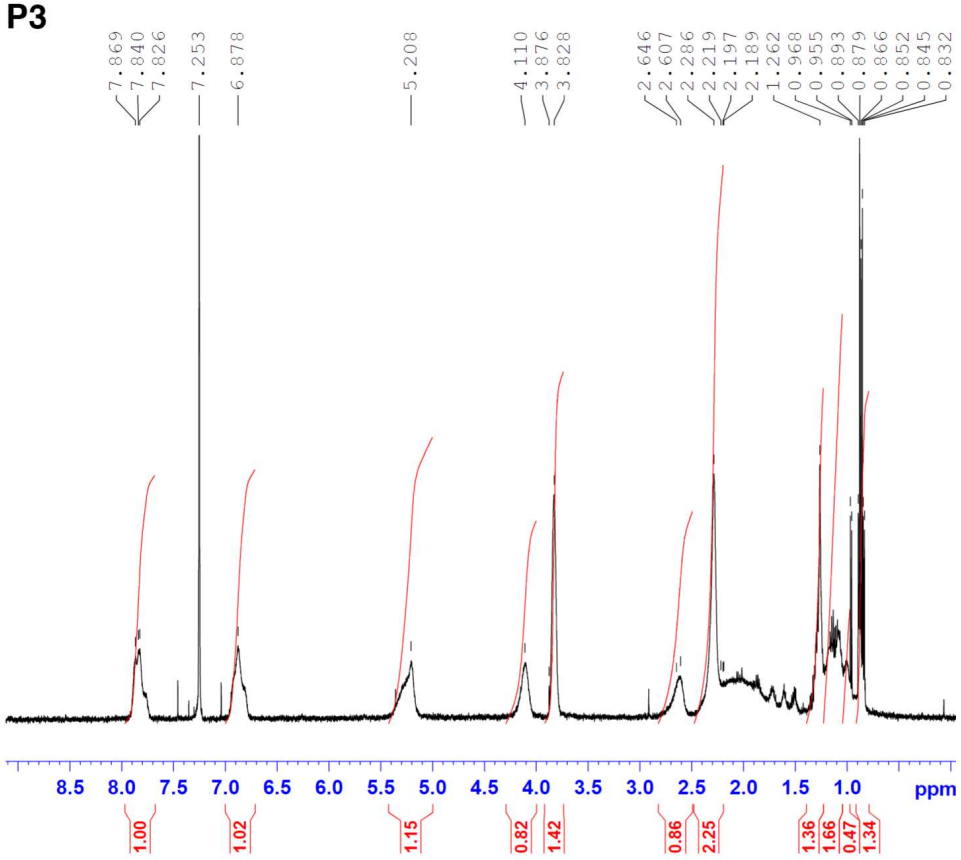
7.869
7.840
7.826
7.253
6.878
5.208
4.110
3.876
3.828
2.646
2.607
2.286
2.219
2.197
2.189
1.262
0.968
0.955
0.893
0.879
0.866
0.852
0.845
0.832
8.5 8.0 7.5 7.0 6.5 6.0 5.5 5.0 4.5 4.0 3.5 3.0 2.5 2.0 1.5 1.0 ppm
1.00
1.02
1.15
0.82
1.42
0.86
2.25
1.36
1.66
0.47
1.34

Chapter 4

Photochemical Control of Noncovalent Interactions in Polyelectrolyte Colloids

Reproduced in part with permission from:
Hu, X.; Feeney, M. J.; McIntosh, E.; Mullahoo, J.; Jia, F.; Xu, Q.; Thomas, S. W., Triggered Release of Encapsulated Cargo from Photoresponsive Polyelectrolyte Nanocomplexes.
ACS Applied Materials & Interfaces **2016**, *8*, 23517-23522.
Copyright 2016 American Chemical Society.

4.1 INTRODUCTION

Polyelectrolyte complexes (PECs) and coacervates are associated complexes between oppositely charged polyelectrolytes that form spontaneously upon mixing solutions of polyanions and polycations under appropriate aqueous conditions. The ion pairing between the oppositely charged polymers, resulting in the release of counterions, together with van der Waals and hydrophobic interactions, provide the driving force for assembly. The formation of PECs can be highly sensitive to parameters such as polymer structure, charge density along polymer chains, polyelectrolyte concentration, mixing ratio between polycations and polyanions, mixing order, salt type, ionic strength.[1-5] The association complexes formed by mixing oppositely charged polyelectrolyte solutions may be precipitates (solid-liquid macrophase separation), coacervates (liquid-liquid phase separation), or colloidal nanoparticles. PECs have been used as carriers to deliver drugs,[6, 7] enzymes,[8] proteins[9] and DNA,[10, 11] and used in other applications such as solar cells,[12] chemical sensors,[13] and membranes.[14, 15]

Stimuli-responsive materials that degrade on demand upon exposure to applied stimuli have received tremendous interest.[16] The photoresponsive PEMs we described in Chapter 3 comprise polycations with photoclevable benzylic ester sidechains that yield carboxylic acid groups upon irradiation with light.[17, 18] This charge-generating characteristic renders PEMs soluble due to the disrupted electrostatic attraction between oppositely charged polyelectrolytes. The potential for preparing light responsive polycations with nitrobenzyl ester groups linking the cationic sidechains with the polymer backbone offers the possibility to “charge-shift” polycations to oppositely charged polyanions. Sullivan, Epps, and coworkers[11] have reported using a charge-shifting cationic diblock copolymer prepared via atom transfer radical polymerization (ATRP), to bind negatively charged DNA for photoinduced nucleic acid delivery.

Chapter 4 describes a charge-shifting polycation **P+** synthesized via free radical random copolymerization of photolabile, positively-charged monomers with the hydrophilic neutral monomer polyethylene glycol methacrylate. Dilute, nonstoichiometric aqueous mixtures of cationic **P+** and anionic poly(styrene sulfonate) (PSS) yield colloidal suspensions of nanoparticles with diameters of 50-100 nm. Upon irradiation, photolysis of the nitrobenzyl groups changes the photolabile polycation **P+** into polyanion **P-** through a charge shifting mechanism as disscused in Chapter 3. The resulting lack of ion-pairing complementarity between P- with poly(styrene sulfonate) (PSS) causes the nanoparticles to dissolve, and the triggered release of the encapsulated guest Nile Red into solution.

4.2 Design and Synthesis of Photolabile Charge-Shifting Polycation

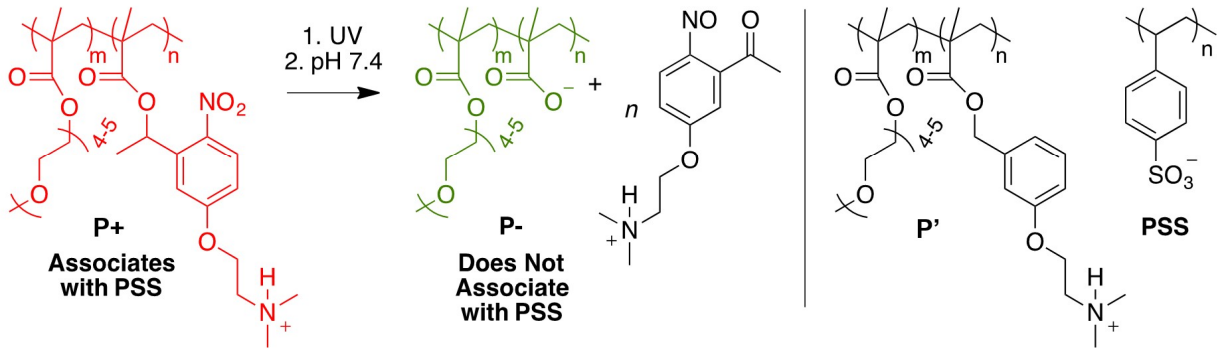

Figure 4.1: *Left*: Photoinduced charge-shifting of positively charged **P+** to negatively charged **P-.** *Right*: Chemical structure of control polycation **P'** and polyanion PSS.

We designed a light responsive polycation (**Figure 4.1**) with nitrobenzyl ester groups linking the cationic sidechains with the polymer backbone offers the possibility to "charge-shift" polycations to oppositely charged polyanions. This methacrylic polycation contains both

hydrophilic oligo(ethylene glycol) and tertiary amine side chains linked to the polymer backbone through α-methylated *ortho*-nitrobenzyl (ONB) ester linkers. Photolysis of the ONB esters cleaves the benzylic C-O bonds through a radical mechanism, separating the amine groups from the polymer and leaving behind carboxylic acid pendants bound to the polymer backbone. At near-neutral pH values, therefore, photolysis events convert pendants of **P+** from having positive formal charges to negative formal charges. As ion pairing of cations and anions is primarily responsible for the association of oppositely charged polyelectrolytes in aqueous media, we hypothesized that such a chemical change would disrupt these interchain interactions and cause such polyelectrolyte complexes to dissolve (**Figure 3.2**).

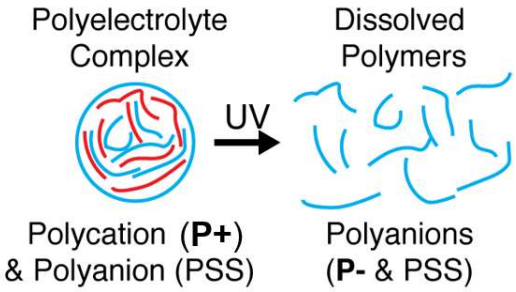

Figure 4.2: Schematic of the light-triggered disruption of nanoscale PECs.

Our synthesis of charge-shifting polycation **P+** and photoinert control polymer **P'** were straightforward (**Scheme 4.1**). Low yields of monomer **M'** resulted from its rapid self-polymerization upon synthesis. Free-radical random co-polymerization, using AIBN as initiator, of either **M+** or **M'** with 1 molar equivalent of commercially available oligo(ethylene glycol) methacrylate (Mw ≈ 300 g/mol, OEGMA) gave **P+** (Mn = 5.1 kDa, Mw = 7.0 kDa, GPC) or **P'** (Mn = 3.5 kDa, Mw = 4.7 kDa, GPC) respectively. The molar ratio of incorporation of OEGMA units and **M+** units in **P+** was 45:55 as determined by ^{1}H NMR spectroscopy. We chose OEGMA

as a comonomer in **P+** and **P'** because: i) it is neutral and will not interfere with the ionic interactions, ii) polyethylene glycol is a widely used nontoxic material to stabilize nanoparticles[19] and iii) it renders **P+** soluble in water—the homopolymer of **M+** had limited water solubility even after protonation.

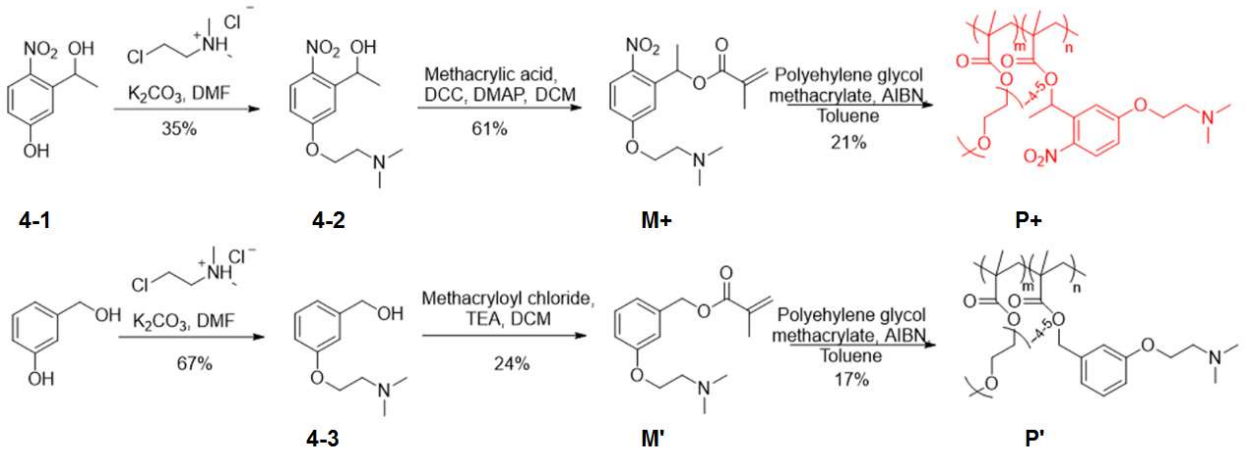

Scheme 4.1: Synthesis of photoreactive polymer **P+** and photoinnert control polymer **P'**.

4.3 Preparation of Polyelectrolyte Colloidal Nanoparticles

Table 4.1. Influence of **P+**/PSS mixing ratios on the size distributions of PECs prepared.

[PSS] (mg/mL)	[**P+**] (mg/mL)	**P1**:PSS[a]	Diameter[b] (nm)	PDI	Zeta potential (mV)
0.070	0.20	1	7700 ± 2200[c]	0.40	-0.13 ± 5
0.070	0.60	3	52 ± 1	0.18	+ 13 ± 1
0.21	0.20	0.33	87 ± 2	0.16	- 31 ± 3

All measurements are the average results of three independent experiments. *a* Molar ratio of charged units. *b* Z-average diameter, *c* PEC solutions with stoichiometric polycation/PSS ratios were not filtered before measurements because the light scattering intensity were too low after filtration.

We then explored conditions for the fabrication of nanoscale colloidal polyelectrolyte complexes by mixing aqueous solutions of **P+** with aqueous solutions of the strong polyanion PSS. Each experiment was performed by injecting a **P+** solution into a PSS solution rapidly while stirring vigorously. In particular, we investigated the influence of the ratio of oppositely charged repeating units (**P+**/PSS*)* on the PECs obtained. Results from dynamic light scattering (DLS) of the resultant suspensions (Table 4.1) show that nanoparticles with relatively narrow size distributions (PDI < 0.2, with Z-average diameters between 50-100 nm) were obtained by using nonstoichiometric ratios of either the cationic or anionic functional groups. When [PSS] = [**P+**], however, macroscale aggregates formed, even though the overall concentration of polymer was lower under these mixing conditions.

Table 4.2. Sizes and zeta potential of PECs upon dilution by 50% (v/v).

		1:3 **P+** : PSS		3:1 **P+** : PSS	
		Before Dilution	After Dilution	Before Dilution	After Dilution
Diluted by water	*d* (nm)	89	85	50	51
	PDI	0.15	0.16	0.16	0.17
	ζ (mV)	-27	-29	+ 14	+14
Diluted by 30 mM pH 7.4 buffer	*d* (nm)	88	86	53	53
	PDI	0.16	0.15	0.18	0.15
	ζ (mV)	-33	-30	+14	+11

This observation, in addition to the sign of zeta potential corresponds to the sign of the excess polyelectrolyte component, is consistent with known behaviour of such complexes:[1, 3, 20] nonstoichiometric mixing ratios of polycations and polyanions yield complexes that consist

of a charge neutral core and a shell enriched in the excess polymer, stabilizing the colloid via electrostatic repulsion between particles. These nonstoichiometric PECs are also stable over our observation time of 3 days and upon dilution with DI water or buffer solution of the same concentration (**Table 3.2**). AFM and SEM images (**Figure 4.3**), as well as visual observation of the Tyndall effect (**Figure 4.4**) are also consistent with nanoparticle formation.

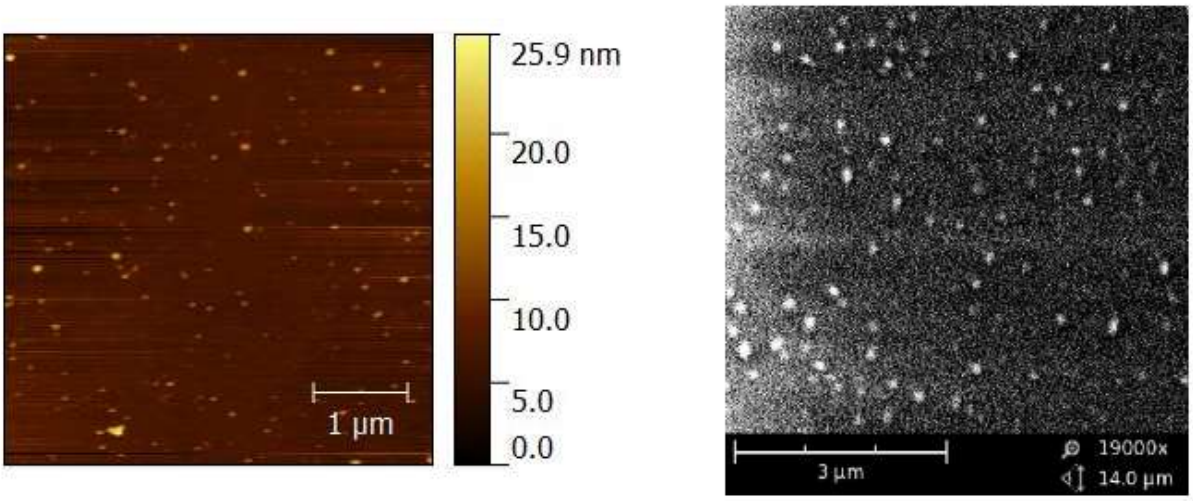

Figure 4.3. AFM and SEM images of the polyelectrolyte nanocomplexes (PSS:**P+** = 3:1, by charged repeating units). Sample preparation: one drop of PEC solution was applied onto a plasma cleaned watch glass using a pipet, and the bulk of the droplet was wicked away using a paper towel. The sample was gently rinsed with 1-2 drops of deionized water to rinse away salt from the buffered solution, then dried using a mild flow of clean compressed air before AFM or SEM measurements.

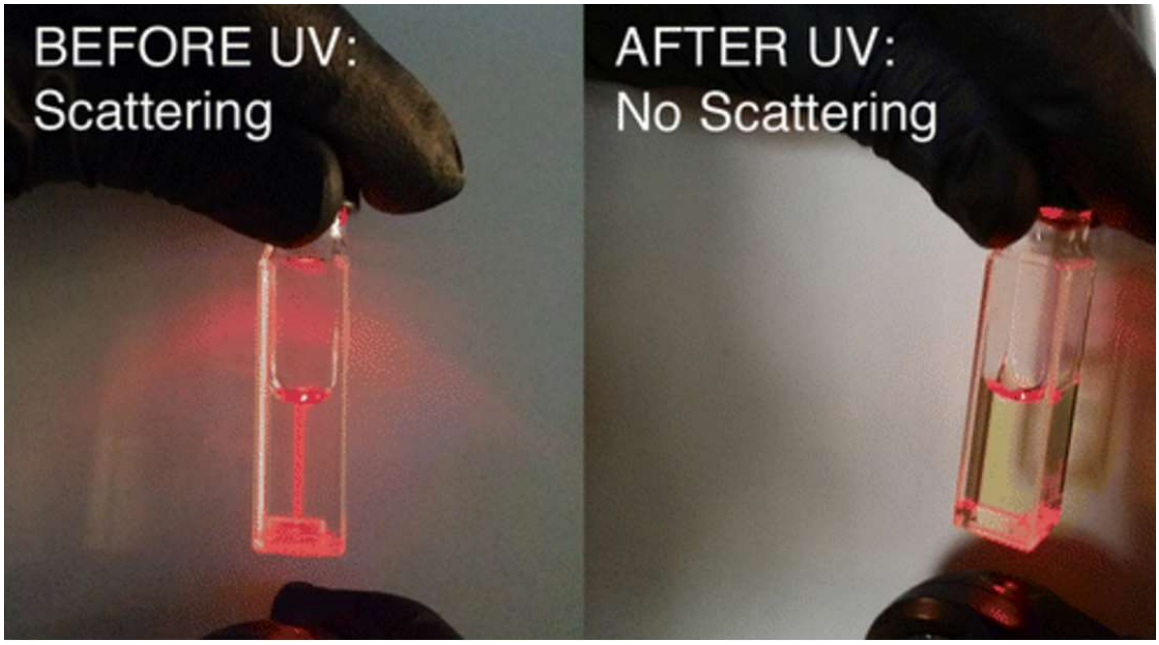

Figure 4.4: Tyndall effect was observed with the PEC solution before photodegradation (*left*), and was absent after photolysis (*right*).

4.4 Photochemical Disruption of Polyelectrolyte Complexes

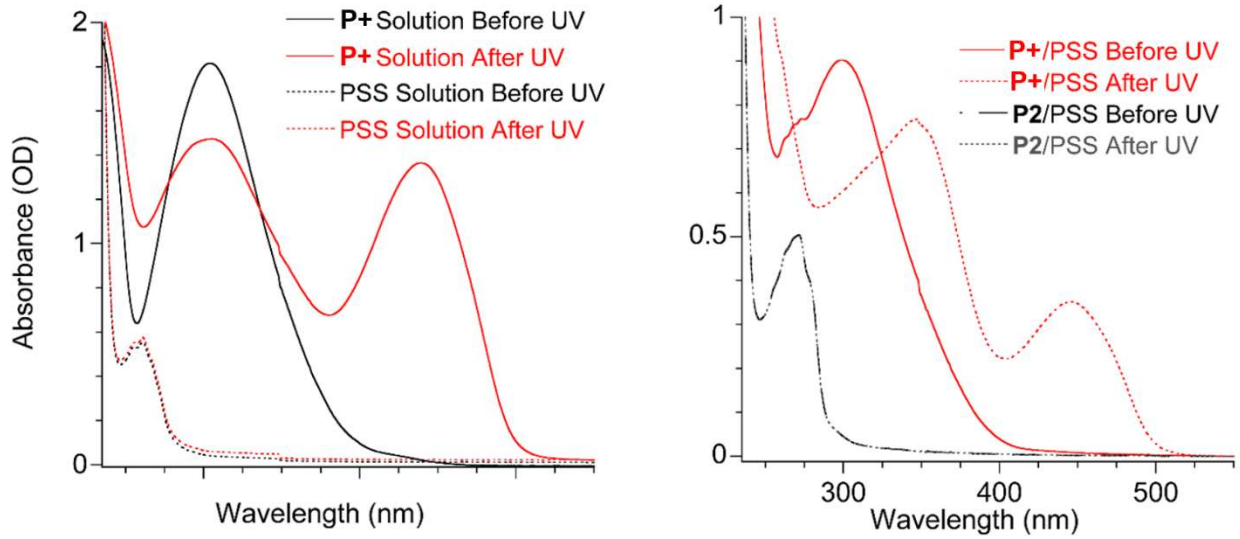

Figure 4.5. UV spectral change of the unmixed polyelectrolytes (*left*) and PECs prepared from a 1:3 **P+**:PSS ratio (*right*) after irradiation (365 nm, 20 mW/cm^2) for 15 minutes in 30 mM pH 7.4 phosphate buffer.

UV/vis spectrophotometry of **P+** in solution and its complexes with PSS provided evidence for photolysis of the nitrobenzyl groups upon irradiation with UV light. After UV irradiation at 365 nm (5.0 mW/cm^2), the characteristic absorption peak of the nitrobenzyl groups in **P+** at 310 nm (Figure 4.5, left) decreased by ~20%, while a new peak at approximately 450 nm emerged, which we attribute to the expected arylnitroso ketone and other downstream photoproducts. PSS showed no significant change in UV/vis spectra after irradiation under identical conditions. Similar spectral changes (Figure 4.5, right) occurred upon irradiation of a sample of **P+**/PSS PEC with molar ratio of 1:3, with a stationary state reached after approximately 15 minutes of irradiation (Figure 4.6), suggesting the complete photolysis of nitrobenzyl groups from **P+**. In a control experiment, an analogous photoinert PEC solution prepared with photoinert polycation **P'** and PSS was irradiated under the same condition. The photoinert PEC solution showed negligible spectral change upon irradiation.

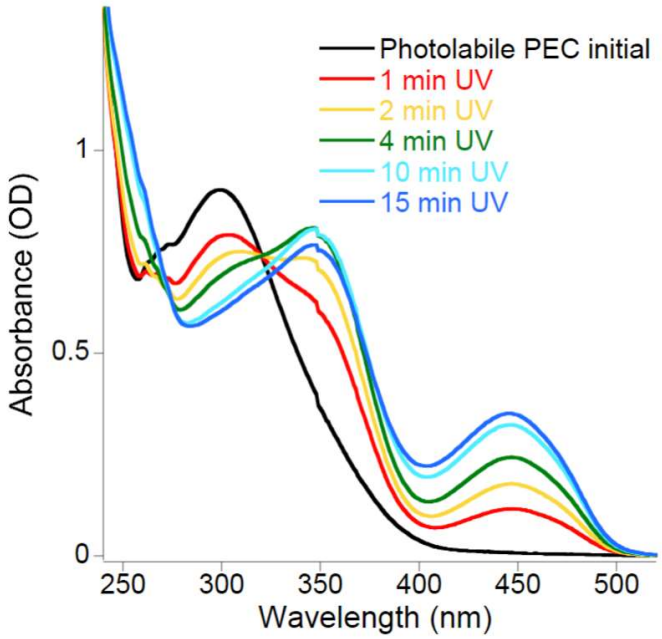

Figure 4.6: UV spectra of the photolabile (1:3 **P+**:PSS) PEC solution depending on irradiation time (365 nm, 20mW/cm^2).

DLS measurements of the nanoscale PECs before and after UV irradiation demonstrated that photolysis of the nitrobenzyl groups did indeed yield PEC dissolution. **Figure 4.7** shows that after 5 minutes of irradiation at 365 nm (20.0 mW/cm^2), the light scattering intensity of the 1:3 **P+**/PSS complex suspension decreased by more than a factor of 50, together with a decrease of the Z-average particle size. UV/vis absorbance spectra acquired during these irradiation experiments (an example is shown in **Figure 4.8**) suggest that approximately 50% conversion of the ONB esters occurs after five minutes of irradiation. Although the complexes prepared using a 3:1 molar ratio of **P+**:PSS largely dissolved after 20 minutes of UV irradiation, the light scattering intensity and nanoparticle size of this sample both increased during the first 10 minutes of photolysis. We preliminarily attribute this observation to initial increased complexation between the photolysis products **P-** and the excess cationic **P+** in solution during early stages of photolysis. As the degree of photolysis of **P+** increases, however, fewer cationic groups on **P+** are available for ion pairing interaction, leading to complex dissolution. Consequently, the light scattering intensity and Z-average size of nanocomplexes observed using DLS decreased. AFM and SEM images of the irradiated samples also confirmed the dissolution of the PECs, as no particles were observed of samples that had been irradiated.

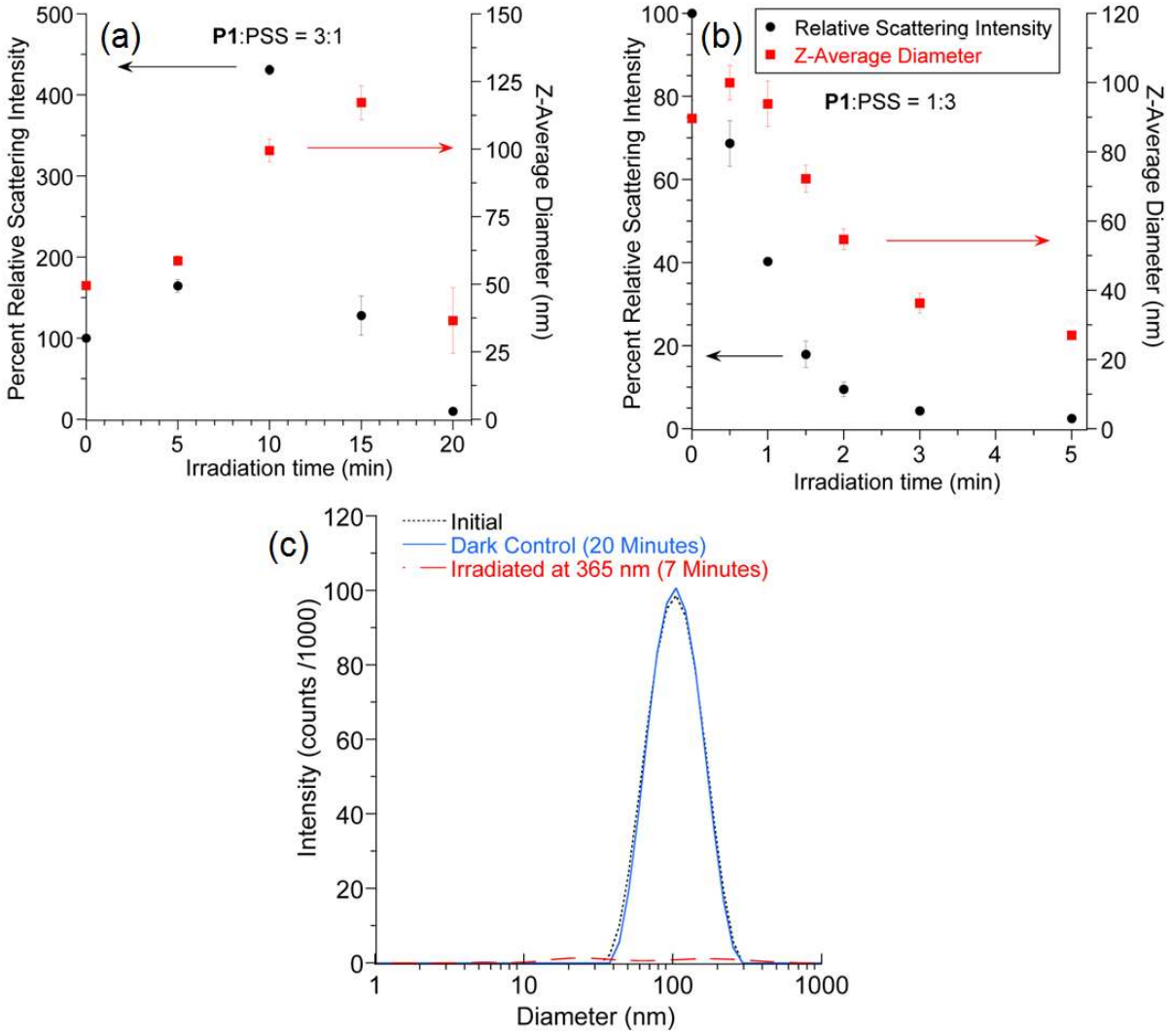

Figure 4.7: Dependence of scattering intensity and Z-average particle diameter, as measured by DLS, for **P**+/PSS polyelectrolyte complexes prepared with 1:3 (*a*) and 3:1 (*b*) molar ratios upon irradiation at 365 nm (20 mW/cm^2). Error bars represent one standard deviation of three independent trials. (*c):* Dynamic light scattering data of a 1:3 **P**+/PSS complex sample before and after irradiation at 365 nm (20 mW/cm^2) for 7 minutes.

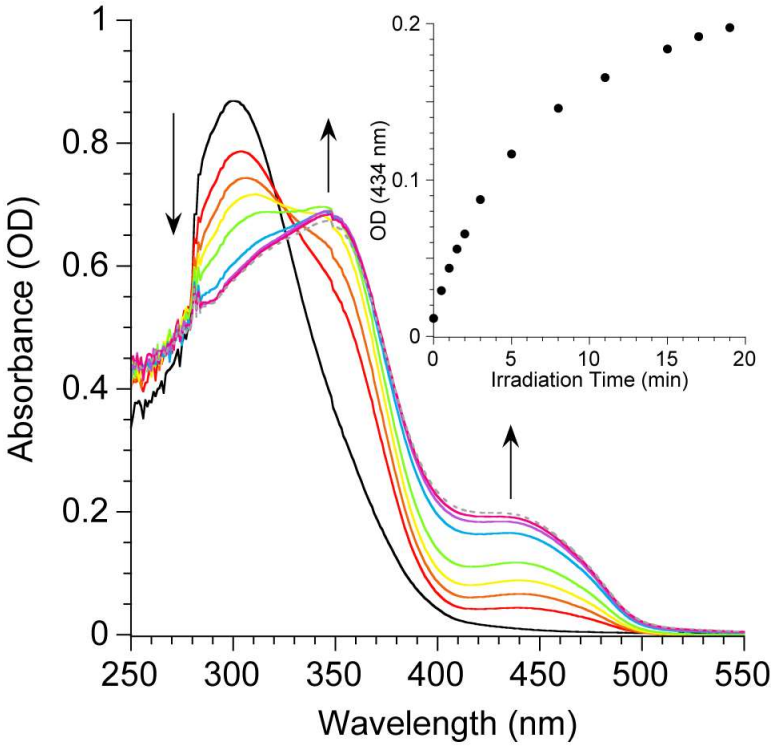

Figure 4.8. Dependence of UV/vis spectra of 1:3 **P**+/PSS nanoparticles on irradiation time. These spectra were acquired as part of the irradiation experiment described in **Figure 4.7**.

In control experiments, the sizes and scattering intensities of **P**+/PSS nanoparticles prepared with either 1:3 and 3:1 molar ratios kept in the dark for 20 minutes decreased by less than 1%. Moreover, exposure of analogous PECs comprising **P'**/PSS in either a 1:3 or 3:1 molar ratio to identical irradiation conditions with UV light induced less than 10% change of the scattering intensities or sizes to the photoinert PECs comprising **P'**/PSS as determined by DLS (**Table 4.3**), and also caused no significant change in UV/vis spectra of the sample (**Figure 4.9**).

Table 4.3: Photostability of photoinert PEC comprising **P'** and PSS

Photoinert PEC (**P'**/PSS=1/3)	Diameter (nm)	Intensity (1000 counts)	PDI	Zeta potential (mV)
Initial	80	286	0.14	-16.5
Irradiated*	85	296	0.15	-10.4

Photoinert PEC (**P'**/PSS=3/1)	Diameter (nm)	Intensity (1000 counts)	PDI	Zeta potential (mV)
Initial	77	135	0.16	+7.9
Irradiated*	75	130	0.19	+7.9

* 365 nm, 20 min, 20 mW/cm^2.

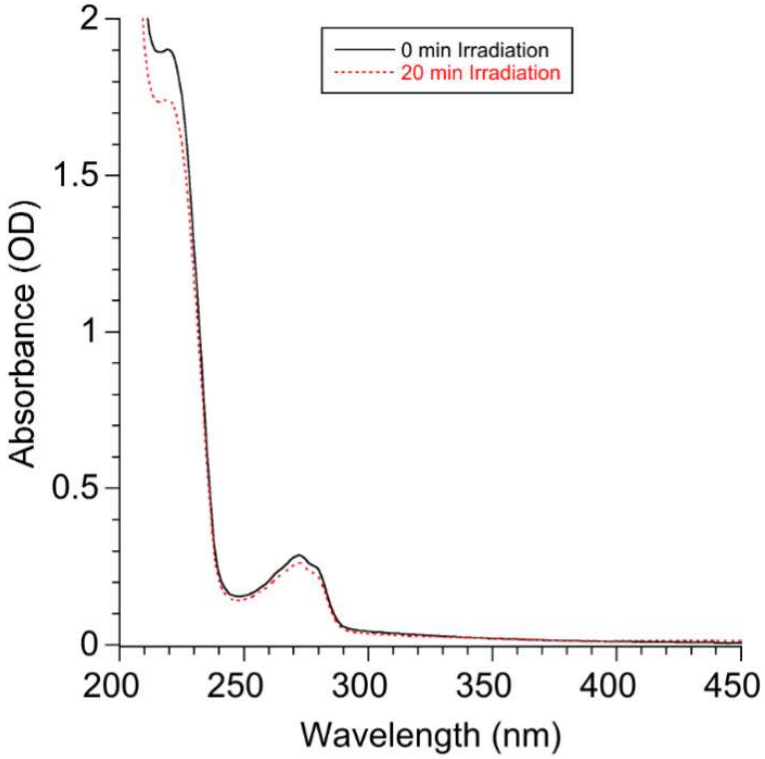

Figure 4.9: Irradiation (365 nm, 20 mW/cm^2, 20 min) of photoinert PEC comprising PS/**P'** (1/3) did not result in any significant change in spectra.

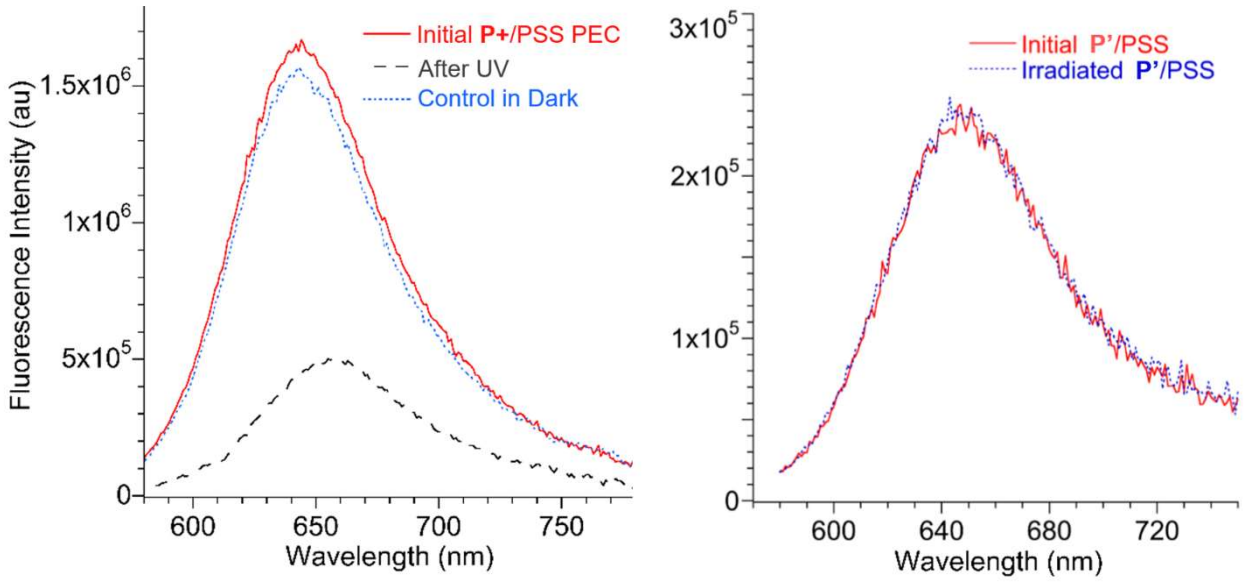

Figure 4.10: Left: Photo-triggered dissolution of photolabile PECs of **P+**/PSS (1:3) resulted in the release of cargo molecule (NR) after 5 minutes of irradiation at 365 nm (20 mW/cm^2). Right: An analogous experiment in which irradiation of photoinert PEC comprising **P'**/PSS (1:3) did not trigger the release of loaded NR.

4.5 Light Triggered Release of Encapsulated Cargo from PEC Colloidal Nanoparticles

To demonstrate that these photolabile complexes were capable of releasing encapsulated cargo, we used Nile Red (NR), a hydrophobic fluorescent molecule with a lower quantum yield of fluorescence in water than in less polar environments, as a guest molecule. The fluorescence of a suspension containing **P+**/PSS (1:3) PECs loaded with NR was monitored before and after UV irradiation. UV irradiation of these PECs for 5 minutes at 365 nm (20 mW/cm^2) caused the fluorescence intensity from NR to decrease (Figure 4.10 *left*), which is indicative of the release of NR into aqueous solution.[21, 22]

To control for UV-induced photobleaching of NR as an alternative explanation for this result, we irradiated a control PEC sample comprising NR encapsulated within **P'**/PSS (1:3) nanoparticles. UV irradiation under identical conditions did not change the fluorescence spectrum or intensity from NR in this sample (Figure 5.10 *right*).

4.6 Conclusions

This chapter demonstrates a photochemical approach to control noncovalent ion-pairing interactions between oppositely charged polyelectrolytes in colloidal nanocomplexes, which has has potential application in phototriggered delivery. The advantages of this approach are i) the simple preparation procedures, both in terms of polymer synthesis and polymer self-assembly, of these photosensitive PECs, ii) the stability of these nanomaterials in buffer over time, and iii) rapid degradation and release upon irradiation.

4.7 Experimental Section

General Considerations

All synthetic manipulations were performed under standard air-free conditions under an atmosphere of argon gas with magnetic stirring. Flash chromatography was performed using silica gel (230-400 mesh) as the stationary phase. NMR spectra were acquired on a Bruker Avance III 500 spectrometer. Chemical shifts are reported relative to residual protonated solvent (7.26 ppm for $CHCl_3$). Polymer molecular weights were determined using a Shimadzu gel permeation chromatography (GPC) system equipped with a Tosoh TSKgel GMHhr-M mixed-bed column and guard column using the UV detector. The column was calibrated with low

polydispersity poly(styrene) standards (Tosoh, PS Quick Kit) with THF as the mobile phase eluting at 0.75 mL/min. Methacryloyl chloride was freshly distilled and used immediately. All other reactants and solvents were purchased from commercial suppliers and used without further purification. Dry THF and dry CH_2Cl_2 were obtained from an Innovative Technologies PureSolv 400 solvent purifier.

All solution optical spectra were acquired of samples in quartz cuvettes (NSG Precision Cells). Electronic absorbance spectra were acquired with a Varian Cary-100 instrument in double beam mode using a solvent-containing cuvette for background subtraction spectra of solution samples. Fluorescence emission spectra were obtained by using a PTI Quantum Master 4 equipped with a 75 W Xe lamp. Fluorescence spectra were corrected for both the output of the lamp and for the response of the photomultiplier tube detector to different wavelengths. Solutions used in the fabrication, processing and response of films were all aqueous solutions unless otherwise mentioned. Dynamic light scattering (DLS) and zeta potential results were collected using a Malvern Zetasizer Nano-ZS. AFM and SEM images were obtained using a Veeco D3100S-1 and a Phenom G2 Pure Table Top SEM (operating at 5 kV), respectively. Detailed synthetic procedures can be found in the Supporting Information.

Preparation of PEC solutions

Buffered solutions (30 mM pH 7.4 phosphate buffer) with various concentrations (0.34 or 1.02 mM, based on charged repeat unit) of **P+** and PSS were prepared. A PEC solution was prepared by rapidly adding a stoichiometric volume of the buffered **P+** solution into a volume of PSS solution while stirring vigorously. The solution was stirred for around 1 min after mixing. All PEC solutions prepared were filtered through a 0.45 nm hydrophilic PTFE filter (A ChemTek Inc.) prior to Dynamic Light Scattering (DLS) measurements, unless otherwise mentioned.

Preparation of a Nile Red (NR) loaded PEC solution

To prepare a NR loaded colloid solution, 5.0 μL acetone solution of NR (0.01%, w/v) was added into 2.0 mL **P+** or **P'** solution (0.20 mg/mL) in pH 7.4 30 mM phosphate buffer), The polycationic solution was then quickly added into 2.0 mL PSS solution (0.21 mg/mL, pH 7.4, 30 mM phosphate buffer). A fluorescence spectrum of the NR loaded PEC solution was collected, then 2.0 mL of the solution was irradiated with 365 nm UV light and the other 2.0 mL solution was kept in the dark.

Irradiation experiments

In each irradiation experiment, 2.0 mL photolabile PEC solution was prepared and filtered as described above. 1.0 mL of the sample was transferred into a cuvette (light path = 10 mm), and subjected to measurement of size by DLS, after which the solution was kept in the dark. The other 1.0 mL was placed under 365 nm UV light for a certain time and also subjected to measurement of size by DLS.

Synthesis Procedures

Compound **4-1** was synthesized as reported in Chapter 2.

Compound **4-2**: To a 50 mL three neck round bottom flask was added compound **4-1** (1.83 g, 0.010 mol), K_2CO_3 (3.45 g, 0.025 mol), and 20 mL DMF. After stirring for 10 min, 2-chloro-N,N-dimethylethylamine hydrochloride (1.44 g, 0.010 mol) was added into the flask. The reaction was stirred at ambient temperature for 1 day, then diluted with 5% Na_2CO_3 solution and extracted with diethyl ether two times. The organic phase was combined and washed with 5%

Na_2CO_3 solution three times, dried over $MgSO_4$, filtered, and concentrated using a rotary evaporator. A light brown liquid was obtained as the product (0.90 g, yield 35 %). ^{1}H NMR (500 MHz, $CDCl_3$) d 8.03 (d, *J* = 9 Hz, 1H), 7.35 (d, *J* = 3 Hz), 1H), 6.86 (dd, *J* = 9 Hz, 3 Hz, 1H), 5.54 (q, *J* = 6 Hz, 2H), 4.15 (t, *J* = 5 Hz, 2H), 2.75 (m, 2H), 2.34 (s, 6H), 1.54 (d, *J* = 6 Hz).

M+: To a 50 mL three neck round bottom flask was added compound **4-2** (0.90 g, 3.5 mmol), DCC (1.0 g, 4.8 mmol), DMAP (0.10 g, 0.82 mmol), methacrylic acid (0.37 g, 4.30 mmol) and 20 mL dry dichloromethane. This mixture was stirred overnight at ambient temperature. The reaction was filtered, concentrated, and purified via flash chromatography using hexane: dichloromethane: TEA (3:1:0.1 by volume) as eluent to yield **M+** as a light yellow solid (0.72 g, yield 61%). (0.1% w/w hydroquinone was added to **M+** as a stabilizer). ^{1}H NMR: (500 MHz, $CDCl_3$) d 8.07 (d, *J* = 9 Hz, 1H), 7.11 (d, *J* = 3 Hz, 1H), 6.87 (dd, *J* = 9 Hz, 3 Hz, 1H), 6.18 (m, 1H), 5.55 (m, 1H), 4.12 (m, 2H), 2.75 (m, 2H), 2.34 (s, 6H), 1.95 (m, 3H), 1.55 (m, 3H). ^{13}C NMR (125 MHz) d 166.1, 163.0, 141.6, 140.5, 136.2, 127.6, 125.9, 112.9, 112.9, 68.7, 66.7, 58.0, 45.9, 22.0, 18.3.

Compound **4-3**: To a 50 mL three neck round bottom flask was added 3-hydroxylbenzyl alcohol (1.24 g, 0.010 mol), K_2CO_3 (4.14 g, 0.030 mol), and 25 mL DMF. After stirring for 10 min, 2-chloro-N,N-dimethylethylamine hydrochloride (1.6 g, 0.011 mol) was added into the flask. The reaction was stirred at ambient temperature for 1 day, then diluted with 5% Na_2CO_3 solution and extracted with diethyl ether two times. The organic phases were combined and washed with 5% Na_2CO_3 solution three times, dried over $MgSO_4$, filtered, and concentrated using a rotary evaporator. An orange liquid was obtained as the product (0.40 g, yield 21%) and carried on without further purification.

M': To a 25 mL three neck round bottom flask was added compound **4-3** (0.30 g, 1.5 mmol), TEA (0.25 mL, 1.8 mmol), and dichloromethane (10 mL). The mixture was cooled to 0°C, and methacryloyl chloride (0.23 g, 2.2 mmol) was added dropwise. The reaction was stirred overnight at ambient temperature, then concentrated, and purified via flash chromatography using hexane: ethyl acetate: TEA (4:1:0.1 by volume) as eluent to yield **M'** as a colorless oil (0.27 g, yield 67%). (0.1% w/w hydroquinone was added to **M'** as a stabilizer). ^{1}H NMR (500 MHz, $CDCl_3$) d 7.27 (m, 1H), 6.83-6.96 (m, 3H), 6.16 (m, 1H), 5.90 (m, 1H), 5.16 (s, 2H), 4.08 (m, 2H), 276 (m, 2H), 2.36 (s, 6H), 1.97 (m, 3H). ^{13}C NMR (125 MHz, $CDCl_3$) d 167.2, 159.0, 137.6, 136.2, 129.6, 125.9, 120.3, 114.2, 114.1, 66.2, 65.9, 58.3, 45.9, 18.4.

P+: To a 25 mL vial was added **M+** (0.25 g), **OEGMA** (0.25 g), AIBN (5.0 mg) and toluene (10 mL). The solution was purged with argon gas for 20 minutes, and then stirred at 60 °C overnight. The reaction was cooled to room temperature, and precipitated into a mixture of hexane and diethyl ether (1:1 v:v). The resulting precipitate was collected by centrifugation. The yellow crude product was dissolved in CH_2Cl_2, and re-precipitated as described above. 0.12 g **P+** was obtained as light yellow gum-like solid (yield 24%). ^{1}H NMR (500 MHz, $CDCl_3$) d 7.9-8.1, 6.8-7.2, 6.1-6.4, 3.8-4.3, 3.5-3.7, 3.3, 2.6-2.9, 2.2-2.4, 1.3-1.9, 0.6-1.0 (all broad signals).

P': To a 10 mL vial was added **M'** (0.12 g), **OEGMA** (0.16 g), AIBN (2.5 mg) and toluene (5 mL). The solution was purged with argon gas for 20 minutes, and then stirred at 60 °C overnight. The reaction was cooled to room temperature, and precipitated into a mixture of hexane and diethyl ether (1:1 v:v). The resulting precipitate was collected by centrifugation. The dark crude product was dissolved in CH_2Cl_2, and re-precipitated as described above. **P'** was obtained as light brown gum-like solid (0.048 g, yield 17%).^{1}H NMR (500 MHz, $CDCl_3$) d 7.2, 6.7-6.9, 4.7-5.0, 3.9-4.1, 3.5-3.7, 3.3, 2.6-2.8, 2.2-2.4, 1.7-2.0, 0.7-1.5 (all broad signals).

4.8 References

1. Zhang, Y., et al., *The influence of ionic strength and mixing ratio on the colloidal stability of PDAC/PSS polyelectrolyte complexes.* Soft Matter, 2015. **11**(37): p. 7392-7401.
2. Priftis, D. and M. Tirrell, *Phase behaviour and complex coacervation of aqueous polypeptide solutions.* Soft Matter, 2012. **8**(36): p. 9396-9405.
3. Chiappisi, L., I. Hoffmann, and M. Gradzielski, *Complexes of oppositely charged polyelectrolytes and surfactants - recent developments in the field of biologically derived polyelectrolytes.* Soft Matter, 2013. **9**(15): p. 3896-3909.
4. Bodnár, K., et al., *Impact of Polyelectrolyte Chemistry on the Thermodynamic Stability of Oppositely Charged Macromolecule/Surfactant Mixtures.* Langmuir, 2016. **32**(5): p. 1259-1268.
5. Li, D. and N.J. Wagner, *Universal Binding Behavior for Ionic Alkyl Surfactants with Oppositely Charged Polyelectrolytes.* Journal of the American Chemical Society, 2013. **135**(46): p. 17547-17555.
6. Zhao, X., et al., *Surface charge-reversible polyelectrolyte complex nanoparticles for hepatoma-targeting delivery of doxorubicin.* Journal of Materials Chemistry B, 2015. **3**(30): p. 6185-6193.
7. He, W., et al., *Nanocarrier for Oral Peptide Delivery Produced by Polyelectrolyte Complexation in Nanoconfinement.* Biomacromolecules, 2015. **16**(8): p. 2282-2287.
8. Caruso, F. and C. Schüler, *Enzyme Multilayers on Colloid Particles: Assembly, Stability, and Enzymatic Activity.* Langmuir, 2000. **16**(24): p. 9595-9603.
9. Kayitmazer, A.B., et al., *Protein-polyelectrolyte interactions.* Soft Matter, 2013. **9**(9): p. 2553-2583.
10. Song, Y., et al., *Cellulose-based polyelectrolyte complex nanoparticles for DNA vaccine delivery.* Biomaterials Science, 2014. **2**(10): p. 1440-1449.
11. Green, M.D., et al., *Catch and release: photocleavable cationic diblock copolymers as a potential platform for nucleic acid delivery.* Polymer Chemistry, 2014. **5**(19): p. 5535-5541.
12. Chang, Y.-M., et al., *Electrostatic Self-Assembly Conjugated Polyelectrolyte-Surfactant Complex as an Interlayer for High Performance Polymer Solar Cells.* Advanced Functional Materials, 2012. **22**(15): p. 3284-3289.
13. Li, C., et al., *A General Strategy To Construct Fluorogenic Probes from Charge-Generation Polymers (CGPs) and AIE-Active Fluorogens through Triggered Complexation.* Angewandte Chemie International Edition, 2012. **51**(2): p. 455-459.
14. Wang, X.-S., et al., *Engineering novel polyelectrolyte complex membranes with improved mechanical properties and separation performance.* Journal of Materials Chemistry A, 2015. **3**(14): p. 7296-7303.
15. Kaner, P., et al., *Layer-by-layer surface modification of polyethersulfone membranes using polyelectrolytes and AgCl/TiO2 xerogels.* Journal of Membrane Science, 2015. **493**: p. 807-819.
16. Theato, P., et al., *Stimuli responsive materials.* Chemical Society Reviews, 2013. **42**(17): p. 7055-7056.
17. Gumbley, P., et al., *Wavelength-Selective Disruption and Triggered Release with Photolabile Polyelectrolyte Multilayers.* Chemistry of Materials, 2014. **26**(3): p. 1450-1456.
18. Hu, X., et al., *Stimuli-Responsive Free-Standing Layer-By-Layer Films.* Advanced Materials, 2016. **28**(4): p. 715-721.
19. Jokerst, J.V., et al., *Nanoparticle PEGylation for imaging and therapy.* Nanomedicine, 2011. **6**(4): p. 715-728.
20. Le Cerf, D., et al., *Formation of polyelectrolyte complexes with diethylaminoethyl dextran: Charge ratio and molar mass effect.* Carbohydrate Polymers, 2014. **113**: p. 217-224.
21. Han, D., X. Tong, and Y. Zhao, *Fast Photodegradable Block Copolymer Micelles for Burst Release.* Macromolecules, 2011. **44**(3): p. 437-439.

22. Goodwin, A.P., et al., *Synthetic Micelle Sensitive to IR Light via a Two-Photon Process.* Journal of the American Chemical Society, 2005. **127**(28): p. 9952-9953.

Chapter 4 Appendix

^{1}H and ^{13}C NMR

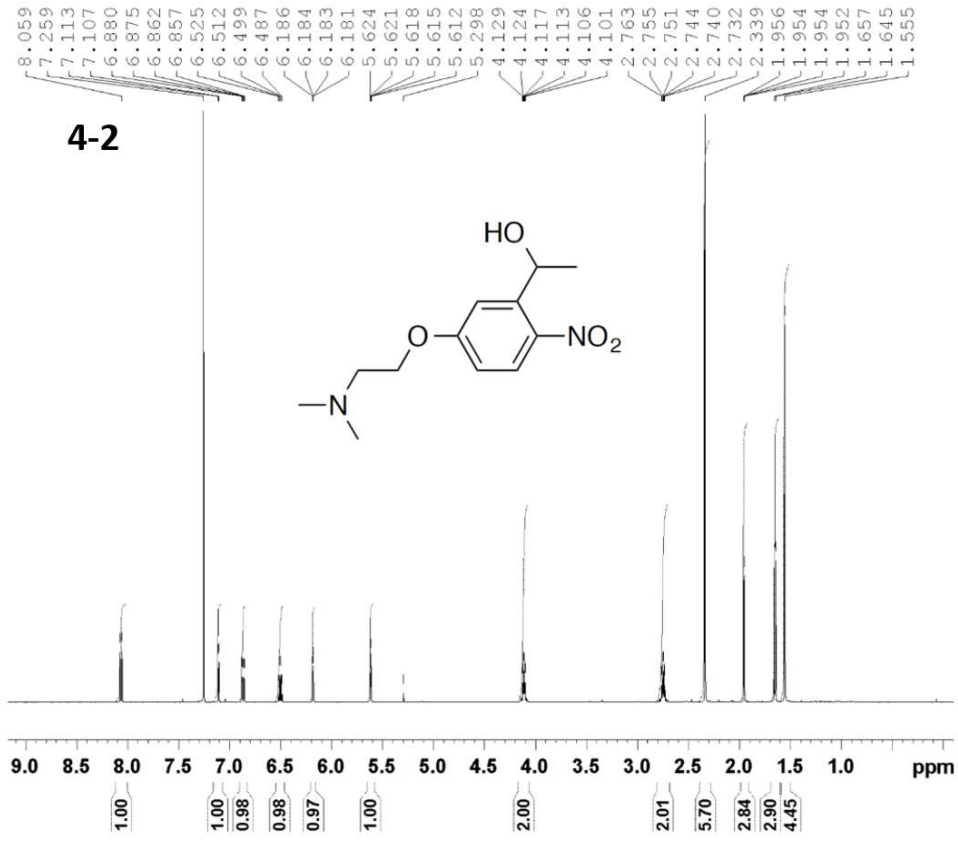
8.059
7.259
7.113
7.107
6.880
6.875
6.862
6.857
6.525
6.512
6.499
6.487
6.186
6.184
6.183
6.181
5.624
5.621
5.618
5.615
5.612
5.298
4.129
4.124
4.117
4.113
4.106
4.101
2.763
2.755
2.751
2.744
2.740
2.732
2.339
1.956
1.954
1.954
1.952
1.657
1.645
1.555
4-2
HO
O
NO2
N
9.0 8.5 8.0 7.5 7.0 6.5 6.0 5.5 5.0 4.5 4.0 3.5 3.0 2.5 2.0 1.5 1.0 ppm
1.00 1.00 0.98 0.98 0.97 1.00 2.00 2.01 5.70 2.84 2.90 4.45

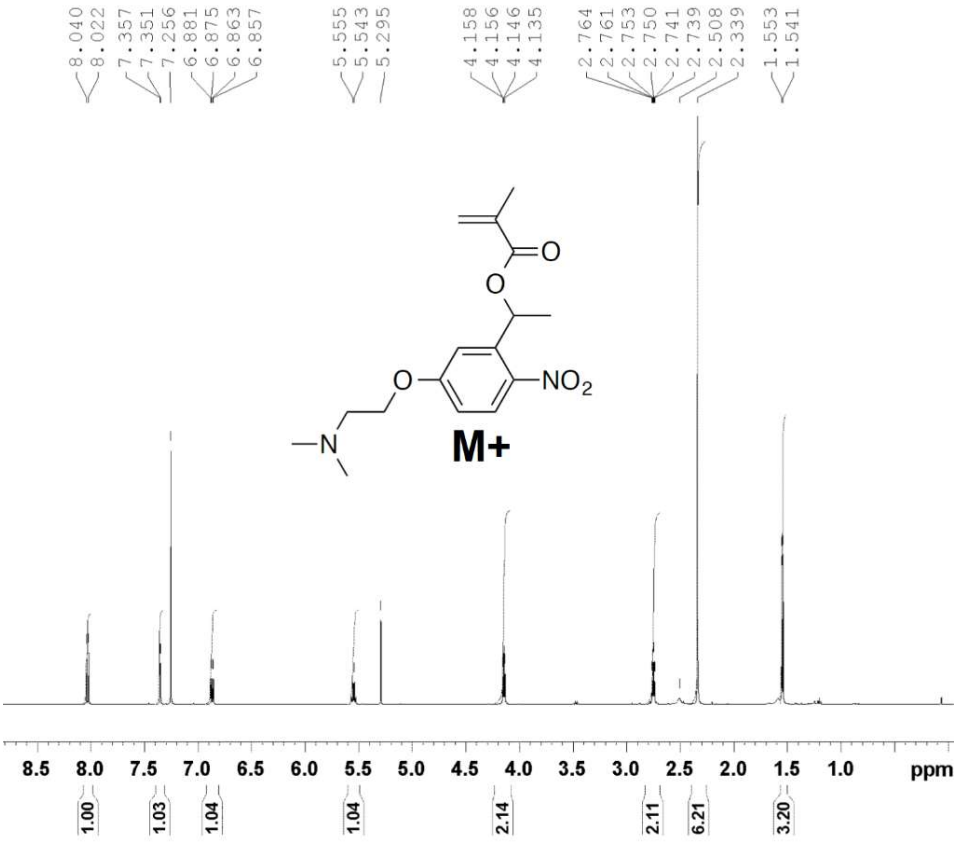
8.040
8.022
7.357
7.351
7.256
6.881
6.875
6.863
6.857
5.555
5.543
5.295
4.158
4.156
4.146
4.135
2.764
2.761
2.753
2.750
2.741
2.739
2.508
2.339
1.553
1.541
O
O
O
NO2
N
M+
8.5 8.0 7.5 7.0 6.5 6.0 5.5 5.0 4.5 4.0 3.5 3.0 2.5 2.0 1.5 1.0 ppm
1.00 1.03 1.04 1.04 2.14 2.11 6.21 3.20

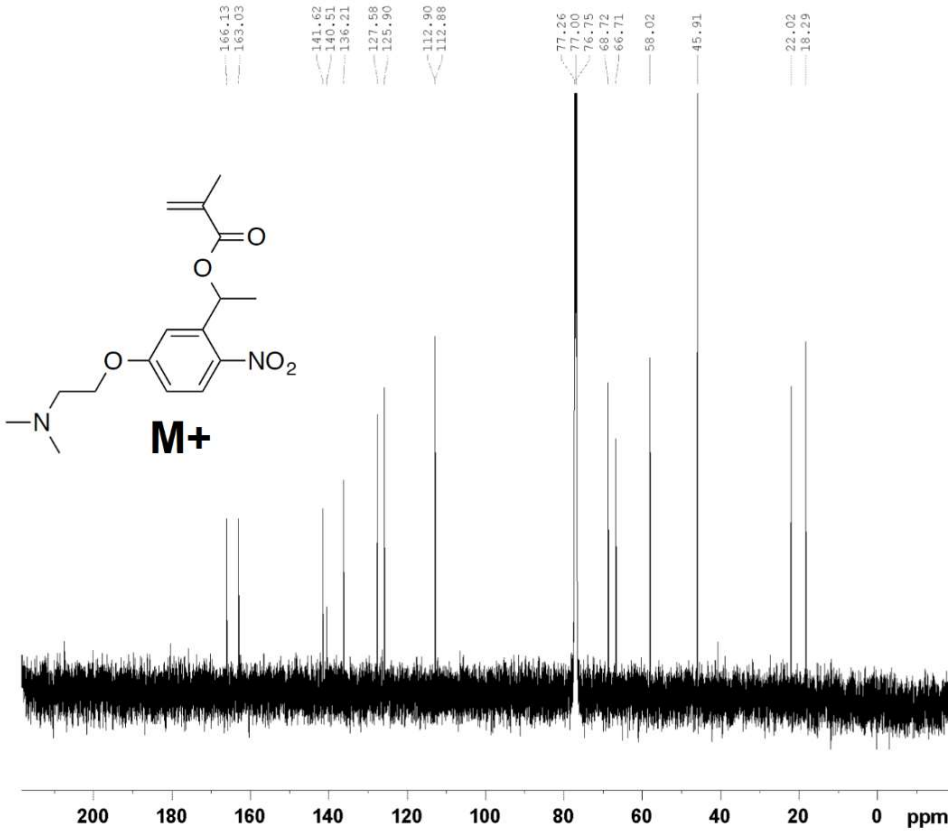
166.13
163.03
141.62
140.51
136.21
127.58
125.90
112.90
112.88
77.26
77.00
76.75
68.72
66.71
58.02
45.91
22.02
18.29
M+
200
180
160
140
120
100
80
60
40
20
0
ppm

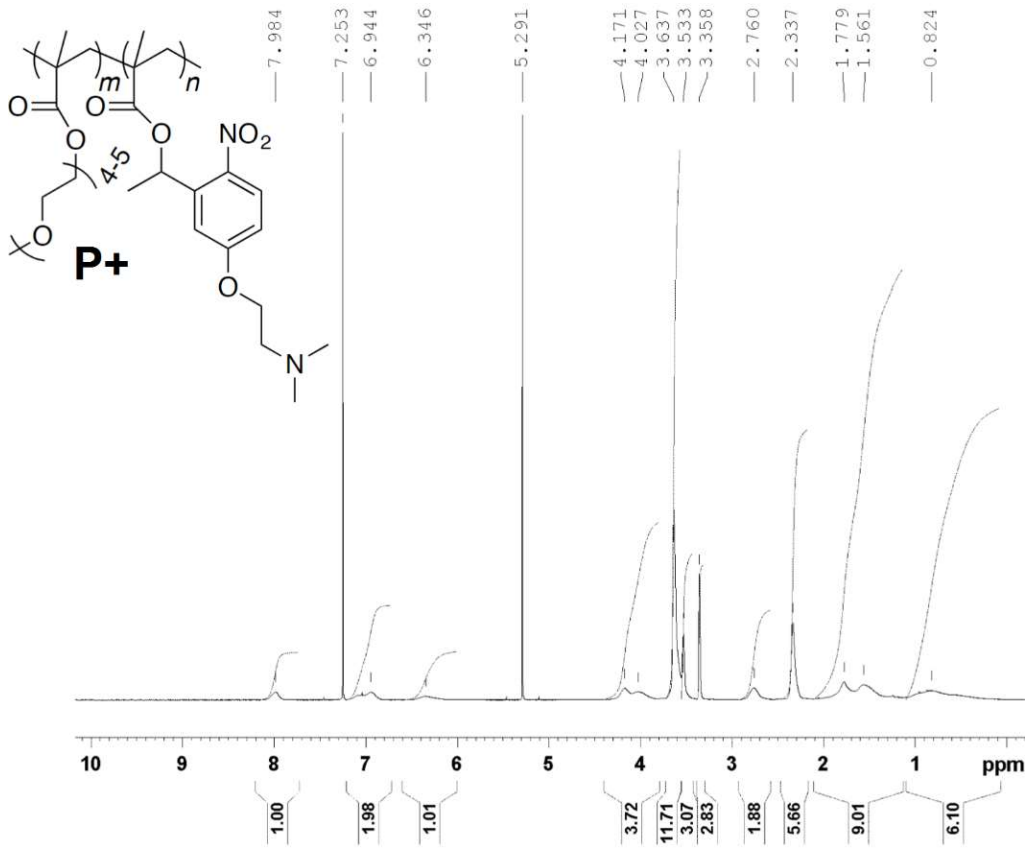
7.984
7.253
6.944
6.346
5.291
4.171
4.027
3.637
3.533
3.358
2.760
2.337
1.779
1.561
0.824
P+
m
n
4-5
NO2
10
9
8
7
6
5
4
3
2
1
ppm
1.00
1.98
1.01
3.72
11.71
3.07
2.83
1.88
5.66
9.01
6.10

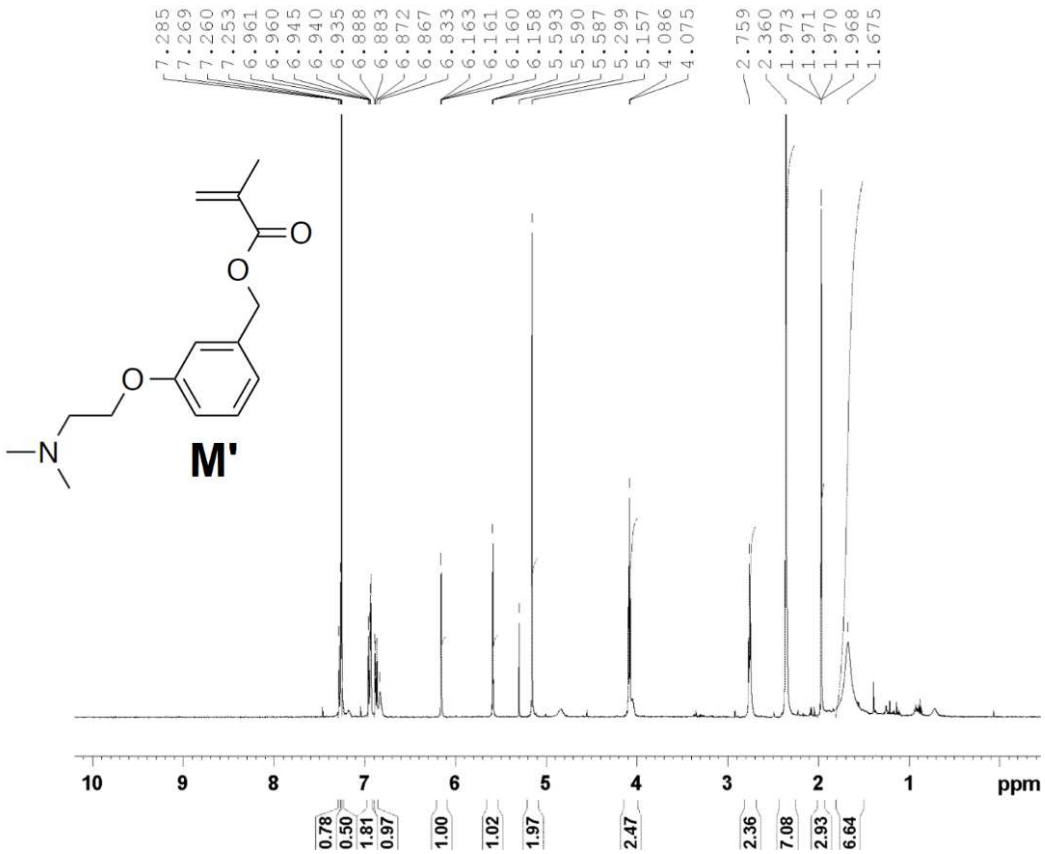
7.285
7.269
7.260
7.253
6.961
6.960
6.945
6.940
6.935
6.888
6.883
6.872
6.867
6.833
6.163
6.161
6.160
6.158
5.593
5.590
5.587
5.299
5.157
4.086
4.075
2.759
2.360
1.973
1.971
1.970
1.968
1.675
M'
10
9
8
7
6
5
4
3
2
1
ppm
0.78
0.50
1.81
0.97
1.00
1.02
1.97
2.47
2.36
7.08
2.93
6.64

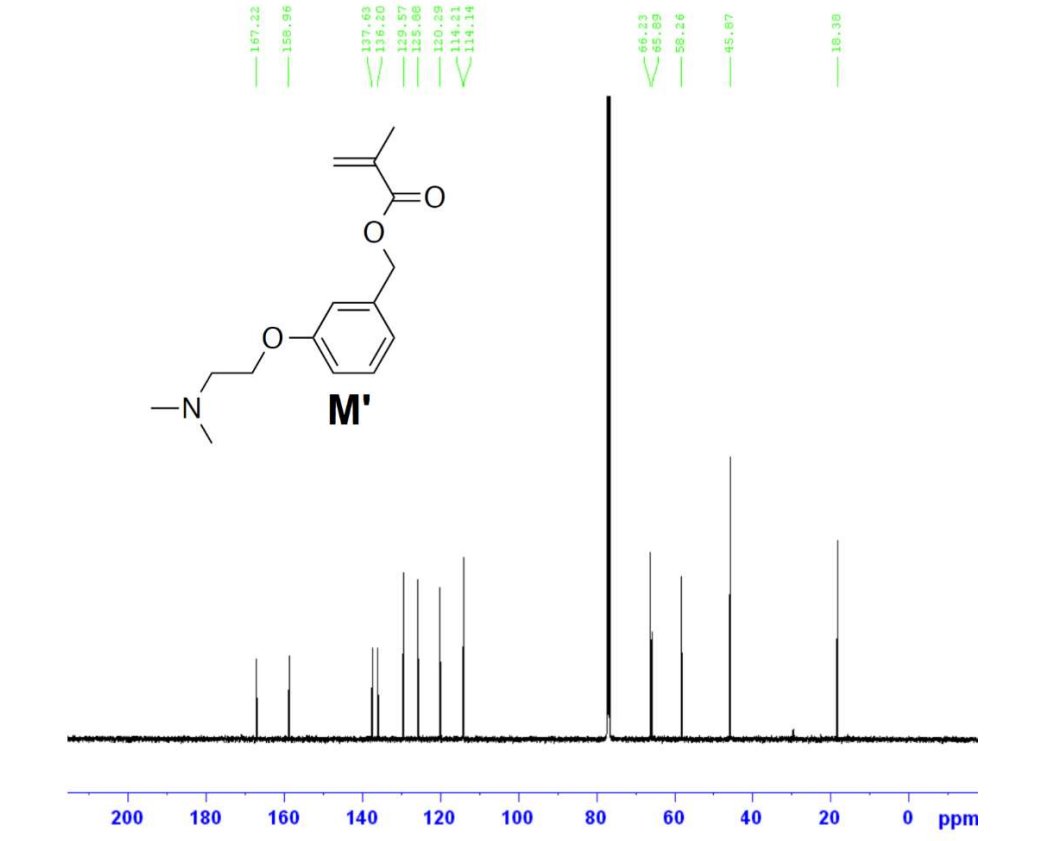
167.22
158.96
137.63
136.20
129.57
125.88
120.29
114.21
114.14
66.33
65.89
58.24
45.87
18.38
M'
200
180
160
140
120
100
80
60
40
20
0
ppm

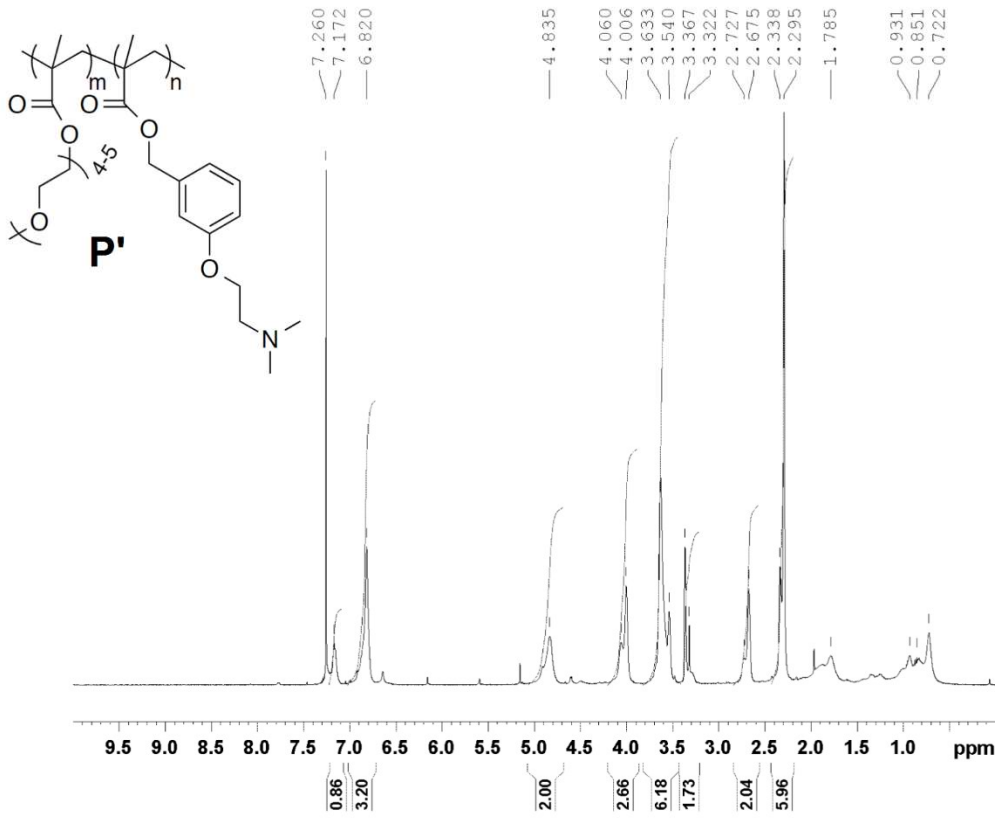
P'
7.260
7.172
6.820
4.835
4.060
4.006
3.633
3.540
3.367
3.322
2.727
2.675
2.338
2.295
1.785
0.931
0.851
0.722
9.5 9.0 8.5 8.0 7.5 7.0 6.5 6.0 5.5 5.0 4.5 4.0 3.5 3.0 2.5 2.0 1.5 1.0 ppm
0.86
3.20
2.00
2.66
6.18
1.73
2.04
5.96

Chapter 5

Photochemical Control of Non-Covalent Intermolecular Forces Governed by Hydrophobicity

—Directly Photopatternable Polythiophene

Reproduced in part from submitted manuscript:
Hu, X.; Mullahoo, J.; Thomas, S. W., Directly Patternable Conjugated Polymer with Phototunable Solubilities for Application in Positive Photolithography, Negative Photolithography and Multi-Level Patterning. Submitted to *Macromolecules*.

5.1 Introduction to Patternable Organic Electronic Materials

The delocalized π-systems of the backbones of conjugated polymers (CPs) give them useful optical and electronic properties, making CPs promising organic semiconducting materials for a variety of applications.[1-7] Two of the most important advantages that CPs have over conventional inorganic semiconductors are solution processability and mechanical flexibility, which can allow for low-cost, large-area flexible electronics such as organic light-emitting devices (OLEDs) and organic thin film transistors (OTFTs). Realization of these characteristics of CPs, however, typically requires incorporation of solubilizing alkyl side chains onto their conjugated backbones.[8-13] There has also been growing interest in developing water soluble CPs with hydrophilic side chains for biological applications.[14-17] Without solubilizing side chains, however, the parent structures of materials such as polythiophene (PT) and poly(phenylene-vinylene) are insoluble in most solvents.

Patterning of semiconducting materials is a key capability in the fabrication of functional devices.[18, 19] Photolithographic patterning is a non-contact, scalable microfabrication method with submicron resolution. Typically, photolithography is an indirect patterning approach in which an intermediate photoresist material is patterned first, followed by transfer of the pattern to an active material.[20] This usually requires additional photoresist materials and extra steps such as photoresist deposition, etching, and lift-off.[19] Driven by the increasing demand of cost-efficient, scalable manufacturing of electronic devices, directly photopatternable electronic materials comprising patterning and optoelectronic functions have attracted considerable attention.[21, 22] Researchers have developed a variety of strategies to realize photoinduced changes in the solubilities of organic optoelectronic materials, such as photochemical cross-linking,[23-33] photochemical cleavage of solubilizing pendants,[9, 10, 34-36]

photoisomerization,[37] photoacid irradiation,[38-40] photoinduced changes in doping,[41, 42] and photoinduced backbone cleavage.[43] Our group has developed negative-tone photoresist conjugated polymers that combine polythiophene or polythiophene-*alt*-benzothiadiazole backbones with photocleavable solubilizing pendants that eliminate from the backbone upon illumination;[9, 34] polymer in the unirradiated areas dissolves in organic solvents while in the irradiated areas, where photolysis of the solubilizing side-chains occurs, polymer remains. Compared with the more commonly adopted negative-tone patterning strategy of photochemical cross-linking, this side chain photocleavage method yields CP micropatterns with increased volume fraction of optoelectronically active backbone because of the removal of the solubilizing pendants after solution processing. This approach may also lower the probability of degradation contributed by side chains (for example, through photoinduced hydrogen atom abstractions).[44]

In comparison to approaches that yield negative-tone photolithography, there have been few reports on positive photoresist organic electronic materials that change from insoluble to soluble upon exposure to light. An example of note is that of Dirk and coworkers, who reported positive-tone photolithography of polythienylene vinylene through photo-oxidative cleavage of the conjugated backbones.[43] A favorable feature of positive photolithography is that the active electronic materials remaining after patterning are protected from irradiation and therefore free from photodegradation. Moreover, to the best of our knowledge, there is no known dual-tone conjugated polymer photoresist: a CP capable of functioning as both positive and negative photoresist. Such a dual-patternable characteristic would enable flexibility to fabricate sophisticated structures with CPs. Examples of reported dual-tone photoresists include those based on *o*-nitrobenzyl-containing hydrogels, in which tuning of composition and irradiation time allows for complex patterns of thickness and stiffness,[45] a polyurethane formulation with

two different nitrophenylpropyl groups with different absorption spectra causing polymerization and depolymerization using different wavelengths of light,[46] polymer networks incorporating coumarin groups[47-50] or other groups[51, 52] that shows photo-switchable cycloaddition reactions (i.e., photo-reversible dimerization reactions), and others.[27, 53-58]

In this chapter, we describe a novel polythiophene derivative **PT$_{o\text{NB}}$** with photocleavable, *ortho*-nitrobenzyl (ONB) functionalized solubilizing alkyl side chains. Photocleavage of ONB linker and the consequential photo-removal of solubilizing alkyl sidechains yield a photolyzed polymer insoluble in nonpolar solvents; on the other hand, photolysis of the ONB junctions reveals carboxylic acid pendant groups on the polymer backbone and therefore increases solubility of the photolyzed polymer in aqueous solutions. Therefore, **PT$_{o\text{NB}}$** has phototunable solubilities programmed through three stages: i) **PT$_{o\text{NB}}$** starting material is soluble in organic solvents and insoluble in aqueous solutions; ii) partially photocleaved polymer is soluble in neither organic nor aqueous solutions; iii) nearly fully photocleaved **PT$_{o\text{NB}}$** is insoluble in organic solvents but soluble in basic aqueous solutions. This approach to phototunable solubility using photolabile solubilizing groups allows for flexibility in processing of conjugated polymers used in organic semiconductor devices: the nature of the developer solution (organic or aqueous) determines whether **PT$_{o\text{NB}}$** behaves as a positive or negative tone photoresist. Harnessing this dual-tone capability, we also demonstrated conjugated film stacking via all-solution processing and micropatterning of a double layer **PT$_{o\text{NB}}$** film.

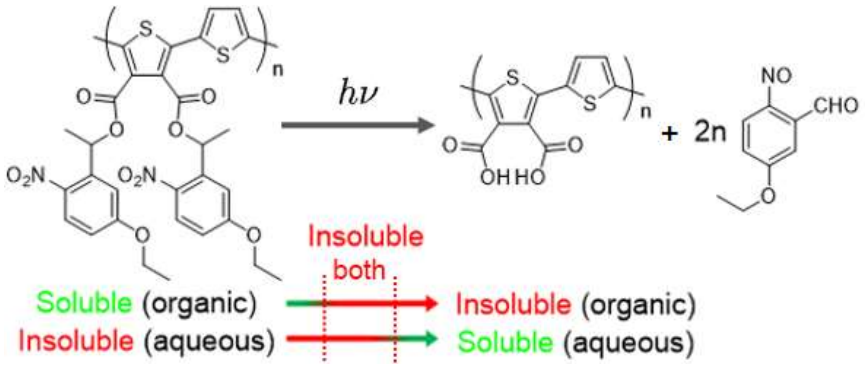

Figure 5.1: Three-stage photochemical control over solubility of **PT*o*NB**.

5.2 Design and Synthesis of Dual-Tone Photoresist PT*o*NB

In order to impart phototunable solubility to polythiophene, we designed ONB functionalized photocleavable hydrophobic sidechains (Compound **1**, Scheme 1). Such pendant groups give **PT*o*NB** sufficient solubility in organic solvents suitable for solution-based processing. The photocleavage of *o*NB groups is a common strategy for deprotecting functional groups in organic synthesis, chemical biology, and functional macromolecules.[54, 59-63] Photolysis of *o*NB esters converts the hydrophobic pendants to hydrophilic carboxylic acid groups. We designed the photolabile 3,4-disubstituted monomer **T1**, which copolymerizes with commercially available monomer 2,5-bis(trimethylstannyl) thiophene via Stille coupling, to yield the functional conjugated copolymer **PT*o*NB**. Complete photo-conversion of **PT*o*NB** would result in a polythiophene photoproduct with stoichiometric molar ratio of carboxylate groups to thiophene rings—PTs with similar ratio of carboxylates to thiophene rings are known to be water-soluble.[64-66] This polythiophene based dual-tone design is different than our previously reported negative-tone photoresist; the photoproducts of those negative-tone photoresists bear only one carboxylic acid group for every two heteroaromatic rings along the main chains, and therefore only have limited solubility in aqueous solutions.[9, 34] We also designed photoinert

control monomer **T2** and polymer analog **PT2** to support our hypothesis regarding the structure-property relationship between the photocleavable chemical functionality and light-induced changes in solubility.

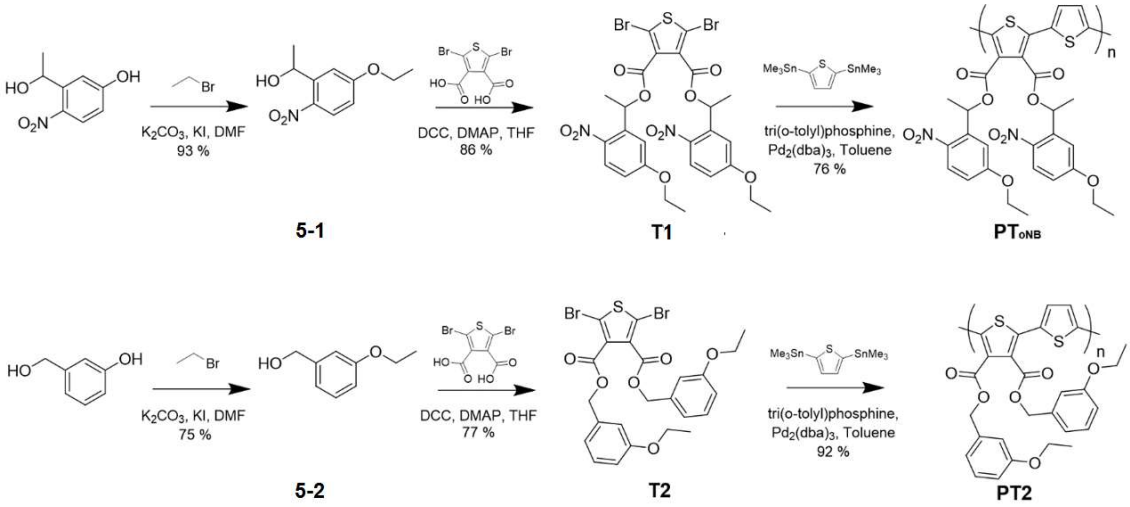

Scheme 5.1 : Synthesis of photoreactive polythiophene **PT*$_{oNB}$*** and control polymer **PT2**.

Synthesis of Polymers: Scheme 1 summarizes our syntheses of *o*NB-functionalized thiophene monomers and polymers. Selective alkylation of the phenol group in 5-hydroxy-α-methyl-2-nitrobenzyl alcohol yielded nitrobenzyl alcohol compound **5-1**. Acylation of compound **5-1** with the known compound 2,5-dibromothiophene-3,4-dicarboxylic acid using *N,N'*-dicyclohexylcarbodiimide as an activating reagent for the carboxylic acids gave monomer **T1**, with photocleavable groups on both the 3 and 4 positions of the thiophene ring. Copolymerization of **T1** with commercially available 2,5-bis(trimethylstannyl)thiophene *via* Stille cross-coupling gave the ONB functionalized polythiophene **PT*$_{o}$*$_{NB}$**, which we isolated by precipitation in methanol, with a number-average molecular weight (M_n) of 5,700 g/mol and polydispersity index (PDI) of 1.5, as determined by gel-permeation chromatography (GPC)

relative to polystyrene standards. The photoinert control polymer **PT2** (M_n = 9.500 g/mol, PDI = 1.6) was prepared similarly, using commercially available 3-hydroxybenzyl alcohol as the starting material.

5.3 Photochemistry

5.3.1 Photolysis of Monomer **T1**:

In order to demonstrate the photoinduced cleavage of solubilizing chains, we monitored the UV/Vis and ^{1}H NMR spectra of a $CDCl_3$ solution of **T1** as a function of irradiation time at $\lambda \approx 300$ - 380 nm with a power density of 5 mW/cm^2. Visually, the solution changed from colorless to brown-yellow in color upon irradiation over tens of minutes. ^{1}H resonances of **T1** disappeared while new resonances corresponding to the photolysis products emerged (**Figure 5.2a**). Concomitantly, the characteristic UV-vis absorption peak of the 5-alkoxy-2-nitrobenzyl group at ~310 nm ($\varepsilon \sim 1.7 \times 10^4$ M^{-1} cm^{-1}) decreased by approximately 30%, while a new peak at approximately 325 nm and two new shoulders at approximately 350 nm and 500 nm emerged (**Figure 5.3**). Such spectral changes are consistent with previous reports[9, 34] concerning nitrobenzyl-functionalized thiophene derivatives. In contrast, **T2** subjected to similar light exposure did not show significant photodegradation as monitored by NMR spectroscopy (**Figure 5.2b**).

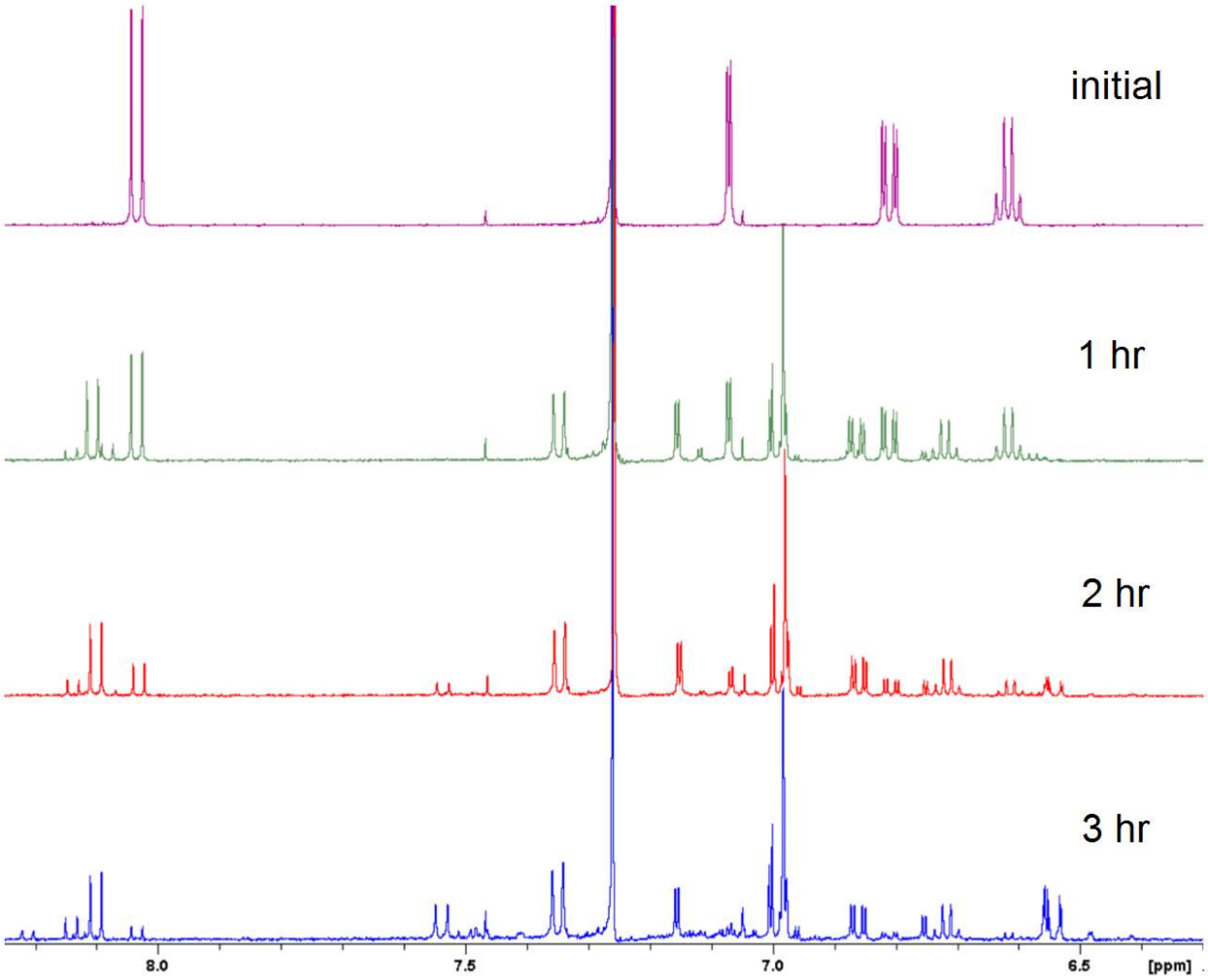

Figure 5.2a: Progression of photochemical degradation of **T1** monitored with NMR spectroscopy. Characteristic peaks of ONB groups [δ 8.03 (d, J = 9 Hz, 2H), 7.07 (d, J = 3 Hz, 2H), 6.81 (dd, J = 9 Hz, 3 Hz, 2H), 6.61 (q, J = 13 Hz, 2H)] near fully disappeared upon 3 hours of UV irradiation in a Rayonet photochemical reactor. Solvent peak: δ 7.26 (residual $CHCl_3$). Purple: initial; green: 1 hour irradiation; red: 2 hours irradiation; blue: 3 hours irradiation.

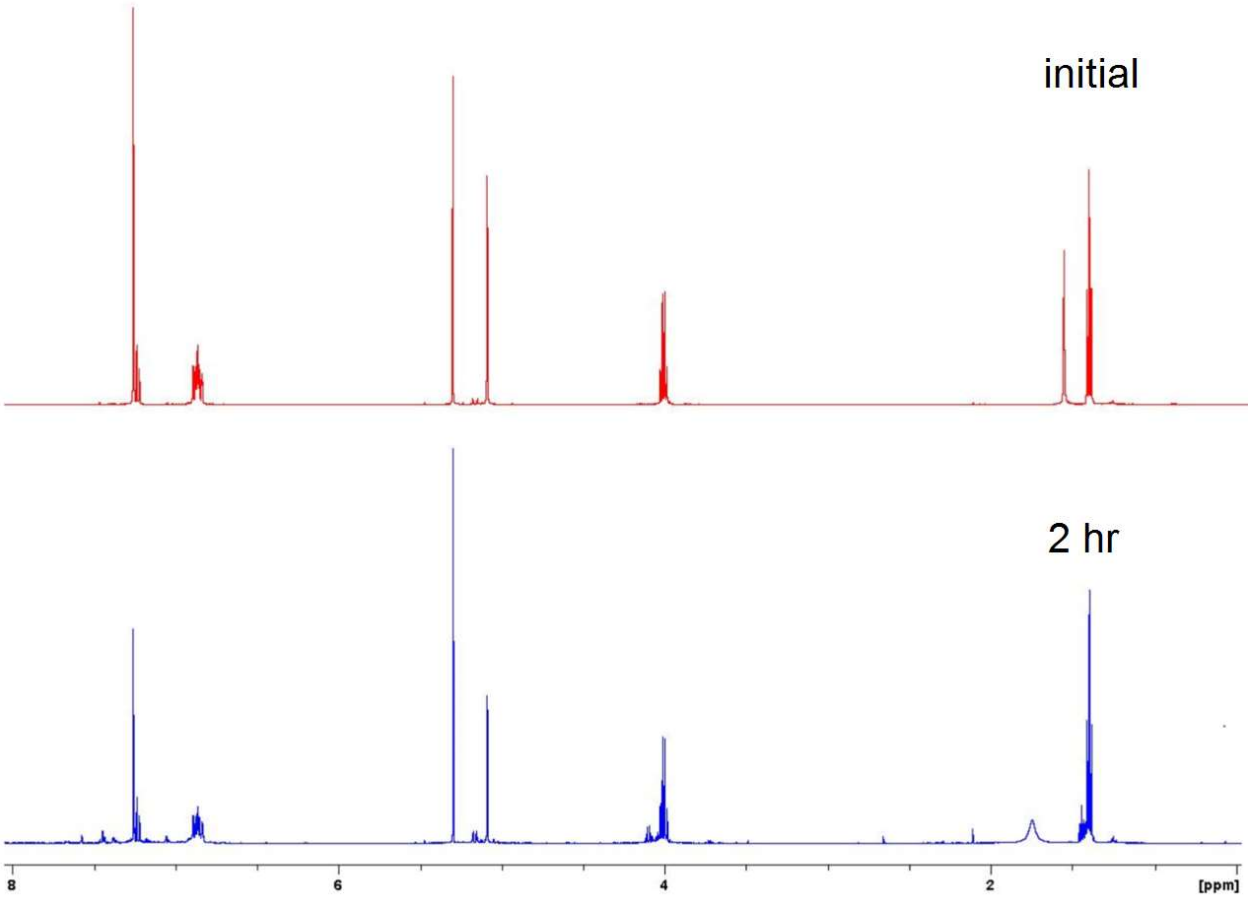

Figure 5.2b: Two hours of UV exposure (same irradiation condition as described in **Figure 5.2a**) did not induce significant degradation of **T2** as shown by NMR results. Characteristic peaks of M2 [δ 7.22-7.25 (m, 2H), 6.83-6.90 (m, 6H), 5.09 (s, 4H), 4.01 (q, J = 7 Hz, 4H), 1.40 (t, J = 7 Hz, 6H)] largely remained. Solvent peaks: δ 7.26 (residual CHCl3), δ 5.32 (residual CH2Cl2, δ 1.56 (residual water). Red: initial; blue: 2 hours irradiation.

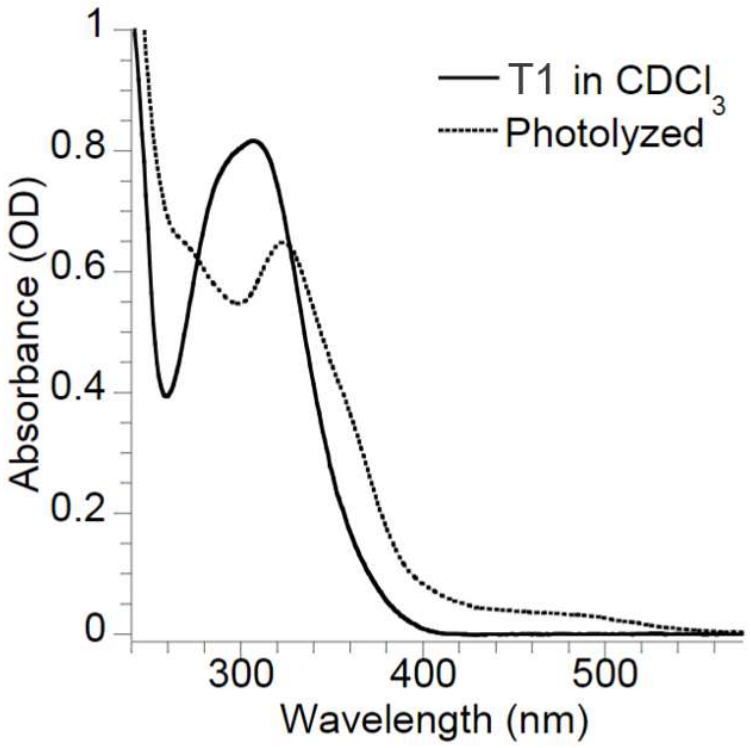

Figure 5.3: Photolysis of monomer **T1** (~ 5 mg/mL in CDCl3) upon exposure to UV light from a Rayonet photochemical reactor using borosilicate glass as the filter. The UV-vis spectra shown were acquired after dilution by 200-fold.

5.3.2 Photolysis of Thin Films

Film Deposition

The incorporation of two ethyl solubilizing side groups on every other thiophene ring gives **PT$_{o\text{NB}}$** a solubility >30 mg/mL in chloroform, rendering it sufficiently soluble for solution-based processing. We prepared **PT$_{o\text{NB}}$** films by spin-casting chloroform solutions of the polymer (2 mg/mL) at 500 rpm for 30 seconds unless otherwise mentioned. We found that **PT$_{o\text{NB}}$** tended to delaminate from quartz substrates upon rinsing in basic aqueous solutions; we therefore spun-

cast thin films onto hydrophobic quartz surfaces silanized with tert-butyltrichlorosilane (advancing water contact angle of silanized quartz substrates = 90° ± 4°). Films prepared in this manner had thicknesses and surface roughnesses of 38 nm ± 6nm and 2.6 nm ± 1.5 nm (RMS), respectively, as determined by atomic force microscopy (AFM). Films deposited on these silanized substrates showed less than a 3 % decrease in absorbance even after 90 minutes of sonication in 0.05 M Na_2CO_3 solutions (pH 12.7). One hour of rinsing in the same solution induced only negligible changes in film thicknesses (<2 nm) and roughnesses (<1 nm).

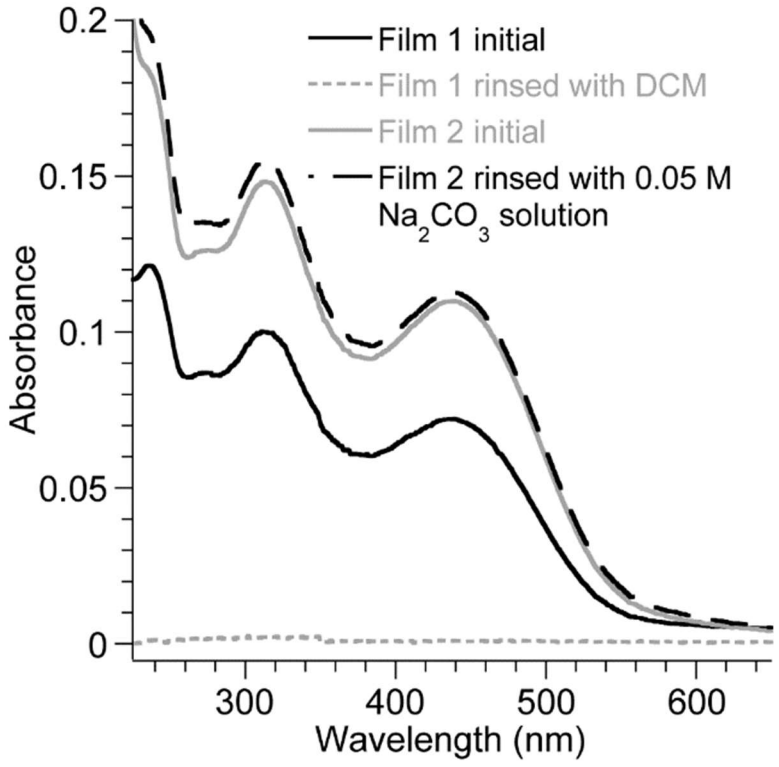

Figure 5.4: Spin-coated **PT$_{o\text{NB}}$** films (*solubility stage 1*) dissolved rapidly in dichloromethane (DCM) rinsing solution (Film 1, rinsed for 10 seconds), while it did not dissolve in 0.05 M Na_2CO_3 solution (Film 2, rinsed for 1 hour).

Photomodulated Solubilities of PT_{oNB} Films

Solubility Stage 1: With the objective of demonstrating that solubility of **PT*o*NB** in both organic solvents and in aqueous solutions changes upon photolysis, we monitored the photolysis and the changes of solubility of **PT*o*NB** films in both dichloromethane (CH_2Cl_2) as well as in 0.05 M aqueous Na_2CO_3 (pH 12.7) using UV-vis spectrophotometry. As expected, unirradiated **PT*o*NB** films (~38 nm-thick) dissolved instantly in organic solvents of low polarity such as dichloromethane and chloroform, but were insoluble in aqueous solutions (**Figure 5.4**).

*Irradiation of **PT*oNB** films:* These films were irradiated using a 200 W Hg/Xe lamp, at $\lambda \approx 300 – 380$ nm with a power density of 5 mW/cm^2. UV-induced changes in the electronic absorbance spectrum of **PT*o*NB** films (**Figure 5.5a**) were similar to those described for monomer **T1**: the band attributed to the nitrobenzyl group at 310 nm decreased by ~ 40% after 90 minutes of irradiation, with a new peak emerging at ~ 350 nm. We attribute the observed bathochromic shifting of the conjugated backbone absorbance (λ_{max} shifting from 441 nm to 465 nm) to increased planarization of the polythiophene backbone, photo-induced aggregation of the polythiophene chains, or both; we have noted similar bathochromic shifts of other solid polythiophenes upon photolysis of nitrobenzyl ester pendants.[9, 34]. Additionally, the increase in hydrophilicity of **PT*o*NB** film upon light exposure, as indicated by the advancing water contact angle of the film before (89° ± 2°) and after 1 hour UV irradiation (81° ± 1°), is also consistent with the expected photochemical conversion of the hydrophobic *o*NB functionalized pendants to the hydrophilic carboxylic acid groups (**Figure 5.1**). In contrast, films of photoinert polythiophene derivative **PT2** showed negligible photoinduced spectral changes (**Figure 5.5b**). The solubility profile of **PT2** (soluble in CH_2Cl_2 and insoluble in aqueous solutions), as well as

hydrophobicity (advancing water contact angle unchanged at 88-89° after of 1 hour of UV irradiation) were also independent of UV irradiation.

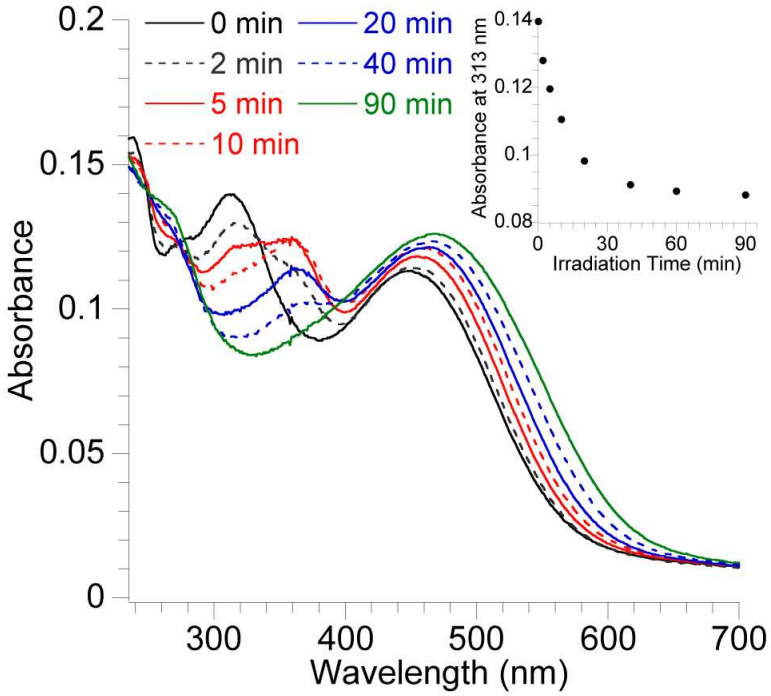

Figure 5.5a: Photolysis of a **PT$_{o\text{NB}}$** film upon exposure to UV light of the photolyzed film monitored by absorbance spectrophotometry. Inset: dependence of film absorbance at 313 nm on irradiation time.

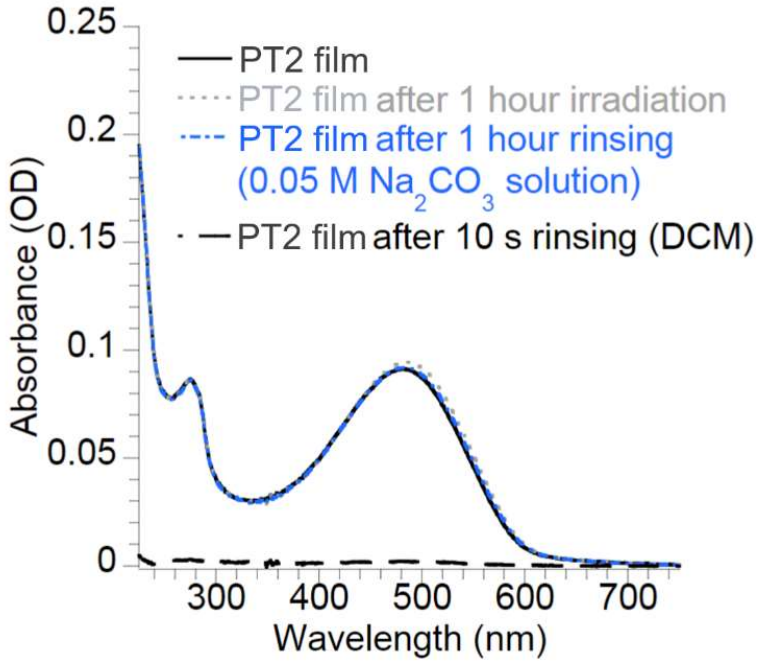

Figure 5.5b: Photoinert control polymer PT2 showed negligible change in absorbance, and maintained its solubility profile (soluble in CH_2Cl_2 and insoluble in aqueous Na_2CO_3) upon exposure to UV irradiation.

Solubility Stage 2: With increasing exposure to UV light, and therefore increasing photolysis of the hydrophobic side chains, **PT$_{o\text{NB}}$** films became increasingly insoluble in CH_2Cl_2, as determined by UV/Vis spectrophotometry (**Figure 5.6**). Upon > 10 minutes of UV irradiation, rinsing these films with CH_2Cl_2 for 20 s caused < 15% decreases of the absorbances of the polythiophene backbone (450 nm) of these films. On the other hand, **PT$_{o\text{NB}}$** subjected to < 30 minutes of irradiation did undergo sufficient conversion to become soluble in aqueous base: films irradiated for < 30 min showed < 5% decrease of backbone absorbance upon rinsing in 0.05 M Na_2CO_3 solution for one hour. These results suggest that the extent of photolysis between 10 and 30 min irradiation (between 50% and 80% of maximum photocleavage, as estimated by

the changes of absorbance at 313 nm in **Figure 5.5a**, yields polymer that is largely insoluble in both CH_2Cl_2 and aqueous Na_2CO_3.

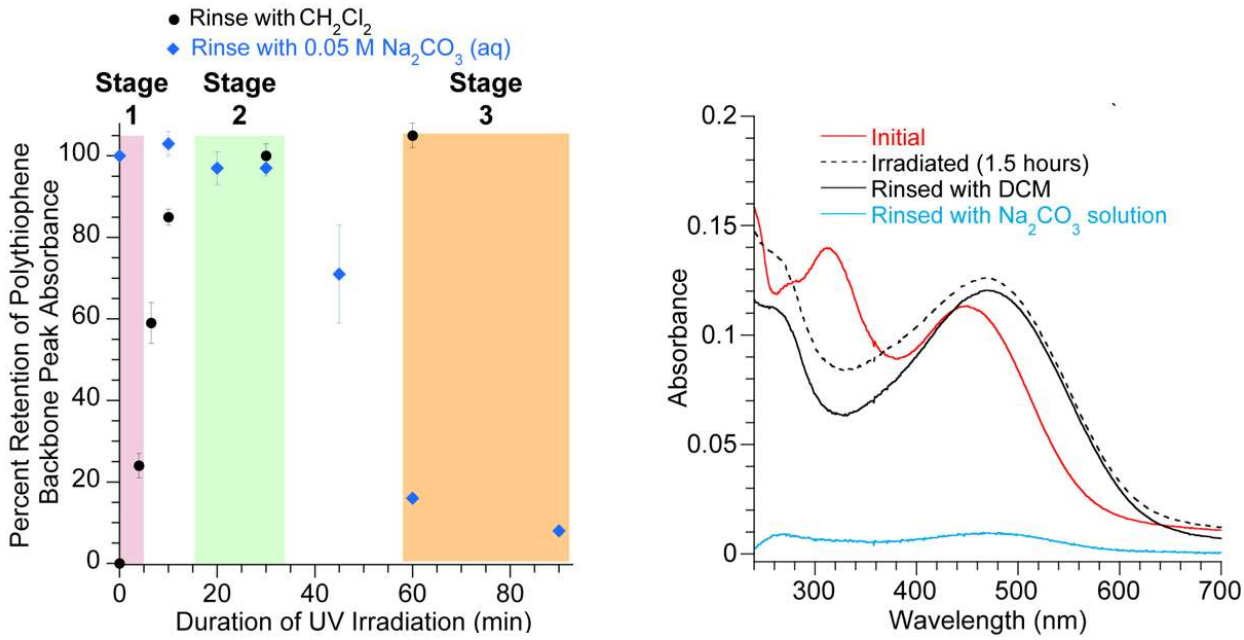

Figure 5.6: Effect of UV irradiation (λ ~ 300 nm – 380 nm, power density 5 mW/cm^2) on the solubility profile of films of **PT$_{o\text{NB}}$**. *Left*: Percentage of polythiophene backbone peak absorption remaining upon rinsing with CH_2Cl_2 for 20 seconds or rinsing with 0.05 M Na_2CO_3 for 1 hour as a function of UV irradiation duration. *Right*: Near fully photolyzed **PT$_{o\text{NB}}$** film resisted dissolution in CH_2Cl_2 (rinsed for 20 seconds) but dissolved in a sequential rinsing step in 0.05 M Na_2CO_3 solution (rinsed for 1 hour) (solubility stage 3). See **Figure 5.5b** for control experiment results with the photoinert polythiophene **PT2**.

Solubility Stage 3: More thoroughly photolyzed films continued to resist dissolution in CH_2Cl_2, as they did in Stage 2, due to the large degree of cleavage of solubilizing hydrocarbon side-chains. The higher degree of photochemical conversion, however, rendered these films soluble in

aqueous solutions of Na_2CO_3 (**Figure 5.6**): polythiophene backbone absorbance of films subjected to 1.5 hours of UV irradiation decreased by > 90% upon rinsing in 0.05 M Na_2CO_3 solution (pH 12.7) for one hour. We attribute the dissolution of these samples in basic solutions to the hydrophilicity gained from the deprotonated, negatively charged carboxylate groups; otherwise identically irradiated films showed less than 10% decrease in backbone absorbance upon rinsing in neutral NaCl solutions of the same ionic strength as 0.05 M Na_2CO_3 (**Figure 5.7**). Photolysis and dichloromethane rinsing also induced a decrease in thickness from 38 nm ± 6 nm (RMS = 2.6 nm) to 18 nm ± 3 nm (RMS = 2.4 nm), as monitored with AFM. We attribute the decreased film thickness, the decreased characteristic nitrobenzyl absorption around 350 nm, and the bathochromic shift of the polymer backbone absorption from 441 nm to 465 nm, to loss of photocleavable sidechains and resulting closer packing of the polymer chains.

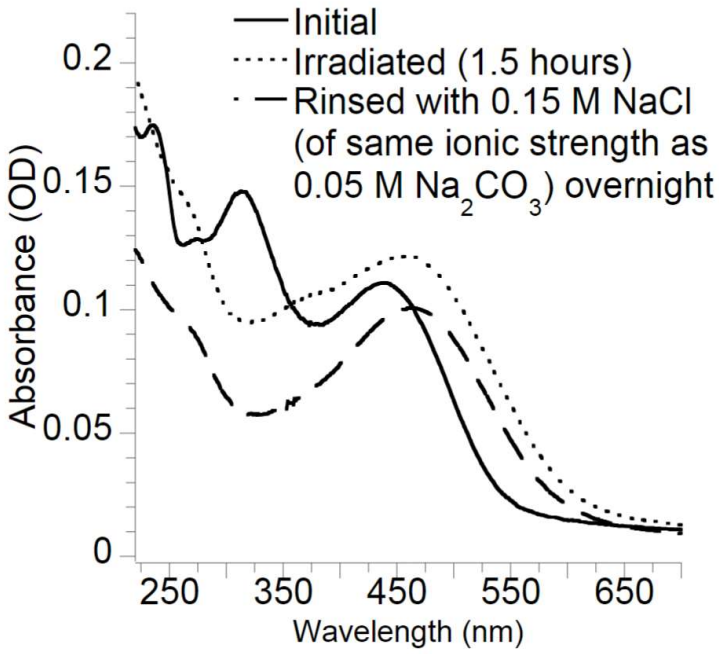

Figure 5.7: Polythiophene backbone in an irradiated PT_{oNB} film largely resisted to dissolution in 0.15 M NaCl solution. Power density = 5mW/cm^2.

5.4 Photopatterning

5.4.1. Dual-Tone Photopatterning with $\mathbf{PT_{oNB}}$

The light-controlled solubility changes of $\mathbf{PT_{oNB}}$ suggests that both positive and negative photolithography are possible with this conjugated polymer, the choice between which depends on the selection of developer solution used after irradiation. We performed photopatterning experiments with two $\mathbf{PT_{oNB}}$ films ("Film+" and "Film-") deposited using 2 mg/mL $CHCl_3$ solutions spun-cast at 500 rpm for 30 seconds. Both films were irradiated through a photomask under identical conditions at $\lambda \approx 300 - 380$ nm (irradiation duration = 1.5 hour; power density = 5 mW/cm^2), such that polymer in the irradiated circles reached solubility stage 3, while polymer in areas protected from UV exposure stayed in solubility stage 1. Film- was developed by rinsing with dichloromethane for 20 s, while Film+ was developed by rinsing with 0.05 M Na_2CO_3 (aq) for 1 hour.

Figure 5.8 shows atomic force microscopy (AFM) analysis of the resulting patterned films. The irradiated circles of CH_2Cl_2-rinsed Film- remained, while the unirradiated areas dissolved, leaving ~15 nm-high circular posts. As described above, this decrease in thickness of the polythiophene-negative tone photoresist based on side-chain photolysis is consistent with our observations in previously reported polymers,[9] for which photolysis rendered the irradiated polymer insoluble in chloroform, but yielded a decrease in thickness—from 33 ± 3.0 nm to 23 ± 1.5 nm after photolysis, and further down to 16 ± 3.0 nm after rinsing with chloroform. In contrast, rinsing identically deposited and irradiated Film+ with 0.05 M Na_2CO_3 after masked irradiation resulted in selective dissolution of the photolyzed polymer in the exposed circular areas, resulting in positive-tone photolithography of the same polythiophene; the remaining

polymer had a thickness of about 34 ± 4 nm, similar to the thicknesses of films before irradiation and rinsing (38 nm ± 6 nm).

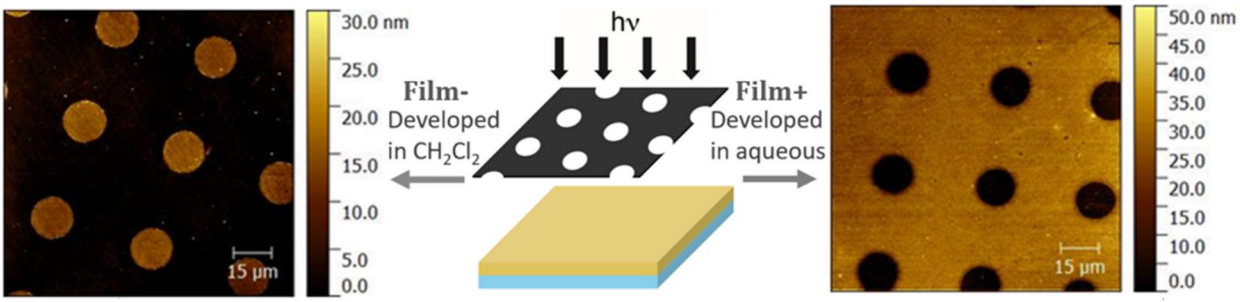

Figure 5.8: Photolithographic patterning of **PT$_{o}$$_{NB}$** films (middle), which were used to generate negative micropatterns using organic developer (CH_2Cl_2), or positive micropatterns using aqueous developer (0.05 M Na_2CO_3 (aq)).

5.4.2 Multi-Level CP Micropatterns:

Although multi-level photopatterning is known using with various non-conjugated polymer photoresists,[67, 68] photolithographic fabrication of multi-level micro-architectures with directly patternable conjugated materials remains an important challenge because of the multi-layer designs of many organic semiconducting devices. To demonstrate such a capability with **PT$_{o}$$_{NB}$,** we first deposited a film comprising two stacked **PT$_{O}$$_{NB}$** films (single-film thickness of approximately 40 nm): one layer of **PT$_{o}$$_{NB}$** was partially photolyzed by 10 min UV exposure in order to render the polymer insoluble in all solvents (solubility stage 2). A subsequent second spin-casting step of **PT$_{o}$$_{NB}$** created a two-layer stacked film, which is only possible after UV irradiation of the first layer; spin coating onto an unirradiated **PT$_{o}$$_{NB}$** film led to no detectable increase of film thickness as the solvent used in subsequent spin-coating steps dissolved the previously deposited layer (**Figure 5.9**).

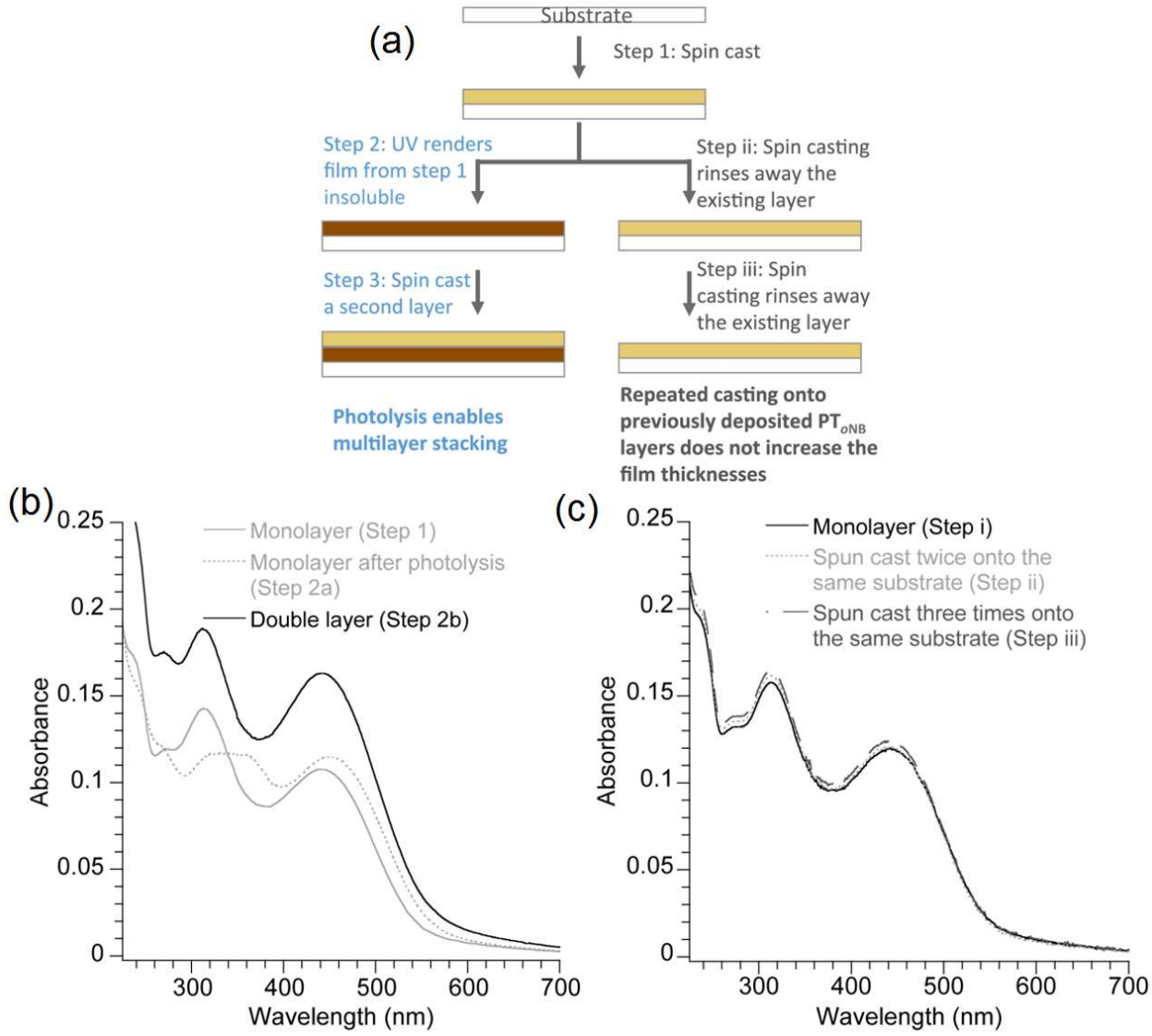

Figure 5.9: (a) Schematic of the photolysis-enabled multilayer stacking. (b) Spin-casting of a second **PT$_{oNB}$** layer onto a photo-desolubilized substrate **PT$_{oNB}$** layer increased the film thickness as monitored with UV/Vis spectroscopy. (c) Spin-casting **PT$_{oNB}$** onto previously deposited **PT$_{oNB}$** layers did not increase the film thicknesses as monitored with UV/Vis.

The photo-modulated, three-stage solubility of **PT$_{oNB}$** allowed fabrication of two-level conjugated polymer microarchitectures through a combination of positive-tone and negative-tone

photolithographies. First, we prepared a bilayer film as described in **Figure 5.9**, with the bottom layer in solubility stage 2 (insoluble in organic and aqueous) and the top layer in solubility stage 1 (soluble in organic, insoluble in aqueous). This two-layer film was then irradiated through a photomask for 10 min and then rinsed with CH_2Cl_2—unirradiated areas in the top layer remained in *solubility stage 1* and dissolved in the CH_2Cl_2, while irradiated polymers in the top layer and the entire bottom layer were in solubility stage 2, resisting dissolution in CH_2Cl_2. Subsequently, this patterned film was irradiated for 90 minutes through the same photomask, oriented perpendicular to the original patterning step. This second patterning step resulted in irradiated areas progressing to solubility stage 3, enabling dissolution of irradiated areas in 0.05 M aqueous Na_2CO_3. The result of these patterning steps is a conjugated polymer film with double level surface microstructures as characterized by AFM (**Figure 5.10** *bottom*), enabled by the unique dual-tone photolithography possible with $\mathbf{PT}_{\boldsymbol{o}\mathbf{NB}}$.

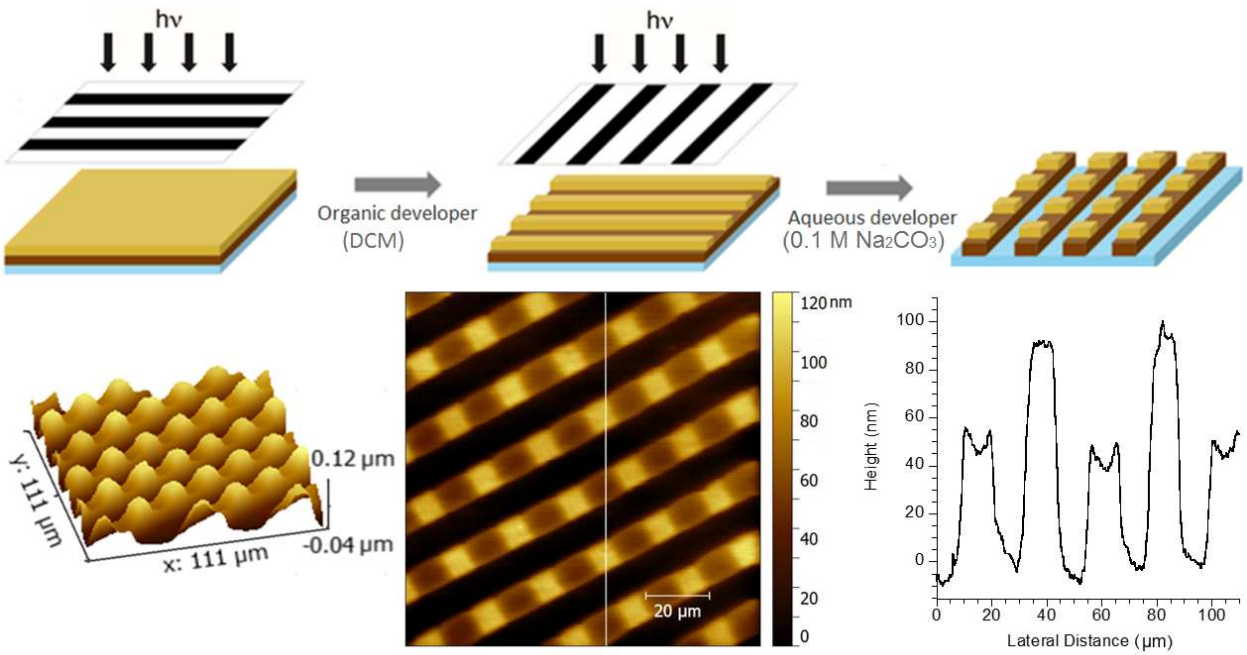

Figure 5.10: *Top*: Schematic of the photolithographic fabrication of double-layer microstructures via two masked irradiation steps. *Bottom*: AFM images of a multi-level photopatterned conjugated polymer film; the plot corresponds to the height profile along the white line in the AFM image.

5.5. Conclusions

Chapter 5 describes a new polythiophene derivative **PT$_{o\text{NB}}$** with photocleavable, *o*NB functionalized side groups with three-stage orthogonal solubilities dictated by the dose of UV irradiation. Such photo-programmable solubility, along with the capability to control spatiotemporal distribution of light, makes **PT$_{o\text{NB}}$** a unique dual-tone optoelectronic photoresist. Photolithography with **PT$_{o\text{NB}}$** via the positive tone approach generates photodegradation-free CP patterns, while the negative tone approach produces CP patterns with increased volume fraction of electroactive materials upon removal of the inactive side groups. This CP photoresist enables

direct photolithographic fabrication of multi-level conjugated polymer microarchitectures. This new approach for conjugated polymer based dual-tone photoresists offers flexibility and feasibility in microfabrication and with potential application in the construction of multilayer organic devices via solution-based processing.

5.6 Experimental Section

General Considerations

All synthetic manipulations were performed under standard air-free conditions under an atmosphere of argon gas with magnetic stirring. Flash chromatography was performed using silica gel (230-400 mesh) as the stationary phase. NMR spectra were acquired on a Bruker Avance III 500 spectrometer. Chemical shifts are reported relative to residual protonated solvent (7.26 ppm for $CHCl_3$). All reactants and solvents were purchased from commercial suppliers and used without further purification. Dry THF, dry CH_2Cl_2, and dry toluene were obtained from an Innovative Technologies PureSolv 400 solvent purifier. Polymer molecular weights were determined using a Shimadzu gel permeation chromatography (GPC) system equipped with a Tosoh TSKgel GMHhr-M mixed-bed column and guard column using the UV detector. The column was calibrated with low polydispersity poly(styrene) standards (Tosoh, PS Quick Kit) in THF as the mobile phase eluting at 0.75 mL/min. AFM images were obtained using a Veeco D3100S-1 working in tapping mode. AFM results were processed using Gwyddion software, version 2.4. The advancing water contact angles of sessile water droplets on the surfaces of the polymer films were determined with a Rame-Hart goniometer (Model 200-U1) at room temperature by adding water from the droplet with a 22-Gauge needle in a stepwise fashion. All

solution optical spectra were acquired of samples in quartz cuvettes. All solid optical spectra were acquired of samples on silanized quartz substrate. Electronic absorbance spectra were acquired with a Varian Cary-100 instrument in double-beam mode.

Irradiation Conditions:

Irradiation experiments with solid films were performed with a 200 W Hg/Xe lamp (Newport-Oriel) equipped with a condensing lens, recirculating water filter, and a combination of a 295 nm long pass filter (Newport) and a UG-11 bandpass filter (Newport).

Irradiation experiments with monomer solution were performed with a Rayonet Photochemical Chamber Reactor, using borosilicate glass as the filter. **T1** solution (about 5 mg/mL) was added into a NMR tube. We first diluted an aliquot (10 uL) of this solution with 2 mL $CDCl_3$ and measured its UV absorbance. We then exposed the NMR tube containing **T1** solution to UV irradiation in a Rayonet photochemical reactor, and monitored the progress of **T1** photodegradation over three hours using ^1H NMR spectroscopy.

Silanization of Quartz Substrates:

A freshly prepared toluene solution of *tert*-butyltrichlorosilane (1 μL/mL) was applied onto a plasma cleaned quartz slide. Another plasma clean quartz was adhered onto that quartz slide, sandwiching the applied silane solution between two slides. This pair of adhered slides was kept in ambient condition for 3 hours, then separated and immediately washed with copious

amounts of CH_2Cl_2. Polymer films were deposited onto these substrates surfaces via spin coating.

Film Deposition via Spin Coating:

Thin films were fabricated by spin-casting of chloroform solutions of polymers (2 mg/mL) onto silanized quartz surfaces using a Laurell Technologies Corporation spin coater (Model WS-400E-6NPP-Lite) at 500 rpm for 30 seconds.

Synthesis

5-hydroxy-α-methyl-2-nitrobenzenemethanol[69] and 2,5-dibromo-3,4-thiophenedicarboxylic acid[70] were synthesized following previously reported methods.

Compound 5-1: 5-hydroxy-α-methyl-2-nitrobenzenemethanol (0.47 g, 2.6 mmol), bromoethane (0.58 g, 5.3 mmol), K_2CO_3 (0.73 g, 5.3 mmol), KI (catalytic) and 10 mL anhydrous DMF were added into a 25 mL three-neck round bottom flask. The reaction was stirred overnight at 50 °C. The reaction mixture was diluted with water and then extracted with diethyl ether 3 times. The combined organic layers were dried over Na_2SO_4, filtered, and concentrated *in vacuo*. The crude product was purified by flash column chromatography using hexane/ethyl acetate (2/1 v/v) as eluent to afford compound **5-1** as a yellow solid. Yield: 0.50 g (93 %). ^{1}H NMR (500 MHz, $CDCl_3$): δ 8.05 (d, J = 9 Hz, 1H), 7.31 (d, J = 3 Hz), 6.84 (dd, J = 9 Hz, 3 Hz, 1H), δ 5.57-5.54 (m, 1H), 4.14 (q, J = 14 Hz, 1H), 2.30 (d, J = 4 Hz, 1H), 1.56 (d, J = 7 Hz, 3H), (t, J = 7 Hz,

3H). ^{13}C NMR (125 MHz, $CDCl_3$): δ 163.4, 144.7, 127.7, 113.4, 112.5, 66.0, 64.3, 53.4, 24.1, 14.6.

Compound 5-2: This compound was synthesized in an analogous manner as compound **5-1**: bromoethane (1.13 g, 10.3 mmol), 3-hydroxybenzenemethanol (0.85 g, 6.9 mmol), K_2CO_3 (1.82 g, 13.2 mmol), KI (catalytic) and 25 mL anhydrous DMF were added into a 100 mL two neck round bottom flask. The reaction was stirred overnight at 50 °C. The reaction mixture was diluted with water and then extracted with diethyl ether 3 times. The combined organic layers were dried over Na_2SO_4, filtered, and concentrated *in vacuo*. The crude product was purified by flash column chromatography using hexane/ethyl acetate (2/1 v/v) as eluent to afford compound **5-2** as a light yellow solid. Yield: 0.78 g (75 %). ^{1}H NMR (300 MHz, $CDCl_3$): δ 7.23-7.27 (m, 1 H), 6.91-6.94 (m, 2H), 6.82 (dd, J = 8 Hz, 2 Hz, 1H), 4.66 (s, 2H), 4.04 (q, J = 7, 2H), 1.41 (t, J = 7, 3H).

T1: To a stirred mixture of 2,5-dibromo-3,4-thiophenedicarboxylic acid (0.20 g, 0.61 mmol), compound **5-1** (0.30 g, 1.4 mmol) and N,N-dimethylaminopyridine (DMAP) (0.030 g, 0.25 mmol) in 25 mL anhydrous THF was added 5 mL of THF solution of N,N'-dicyclohexylcarbodiimide (DCC) (0.35 g, 1.7 mmol) in a dropwise manner. The reaction mixture was stirred over two days at ambient temperature. After filtration, the solution was concentrated, then dispersed into DCM/hexane (1/4 v/v, 5 mL). The dispersion was left in a freezer for about two hours to precipitate most of the byproduct N,N'-dicyclohexylurea, which was removed by filtration. The crude product was purified by flash column chromatography using hexanes/ethyl acetate (9/1 v/v) to afford two isomers of **T1** ($R_f \approx 0.1$ and 0.15) as a white solid and a light yellow solid, respectively. Yield: 0.35 g (86 %) (two isomers combined). ^{1}H NMR (500 MHz, $CDCl_3$): δ 8.03 (d, J = 9 Hz, 2H), 7.07 (d, J = 3 Hz, 2H), 6.81 (dd, J = 9 Hz, 3 Hz, 2H), 6.61 (q, J

= 13 Hz, 2H), 4.06-4.17 (m, 4H), 1.63 (d, J = 7 Hz, 6H), 1.42-1.46 (m, 6H). ^{13}C NMR (125 MHz, $CDCl_3$): δ 163.5, 160.3, 140.3, 139.4, 133.1, 127.8, 116.5, 113.8, 112.5, 70.8, 64.5, 22.3, 14.6. HRMS: calculated for $C_{26}H_{24}Br_2N_2O_{10}S$ $(M + Na)^+$: 738.9401; found, 738.9405.

T2: This monomer was synthesized using a similar method as that for **T1**. To a stirred mixture of 2,5-dibromo-3,4-thiophenedicarboxylic acid (0.40 g, 1.2 mmol), compound **5-2** (0.60 g, 4.0 mmol) and DMAP (0.070 g, 0.57 mmol) in 50 mL anhydrous THF was added 10 mL of a THF solution of DCC (0.75 g, 3.6 mmol) in a dropwise manner. The reaction mixture was stirred over two days at ambient temperature. After filtration, the solution was concentrated, then dispersed into a DCM/hexane mixture (1/4 v/v, 5 mL). The dispersion was left in freezer for about two hours to precipitate most of the by-product N,N'-dicyclohexylurea, which was removed by filtration. The crude product was purified by flash column chromatography using hexanes/ethyl acetate (9/1 v/v) to yield **T2** ($R_f \approx 0.35$) as a light yellow oil. Yield: 0.51 g (77 %). ^{1}H NMR (500 MHz, $CDCl_3$): δ 7.22-7.25 (m, 2H), 6.83-6.90 (m, 6H), 5.09 (s, 4H), 4.01 (q, J = 7 Hz, 4H), 1.40 (t, J = 7 Hz, 6H). ^{13}C NMR (125 MHz, $CDCl_3$): δ 161.2, 159.1, 136.3, 133.4, 129.6, 120.5, 116.2, 114.7, 114.4, 67.7, 63.4, 14.8. HRMS: calculated for $C_{24}H_{22}Br_2O_6S$ $(M + Na)^+$: 620.9385; found, 620.9379.

PT$_{o\text{NB}}$: A round bottom flask was charged with tris(dibenzylideneacetone)dipalladium(0) (13 mg, 0.014 mmol) and tri(*o*-tolyl)phosphine (36 mg, 0.12 mmol). The flask was evacuated and refilled with argon three times. A 5 mL anhydrous toluene solution of **T1** (combined mixture of two isomers of **T1** was used in this step; 205 mg, 0.29 mmol) and 2,5-bis(trimethylstannyl)thiophene (117 mg, 0.29 mmol) was purged with argon for 20 min, then transferred into the round bottom flask under argon flow. The reaction mixture was left to reflux for 3 days. The reaction mixture was cooled to ambient temperature, and added dropwise to

methanol to precipitate the polymer. After centrifugation, the polymer was dissolved in CH_2Cl_2 and precipitated two additional times. The precipitate was dried in a vacuum oven at 50 °C over two days to give **PT*o*NB** as an orange solid. Yield: 140 mg (76 %). ^{1}H NMR (500 MHz, $CDCl_3$): (all broad signals) δ 7.90-8.15 (2H), 6.40-7.40 (8H), 3.70-4.30 (4H), 0.75-2.00 (12H). GPC: M_n = 5.7 kDa, M_w = 8.6 kDa, PDI = 1.51.

PT2: The polymer was synthesized in an analogous way as **PT*o*NB**, using tris(dibenzylideneaceton)dipalladium(0) (15 mg, 0.016 mmol), tri(o-tolyl)phosphine (42 mg, 0.138 mmol), **T2** (200 mg, 0.34 mmol) and 2,5-bis(trimethylstannyl)thiophene (137 mg, 0.34 mmol) as starting materials. 162 mg **PT2** was obtained as a red solid (yield: 92 %). ^{1}H NMR (500 MHz, $CDCl_3$): (all broad signals) δ 7.00-7.26 (4H), 6.65-6.69 (6H), 4.90-5.20 (4H), 3.85-4.05 (4H), 1.25-1.50 (6H). GPC: M_n = 9.5 kDa, M_w = 15.5 kDa, PDI = 1.63.

5.7 References

1. Mei, J., et al., *Integrated Materials Design of Organic Semiconductors for Field-Effect Transistors.* Journal of the American Chemical Society, 2013. **135**(18): p. 6724-6746.
2. Brabec, C.J., et al., *Polymer–Fullerene Bulk-Heterojunction Solar Cells.* Advanced Materials, 2010. **22**(34): p. 3839-3856.
3. Facchetti, A., *π-Conjugated Polymers for Organic Electronics and Photovoltaic Cell Applications.* Chemistry of Materials, 2011. **23**(3): p. 733-758.
4. Thomas, S.W., G.D. Joly, and T.M. Swager, *Chemical Sensors Based on Amplifying Fluorescent Conjugated Polymers.* Chemical Reviews, 2007. **107**(4): p. 1339-1386.
5. Jensen, J., et al., *Development and Manufacture of Polymer-Based Electrochromic Devices.* Advanced Functional Materials, 2015. **25**(14): p. 2073-2090.
6. Muller, C.D., et al., *Multi-colour organic light-emitting displays by solution processing.* Nature, 2003. **421**(6925): p. 829-833.
7. Müllen, K. and W. Pisula, *Donor–Acceptor Polymers.* Journal of the American Chemical Society, 2015. **137**(30): p. 9503-9505.
8. Mei, J. and Z. Bao, *Side Chain Engineering in Solution-Processable Conjugated Polymers.* Chemistry of Materials, 2014. **26**(1): p. 604-615.
9. Smith, Z.C., et al., *Thiophene-Based Conjugated Polymers with Photolabile Solubilizing Side Chains.* Macromolecules, 2015. **48**(4): p. 959-966.
10. Schelkle, K.M., et al., *Light-Induced Solubility Modulation of Polyfluorene To Enhance the Performance of OLEDs.* Angewandte Chemie International Edition, 2015. **54**(48): p. 14545-14548.
11. Kline, R.J., et al., *Critical Role of Side-Chain Attachment Density on the Order and Device Performance of Polythiophenes.* Macromolecules, 2007. **40**(22): p. 7960-7965.
12. Jaymand, M., M. Hatamzadeh, and Y. Omidi, *Modification of polythiophene by the incorporation of processable polymeric chains: Recent progress in synthesis and applications.* Progress in Polymer Science, 2015. **47**: p. 26-69.
13. Guo, Z.-H., et al., *A side-chain engineering approach to solvent-resistant semiconducting polymer thin films.* Polymer Chemistry, 2016. **7**(3): p. 648-655.
14. Cao, B., et al., *Integrated zwitterionic conjugated poly(carboxybetaine thiophene) as a new biomaterial platform.* Chemical Science, 2015. **6**(1): p. 782-788.
15. Lee, S.H., et al., *Water-Soluble Conjugated Polyelectrolytes with Branched Polyionic Side Chains.* Macromolecules, 2011. **44**(12): p. 4742-4751.
16. Traina, C.A., R.C. Bakus, and G.C. Bazan, *Design and Synthesis of Monofunctionalized, Water-Soluble Conjugated Polymers for Biosensing and Imaging Applications.* Journal of the American Chemical Society, 2011. **133**(32): p. 12600-12607.
17. Gaylord, B.S., A.J. Heeger, and G.C. Bazan, *DNA detection using water-soluble conjugated polymers and peptide nucleic acid probes.* Proceedings of the National Academy of Sciences, 2002. **99**(17): p. 10954-10957.
18. Pease, R.F. and S.Y. Chou, *Lithography and Other Patterning Techniques for Future Electronics.* Proceedings of the IEEE, 2008. **96**(2): p. 248-270.
19. Kahn, B.E., *Patterning Processes for Flexible Electronics.* Proceedings of the IEEE, 2015. **103**(4): p. 497-517.
20. Taylor, P.G., et al., *Orthogonal Patterning of PEDOT:PSS for Organic Electronics using Hydrofluoroether Solvents.* Advanced Materials, 2009. **21**(22): p. 2314-2317.
21. Menard, E., et al., *Micro- and nanopatterning techniques for organic electronic and optoelectronic systems.* Chemical Reviews, 2007. **107**(4): p. 1117-1160.
22. DeFranco, J., et al., *Photolithographic Patterning of Organic Electronic Materials*, in *Functional Supramolecular Architectures*. 2011, WILEY-VCH Verlag & Co. KGaA. p. 399-420.

23. Jensen, J., et al., *Direct Photopatterning of Electrochromic Polymers.* Advanced Functional Materials, 2013. **23**(30): p. 3728-3737.
24. Leliège, A., S. Barik, and W.G. Skene, *Photopatternable Electrochromic Materials from Oxetane Precursors.* ACS Applied Materials & Interfaces, 2014. **6**(9): p. 6920-6929.
25. Pal, R.K., et al., *Photolithographic Micropatterning of Conducting Polymers on Flexible Silk Matrices.* Advanced Materials, 2016. **28**(7): p. 1406-1412.
26. Davis, A.R. and K.R. Carter, *Controlling Optoelectronic Behavior in Poly(fluorene) Networks Using Thiol–Ene Photo-Click Chemistry.* Macromolecules, 2015. **48**(6): p. 1711-1722.
27. Blasco, E., M. Wegener, and C. Barner-Kowollik, *Photochemically Driven Polymeric Network Formation: Synthesis and Applications.* Advanced Materials, 2017: p. n/a-n/a.
28. Marrocchi, A., et al., *Click-chemistry approaches to [small pi]-conjugated polymers for organic electronics applications.* Chemical Science, 2016. **7**(10): p. 6298-6308.
29. Bender, M., et al., *Photo-Cross-Linkable Polyfluorene–Triarylamine (PF–PTAA) Copolymer Based on the [2 + 2] Cycloaddition Reaction and Its Use as Hole-Transport Layer in OLEDs.* Macromolecules, 2016. **49**(8): p. 2957-2961.
30. Derue, L., et al., *All-Solution-Processed Organic Light-Emitting Diodes Based on Photostable Photo-cross-linkable Fluorescent Small Molecules.* ACS Applied Materials & Interfaces, 2016. **8**(25): p. 16207-16217.
31. Png, R.-Q., et al., *High-performance polymer semiconducting heterostructure devices by nitrene-mediated photocrosslinking of alkyl side chains.* Nature Materials, 2010. **9**(2): p. 152-158.
32. Schelkle, K.M., et al., *Photo-Cross-Linkable Polymeric Optoelectronics Based on the [2 + 2] Cycloaddition Reaction of Cinnamic Acid.* Macromolecules, 2016. **49**(5): p. 1518-1522.
33. Gather, M.C., et al., *Solution-processed full-color polymer organic light-emitting diode displays fabricated by direct photolithography.* Advanced Functional Materials, 2007. **17**(2): p. 191-200.
34. Smith, Z.C., R.H. Pawle, and S.W. Thomas, *Photoinduced Aggregation of Polythiophenes.* ACS Macro Letters, 2012. **1**(7): p. 825-829.
35. Schelkle, K.M., et al., *Emission Turn-On and Solubility Turn-Off in Conjugated Polymers: One- and Two-Photon-Induced Removal of Fluorescence-Quenching Solubilizing Groups.* Macromolecular Rapid Communications, 2015. **36**(1): p. 31-37.
36. Li, B.W., et al., *Polymer composites with photo-responsive phthalocyanine for patterning in color and fluorescence.* European Polymer Journal, 2017. **89**: p. 399-405.
37. Katayama, H., et al., *Stereocontrolled Synthesis and Optical Properties of All-cis Poly(phenylene vinylenes) (PPVs): A Method for Direct Patterning of PPVs.* Journal of the American Chemical Society, 2005. **127**(12): p. 4350-4353.
38. Yang, K., et al., *Patternable Conjugated Polymers with Latent Hydrogen-Bonding on the Main Chain.* Macromolecules, 2014. **47**(24): p. 8479-8486.
39. Johnson, R.S., D.R. Wheeler, and S.M. Dirk, *Photolithographic patterning of alkoxy substituted poly(p-phenylenevinylene)s from xanthate precursors.* Journal of Materials Chemistry C, 2013. **1**(7): p. 1428-1433.
40. Bouffard, J., et al., *Photopatterning of Poly(arylene dienylene) by the Photoacid-Catalyzed Deprotection−Elimination Reaction of a Precursor Polymer.* Macromolecules, 2010. **43**(3): p. 1425-1429.
41. Jacobs, I.E., et al., *Direct-Write Optical Patterning of P3HT Films Beyond the Diffraction Limit.* Advanced Materials, 2017. **29**(2).
42. Fuzell, J., et al., *Optical Dedoping Mechanism for P3HT:F4TCNQ Mixtures.* Journal of Physical Chemistry Letters, 2016. **7**(21): p. 4297-4303.
43. Johnson, R.S., et al., *Conjugated Polymer Patterning through Photooxidative Backbone Cleavage.* Macromolecular Rapid Communications, 2014. **35**(12): p. 1116-1120.
44. Aoyama, Y., et al., *Photo-induced oxidation of polythiophene derivatives: Dependence on side chain structure.* Polymer Degradation and Stability, 2013. **98**(4): p. 899-903.

45. Xue, C., D.Y. Wong, and A.M. Kasko, *Complex Dynamic Substrate Control: Dual-Tone Hydrogel Photoresists Allow Double-Dissociation of Topography and Modulus.* Advanced Materials, 2014. **26**(10): p. 1577-1583.
46. García-Fernández, L., et al., *Dual Photosensitive Polymers with Wavelength-Selective Photoresponse.* Advanced Materials, 2014. **26**(29): p. 5012-5017.
47. Maddipatla, M.V.S.N., et al., *Photoresponsive Coumarin Polyesters That Exhibit Cross-Linking and Chain Scission Properties.* Macromolecules, 2013. **46**(13): p. 5133-5140.
48. Zhao, C., et al., *A pH-UV Dual-Responsive Photoresist for Nanoimprint Lithography That Improves Mold Release.* The Journal of Physical Chemistry C, 2017. **121**(21): p. 11428–11436.
49. Lee, J., et al., *Kinetics of UV Irradiation Induced Chain Scission and Cross-Linking of Coumarin-Containing Polyester Ultrathin Films.* Macromolecules, 2014. **47**(9): p. 2891-2898.
50. Jellali, R., M. Alexandre, and C. Jerome, *Photosensitive polydimethylsiloxane networks for adjustable-patterned films.* Polymer Chemistry, 2017. **8**(16): p. 2499-2508.
51. Manhart, J., et al., *Design and application of photo-reversible elastomer networks by using the [4πs+4πs] cycloaddition reaction of pendant anthracene groups.* Polymer, 2016. **102**: p. 10-20.
52. Kaur, G., P. Johnston, and K. Saito, *Photo-reversible dimerisation reactions and their applications in polymeric systems.* Polymer Chemistry, 2014. **5**(7): p. 2171-2186.
53. Hallett-Tapley, G.L., et al., *Single component photoacid/photobase generators: potential applications in double patterning photolithography.* Journal of Materials Chemistry C, 2013. **1**(15): p. 2657-2665.
54. Radl, S.V., et al., *Photo-responsive thiol-ene networks for the design of switchable polymer patterns.* Polymer Chemistry, 2017. **8**(9): p. 1562-1572.
55. He, C. and M.P. Stoykovich, *Photopatterning of Cross-Linkable Epoxide-Functionalized Block Copolymers and Dual-Tone Nanostructure Development for Fabrication Across the Nano- and Microscales.* Small, 2015. **11**(20): p. 2407-2416.
56. Wolfberger, A., et al., *Photolithographic patterning of cellulose: a versatile dual-tone photoresist for advanced applications.* Cellulose, 2015. **22**(1): p. 717-727.
57. Fonseca, C., et al. *Advances and challenges in dual-tone development process optimization*. 2009.
58. Jen, W.L.K., et al., *Self-aligned patterning on a flexible substrate using a dual-tone, thermally activated photoresist.* Journal of Vacuum Science & Technology B, 2012. **30**(1).
59. Klán, P., et al., *Photoremovable Protecting Groups in Chemistry and Biology: Reaction Mechanisms and Efficacy.* Chemical Reviews, 2013. **113**(1): p. 119-191.
60. Thomas, S.W., *New Applications of Photolabile Nitrobenzyl Groups in Polymers.* Macromolecular Chemistry and Physics, 2012. **213**(23): p. 2443-2449.
61. Zhao, H., et al., *o-Nitrobenzyl Alcohol Derivatives: Opportunities in Polymer and Materials Science.* Macromolecules, 2012. **45**(4): p. 1723-1736.
62. Hu, X., et al., *Triggered Release of Encapsulated Cargo from Photoresponsive Polyelectrolyte Nanocomplexes.* ACS Applied Materials & Interfaces, 2016. **8**(36): p. 23517-23522.
63. Hu, X., et al., *Stimuli-Responsive Free-Standing Layer-By-Layer Films.* Advanced Materials, 2016. **28**(4): p. 715-721.
64. Nilsson, K.P., et al., *Imaging distinct conformational states of amyloid-beta fibrils in Alzheimer's disease using novel luminescent probes.* ACS Chemical Biology, 2007. **2**(8): p. 553-560.
65. Mawad, D., et al., *A Single Component Conducting Polymer Hydrogel as a Scaffold for Tissue Engineering.* Advanced Functional Materials, 2012. **22**(13): p. 2692-2699.
66. Bertran, O., et al., *Poly(2-thiophen-3-yl-malonic acid), a Polythiophene with Two Carboxylic Acids Per Repeating Unit.* Journal of Physical Chemistry B, 2010. **114**(19): p. 6281-6290.
67. Hu, X., Z. Qureishi, and S.W. Thomas, *Light Controlled Selective Disruption, Multi-Level Patterning, and Sequential Release with Polyelectrolyte Multilayer Films Incorporating Four Photocleavable Chromophores.* Chemistry of Materials, 2017. **29**: p. 2951-2960.
68. Nie, Z.H. and E. Kumacheva, *Patterning surfaces with functional polymers.* Nature Materials, 2008. **7**(4): p. 277-290.

69. Hu, X., J. Shi, and S.W. Thomas, *Photolabile ROMP gels using ortho-nitrobenzyl functionalized crosslinkers.* Polymer Chemistry, 2015. **6**(27): p. 4966-4971.
70. Chen, X., et al., *Copolymers from naphtho[2,3-c]thiophene-4,9-dione derivatives and benzodithiophene: synthesis and photovoltaic applications.* RSC Advances, 2012. **2**(19): p. 7439-7448.

Chapter 5 Appendix

^{1}H and ^{13}C NMR

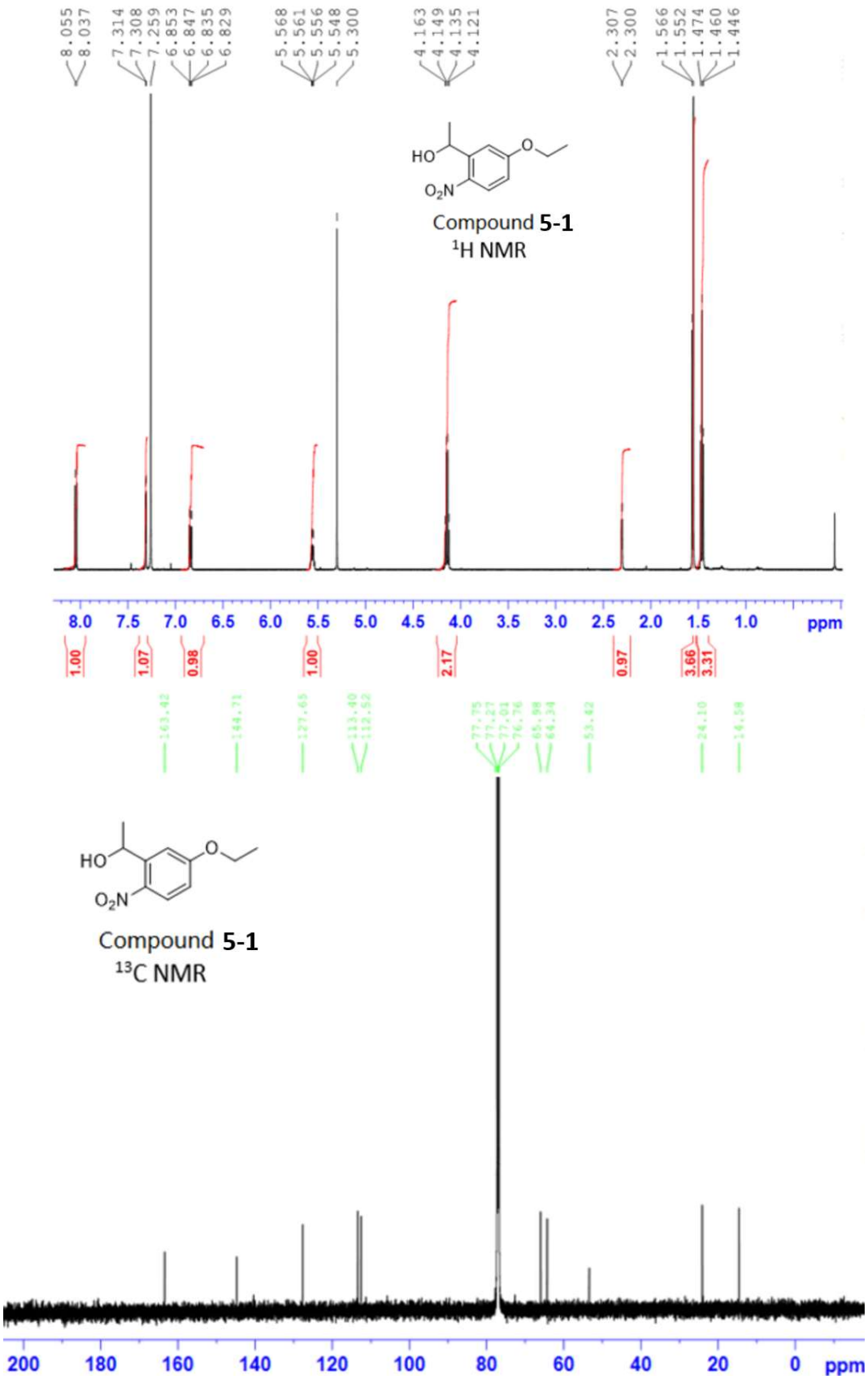
8.055
8.037
7.314
7.308
7.259
6.853
6.847
6.835
6.829
5.568
5.561
5.556
5.548
5.300
4.163
4.149
4.135
4.121
2.307
2.300
1.566
1.552
1.474
1.460
1.446
HO
O
O2N
Compound 5-1
1H NMR
8.0
7.5
7.0
6.5
6.0
5.5
5.0
4.5
4.0
3.5
3.0
2.5
2.0
1.5
1.0
ppm
1.00
1.07
0.98
1.00
2.17
0.97
3.66
3.31
163.42
144.71
127.65
133.40
112.52
77.35
77.27
77.01
76.76
65.98
64.34
53.42
24.10
14.58
HO
O
O2N
Compound 5-1
13C NMR
200
180
160
140
120
100
80
60
40
20
0
ppm

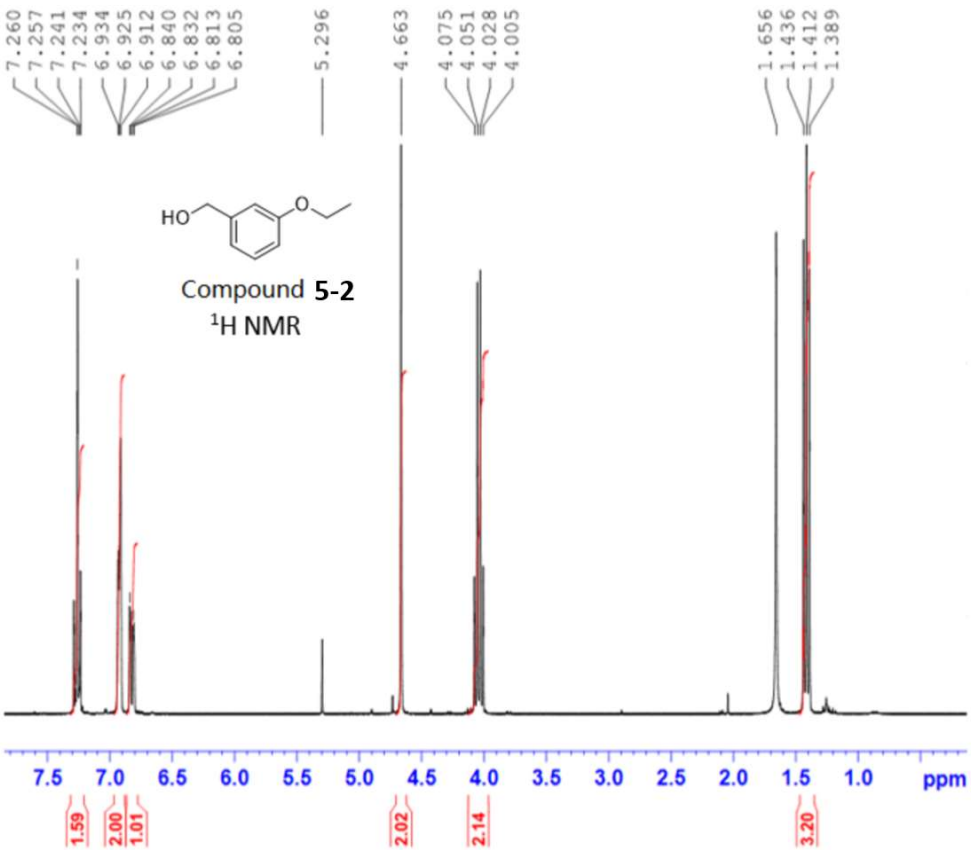
7.260
7.257
7.241
7.234
6.934
6.925
6.912
6.840
6.832
6.813
6.805
5.296
4.663
4.075
4.051
4.028
4.005
1.656
1.436
1.412
1.389
HO
O
Compound 5-2
1H NMR
7.5
7.0
6.5
6.0
5.5
5.0
4.5
4.0
3.5
3.0
2.5
2.0
1.5
1.0
ppm
1.59
2.00
1.01
2.02
2.14
3.20

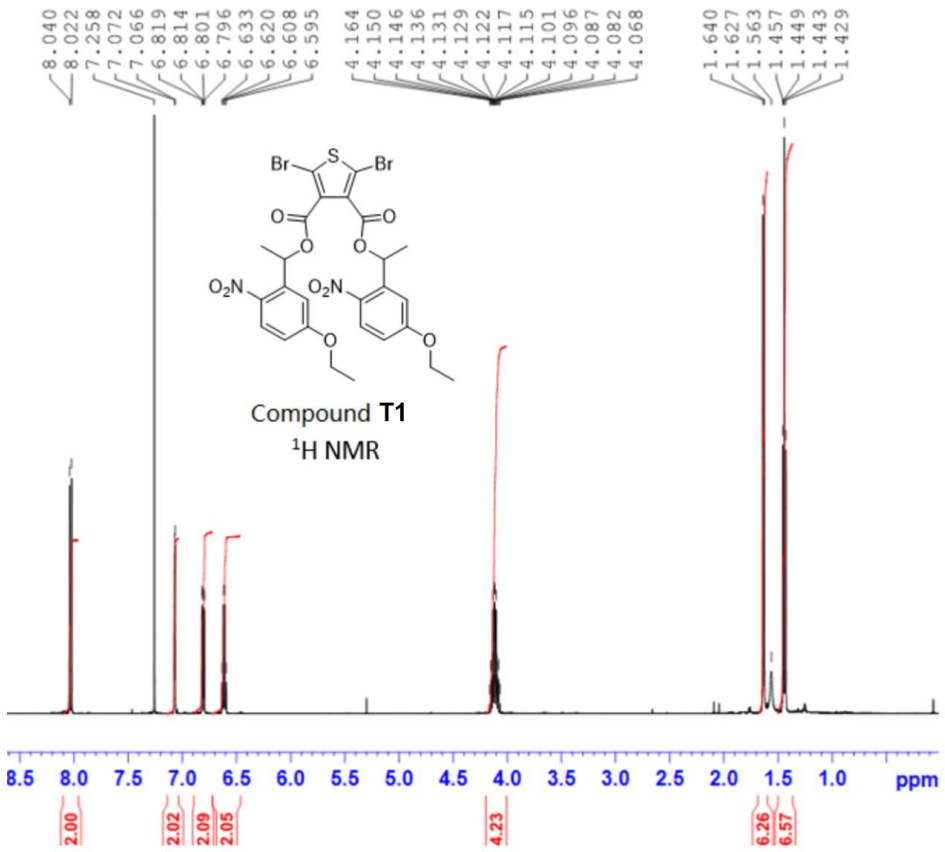
8.040
8.022
7.258
7.072
7.066
6.819
6.814
6.801
6.796
6.633
6.620
6.608
6.595
4.164
4.150
4.146
4.136
4.131
4.129
4.122
4.117
4.115
4.101
4.096
4.087
4.082
4.068
1.640
1.627
1.563
1.457
1.449
1.443
1.429
Br
S
Br
O
O
O
O
O2N
O2N
O
O
Compound T1
1H NMR
8.5
8.0
7.5
7.0
6.5
6.0
5.5
5.0
4.5
4.0
3.5
3.0
2.5
2.0
1.5
1.0
ppm
2.00
2.02
2.09
2.05
4.23
6.26
6.57

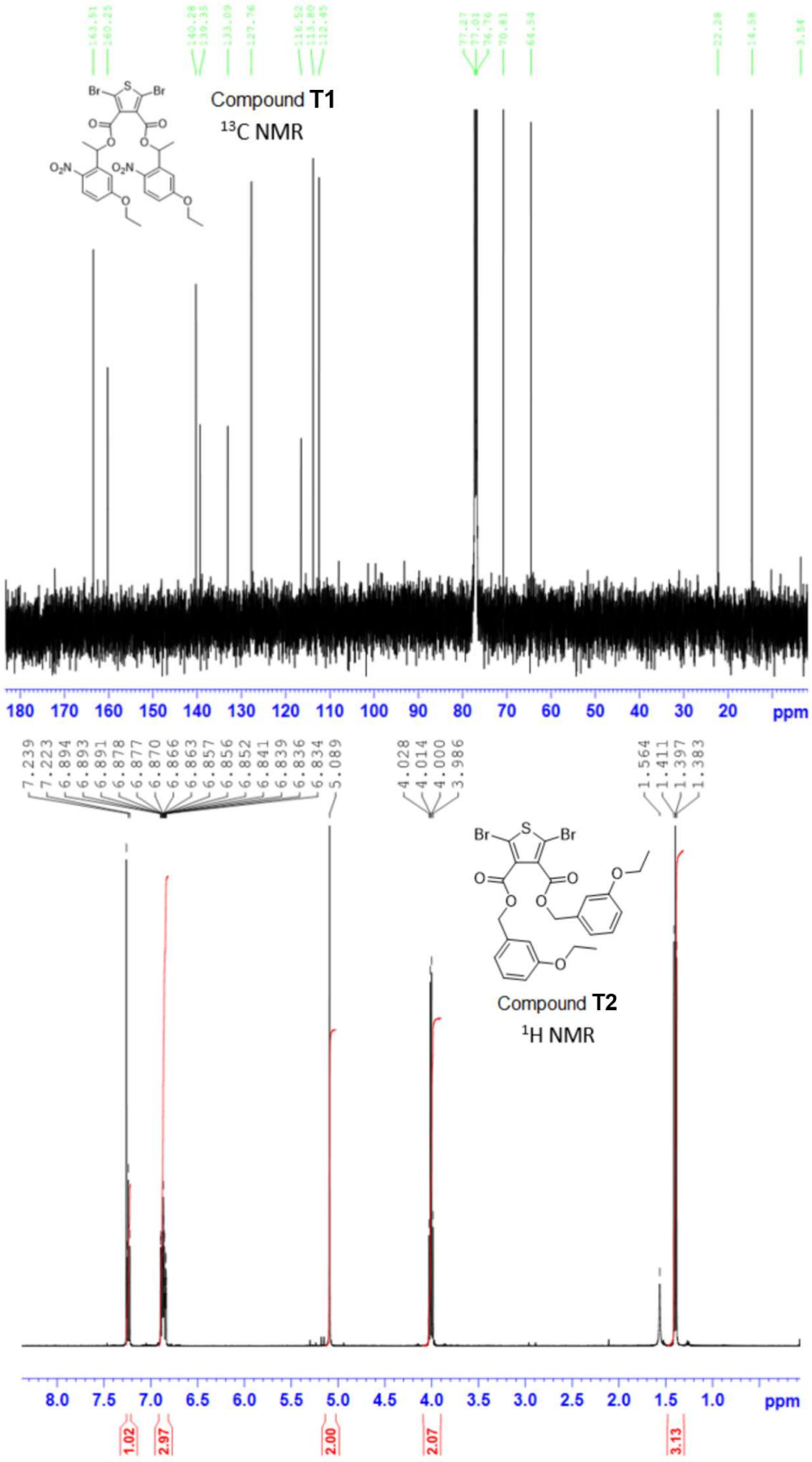
Compound T1
13C NMR
Compound T2
1H NMR
ppm

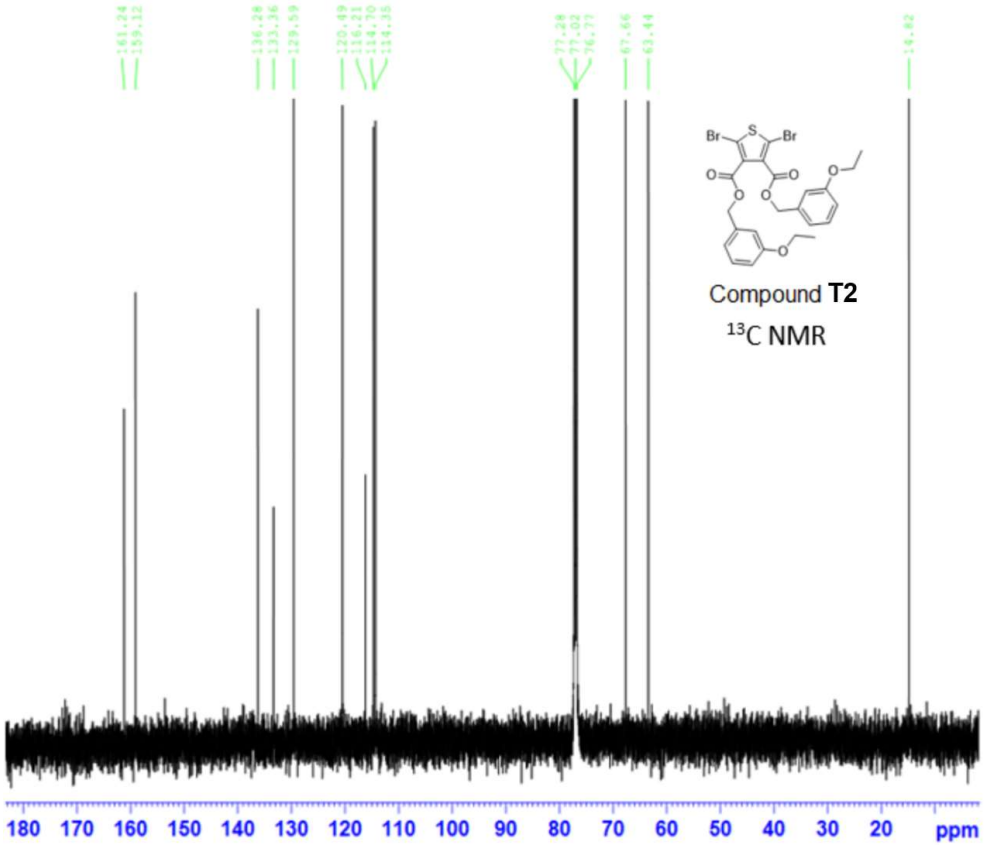
161.24
159.12
136.28
133.36
129.59
120.49
116.21
114.70
114.35
77.29
77.02
76.77
67.66
63.44
16.82
Br
S
Br
O
O
O
O
O
O
Compound T2
13C NMR
180 170 160 150 140 130 120 110 100 90 80 70 60 50 40 30 20 ppm

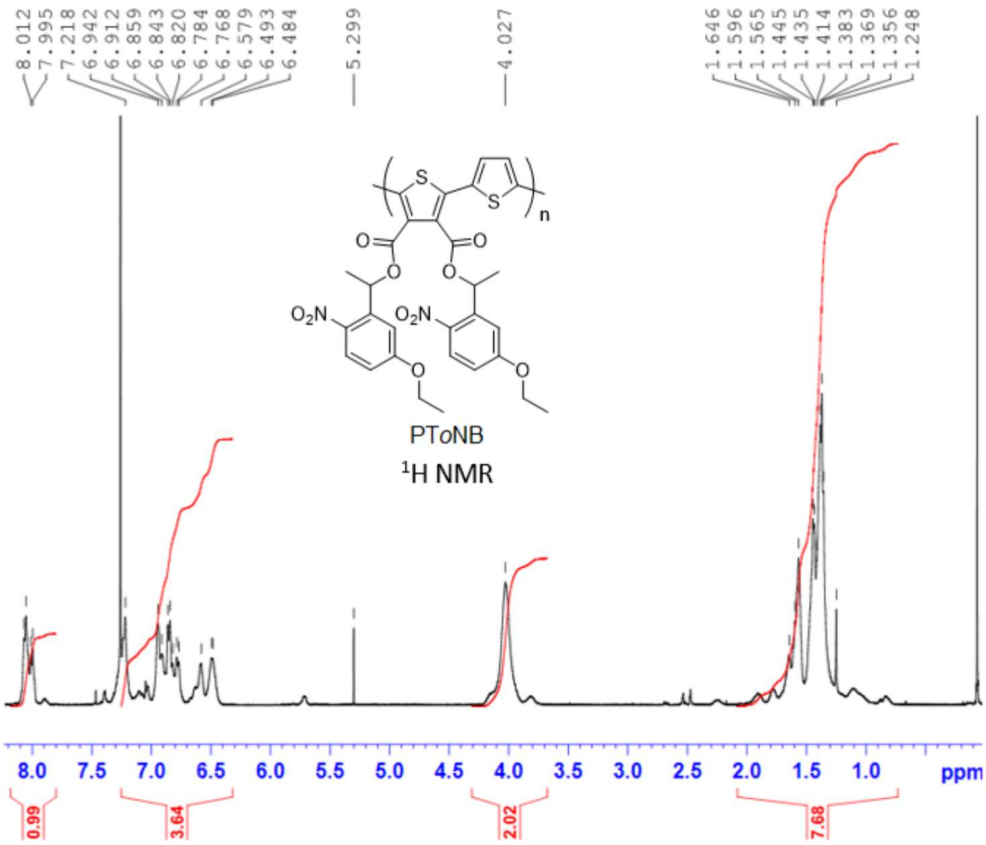
8.012
7.995
7.218
6.942
6.912
6.859
6.843
6.820
6.784
6.768
6.579
6.493
6.484
5.299
4.027
1.646
1.596
1.565
1.445
1.435
1.414
1.383
1.369
1.356
1.248
S
S
n
O
O
O
O
O2N
O2N
O
O
PToNB
1H NMR
8.0 7.5 7.0 6.5 6.0 5.5 5.0 4.5 4.0 3.5 3.0 2.5 2.0 1.5 1.0 ppm
0.99
3.64
2.02
7.68

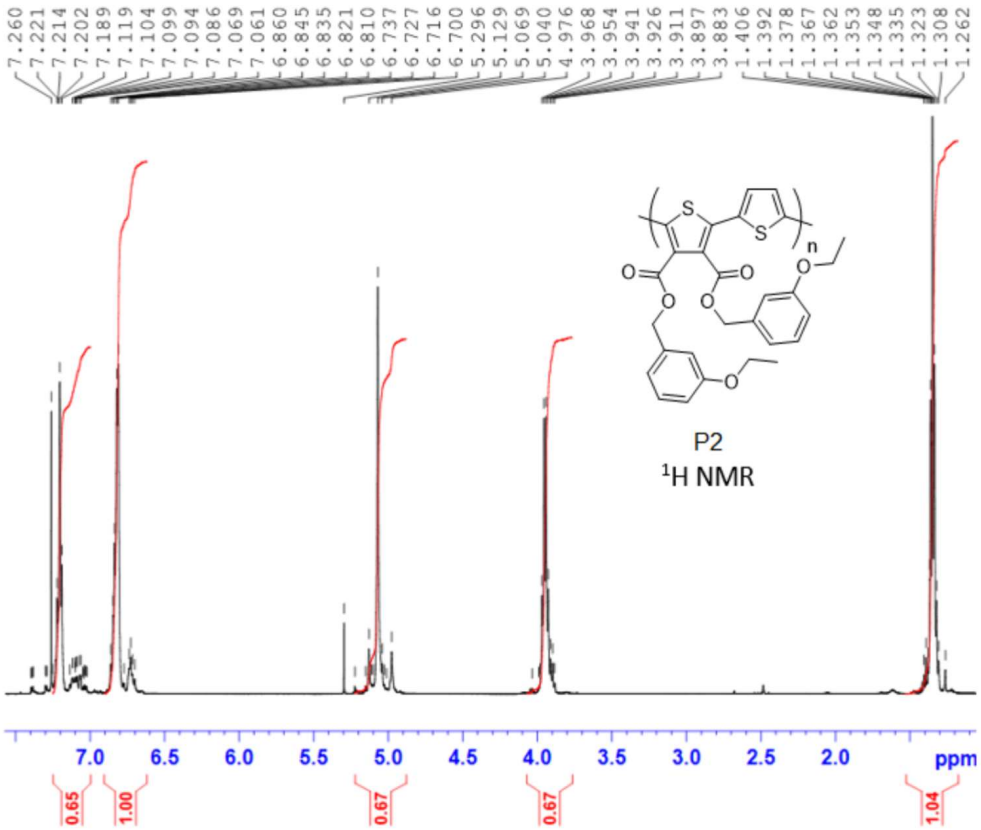
7.260
7.221
7.214
7.202
7.189
7.119
7.104
7.099
7.094
7.086
7.069
7.061
6.860
6.845
6.835
6.821
6.810
6.737
6.727
6.716
6.700
5.296
5.129
5.069
5.040
4.976
3.968
3.954
3.941
3.926
3.911
3.897
3.883
1.406
1.392
1.378
1.367
1.362
1.353
1.348
1.335
1.323
1.308
1.262
S
S
n
O
O
O
O
O
O
P2
1H NMR
7.0
6.5
6.0
5.5
5.0
4.5
4.0
3.5
3.0
2.5
2.0
ppm
0.65
1.00
0.67
0.67
1.04